

**Identification of proteins involved in genome stability by
high-throughput screening of overexpression ORFeome**

A thesis submitted for the degree of

Doctor of Philosophy

by

Priya Jaitly



Molecular Biology and Genetics Unit

Jawaharlal Nehru Centre for Advanced Scientific Research

Jakkur, Bangalore-560064

September 2021

Dedicated to my family

DECLARATION

I hereby declare that the work described here in this thesis entitled '**Identification of proteins involved in genome stability by high-throughput screening of overexpression ORFeome**' has originally been carried out by myself under the guidance and supervision of **Dr. Kaustuv Sanyal**, Professor, Molecular Biology and Genetics Unit (MBGU), Jawaharlal Nehru Centre for Advanced Scientific Research (JNCASR), Bangalore-560064, India and that this work has not been submitted elsewhere for the award of any other degree. In keeping with the norm of reporting the scientific observations, due acknowledgements have been made whenever the work described was carried out in collaboration with other researchers or was based on findings of other investigators. Any omission, which might have occurred by oversight or misjudgement, is regretted.



Priya Jaitly

Place: Bangalore

Date: 23 September, 2021



Jawaharlal Nehru Centre for Advanced Scientific Research

Autonomous Institution under Dept. of Science & Technology, Govt. of India and an Institution Deemed to be University

जवाहरलाल नेहरू उन्नत वैज्ञानिक अनुसंधान केंद्र (ज.ने.उ.वै.अ.के.)

(विज्ञान एवं प्रौद्योगिकी विभाग, भारत सरकार के अधीन एक स्वायत्त संस्था तथा सम विश्वविद्यालय संस्थान)

Kaustuv Sanyal, PhD

Professor & JC Base National Fellow
Molecular Biology & Genetics Unit
Visiting Professor, Osaka University

Certificate

This is to certify that the work described in this thesis entitled '*Identification of proteins involved in genome stability by high-throughput screening of overexpression ORFeome*' is the result of investigations carried out by **Ms. Priya Jaitly** in the Molecular Biology and Genetics Unit (MBGU), Jawaharlal Nehru Centre for Advanced Scientific Research (JNCASR), Bangalore 560064, India under my supervision and guidance. The results presented in this thesis have not previously formed the basis for the award of any other diploma, degree or fellowship.

Place: Bangalore

Kaustuv Sanyal

Date: 23 September 2021

ACKNOWLEDGEMENTS

The work carried out in this thesis has been made possible by the support and help from many individuals and organizations. I take this opportunity to express my gratitude to all those people who directly or indirectly contributed to this study.

First and foremost, I want to thank my research supervisor Prof. Kaustuv Sanyal for his constant support and encouragement. I thank him sincerely for instilling confidence in me to pursue my research problem. His enthusiasm for the topic made a strong impression on me. His scientific temperament and approach towards the subject helped me understand my scientific problem better. His valuable insights, support and scholarly guidance have given this story the necessary impetus that it needed.

I would like to express my gratitude towards all the faculty members of the Molecular Biology and Genetics Unit. I am thankful to Prof. Maneesha Inamdar, chairperson of MBGU, under whom I did my first lab rotation. She taught me the preliminary concept of developmental biology and how to approach a scientific question. The guidance received from her during my lab rotation helped me in experimental designing and proper cataloging of the results. The various courses taken during the program have been very useful to me towards understanding the basic concepts and techniques of molecular biology. Hence, I thank all the faculties, Prof. M.R.S Rao, Prof. Anuranjan Anand, Prof. Tapas Kundu, Prof. Ranga Uday Kumar, Prof. Namita Surolia, Prof. Hemalatha Balaram, Prof. Maneesha Inamdar, Dr. Ravi Manjithaya, Dr. James Chelliah, Dr. Kushagra Bansal and Dr. G.R. Ramesh for their constructive criticism throughout.

I am thankful to our collaborators Prof. Christophe d'Enfert and Mélanie Legrand from Institut Pasteur, Paris, France for providing the *E. coli* overexpression collection and sharing the protocols and reagents for high-throughput assays. Online discussions with them have always been a learning experience. I feel lucky that I got an opportunity to work in Prof. Christophe's lab for three months. I thank Prof. Christophe and all his lab members for their help and support during my stay.

I thank Dr. N. Nala at the flow cytometry facility, JNCASR, for assisting flow cytometry and cell sorting experiments. Carrying out flow cytometry analysis for so many strains would not have been possible without his support. I sincerely thank him for his availability during the weekends and post-working hours. He also helped me in standardizing flow cytometry-related experiments.

I thank JNCASR for providing excellent facilities and environment to conduct research. The inhouse facilities including the central instruments facilities have been very useful in case of break-down of the lab instruments. I also want to thank JNC admin staff, academic staff and MBGU staff for their help.

I thank Indo-French Centre for the Promotion of Advanced Research (CEFIPRA) for funding the project and aiding the travel between the Indian and French labs.

The acknowledgement section is incomplete without mentioning the members of Molecular Mycology lab. Firstly, I want to thank Lakshmi whom I considered my second mentor in the lab. The patience, the focus and the accuracy that is needed to perform any experiment was all taught by her to me. Words are certainly not enough to express my gratitude to her. Special thanks to Krishnendu who helped me with the phylogenetic analysis. Special thanks to Abhijit and Tejas who helped in constructing the overexpression library and generating various deletions and tagging cassettes. I want to thank Laxmi and Neha for teaching me the initial basic techniques related to the yeast genetics. I thank Vikas for teaching me how to have a balanced life while working in the lab. I thank Sundar and Rima for being such excellent trouble-shooters. I thank Priya B, Satya, Rashi, Kuladeep and Hashim for sharing the reagents during emergency. My thanks and appreciations also go to other members of the lab (past and present), Shreyas, Aswathy, Shweta, Promit, Rohit, Srijana, Ankita, Srikrishna, Nidhi, Harshit, Deepam for their stimulating suggestions and encouragement. I thank Amrutha, Vanshika and Arghakusum who helped me with the intra-species characterization part. Special thanks to Nagaraja and Sahana for making lab reagents available on time.

I have been blessed with good friends in JNCASR. I would like to thank Divyesh, Payel, Deeti, Shashank, Ronak, Diana, Arindam, Rahul, Preeti, Aksa, Kajal, Pallabi, Siddharth, Veena, Bhavana. Talking to them was the biggest stress buster for me. They have helped immensely during my stay at JNCASR.

I thank all my MBGU seniors and juniors, who are too numerous to be named, but who, nevertheless, have inspired me, at some moment or the other through their work or personal interactions.

I personally felt lucky to have Jigyasa and Piyush as my friends. They have always supported and guided me throughout my PhD tenure. Most importantly none of this could have happened without my family. To my mother, father, brother and sister-in-law, every time I was sad or depressed, you were there to make me smile. I am forever grateful to your unconditional love and encouragement.

TABLE OF CONTENTS

Chapter 1: Introduction	1
Genome stability and its importance	2
Cross-talk between genome stability and cell cycle	4
Yeast as a powerful tool for studying cell cycle and genome stability	6
Role of DNA replication in maintaining genome stability	6
Chromosome segregation as a major determinant of genome stability	8
Centromeres and kinetochores	9
MTOCs, the site for MT nucleation	11
Spatial organization of the KTs near SPB	13
MTs and their accessory proteins	15
Role of MTs and MAPs in nuclear migration	16
Beyond nuclear division, exiting mitosis	19
Role of mitotic checkpoints in regulating genome stability	20
<i>Candida albicans</i> as a model system for studying eukaryotic genome biology	23
Taxonomic position	24
Morphology	25
Chromosomal elements	27
Genome plasticity and its significance	29
Molecular mechanisms leading to genome diversity	32
Purpose of the present study	33
Summary of the current work	33

Chapter 2: Results (Part I)	36
Screening of <i>C. albicans</i> overexpression library identifies <i>chromosome stability (CSA)</i> genes	36
A reporter system for monitoring chromosome stability in <i>C. albicans</i>	37
Generation and screening of <i>C. albicans</i> overexpression library to identify regulators of genome stability	40
Molecular mechanisms underlying CIN in <i>CSA</i> overexpression mutants	44
Chapter 3: Results (Part II)	48
Csa6 is a spindle pole body localizing protein required for mitotic progression and mitotic exit in <i>C. albicans</i>	48
Csa6, a previously uncharacterized protein, as a key regulator of mitotic progression in <i>C. albicans</i>	49
SAC inactivation bypasses the <i>CSA6</i> overexpression-induced G2/M arrest	52
Csa6 regulates mitotic exit network and is essential for viability in <i>C. albicans</i>	55
Csa6 is an SPB-localizing protein, present in a subset of CUG-Ser clade species of fungi	59
Chapter 4: Discussion and future perspectives	64
Chapter 5: Materials and methods	72
Strains, plasmids and primers	73
Strain Construction	73
Media and growth conditions	80
Flow cytometry analysis	81
96-well plasmid miniprep by boiling lysis method	81
<i>C. albicans</i> colony PCR	81
Primary and secondary overexpression screening	82
Cell sorting and marker analysis	82

Cell cycle analysis	83
Fluorescence microscopy	83
Protein preparation and western blotting	84
Statistical analysis	85
Chapter 6: References	96
Appendix: Results of the primary screen	108
List of Publications	133

LIST OF FIGURES AND TABLES

Chapter 1: Introduction		
Figure 1.1	Different forms of genome instability	2
Figure 1.2	Endogenous stresses leading to genome instability	3
Figure 1.3	Regulation of eukaryotic cell division cycle	4
Figure 1.4	Role of the origin recognition complex (ORC) in the assembly of pre-replication complex	7
Figure 1.5	Genome instability due to replication fork stalling	8
Figure 1.6	An overview of KT architecture	10
Figure 1.7	Organization of SPB components in the budding yeast and the fission yeast	12
Figure 1.8	KT clustering in fungi	14
Figure 1.9	Structure and types of MTs in the budding yeast	16
Figure 1.10	Dynamics of nuclear segregation mechanisms in fungi	17
Figure 1.11	The two pathways for nuclear positioning in <i>S. cerevisiae</i>	18
Figure 1.12	The MEN pathway in <i>S. cerevisiae</i>	20
Figure 1.13	Principles of SAC activation	21
Figure 1.14	Mechanisms leading to SPOC activation	23
Figure 1.15	Position of <i>C. albicans</i> in the fungal phylogenetic tree	24
Figure 1.16	Plasticity of <i>C. albicans</i> cell morphology	25
Figure 1.17	DNA-damage-induced morphological transition in <i>C. albicans</i>	26
Figure 1.18	Schematic of essential chromosomal elements in <i>C. albicans</i>	28
Figure 1.19	The unique haploid-diploid-tetraploid life cycle of <i>C. albicans</i>	31
Figure 1.20	Plasticity of <i>C. albicans</i> genome	32

Chapter 2: Results (Part I)		
Figure 2.1	The CSA reporter system for detecting chromosome instability (CIN) in <i>C. albicans</i>	37
Figure 2.2	Functional validation of the CSA reporter	39
Figure 2.3	Primary and secondary screening of the <i>C. albicans</i> overexpression strains identifies six <i>CSA</i> genes	41
Figure 2.4	CIN associated with overexpression of <i>CSA</i> genes is regulated via distinct mechanisms	45
Table 2.1	Quantification of BFP/GFP loss frequency in EV	42
Table 2.2	BFP/GFP loss frequency in the primary hits	43
Table 2.3	Overexpression phenotypes of <i>CSA</i> genes in <i>C. albicans</i> and <i>S. cerevisiae</i>	46
Chapter 3: Results (Part II)		
Figure 3.1	Overexpression of <i>Csa6</i> leads to G2/M arrest in <i>C. albicans</i>	49
Figure 3.2	Overexpression of <i>CSA6</i> affects cell growth but does not perturb kinetochore integrity in <i>C. albicans</i>	51
Figure 3.3	Overexpression of <i>Csa6</i> alters the morphology of the mitotic spindle	51
Figure 3.4	The G2/M cell cycle arrest in <i>CSA6^{OE}</i> mutant is mediated by Mad2.	52
Figure 3.5	<i>CSA6^{OE}</i> associated G2/M arrest is relieved upon <i>mad2</i> deletion	53
Figure 3.6	<i>CSA6^{OE}</i> associated G2/M arrest is not relieved upon <i>bub2</i> deletion	54
Figure 3.7	<i>Csa6</i> depletion causes late anaphase/telophase arrest in <i>C. albicans</i>	55
Figure 3.8	<i>Csa6</i> depleted cells duplicate and segregate their nuclei	56
Figure 3.9	<i>Csa6</i> depletion leads to hyper-extended mitotic spindle in <i>C. albicans</i>	57
Figure 3.10	<i>Csa6</i> is required for mitotic exit in <i>C. albicans</i>	58

Figure 3.11	Csa6 is localized to the spindle pole bodies throughout the cell cycle in <i>C. albicans</i>	61
Figure 3.12	Restricted presence of Csa6 in CUG-Ser clade species	62
Figure 3.13	Conservation and ectopic expression of CdCsa6	62
Figure 3.14	CdCsa6 localizes to the SPB and functionally complements CaCsa6	63
Chapter 4: Discussion and future perspectives		
Figure 4.1	Csa6 levels are fine-tuned at various stages of the cell cycle to ensure both mitotic progression and mitotic exit in <i>C. albicans</i>	65
Figure 4.2	Proposed mechanisms by which aberrant centrosome dynamics can promote KT-MT misattachments	68
Figure 4.3	Comparison of the process of mitotic exit in yeast species	69
Figure 4.4	Role of <i>C. albicans</i> Cdc14-interacting proteins in cell cycle	69
Figure 4.5	Predicted structural features of Csa6 in <i>C. albicans</i>	70
Chapter 5: Materials and methods		
Table 5.1	Strains used in this study	85
Table 5.2	Primers used in this study	90
Table 5.3	Plasmids used in this study	94

ABBREVIATIONS

3'	3-prime
5'	5-prime
bp	Base pair
°C	Degree Celsius
DNA	Deoxyribonucleic acid
EDTA	Ethylenediaminetetraacetic acid
h	Hour
kb	Kilo base pairs
kDa	Kilodalton
Mb	Mega base pairs
μg	Micrograms
μl	Microlitre
μm	Micrometre
μM	Micromolar
mg	Milligrams
ml	Millilitre
mM	Millimolar
min	Minutes
M	Molar
ng	Nanograms
nm	Nanometre
NCBI	National Center for Biotechnology Information

NAT	Nourseothricin acyl transferase
OD ₆₀₀	Optical density at 600 nm
ORF	Open reading frame
%	Percent
PBS	Phosphate buffer saline
PCR	Polymerase chain reaction
pH	Potential of hydrogen
rpm	Revolutions per minute
RNA	Ribonucleic acid
s	Second
SDS	Sodium dodecyl sulphate

Chapter 1

Introduction

Genome stability and its importance

Cells are the fundamental unit of all living organisms (Schleiden 1838; Schwann and Hünslser 1910), capable of growing and dividing on their own. The structure and function of a cell are specified by its genetic material, a linear DNA sequence, packaged into a thread-like structure called the chromosomes and inherited from a parent to its progeny during cell division. Thus, one of the crucial attributes of a living cell is to ensure genome stability, that is, to preserve and faithfully transfer the genetic material from one generation to the other. Failure to achieve this purpose can introduce genetic alterations or genome instability, leading to abnormal cell functioning or phenotypes in the progeny (Figure 1.1). Genome instability has been intimately associated with aneuploidy, presence of abnormal chromosomal numbers (Potapova et al. 2013) and is one of the potential drivers of human genetic and neurodegenerative disorders (Taylor et al. 2019; Yurov et al. 2019), aging (Petr et al. 2020) and several cancers (Negrini et al. 2010). Although primarily considered harmful for a cell or an organism, genome instability may also contribute to generating variations and driving evolution, especially in unicellular eukaryotes (Guin et al. 2020a; Sankaranarayanan et al. 2020).

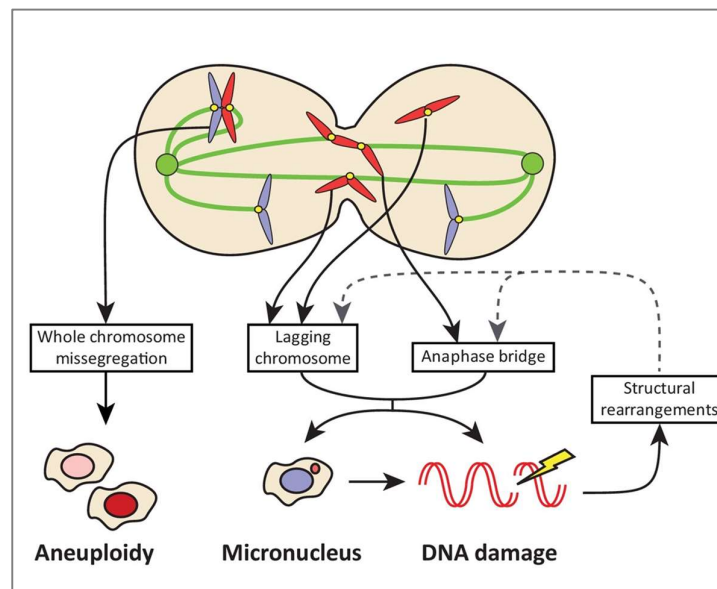


Figure 1.1. Different forms of genome instability. Erroneous chromosome segregation can lead to CIN in the form of whole chromosome missegregation (aneuploidy), lagging chromosomes, anaphase bridges, etc. Lagging chromosomes and anaphase bridges may result in DNA damage or the formation of a micronucleus. DNA damage may also occur due to endogenous stresses or exposure to exogenous mutagens. Erroneous DNA damage repair

may, in turn, result in structural rearrangements causing CIN. Adapted from (van Jaarsveld and Kops 2016).

At the molecular level, genome instability predominantly arises as a consequence of DNA lesions, of which DNA double-strand break (DSB) accounts for the most detrimental of DNA lesions. Two major pathways by which DSBs are repaired include homologous recombination (HR) and non-homologous end-joining (NHEJ) (Mehrotra and Mittra 2020). HR employs an equivalent region of DNA from either sister chromatid or homologous chromosome as a template to repair DSBs. On the contrary, NHEJ ligates the two ends of DNA lesions without using an identical DNA sequence as a template. Thus, HR-mediated DSB repair represents a high-fidelity, less erroneous mode of DNA repair as compared to NHEJ which is more error-prone and often results in mutations at the break site. If not repaired properly, DSBs can give rise to genetic alterations. These alterations include but are not limited to point mutations, insertions and deletions of bases in specific genes and/or gain, loss and rearrangements of chromosomes, together referred to as chromosome instability (CIN) (Aguilera and Gomez-Gonzalez 2008). Besides defective DNA repair pathways, genotoxic stresses from other endogenous sources such as infidelity in DNA replication and segregation can also imperil genome integrity by inducing DNA lesions or aneuploidy (Figure 1.2). In addition, exposure to multiple exogenous agents such as ultraviolet (UV) light, ionizing radiation, DNA chelating agents and chemical mutagens can evoke genome instability by generating DSBs, base deletions, insertions or substitutions (Chatterjee and Walker 2017).

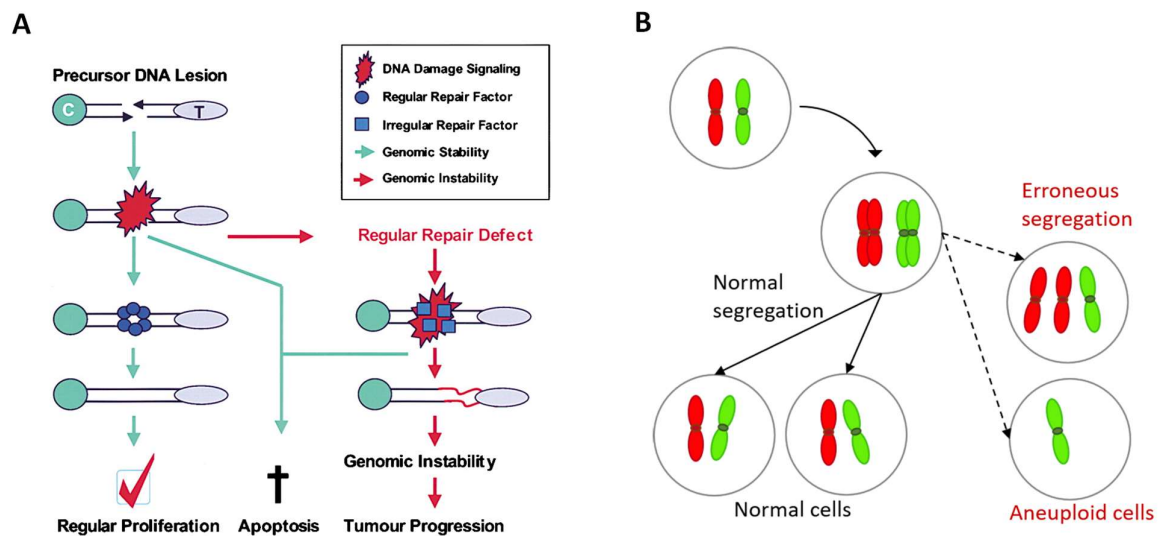


Figure 1.2. Endogenous stresses leading to genome instability. (A) Defective repair of DNA lesions due to replication errors or exposure to mutagens can lead to genomic instability. Adapted and modified from (Schar 2001). **(B)** Errors in chromosome segregation can result in whole chromosome loss, leading to aneuploidy.

Cross-talk between genome stability and cell cycle

High fidelity transmission of the genetic material from a mother to its daughter cells is an important predicate of genome stability, achieved through the proper execution of cell division cycle. Cell division is a fundamental aspect of all living organisms required for supporting growth, reproduction and replenishment of dead or damaged cells. Although species-specific differences in terms of the molecular players and mechanisms exist, the overall process and occurrence of various cell cycle events remain conserved from unicellular yeasts to more complex metazoans including humans. The eukaryotic mitotic cell division constitutes an ordered set of events by which a cell divides to produce two daughter cells (Figure 1.3A). The key events of a mitotic cell cycle governing genome stability include the S (synthesis) phase during which the genetic material is duplicated followed by the M (mitosis) phase in which equal segregation of the duplicated genetic material occurs. Separating the S and M phases are the two gap phases (G1 and G2), which together with the S phase comprise the interphase stage of the cell cycle. In G1 and G2 phases, cells grow in size, gain mass and prepare themselves for the subsequent stages. The M phase is further subdivided into prophase, metaphase, anaphase and telophase, after which cells exit mitosis and undergo cytokinesis (Figure 1.3A). In cytokinesis, the cytoplasm, organelles and cell membrane divide to finally give rise to two identical cells, marking the end of mitosis.

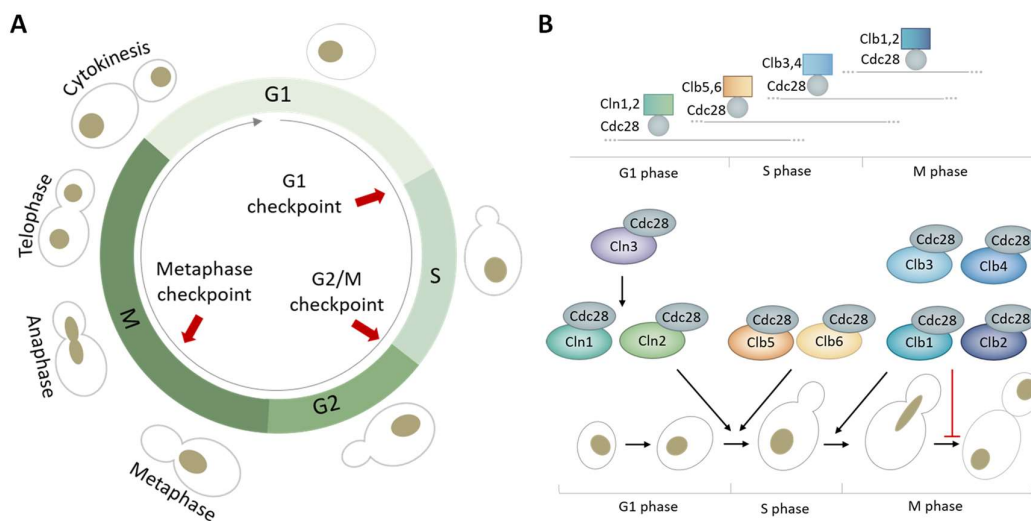


Figure 1.3. Regulation of eukaryotic cell division cycle. (A) Schematic of nuclear segregation in the budding yeast, a pronounced eukaryotic model system. A mitotic cell cycle in yeast begins with an unbudded mother cell in the G1 stage which forms a small bud (daughter bud) during G1/S and duplicates its genetic material during the S phase. Post-S phase, the daughter bud continues to grow and the genetic material, entrapped inside the nucleus (yellow), is segregated to finally give rise to the two daughter cells. Various cell cycle checkpoints are marked in red arrows. (B) Major Cdk-cyclin complexes involved in the budding yeast cell cycle. In budding yeast, a single Cdk, Cdc28, can regulate transitions to various cell cycle phases by associating with multiple stage-specific cyclins. Three G1 cyclins, Cln1-3, regulate the G1 checkpoint (also known as Start in the budding yeast). Clb1-4 regulates entry into the M phase and Clb5-6 governs entry into the S phase. *Top*, approximate activation timings of the indicated complexes during cell cycle. Cln3 promotes entry into the Start and can be detected throughout the cell cycle (Wijnen et al. 2002). *Bottom*, schematic showing functions associated with indicated complexes at various cell cycle stages. Adapted and modified from (Morgan 1997; Bloom and Cross 2007).

The accuracy of several cell cycle events starting from DNA replication to chromosome segregation is crucial for maintaining genome integrity (Figure 1.2). Cell cycle checkpoints are the cellular surveillance mechanisms by which the integrity and fidelity of various cell cycle events are monitored. They play a critical role in ensuring genome stability by halting the progression of a cell to the next phase in response to an error or damage until it is repaired. In a mitotic cell cycle, three major checkpoints monitor the fidelity of various cell cycle events (Figure 1.3A); (i) The cell size checkpoints at G1 and G2 phases coordinate the cell size with cell cycle progression (Barnum and O'Connell 2014). Control of cell size is important for regulating the cellular distribution of nutrients and biosynthetic materials during cell division. (ii) The DNA damage checkpoint operates at G2/M stages and functions in response to any kind of DNA damage due to exogenous or endogenous factors. (iii) The spindle checkpoint pathway functions during mitosis and ensures fidelity of chromosome segregation at metaphase-anaphase transition. Failure of any of the error-correcting mechanisms can thus introduce genetic alterations, causing genome instability in the progeny.

Progression of the cell cycle through various checkpoints is mediated by two groups of proteins, cyclins and cyclin-dependent kinases (Cdks) (Figure 1.3B). Cyclins are a family of proteins whose levels oscillate throughout the cell cycle (Figure 1.3B). Cyclins regulate cell cycle events when they are tightly bound to Cdks, which are enzymes (kinases) that phosphorylate other proteins. The proteins phosphorylated by Cdks facilitate transitions to various cell cycle stages. Cdks are active when bound to cyclins and hence, their activity is

dependent on the periodic expression of the cyclins. Activation of cell cycle checkpoints in response to an error or damage influences the activity of the Cdk/cyclin complex, thus delaying the transition to subsequent cell cycle stage during cell division.

Yeast as a powerful tool for studying cell cycle and genome stability

Yeasts are single-celled eukaryotes belonging to the fungal kingdom. For decades, budding and fission yeasts have served as uncontested model systems for exploring fundamental aspects of eukaryotic cell biology, that are otherwise difficult to study in developmentally complex humans. The key regulators of the cell division cycle including Cdks, cyclins and cell cycle checkpoints were deciphered using baker's yeast, *Saccharomyces cerevisiae*, and the fission yeast, *Schizosaccharomyces pombe* as biological systems (Hartwell et al. 2001; Pray 2008). Moreover, the ease of amenability, the availability of a plethora of genetic tools, a shorter life span, and an excellent opportunity to work with a large number of individuals within a single generation make yeast an ideal model organism for elucidating the underlying mechanisms of genome stability in eukaryotes. Recent advancements in molecular tools, sequencing technologies and computational methods made several fungal genomes fully sequenced and assembled. This unprecedented scientific advancement facilitated bioinformatic analysis of the array of genes, including cell cycle-related genes, that are conserved, lost or gained in fungi during evolution. *Candida albicans*, which diverged from the budding yeast *S. cerevisiae* ~235 million years ago (Steenwyk et al. 2021), is one such fungal species with a well-assembled genome (van het Hoog et al. 2007; Skrzypek et al. 2017) and has been employed as a model system in our study.

Role of DNA replication in maintaining genome stability

DNA replication is a tightly regulated biological process responsible for generating two identical copies of DNA from the original DNA molecule, essential for preserving genomic integrity in the daughter cells. In eukaryotes, DNA replication starts at multiple distinct sites on every chromosome, called the replication origins. These initiator sequences act as a platform for assembling multi-protein complexes that facilitate the opening up of the double-stranded DNA to form replication bubbles (Bell and Labib 2016). One of the most upstream complexes to bind and flag mark the potential replication origin sites include the origin recognition complex (ORC), a hexameric complex consisting of ORC1-6 polypeptides (Figure 1.4). In late mitosis and early G1, ORC along with Cdc6 and Cdt1 recruit the inactive ring-shaped minichromosome maintenance (Mcm) helicase complex, Mcm2-7, to form the

pre-replication complex (pre-RC), also known as origin licensing. At the G1/S transition, the pre-RC is converted to the pre-initiation complex, Mcm helicases get activated and additional factors such as DNA polymerases are recruited at the origins to complete the replisome assembly. Following DNA melting, DNA polymerase starts synthesizing the new DNA molecule, forming a replication fork, in a semi-conservative manner.

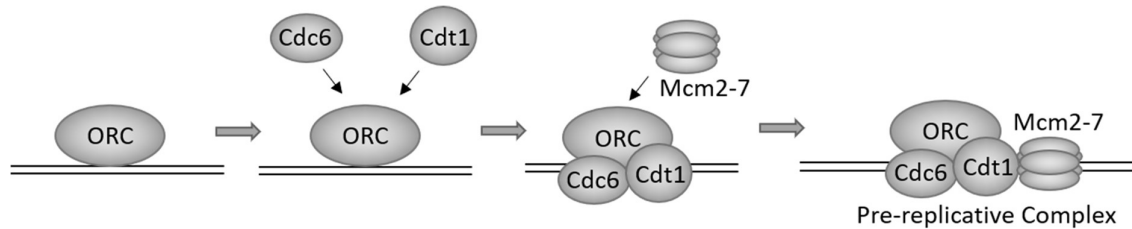


Figure 1.4. Role of the origin recognition complex (ORC) in the assembly of pre-replication complex. The pre-RC components are recruited to the replication origin in a step-wise manner, with ORC being the foremost component to be loaded followed by Cdc6, Cdt1 and the Mcm2-7 complex. The formation of the pre-RC complex licenses the replication origin sites to initiate DNA replication during S phase. Modified from (Takeda and Dutta 2005).

The fork progression during DNA replication is hindered upon encountering physical impediments in the form of DNA lesions, unusual DNA structures, transcriptional machinery or depletion of key biomolecules required for DNA synthesis - all of which either slow down or stall replication fork progression (Figure 1.5). Most stalled forks resume their activity after any DNA damage is repaired by DNA damage response (DDR) pathways (Sirbu and Cortez 2013; Chatterjee and Walker 2017). However, if DNA replication failed to restart, stalled fork collapses, leaving behind unreplicated DNA, resulting in CIN due to incorrect repair and more error-prone replication (Cortez 2015). Fork collapse thus poses a major threat to genome integrity. Besides DDR pathways, the regulation of several replisome components ensures genomic integrity (Mehrotra and Mitra 2020). Periodic expression of cyclins and their Cdk prevents reduplication of the genome during the same cell cycle by promoting scheduled localization of the pre-RC components at origins. Low Cdk activities during late mitosis/early G1 facilitate origin silencing, while high Cdk activities during S phase prevent re-licensing of the DNA replication origins before the end of mitosis. In addition, accumulation of Cdc6 and Cdt1 has been shown to induce reduplication and the associated

genome instability (Vaziri et al. 2003). Overexpression of Cdc6, Cdt1 and Mcm7 have also been linked with oncogenesis and cancer progression (Ren et al. 2006; Mahadevappa et al. 2017).

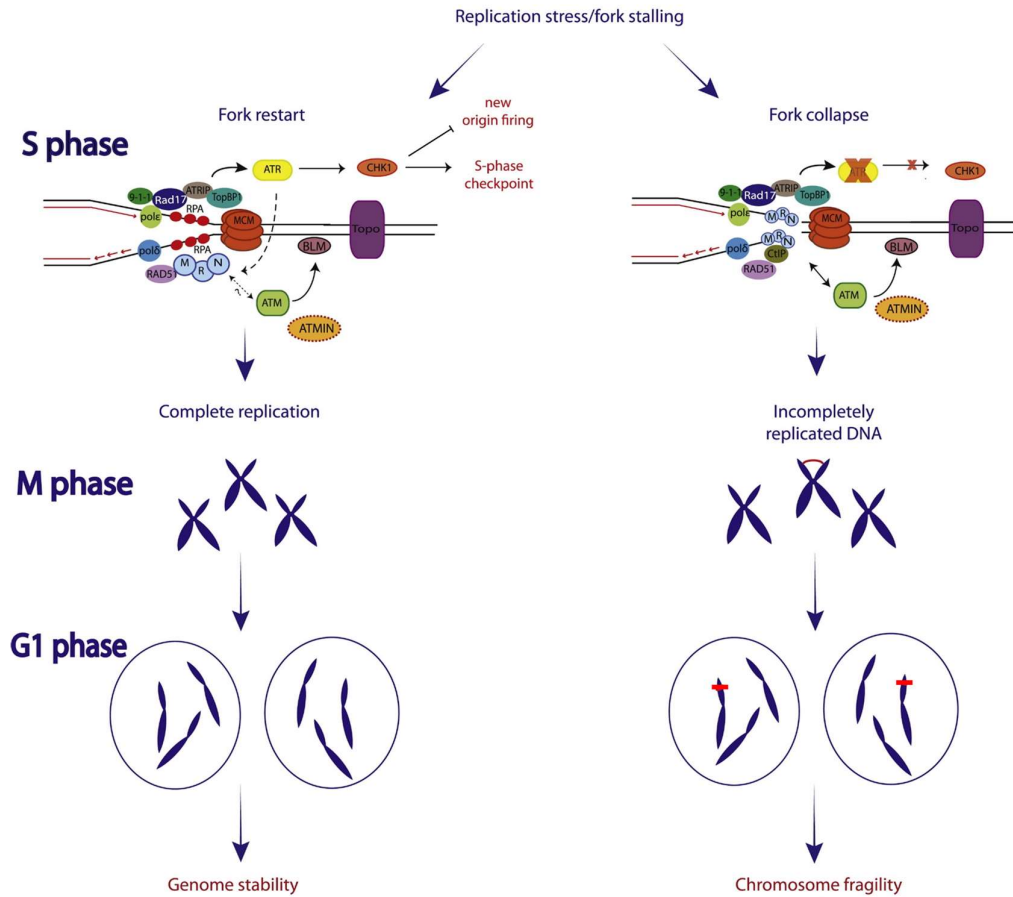


Figure 1.5. Genome instability due to replication fork stalling. Schematic representing the possible outcomes of fork stalling upon encountering damaged DNA. The resumption of the replication fork activity after DNA repair facilitates DNA replication preventing genome instability, whereas fork collapse results in incomplete DNA replication, leading to CIN. Adapted and modified from (Mazouzi et al. 2014).

Chromosome segregation as a major determinant of genome stability

Chromosome segregation during M phase is one of the pivotal steps governing genome stability in the daughter cells during cell division. In eukaryotes, the assembly of a bipolar spindle structure, predominantly consisting of microtubules (MTs)- emanating from the microtubule-organizing centers (MTOCs), drives the separation of the duplicated chromosomes. MTs interact with chromosomes through the kinetochore, a macromolecular

structure that assembles on centromeric DNA. During mitosis, sister kinetochores attach to the MTs emanating from the opposite poles (bipolar attachment) and migrate towards the respective poles with the help of MTs and MT-associated proteins (MAPs). Failure or erroneous chromosome-spindle attachment may lead to chromosome missegregation resulting in additional or fewer chromosomes in the daughter cells, causing aneuploidy- the potential driver of several cancers and genetic disorders. In the subsequent sections, we discuss the key mitotic players along with their structure-function and spatial organization to explain the major aspects of mitotic chromosome segregation.

Centromeres and kinetochores

The chromosomal locus where all the kinetochore (KT) subunits assemble is known as the centromere (CEN) which also serves as a site for sister chromatid attachment. Although this function of CEN remains conserved from yeast to humans, the DNA sequence composition and size of the CEN are poorly conserved across the eukaryotes. The budding yeast *S. cerevisiae* contains a defined CEN DNA sequence of ~125bp, known as point CENs. In contrast, CENs of most organisms ranging from the fission yeast to humans do not contain any defined sequence. These organisms have regional CENs of larger sizes (40-4000 kb), with repetitive and AT-rich sequences. The fission yeast CEN contains a non-repetitive central core, flanked by inverted repeat regions while CENs in metazoans such as humans are composed of highly repetitive DNA sequences (Guin et al. 2020b). So far, all known fungal species have been reported to possess monocentric chromosomes (one localized CEN per chromosome) that are mostly specified by the presence of a CEN-specific histone H3 variant, CENP-A (Cse4 in budding yeasts). CENP-A regulates the recruitment of KT subunits onto centromeric DNA (Howman et al. 2000; Fachinetti et al. 2013) and is sufficient to trigger KT assembly upon ectopic CENP-A localization.

The KT is a large multi-protein complex that serves as a platform for connecting the MTs to the chromosomes (Figure 1.6). The overall structure of the KT complex remains conserved from yeast to humans (Meraldi et al. 2006). The KT consists of two major layers called the CEN-proximal inner layer and the MT-binding outer layer (Musacchio and Desai 2017). The inner layer constitutes a group of CEN proteins (CENPs), forming the Constitutive Centromere Associated Network (CCAN), which helps in linking the centromeric chromatin to the outer KT (Figure 1.6). The CCAN consists of 16 CENPs, organized in various subcomplexes viz. CENP-A-CENP-C, CENP-T-W-S-X, CENP-O-P-Q-U, CENP-H-I-K-M,

and CENP-L-N. Specifically, CENP-A/CENP-C and CENP-T/U subunits are involved in recruiting the outer KT proteins and linking them to centromeric chromatin (Kixmoeller et al. 2020). The KT attaches to the MTs with the help of its outer layer, which mainly consists of the KMN protein complexes and the fungus-specific Dam1/DASH complex (Figure 1.6) (Musacchio and Desai 2017; Kixmoeller et al. 2020). Although both, the Ndc80 complex as well as the Knl1 complex of the KMN network can bind to the MTs directly, it is the Ndc80 complex that recruits accessory MT attachment factors like the Dam1/DASH complex at the KT. Besides associating the chromosomes with the MTs, KTs also recruit a cellular surveillance mechanism, called the spindle assembly checkpoint that monitors proper KT-MT attachments during mitosis.

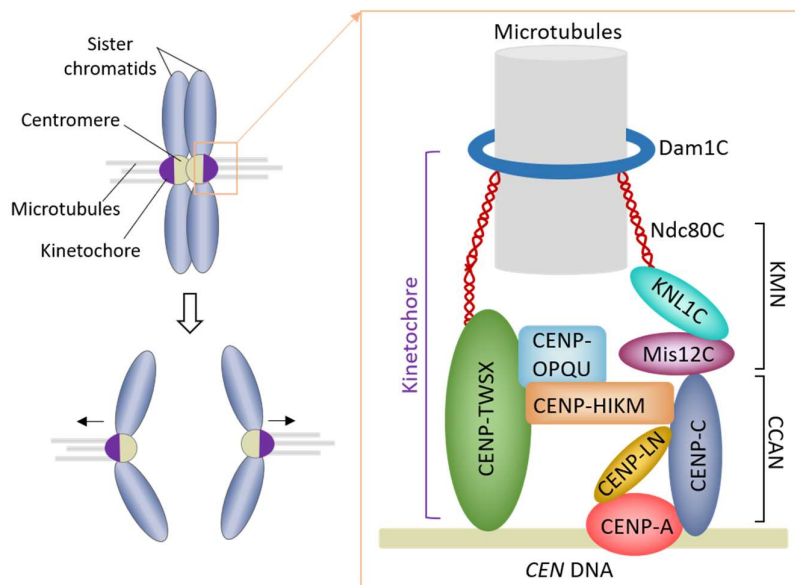


Figure 1.6. An overview of KT architecture. *Left*, mitotic chromosome segregation facilitated by the key players, centromere (CEN), kinetochore (KT) and microtubules (MTs). KT attaches to the MTs emanating from the opposite poles (bipolar attachment), segregating sister chromatids. *Right*, schematic showing the approximate position of various KT subcomplexes. The CCAN forms the inner KT whereas the KMN and the Dam1 complex form the outer kinetochore to provide a platform for MT binding.

The timing and the dependency of KT subunits to assemble at the CEN also shows remarkable variations across different fungal species. In both *S. cerevisiae* and *C. albicans*, the KT remains assembled throughout the cell cycle (Roy et al. 2013). In *S. cerevisiae*, a

stepwise assembly of the KT proteins is evident (De Wulf et al. 2003). The CBF3 complex, along with CBF1, recognizes the specific point CENs and promotes CENP-A loading, followed by the recruitment of other inner KT proteins. The inner KT proteins then act as a scaffold for recruiting the outer KT proteins. In contrast, KT assembly in *C. albicans* is coordinated and interdependent (Thakur and Sanyal 2012). Depletion of any KT protein results in delocalization and degradation of CENP-A, collapsing the whole KT architecture. In *S. pombe*, the inner and most of the outer KT proteins remain assembled throughout the cell cycle. The Dam1/DASH complex barring Dad1 (present throughout cell cycle), localizes to the CEN only during mitosis (Liu et al. 2005; Sanchez-Perez et al. 2005).

MTOCs, the site for MT nucleation

The MTOCs are morphologically diverse subcellular structures responsible for nucleating MT filaments. While centrosomes serve as the primary site for MT nucleation in metazoans, its functional homolog in fungi is called the spindle pole body (SPB). In contrast to open mitosis observed in most metazoans where a complete breakdown of the nuclear envelope (NE) takes place, many fungal species predominantly undergo closed mitosis wherein the NE remains intact throughout the cell cycle. The presence of the NE barrier makes it challenging for the SPBs to nucleate MTs that can reach the chromosomes. The two ascomycetes, *S. cerevisiae* and *S. pombe*, which undergo closed mitosis, overcome this barrier by inserting the SPBs within the nuclear membrane at all or some stages of the cell cycle, respectively (Figure 1.6A) (Cavanaugh and Jaspersen 2017).

The SPB consists of several proteins that have been identified using genetic, biochemical, and bioinformatics approaches. A major understanding of the function of each of these proteins has come from the studies carried out in *S. cerevisiae* and *S. pombe* (Figure 1.7A, B) (Cavanaugh and Jaspersen 2017). Within SPB, two major complexes called the γ -tubulin complex (γ -TuC) and the γ -tubulin complex receptors (γ -TuCr), together, are responsible for nucleating cytoplasmic as well as nuclear MTs (Figure 1.7A). The γ -TuCr consists of the linker proteins that act as a receptor for the γ -TuC, which harbors the MT nucleating activity. The γ -TuC of *S. cerevisiae*, also known as γ -tubulin small complex (γ -TuSc), represents the minimal module required for MT formation (Kollman et al. 2010) and is highly conserved across fungal species (Lin et al. 2015). In contrast, γ -TuC of many other fungi including *S. pombe* is known as the γ -tubulin ring complex (γ -TuRC) and consists of several additional proteins for MT nucleation (Figure 1.7B) (Kollman et al. 2011). Interestingly, Mzt1, a protein

linked to the γ -TuRC, remains highly conserved across fungal species except in *S. cerevisiae* (Lin et al. 2015). Why *S. cerevisiae* lost Mzt1 and *C. albicans*, an ascomycete with γ -TuSc subunits for MT nucleation retained it during the course of evolution, remains unclear (Lin et al. 2015; Cavanaugh and Jaspersen 2017).

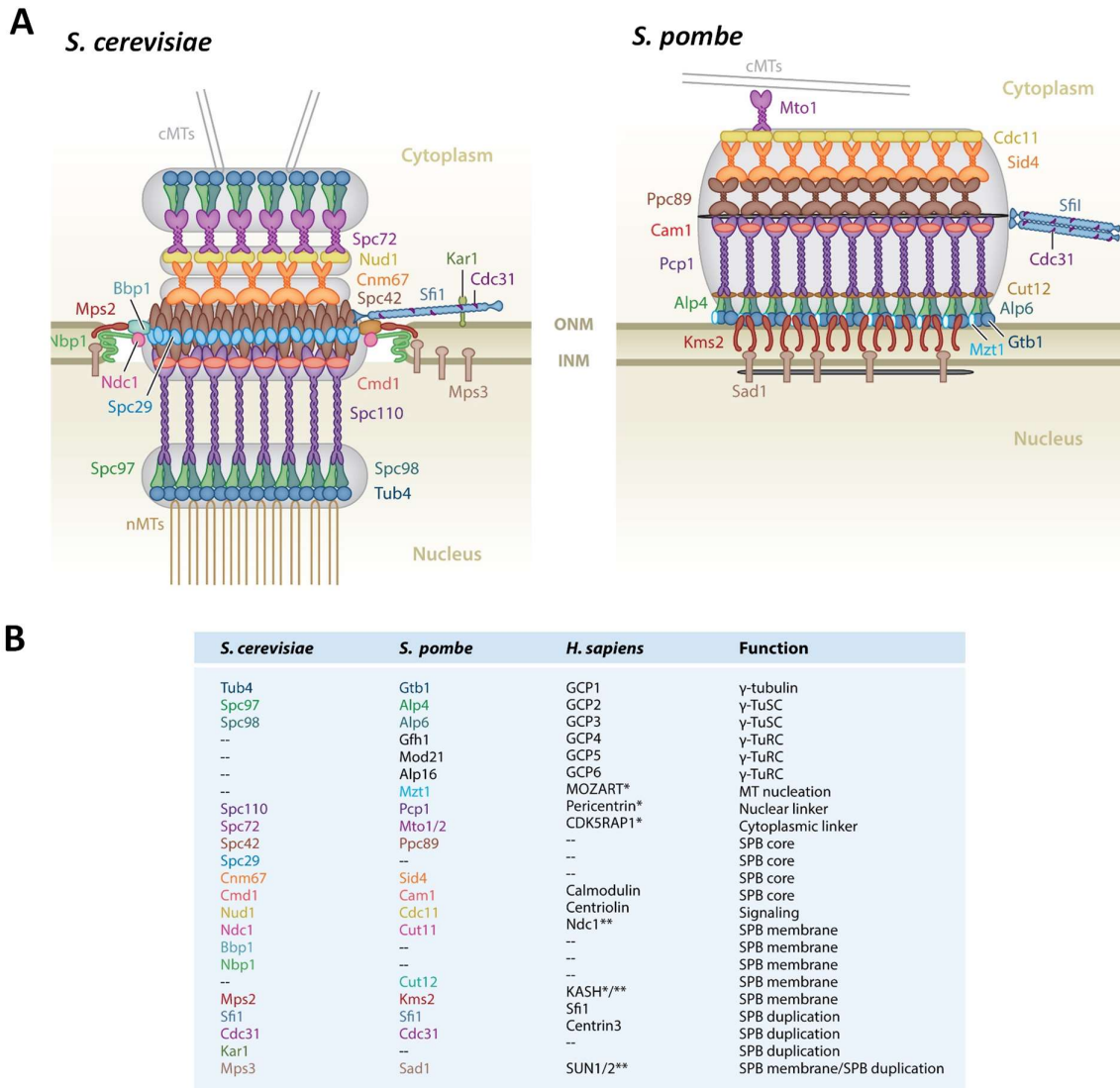


Figure 1.7. Organization of SPB components in the budding yeast and the fission yeast. (A) The multi-layered SPB structure in the indicated species. (B) Chart depicting the function of various orthologous SPB components or proteins that perform similar functions (as shown in panel A), in the indicated species. Adapted and modified from (Cavanaugh and Jaspersen 2017).

Besides MT nucleating subunits, the SPB complex contains additional proteins that are crucial for its functioning (Figure 1.7A, B). In both *S. cerevisiae* and *S. pombe*, SPB duplication occurs with the help of an extended structure, known as the half-bridge (Cavanaugh and Jaspersen 2017). The half-bridge acts as an assembly site for the daughter SPB, called the satellite, consisting of the core SPB proteins (Figure 1.7A, B) (Cavanaugh and Jaspersen 2017). As *S. cerevisiae* and *S. pombe* undergo closed mitosis, the new SPB molecule in these species gets inserted into the NE with the help of the SPB membrane proteins (Figure 1.7A, B). One of the highly conserved SPB components called Nud1 in *S. cerevisiae* and Cdc11 in *S. pombe*, also engages SPBs in the cellular signaling pathway, known as the mitotic exit network and septation initiation pathway, respectively.

Although SPB remains the primary nucleation site for MT polymerization, many fungal species also employ non-SPB MTOCs for MT nucleation. In *S. pombe*, two types of non-SPB MTOCs called the interphase MTOC (iMTOC) and equatorial MTOC (eMTOC) contribute to MT nucleation during different cell cycle stages. While the iMTOCs are present on the NE, MTs, and in the cytoplasm, the eMTOCs form the post anaphase array at the site of cell division (Sawin and Tran 2006). A pool of highly dynamic and cell cycle-regulated MTs, whose origin is poorly understood, has also been observed in *C. albicans* (Finley and Berman 2005). Perhaps, these free MTs also arise from the yet to be identified non-SPB MTOCs in *C. albicans*.

Spatial organization of the KTs near SPB

KT clustering is a general phenomenon in many organisms and cell types (Takeo et al. 2011; Guin et al. 2020b). Fluorescence microscopy analyses show that KT proteins of many fungal species cluster towards the nuclear periphery and close to the SPBs, at some or all the stages of the cell cycle (Figure 1.8A-C). The biological significance of this spatial organization of the KT is not very well understood. Perhaps, such an arrangement aids in MT capturing, especially when there is no metaphase plate arrangement for the chromosomes to align (Guacci et al. 1997).

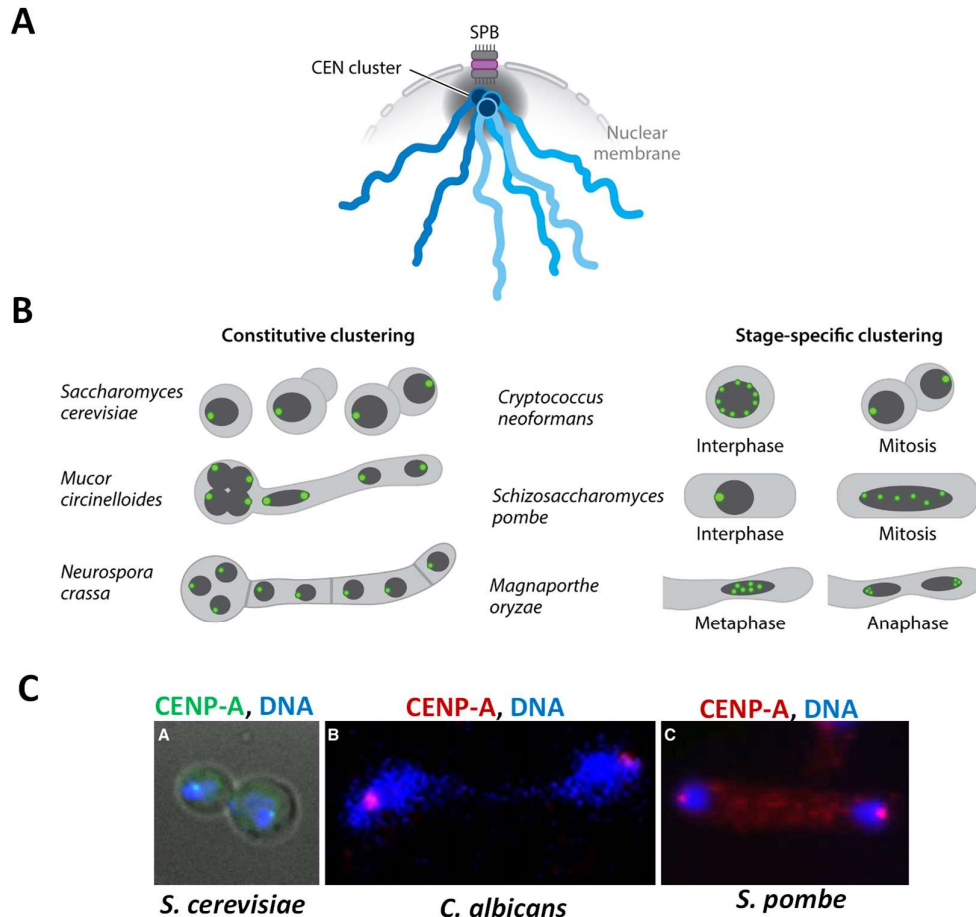


Figure 1.8. KT clustering in fungi. (A) Schematic showing the Rab1-like configuration of the chromosomes wherein CENP-A molecules are clustered together towards the SPB. Adapted from (Guin et al. 2020b). (B) Spatial clustering of the KTs (green) at the periphery of the nuclear mass (dark grey) in the indicated species at various cell cycle stages. Adapted from (Guin et al. 2020b). (C) Micrographs showing clustered CENP-A molecules in the indicated species during anaphase. Adapted and modified from (Kursel and Malik 2016).

In *S. cerevisiae*, KTs remain attached to the MTs and cluster close to SPB throughout the cell cycle (Figure 1.8B, C) (Jin et al. 2000). The KT clustering is affected in KT mutants and upon treatment with the MT depolymerizing drugs, suggesting the significance of the KT-MT attachment in maintaining the clustered state of the KTs (Jin et al. 2000; Janke et al. 2001). Additionally, a KT protein called Slk19 is shown to help KTs glue together in the presence of an MT depolymerizing drug (Richmond et al. 2013). The distance between SPBs and KTs is, however, maintained by the two non-essential inner KT proteins, Chl4 and Ctf19 (Sau et al. 2014). In *C. albicans*, similar to *S. cerevisiae*, KTs remain clustered close to the SPB,

throughout the cell cycle (Figure 1.8B, C) (Sanyal and Carbon 2002; Thakur and Sanyal 2012). However, the integrity of the KT structure and not the mitotic spindle affects KT clustering in *C. albicans* (Thakur and Sanyal 2012). The KTs in *S. pombe* are clustered near SPBs during interphase, but, undergo a brief declustering during mitosis (Figure 1.8B, C) (Takahashi et al. 2000). During interphase, KTs are associated with SPBs without the involvement of the MTs. Instead, *S. pombe* uses the linker of nucleoskeleton and cytoskeleton complex (LINC), which consists of the SUN-KASH domain proteins, to establish an indirect connection with the SPBs (Miki et al. 2004; Hou et al. 2012).

MTs and their accessory proteins

MTs are hollow, cylindrical structures that, along with actin and intermediate filaments, form a part of the cytoskeleton in eukaryotic cells. The MT filament is a long polymer, comprising of conserved tubulin subunits. Most eukaryotic cells contain multiple isoforms of tubulin. The α - and β -tubulin subunits associate to form heterodimers and constitute the main body of the MTs (Figure 1.9A). While the β -tubulins are exposed at the faster polymerizing plus end of the MT, the α -tubulins are exposed at the slow-growing minus end of the MTs. The γ -tubulin is a key component of the MTOCs, responsible for nucleating MT filaments. The budding yeast MTOC, also known as the SPB, remains embedded within the nucleus and nucleates two types of MTs, astral or cytoplasmic MTs (cMTs) and nuclear MTs. The nuclear MTs further consist of kinetochore MTs (kMTs) or k-fibers that connect spindle poles to the KTs and interpolar MTs that interdigitate with each other at the spindle midzone (Figure 1.9B). While cMTs aid in nuclear positioning during cell division, the nuclear MTs facilitate sister chromatid separation. Within the mitotic spindle, the MTs are organized with their minus end facing the spindle poles and their plus ends extending away from the poles (Figure 1.9B).

The dynamicity of MTs is regulated by MAPs (Goodson and Jonasson 2018; Bodakuntla et al. 2019). MAPs belong to a loosely defined group of proteins that bind to MTs and regulate various aspects of MTs including MT nucleation and polymerization. Different classes of MAPs include;

1. *Stabilizers* promote polymerization or slow depolymerization of the MTs.
2. *Destabilizers* prevent free tubulin subunits from polymerizing.
3. *Capping proteins* adhere to the minus or plus end of the MTs and are thus capable of stopping dimer association and dissociation.

4. *Bundlers and crosslinkers* promote the lateral association of the MT filaments.

5. *MT motor proteins* move along the MT filaments by hydrolyzing ATP and consist of two groups of proteins called dyneins and kinesins. While kinesins walk towards the plus end of the MTs, dyneins move towards the minus end of the MTs.

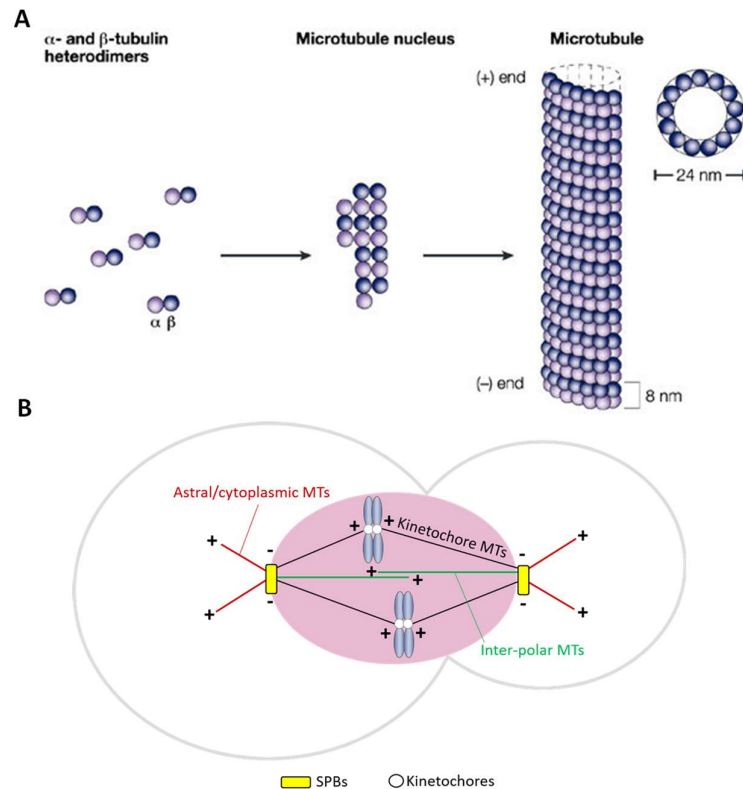


Figure 1.9. Structure and types of MTs in the budding yeast. (A) Formation of MT filament from the nucleation of α and β subunits. Adapted from (Jordan and Wilson 2004). (B) Three types of MTs being emanated from the SPB of the budding yeast. The nuclear MTs further consist of kinetochore MTs (kMTs) and inter-polar MTs. The position of plus (+) and (-) end of the MT is indicated. The nucleus is shown in light pink.

Role of MTs and MAPs in nuclear migration

Many fungal species undergo polarized cell division in which the cortical site for the daughter cell is pre-determined (Chiou et al. 2017). Nuclear positioning along the plane of cell division is an important prerequisite for chromosome segregation in these fungal species (Figure 1.10) (Varshney and Sanyal 2019b). This is achieved by the combined efforts of several mitotic players, including MTOCs, MTs, and MAPs.

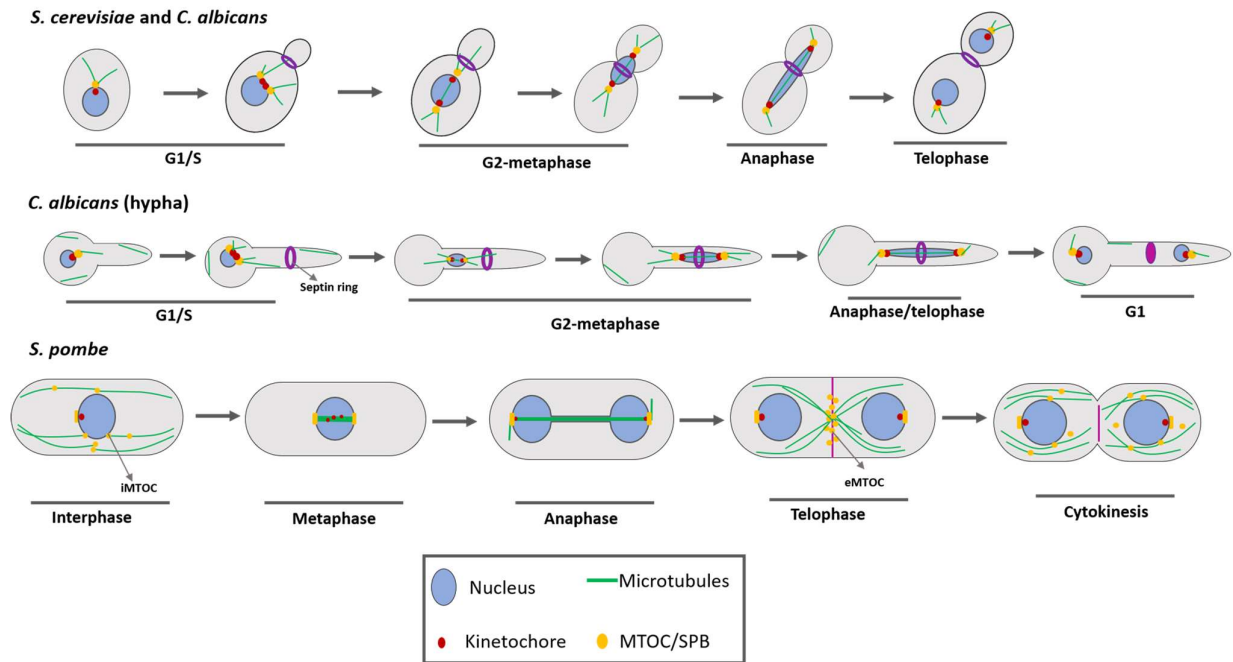


Figure 1.10. Dynamics of nuclear segregation mechanisms in fungi. Diagrammatic representation of various stages of nuclear division in the indicated fungal species. Nuclear migration to the bud neck is a key event during nuclear division in *S. cerevisiae* and *C. albicans* yeast cells. In *C. albicans* hyphal cells, the nucleus first moves ~10-20 μm into the germ tube to the presumptum, the site of germ tube division and septum formation and then undergoes division. Unlike *S. cerevisiae* and *C. albicans* which divide by budding, *S. pombe* divides by fission. In *S. pombe*, apart from SPBs that nucleate spindle MTs, non-SPB MTOCs, such as interphase MTOCs (iMTOCs), primarily at the NE and equatorial MTOCs (eMTOCs), at the site of septation, nucleate MTs during interphase and post anaphase, respectively.

Nuclear migration in *S. cerevisiae* is mediated by two redundant pathways, called the Kar9- and dynein-dependent pathways (Figure 1.11) (Huisman and Segal 2005; Fraschini et al. 2008; Varshney and Sanyal 2019b). During the G1 phase, the cortical capture of the cytoplasmic MTs at the bud-neck occurs through the binding of Kar9 with the myosin motor Myo2. Movement of Myo2 along the actin cables then transports the cMTs, emanating from the old SPB into the bud region. After SPB duplication, the old SPB is held at the mother-bud junction preventing the cMTs of the new SPB from entering into the daughter bud. At this stage, the fate of the old SPB (daughter-bound) and new SPB (mother-bound) is decided. As SPB remains embedded within the nucleus during mitosis, the cortical capturing of the cMTs also results in the simultaneous movement of the nucleus. During the G2/M phase, a short

mitotic spindle is formed which gets aligned along the mother-bud axis under the surveillance of the spindle positioning checkpoint (Caydasi et al. 2010). The mitotic spindle is then pulled into the mother-bud junction with the help of dynein, a minus-end directed motor protein (Adames and Cooper 2000). The dynein-pull happens first in the daughter bud and later in the mother bud, resulting in an elongated anaphase spindle, delivering a single nucleus to each daughter cell.

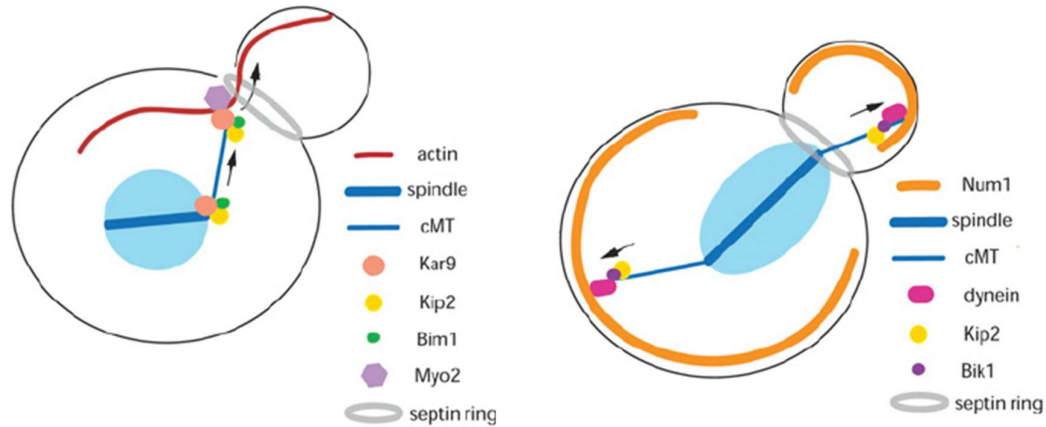


Figure 1.11. The two pathways for nuclear positioning in *S. cerevisiae*. *Left*, the Kar9 pathway. Kar9 is preferentially localized to the SPB which goes into the daughter cell and is translocated to the MT plus end through interaction with the plus end-directed motor protein Kip2. Bim1 is a MAP that binds to the plus end of the MT and interacts with Kar9. Kar9 thus acts as an adapter between Bim1 and Myo2 and helps in guiding the MTs along the actin cables. *Right*, the dynein pathway. Dynein is a minus end-directed motor protein that associates with the cortical anchor protein, Num1. Dynein is targeted to the plus end of the MT with the help of Bik1 plus-end tracking protein and Kip2. Adapted from (Fraschini et al. 2008).

Nuclear migration in *C. albicans*, similar to *S. cerevisiae*, involves the movement of the nucleus towards the bud neck. Apart from the budding yeast form, *C. albicans* also displays diverse morphological forms including pseudohyphae and true hyphae. The dynamics of nuclear positioning in pseudohyphae is similar to that in the budding yeast form. However, there is a variation in the nuclear positioning in the true hyphal cells: the nucleus moves 10-20 μm into the growing germ tube and then divides across the presumptum, the site of septum formation (Figure 1.10) (Finley and Berman 2005). Unlike most yeasts, which use dynein-dependent MT pulling forces to position the nucleus, *S. pombe* uses MT pushing mechanisms to position the nucleus (Figure 1.10) (Tran et al. 2001; Daga and Chang 2005; Daga et al.

2006). The interphase stage of *S. pombe* consists of approximately three to five MT bundles, nucleated by iMTOCs and distributed on either side of the nucleus. These interphase MTs are arranged in an anti-parallel fashion where the minus ends are present towards the nucleus and the plus ends occupy the cell tip (Tran et al. 2001). This mode of arrangement helps in the dynamic positioning of the nucleus towards the center of the cell, which further dictates the site of cell division (Daga and Chang 2005; Piel and Tran 2009).

Beyond nuclear division, exiting mitosis

Progression through mitosis is facilitated by the activity of Cdks in association with mitotic cyclins. Exit from mitosis thus requires the inactivation of Cdks and reversion of the Cdk-dependent phosphorylation events, failure of which can lead to an indefinite arrest in the late anaphase/telophase stage. Mitotic exit is, therefore, essential for subsequent entry into the next cell cycle. In budding yeast, mitotic exit is mediated by a conserved protein phosphatase called Cdc14. Cdc14 is kept inactive inside the nucleolus from G1 until anaphase through association with its inhibitor Net1. During anaphase, activation of Cdc14 is achieved in two steps. In the first step, which occurs during early anaphase, the Cdc14 early anaphase release (FEAR) network promotes Cdk-dependent phosphorylation of Net1, resulting in the partial release of Cdc14 from nucleolus into the nucleoplasm (Rock and Amon 2009). The Cdc14 activation by the FEAR network is not essential for the mitotic exit but is critical for accomplishing anaphase-related tasks, including stabilization of the anaphase spindle. The second and the complete activation of Cdc14 is achieved during late anaphase through the activity of the mitotic exit network (MEN) (Figure 1.12). The MEN facilitate and sustains the complete release of Cdc14 from nucleoplasm to the cytoplasm, thus facilitating mitotic exit.

Occurring at the SPBs, MEN is a signalling cascade driven by the Ras-like GTPase Tem1 (Figure 1.12) (Hotz and Barral 2014). Active Tem1 (GTP bound) recruits the downstream kinase Cdc15 at the SPB which in turn activates the Dbf2-Mob1 kinase complex. Activated Dbf2-Mob1 translocate to the nucleus and promotes dissociation of Cdc14 from Net1. Once in the cytoplasm, Cdc14 dephosphorylates its targets including the CDK inhibitor Sic1, transcription factor Swi5 and anaphase-promoting complex (APC) activator Cdh1, to promote mitotic exit (Bloom and Cross 2007). Besides exiting the cells from mitosis, MEN is also required for cytokinesis in budding yeast (Meitinger et al. 2012).

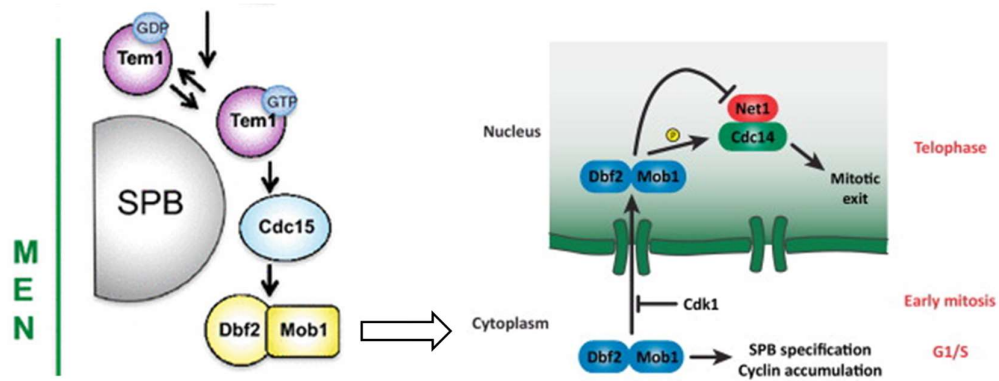


Figure 1.12. The MEN pathway in *S. cerevisiae*. Schematic showing step-wise activation of the MEN pathway at the SPBs. Shuttling of the active Dbf2-Mob1 complex into the nucleus during anaphase/late telophase results in Cdc14 activation, thereby triggering mitotic exit and cytokinesis. Adapted and modified from (Hotz and Barral 2014; Juanes and Piatti 2016).

The MEN in other fungal systems is comparatively less explored. In *C. albicans*, the major components of the MEN pathway, including Tem1, Cdc15, Dbf2 and Cdc14 have been characterized (Clemente-Blanco et al. 2006; Gonzalez-Novo et al. 2009; Milne et al. 2014; Bates 2018). Strikingly, Cdc14 is shown to be non-essential in *C. albicans* with functions in cell separation following cytokinesis. In contrast, Dbf2 has been reported to be essential for proper nuclear segregation, actomyosin ring contraction, and cytokinesis in *C. albicans*. Thus, the MEN components in *C. albicans* had undergone a major rewiring with a yet to be identified critical counterpart of Cdc14 phosphatase. The MEN orthologous signalling pathway in fission yeast is called the septation initiation network (SIN). The SIN in *S. pombe* controls the formation of the septum and the onset of cytokinesis (Simanis 2015). Although the outputs of MEN and SIN are different, their components are highly conserved between the two species including a scaffolding component, an NDR-family kinase and upstream regulation by GAP components and a polo kinase (Bardin and Amon 2001; Hergovich and Hemmings 2012; Cavanaugh and Jaspersen 2017).

Role of mitotic checkpoints in regulating genome stability

Faithful completion of mitosis relies on the proper execution of two pivotal events: bipolar attachment of chromosomes to the mitotic spindle at metaphase and sister chromatid separation during anaphase after which cells are allowed to exit mitosis. In budding yeast, two surveillance mechanisms called the spindle assembly checkpoint (SAC) (Figure 1.13)

and spindle position checkpoint (SPOC) (Figure 1.14) guarantee successful completion of mitosis.

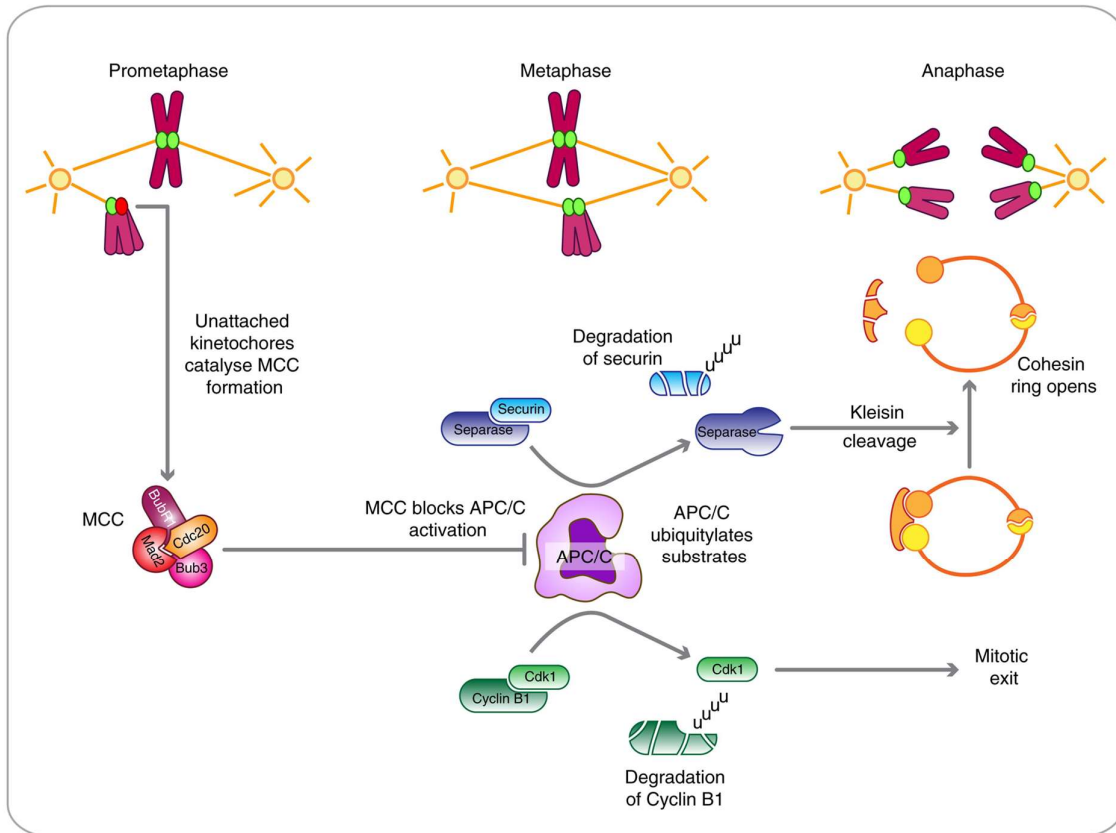


Figure 1.13. Principles of SAC activation. Unattached or wrongly attached KT (prometaphase) catalyze the formation of MCC, resulting in the inhibition of APC/C. The formation of a bipolar spindle (metaphase) ceases MCC generation and activates APC/C which then ubiquitinates securin and mitotic cyclins. Degradation of securin activates separase which in turn opens the ring structure of the cohesion by cleaving one of its subunits, thus allowing sister chromatids to separate (anaphase). Meanwhile, degradation of mitotic cyclins inactivates Cdk1, leading to mitotic exit. Adapted from (Lara-Gonzalez et al. 2012).

SAC prevents metaphase-anaphase transition until sister chromatids are properly attached to the sister poles (bipolar attachment). The KMN network of the outer KT acts as a molecular platform for the recruitment of SAC components (Musacchio and Desai 2017). In response to unattached KTs, SAC generates a diffusible stop signal known as the mitotic checkpoint complex (MCC) that inhibits E3 ubiquitin ligase called the anaphase-promoting complex or cyclosome (APC/C) (Figure 1.13). MCC consists of Cdc20, Mad2, BubRI/Mad3, and Bub3.

The BubRI/Mad3 of MCC acts as a pseudo-substrate, inhibiting the ubiquitylation of B-type cyclins and securing, the substrates of APC/C. Upon proper KT-MT attachments, SAC is silenced, and APC/C inhibition is relieved, resulting in the degradation of B-type mitotic cyclins and securin, thus promoting sister chromatid separation. Tension across the sister KTs also regulates the fidelity of chromosome segregation. Tensionless KT-MT attachments result in the missegregation of the chromosomes. SAC can efficiently detect unattached KTs but fails to recognize tensionless KT-MT attachments. An error correction kinase, called Aurora B (Ipl1 in budding yeast) localizes to the CENs and monitors the tension across the sister KTs (Tanaka et al. 2002; Lampson et al. 2004). It destabilizes the tensionless KT-MT interactions by phosphorylating outer KT components. This results in detachment of the MTs from the KTs, thus, allowing the SAC machinery to correct the improper KT-MT attachments (Carmena et al. 2012).

SPOC on the other hand prevents cells from exiting mitosis until the mitotic spindle is properly aligned along the mother-daughter axis. This is achieved by inhibiting the upstream MEN component, Tem1, the small Ras-like GTPase (Figure 1.14) (Caydasi et al. 2010; Caydasi and Pereira 2012). The key components of SPOC include the bipartite GAP complex Bfa1-Bub2, the polo-like kinase Cdc5 and the kinase Kin4. The GAP function of the Bfa1-Bub2 complex activates the GTP hydrolysis of Tem1, thus reducing the active form of Tem1 and inhibiting mitotic exit. While the phosphorylation of Bfa1-Bub2 at the SPB by Cdc5 inhibits the GAP activity of the complex, the phosphorylation by Kin4 induces the GAP activity of the Bfa1-Bub2 complex. During anaphase, Bfa1-Bub2 has a preferential localization to one of the SPBs which is destined to go to the daughter cell (dSPB) and Kin4 is primarily localized to the mother cell cortex. Upon spindle misalignment, Kin4 localizes to SPBs and gains access to phosphorylate Bfa1-Bub2 (Figure 1.14). This, in turn, destabilizes the SPB binding of the GAP complex, decreasing their levels at the dSPB and resulting in their symmetric localization at both the SPBs. How exactly Bfa1-Bub2 inhibits mitotic exit upon spindle misalignment is not fully understood, but inhibition of Tem1 can occur in two ways; i) As Tem1 localization to the SPB in early anaphase is dependent on the GAP complex, the Tem1 levels also reduce in response to decreased Bfa1-Bub2 levels. ii) Increased turnover rate of Bfa1-Bub2 may prevent the complex from inhibitory phosphorylation by Cdc5 which in turn could activate the GAP complex and hence inhibit Tem1. Altogether, the Bfa1-Bub2 complex delays mitotic exit through inhibition of Tem1 until the spindle positions itself correctly along the mother-bud direction. If the spindle is

properly aligned, Cdc5 phosphorylates Bfa1-Bub2, thus inactivating the GAP complex and leading to the mitotic exit.

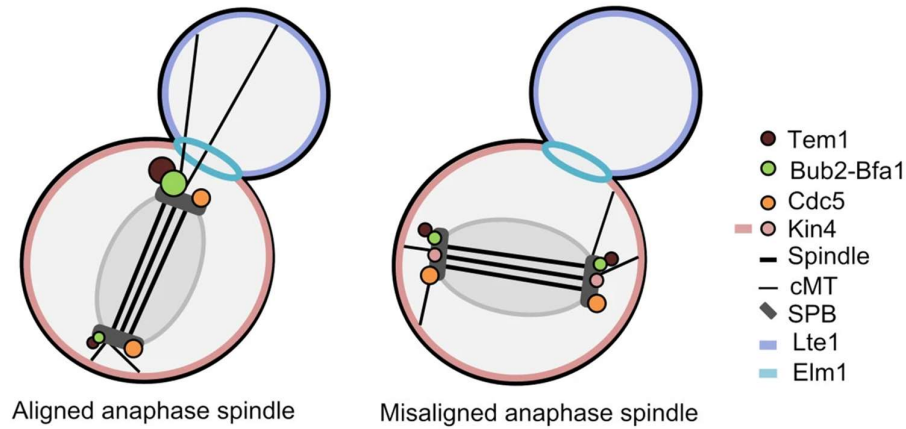


Figure 1.14. Mechanisms leading to SPOC activation. Schematic showing the localization of SPOC proteins when the spindle is properly aligned (left) or misaligned (right). Note changes in the localization of Bfa1-Bub2, Tem1 and Kin4 from asymmetric to symmetric upon spindle misalignment. Adapted from (Caydasi et al. 2010).

***Candida albicans* as a model system for studying eukaryotic genome biology**

S. cerevisiae and *S. pombe* have served as uncontested model systems for studying numerous aspects of eukaryotic cell biology. The discoveries made in these two species have unraveled several biological players and processes that are proven to be relevant across eukaryotes. *C. albicans*, an ascomycete belonging to the CUG-Ser clade (Figure 1.15) is an emerging yeast model system that has gathered much attention due to its clinical relevance as a dreaded human pathogen (Legrand et al. 2019). *C. albicans* is a commensal of the mucosal linings of the human reproductive tract, gastrointestinal tract, urinary tract, mouth, skin, etc. (Soll 2002). However, under certain host conditions, such as weakened immunity, burns, gastrointestinal disease, cancer or treatment with antibiotics, *C. albicans* may transit from a harmless commensal to an opportunistic pathogen causing Candidiasis (Berdal et al. 2014). *C. albicans* remains the most frequently isolated fungal pathogen from humans and is responsible for the majority of *Candida* infections (Brown et al. 2012; Friedman and Schwartz 2019). In subsequent sections, we discuss several characteristic features of *C. albicans* as an attractive biological system for understanding the regulation of genome stability in eukaryotes.

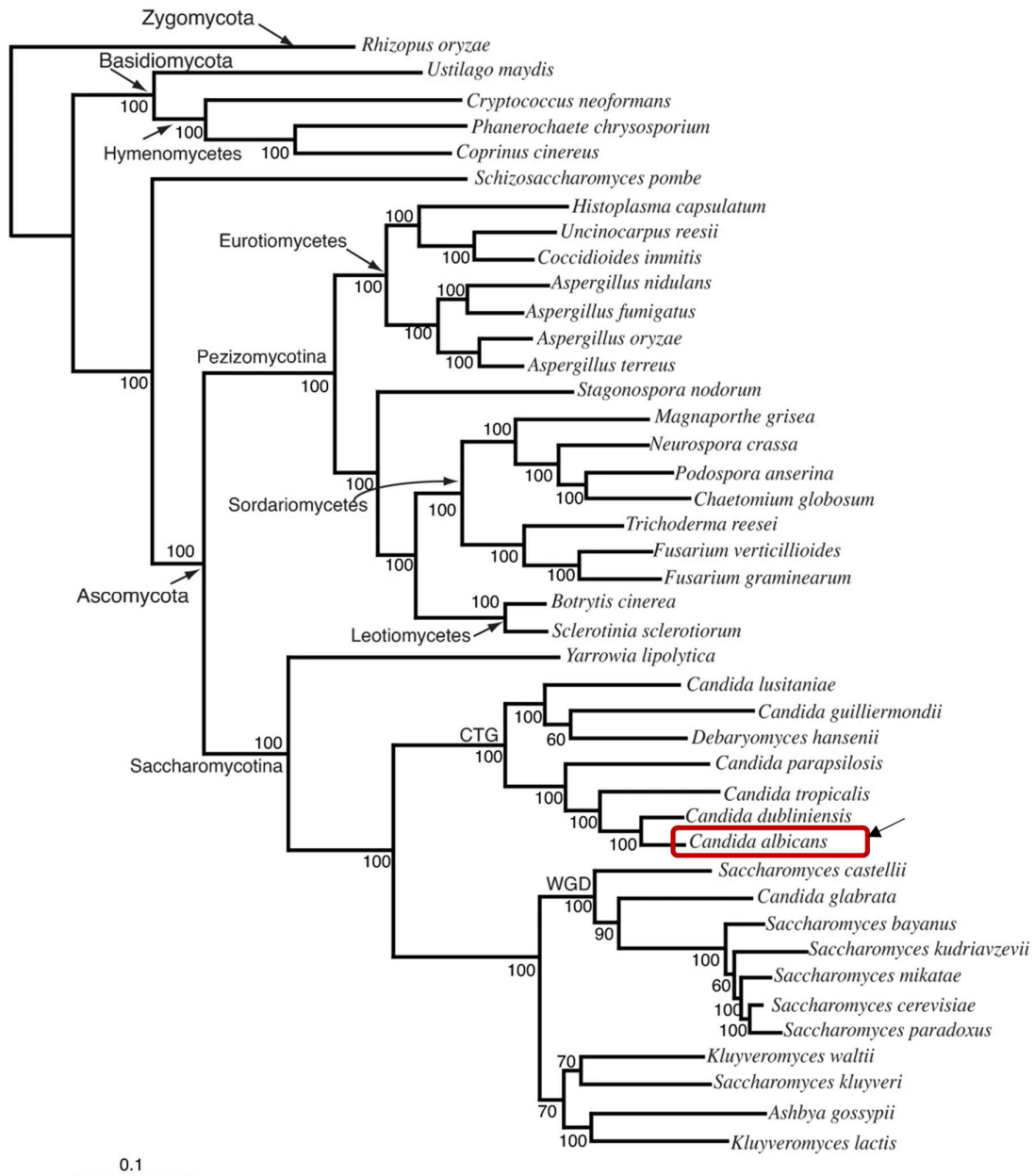


Figure 1.15. Position of *C. albicans* in the fungal phylogenetic tree. The tree was constructed using the maximum likelihood method constituting the alignment of 153 universally distributed fungal genes. Adapted from (Fitzpatrick et al. 2006).

Taxonomic position

Kingdom: Fungi

Phylum: Ascomycota

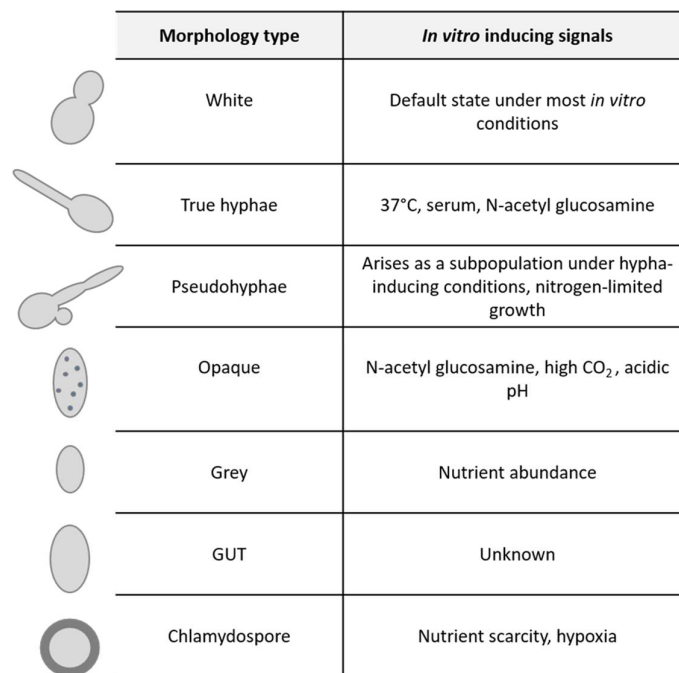
Subphylum: Saccharomycotina

Class: Saccharomycetes

Order: Saccharomycetales
 Family: Debaryomycetaceae
 Genus: *Candida*
 Species: *albicans*

Morphology

One of the most striking features of *C. albicans* is its ability to undergo phenotypic transitions between different morphological states under various environmental conditions (Figure 1.16) (Noble et al. 2017).










	Morphology type	<i>In vitro</i> inducing signals
	White	Default state under most <i>in vitro</i> conditions
	True hyphae	37°C, serum, N-acetyl glucosamine
	Pseudohyphae	Arises as a subpopulation under hypha-inducing conditions, nitrogen-limited growth
	Opaque	N-acetyl glucosamine, high CO ₂ , acidic pH
	Grey	Nutrient abundance
	GUT	Unknown
	Chlamyospore	Nutrient scarcity, hypoxia

Figure 1.16. Plasticity of *C. albicans* cell morphology. Tabular representation of various morphological forms of *C. albicans* under indicated environmental conditions.

Among the diverse phenotypes that have been reported so far, the form that best describes the default state of *C. albicans* under *in vitro* growth conditions is the yeast or the white form. The white cells of *C. albicans* are considered to be unicellular with a round to oval-shaped morphology, similar to *S. cerevisiae*. In contrast, the filamentous forms of *C. albicans* propagate as multicellular, long, branching structures, known as mycelia. The filaments of *C. albicans* can be further characterized into two types; i) true hyphae, comprising of long tubular-shaped cells with parallel-sided walls, or ii) pseudohyphae, consisting of elongated

cells with constrictions at the septal junction. The opaque form is the mating competent form of *C. albicans* characterized by the presence of cell surface ‘pimples’, larger size and elongated shape as compared to the white cells. Unlike opaque cells, the grey cells of *C. albicans* are much smaller than conventional yeasts, possess a smooth-surfaced cell wall and mate with very low efficiency. Under limited availability of nutrients or oxygen-depleted conditions, the terminal cells in *C. albicans* mycelia can form chlamydozoospores- large, thick-walled, spherical cells, whose biological significance remains undefined. *C. albicans* can also switch into a unique gastrointestinally induced transition (GUT) state in response to the cues from the mammalian gastrointestinal tract. Similar to opaque cells, GUT cells are also elongated-shaped, but lack cell surface pimples and are mating incompetent.

The yeast-hyphal transition is considered as one of the important virulence traits of *C. albicans*. While the yeast forms are mostly found as harmless commensals in various infection models, the filamentous forms have been associated with tissue invasion and damage (Braun and Johnson 1997; Lo et al. 1997; Saville et al. 2003). In addition, the hyphal transition is an important prerequisite during *C. albicans* biofilm formation on abiotic surfaces (Finkel and Mitchell 2011). *C. albicans* cells also undergo a morphological transition to a unique filamentous growth, which is different from the conventional yeast-hyphal switching, in response to genotoxic stresses (Legrand et al. 2019) (Figure 1.17). Treatment of *C. albicans* with a DNA-damaging agent or an inhibitor of MT-polymerizing agent leads to polarized growth and termination of cell cycle progression (Legrand et al. 2019). A similar phenotype has also been observed in mutants with altered expression of genes coding for proteins involved in DNA damage response and cell cycle regulation (Legrand et al. 2019).

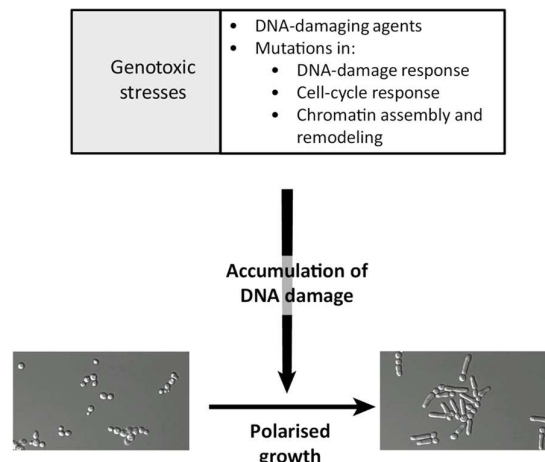


Figure 1.17. DNA-damage-induced morphological transition in *C. albicans*. Schematic depicting polarized growth in *C. albicans* in response to various genotoxic stresses. Adapted from (Legrand et al. 2019).

Chromosomal elements

The essential elements of a eukaryotic chromosome – namely CENs, DNA replication origins and telomeres – have been identified in *C. albicans* (Figure 1.18). The CEN DNA sequences of *C. albicans* are 3-5 kb long and are all unique and different from each other, devoid of any common sequence motif or repeat (Figure 1.18A) (Sanyal et al. 2004). The absence of a CEN-specific DNA sequence and the inability of the exogenously introduced CEN DNA to function as a native CEN suggested epigenetic regulation of CEN identity in *C. albicans* (Baum et al. 2006). However, upon CEN deletion, neocentromeres are formed efficiently in *C. albicans*, mostly proximal and rarely distal to the native CEN (Ketel et al. 2009; Thakur and Sanyal 2013). Similar to native CENs clustering (Sreekumar et al. 2019; Guin et al. 2020b), neocentromeres also cluster in three-dimension with other functional CENs (Burrack et al. 2016). Gene conversion at the CENs can interchange the deleted CEN with the native CEN (Thakur and Sanyal 2013) and possibly explains the low frequency of single nucleotide polymorphism across *C. albicans* CENs. Besides CEN clustering, the structural integrity of the kinetochore is required for CEN function in *C. albicans*. Depletion of an essential kinetochore protein disrupts the integrity of the kinetochore architecture (Roy et al. 2011; Thakur and Sanyal 2012) and also results in delocalisation and degradation of CENP-A (Thakur and Sanyal 2012) that forms centromeric chromatin.

DNA replication initiates from multiple discrete genetic loci – the DNA replication origins (*ORI*). Based on the location, *ORIs* in *C. albicans* are two types (Tsai et al. 2014); a) arm *ORIs*, which are located on the chromosomal arms and b) centromeric *ORIs*, which are present on (Koren et al. 2010) or close to the *CENs* (Mitra et al. 2014) (Figure 1.18B). While a subset of arm *ORIs* is defined by a 15-bp AC-rich consensus motif and a nucleosome-depleted pattern, centromeric *ORIs* are defined by epigenetic mechanisms (Tsai et al. 2014) and replicate the earliest in the genome (Koren et al. 2010). The centromeric *ORIs* together with homologous recombination (HR) proteins, Rad51 and Rad52, play a key role in loading CENP-A to the CENs (Mitra et al. 2014). The centromeric *ORIs* together with homologous recombination (HR) proteins, Rad51 and Rad52, play a key role in loading CENP-A to the CENs (Mitra et al. 2014). While replicating CEN DNA, the moving replication forks from

CEN-proximal *ORIs* stall at *CEN* due to the presence of the kinetochore acting as a physical barrier (Mitra et al. 2014). The fork stalling accumulates single-stranded DNA which attracts HR proteins Rad51 and Rad52, which are shown to interact with CENP-A in *C. albicans* (Mitra et al. 2014). As a consequence, CENP-A gets deposited onto the *CENs*. Consistent with this, in a *CEN*-deleted strain, neocentromere becomes the earliest replicating region (Koren et al. 2010).

A telomere, at the termini of a eukaryotic chromosome, ensures chromosome end replication and protects them from degradation or end-to-end chromosome fusion. *C. albicans* telomeres are unique in containing tandem copies of unusually long 23 bp repeating unit (McEachern and Hicks 1993) (Figure 1.18C). However, they are assembled into heterochromatin via the classical Sir2-mediated pathway (McEachern and Hicks 1993; Freire-Beneitez et al. 2016). The subtelomeric regions of *C. albicans* consist of the telomere-associated (*TLO*) family of genes which encode for the subunits of the mediator complex, a crucial component for transcription initiation (Zhang et al. 2012a). There are in total 15 *TLO* genes (including one pseudogene) in *C. albicans* but other non-*C. albicans* species have either one or two *TLO* genes (Jackson et al. 2009). In addition, overexpression of *TLO* genes in *C. albicans* influences many growth and virulence-related properties (Dunn et al. 2018). The expansion in the number of *TLO* genes could thus explain the ability of *C. albicans* to adapt in various host niches.

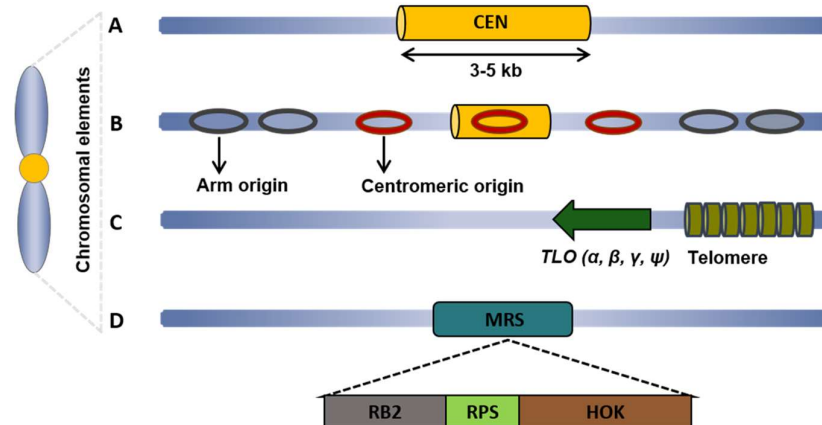


Figure 1.18. Schematic of essential chromosomal elements in *C. albicans*. (A) A 3-5 kb long CENP-A-rich centromere (*CEN*) that lacks any common DNA sequence element or

pericentric repeat. **(B)** DNA replication origins (*ORIs*), identified as ORC-bound regions, are categorized into arm *ORIs* and centromeric *ORIs*. Like *CENs*, centromeric *ORIs* do not contain any common DNA sequence motif. **(C)** Telomere repeats in *C. albicans* are unusually long and the subtelomeric regions contain an unusually high number of *TLO* genes. **(D)** MRS, which further consists of three sequence elements, namely, RB2, RPS and HOK. The RB2 (~6kb) and HOK (~8kb) elements are non-repetitive sequences that occur only once per MRS, flanking the RPS element. The repeated sequence (RPS) is ~2kb long repetitive sequence whose number can vary in an MRS. Each RPS unit carries a SfiI restriction enzyme site. SfiI mapping of the *C. albicans* genome served as a valuable tool to study chromosomal rearrangements before the whole genome sequence was available. Adapted and modified from (Legrand et al. 2019).

A special feature of the *C. albicans* genome is the major repeat sequences (MRS). MRS is a long tract (10-100kb) of repetitive DNA that is present on all chromosomes, except chromosome 3. Structurally, an MRS is composed of three subunits: the repetitive RPS subunit flanked by non-repetitive elements, RB2 and HOK (Figure 1.18D). Chromosome 3 contains only the RB2 element without the RPS or HOK unit (Chibana and Magee 2009). Surprisingly, MRS, being a repetitive region, is not assembled into classical heterochromatin but carries marks of both euchromatin and heterochromatin (Freire-Beneitez et al. 2016). MRS covers about 3% of the total genome, yet its function remains elusive, except that it is considered to be a hotspot for genome rearrangements in *C. albicans* (Lephart et al. 2005). MRS is a preferred site for chromosomal translocations (Chibana and Magee 2009), and the expansion and contraction of its RPS region give rise to chromosome length polymorphism (Chibana et al. 2000). Further, the presence of MRS affects the frequency of non-disjunction whereby a homolog bearing a larger MRS is more likely to be lost at the time of chromosome segregation (Lephart et al. 2005). Thus, MRS serves as an important means of generating karyotypic diversity in *C. albicans* and needs to be studied in greater detail for its function and origin.

Genome plasticity and its significance

Similar to phenotypic plasticity, the genome of *C. albicans* also exhibits remarkable flexibility in terms of tolerating genome instability events upon exposure to oxidative stress, elevated temperature, antifungals or in presence of certain host factors (Selmecki et al. 2010; Legrand et al. 2019). These events can be categorized as single nucleotide polymorphisms (SNPs), ploidy variations and chromosomal rearrangements.

SNPs and loss of heterozygosity (LOH)

Heterozygosity is defined as a particular region or a gene on a chromosome for which two copies, that differ in the DNA sequence, are present. Whole-genome sequencing of *C. albicans* revealed that its genome is exceptionally heterozygous, with an average density of 1 SNP per 237-283 bp (Jones et al. 2004; Muzzey et al. 2013; Legrand et al. 2019). This SNP frequency is higher than the SNP density of *S. cerevisiae*, with 1 SNP every 28,000 -60,000 bp (Magwene et al. 2011) or humans in which SNP occurs every 1000-2000 bp (Sachidanandam et al. 2001). The heterozygous state of the *C. albicans* genome is often influenced by LOH events. Although LOH can be detected on all the chromosomes of *C. albicans*, several studies have reported that for some chromosomes, one haplotype or even a part of it can never exist in the homozygous state. This is because of the presence of recessive lethal or deleterious alleles on some haplotypes (Legrand et al. 2019). In particular, this homozygous bias has been observed for chromosome R, 1, 2, 3, 4, 6 and 7 (Bennett and Johnson 2003; Hickman et al. 2013). While both homozygosity and heterozygosity of some alleles can confer a fitness advantage to *C. albicans* (Holmes et al. 2006; Hickman et al. 2013), why the latter is preferred in this organism, remains an enigma.

Ploidy variations and parasexual cycle

The predominant ploidy state of *C. albicans* is diploid, but it can also exist as a haploid or a tetraploid. Unlike *S. cerevisiae*, which forms haploids by undergoing reductional division (meiosis), ploidy reduction in *C. albicans* occurs through random concerted chromosome loss. To form tetraploids, *C. albicans* cells goes through a non-meiotic parasexual cycle in which diploid white cells, heterozygous for *MTL* (mating type-locus) a or α loci, morphologically switches into the opaque form to undergo mating, forming tetraploids (Bennett and Johnson 2003). These tetraploids can then come back to the diploid or near-diploid state through the process of concerted chromosome loss (Bennett and Johnson 2003) (Figure 1.19).

Chromosomal rearrangements

Besides ploidy changes and polymorphism at the nucleotide level, the *C. albicans* genome can exhibit chromosomal alterations in the form of;

1. *Whole-chromosomal aneuploidy*: gain (trisomy) or loss (monosomy) of an entire chromosome

alternative carbon sources or undergo white-opaque switching following the loss of MTL (Magee and Magee 2000; Lockhart et al. 2002; Miller and Johnson 2002).

Molecular mechanisms leading to genome diversity

Genome instability in *C. albicans* can arise at the time of DSB repair, in response to DNA damage, or due to chromosome non-disjunction during mitosis. While the latter is associated with whole chromosome loss, resulting in aneuploidy (Figure 1.20), DNA-DSB repair can result in either short-range or long-range LOH (Feri et al. 2016; Legrand et al. 2019) (Figure 1.20). Short-range LOH events are restricted to the site of DNA damage and can occur as a consequence of DSB repair by gene conversion without crossover. In contrast, long-range LOH events extend from the site of DNA damage to the telomeres and can occur when DSB is repaired by either gene conversion with cross-over or break-induced replication. If left unrepaired, DSBs can also result in chromosome truncation or segmental aneuploidies (Figure 1.20).

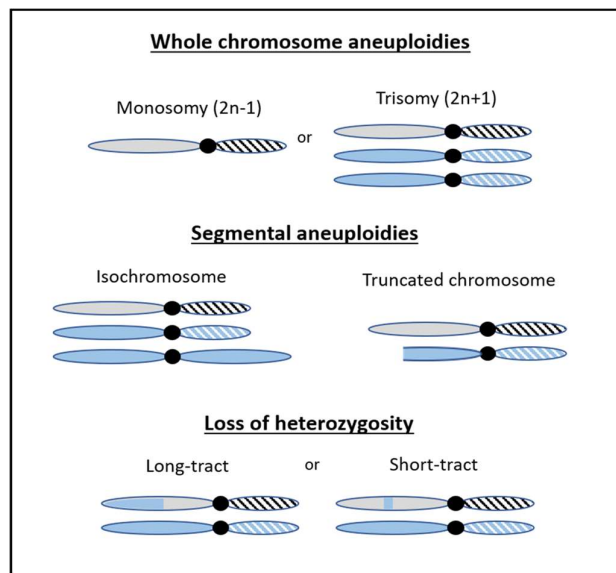


Figure 1.20. Plasticity of *C. albicans* genome. Diagrammatic representation of various forms of genetic alterations in *C. albicans*. Adapted and modified from (Legrand et al. 2019).

As noted previously, the two major pathways involved in repairing DSB include HR and NHEJ. Characterization of the proteins involved in either pathway revealed that HR plays a major role in DNA damage repair in *C. albicans* as compared to NHEJ, which rarely occurs in this ascomycete (Legrand et al. 2019). Consequently, genes involved in homologous

recombination, such as *MRE11* and *RAD50*, and DNA damage checkpoint pathway, including *MEC1*, *RAD53* and *DUN1*, are required to prevent genome instability in *C. albicans* (Legrand et al. 2007; Legrand et al. 2011; Loll-Krippelber et al. 2014). A recent screen using a collection of 124 overexpression mutants has identified additional genes, namely, *CDC20*, *BIMI* and *RAD51*, whose overexpression resulted in an increased LOH-driven genome instability in *C. albicans* (Loll-Krippelber et al. 2015). However, ~70% of genes are still uncharacterized in *C. albicans* and have not been annotated for any function (Skrzypek et al. 2017; Thomas et al. 2020). Systematic approaches are thus needed to exhaustively define the drivers of *C. albicans* genome maintenance and outline species-specific processes as well as commonalities with other eukaryotes.

Purpose of the present study

Genome instability has been intimately associated with oncogenesis, genetic disorders and karyotypic evolution. A series of studies performed in a wide range of organisms ranging from yeasts to humans have highlighted the coherent efforts of high-fidelity DNA replication, DNA repair, chromosome segregation and cell cycle control by checkpoints in regulating genomic stability. Considering the vast diversity in the mechanisms of chromosome segregation in eukaryotes, including the fungal kingdom, it is conceivable that many genes involved in genome maintenance are yet to be discovered. An opportunistic human fungal pathogen *C. albicans* is gaining much attention due to its genome plasticity and emerging antifungal resistance. The ability of *C. albicans* genome to tolerate CIN in the form of whole chromosomal or segmental aneuploidy, isochromosome formation, chromosome truncation, or mitotic crossing-over raises intriguing questions on the functioning of genome stability-regulators in this fungal pathogen. While perturbation of a candidate gene's function to decipher its role in a cellular pathway has been a classical strategy in biological research, screening of mutant collections aids in uncovering additional molecular players and cellular pathways in an unbiased manner. Here, using a clinically relevant fungal species, *C. albicans*, as a model system, we have performed a large-scale screen aimed at identifying regulators of genome stability, some of which may serve as new targets for therapeutic interventions of fungal infections.

Summary of the current work

In this study, we sought to identify genes that are involved in regulating genome stability in *C. albicans*. For this, we first developed a chromosome stability (CSA) reporter system in

which CIN due to chromosome loss can be easily identified at the single-cell level. The left arms of the chromosome 4 homologs (Ch4A and Ch4B) in CSA reporter were engineered to carry the green fluorescent protein (GFP) and blue fluorescent protein (BFP) genes, respectively. These genes are integrated at the same intergenic locus in both the homologs. The right arm of Ch4B in CSA reporter carries the red fluorescent protein (RFP) gene. In this setup, while the loss of either BFP or GFP fluorescence suggests a chromosome instability event at the BFP/GFP locus of Ch4, the concomitant loss of the two unlinked markers (BFP and RFP) indicate a whole chromosome loss for Ch4B. After validating the functionality of the CSA reporter system by inducing chromosome loss with a known gene, we used the CSA reporter as a parent strain for generating a library of 1067 *C. albicans* overexpression strains that can be individually monitored for CIN events by flow cytometry. Each of these strains, carrying a unique ORF under the control of an inducible tetracycline promoter, can be overexpressed in the presence of tetracycline. Primary and secondary screening of these 1067 overexpression strains identified six *CSA* genes which we named as *CSA1* (*CLB4*), *CSA2* (*ASE1*), *CSA3* (*KIP2*), *CSA4* (*BFA1*), *CSA5* (*MCM7*) and *CSA6* (*ORF19.1447* encoding a protein of unknown function). Further characterization of the underlying mechanisms of genome instability in *CSA* overexpression mutants revealed; a) Overexpression of either *CSA1^{CLB4}*, *CSA2^{ASE1}* or *CSA3^{KIP2}* induced CIN mostly through non-chromosomal loss events. b) Overexpression of either *CSA4^{MCM7}*, *CSA5^{BFA1}* or *CSA6* arrested cells at different cell cycle phases with the G2/M equivalent DNA content (4N). We discuss the implications of identifying these genes, except *CSA6*, in the light of their conserved roles in cell cycle progression.

We performed an in-depth analysis to elucidate the function of *CSA6* in *C. albicans*. Overexpression studies of *CSA6* (*CSA6^{OE}*) indicated that *CSA6^{OE}* leads to Mad2-mediated metaphase arrest in *C. albicans* with unsegregated nuclei and aberrant mitotic spindle formation. In contrast, promoter shut down of *CSA6* (*CSA6^{PSD}*) leads to cell cycle arrest at late anaphase/telophase, with segregated nuclear masses and a hyper-extended mitotic spindle. The anaphase arrest in *CSA6^{PSD}* is bypassed upon overexpression of *Soll1*, a Cdk substrate, indicating *Csa6*'s role in mitotic exit. We further carried out sub-cellular localization studies with *Csa6* and found that it is constitutively localized to the SPBs in *C. albicans*. We discuss dual functions of *Csa6* in cell cycle, first during the G2/M phase for proper assembly of the mitotic spindle and then later during anaphase to exit the cells from mitosis. We allude that localized at the SPBs, *Csa6* regulates two critical events of mitosis,

viz. metaphase-anaphase transition and mitotic exit. We analyzed the presence of Csa6 across various fungi using protein homology, synteny analysis and found its restricted existence in a subset of fungal species belonging to the CUG-Ser clade. Lastly, we analyzed intra-species conservation of Csa6 by ectopically expressing Csa6 of another CUG-Ser clade species, *Candida dubliniensis*, in *C. albicans*. We found similar to CaCsa6, CdCsa6 also localizes to the SPBs and functionally complements CaCsa6. We suggest the functional conservation of Csa6 in a subset of *Candida* species and allude its implication as a potential target for antifungal therapies.

Chapter 2

Results (Part I)

Screening of *C. albicans* overexpression library identifies chromosome stability (*CSA*) genes

A reporter system for monitoring chromosome stability in *C. albicans*

To understand the molecular mechanisms underlying genome instability, we wanted to develop a reporter system in which chromosome loss (CL) can be distinguished from non-CL events such as break-induced replication, gene conversion, chromosome truncation or mitotic cross over (Loll-Krippleber et al. 2015; Feri et al. 2016). A LOH reporter strain, co-expressing the green fluorescent protein (GFP) and the blue fluorescent protein (BFP) genes, has been previously employed to analyze LOH occurrence in *C. albicans* (Loll-Krippleber et al. 2015; Feri et al. 2016). In the LOH reporter system (Feri et al. 2016), the GFP and BFP genes (associated with the *ARG4* and *HIS1* auxotrophic markers, respectively) have been integrated at the same intergenic locus on the left arm of Ch4A and Ch4B, respectively (Figure 2.1A). In this setup, the occurrence of a CIN event at the BFP or GFP locus leads to the expression of either BFP or GFP reporter genes (Feri et al. 2016). To differentiate CL from non-CL events, we modified this LOH reporter strain (Feri et al. 2016) by integrating a red fluorescent protein (RFP) reporter gene (associated with the hygromycin B (Hyg B) resistance marker) on the right arm of Ch4B (Figure 2.1A). In the resulting reporter strain, called the CSA reporter (CEC5201, *P_{TDH3}GFP/BFP/RFP*), while the loss of either BFP or GFP suggests a CIN event at the BFP/GFP locus of Ch4, the concomitant loss of the two unlinked markers (*BFP-HIS1* and *RFP-HYGB*) but retention of *GFP-ARG4* indicates loss of Ch4B haplotype (Figure 2.1B). The fluorescence intensity histogram of GFP, BFP and RFP in the CSA reporter system was validated by flow cytometry (Figure 2.1C).

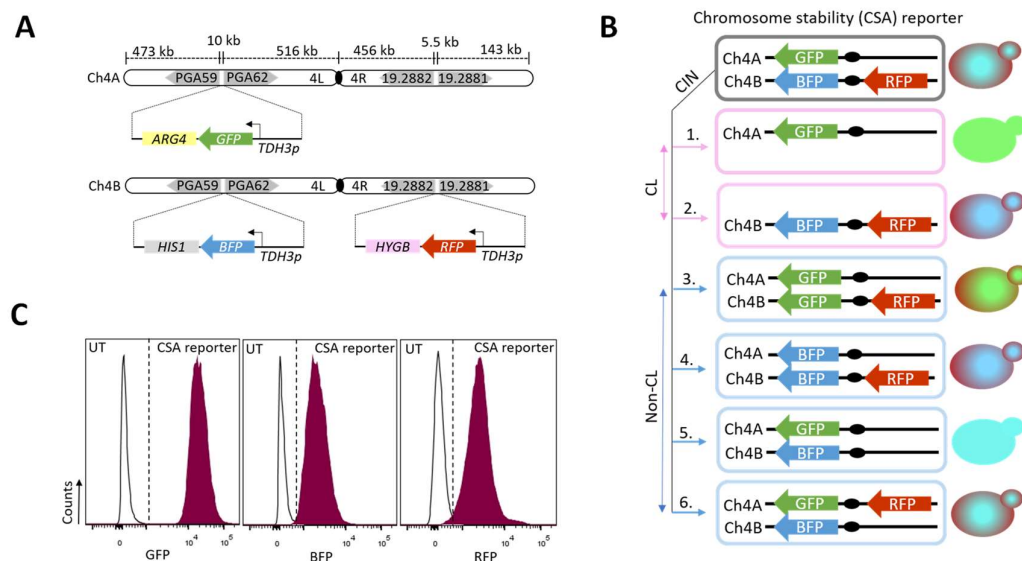


Fig. 2.1. The CSA reporter system for detecting chromosome instability (CIN) in *C. albicans*. (A) A line diagram of Chromosome 4 (Ch4). As indicated, BFP/GFP-expressing cassettes were integrated into the left arm of both the homologs of Ch4 in the *PGA59-PGA62* intergenic region, while the RFP-expressing cassette was integrated into the right arm of Ch4 in the *ORF19.2882-ORF 19.2881* intergenic region. Expression of BFP, GFP and RFP is under control of the *TDH3* promoter and is associated with respective selectable markers, as mentioned in the diagram. (B) Possible outcomes of CIN at the BFP/GFP and RFP loci. 1-4, CIN at the BFP or GFP locus, because of chromosome loss (CL) or non-CL events, will lead to the expression of either GFP or BFP, respectively. CIN due to CL can be specifically identified by the concomitant loss of BFP and RFP, as shown in 1. 5 and 6, cells undergoing non-CL events at the RFP locus will continue to express BFP and GFP. (C) Histograms showing fluorescence intensity measurements of an untagged strain (SN148) and CSA reporter strain (CEC5201) by flow cytometry. The CSA reporter strain on the right exhibited higher fluorescence intensity for GFP, BFP and RFP laser than the untagged (UT) strain.

The BFP/GFP reporter system has been successfully used for identifying regulators of LOH in *C. albicans* (Loll-Krippleber et al. 2015). One such gene that was identified included *CDC20*, which is important for anaphase onset and the spindle checkpoint and whose overexpression induces whole chromosome loss in *C. albicans* (Loll-Krippleber et al. 2015). Hence, we used *CDC20* overexpression as a genetic tool to functionally validate the concomitant loss of *BFP-HIS1* and *RFP-HYGB* (loss of Ch4B) in the CSA reporter strain (CEC5201, *P_{TDH3}GFP/BFP/RFP*). In *C. albicans*, loss of Ch4A has not been observed due to the presence of recessive lethal alleles on Ch4B (Feri et al. 2016). To overexpress *CDC20*, we used the tetracycline-inducible *TET* promoter (*P_{TET}*) (Chauvel et al. 2012; Loll-Krippleber et al. 2015) and analyzed the loss of BFP or GFP by flow cytometry (Figure 2.2A, B) (Loll-Krippleber et al. 2015). As reported earlier (Loll-Krippleber et al. 2015), cells overexpressing *CDC20* (*CDC20^{OE}*) displayed a higher population of BFP⁺GFP⁻ and BFP⁻GFP⁺ cells as compared to the empty vector (EV) (Figure 2.2B, C), indicating increased CIN in this mutant. Next, we isolated BFP⁻GFP⁺ cells of EV and *CDC20^{OE}* using flow cytometry and plated them for subsequent analysis of auxotrophic/resistance markers (Figure 2.2D). Upon incubation of the sorted BFP⁻GFP⁺ cells, we observed the appearance of small and large colonies, as was reported earlier (Loll-Krippleber et al. 2015) (Figure 2.2D). Small colonies have been previously shown to always result from the loss of Chr4B and are predicted to be a consequence of Ch4A monosomy, eventually yielding large colonies upon reduplication (Loll-Krippleber et al. 2015). We, therefore, performed the marker analysis on large colonies and found that 85% of the BFP⁻GFP⁺ derived colonies of *CDC20^{OE}* mutant concomitantly

lost both *HIS1* and *HYGB* but retained *ARG4* (Figure 2.2E) suggesting the loss of Ch4B homolog; flow cytometry analysis further confirmed the loss of BFP and RFP signals in these colonies. The remaining 15% of colonies retained *GFP-ARG4* and *RFP-HYGB* but not *BFP-HIS1* (Figure 2.2E) indicating that more localized events including gene conversion, rather than whole chromosome loss, were responsible for loss of the BFP signals in these cells. The above data indicate that the CSA reporter system that we engineered enables precise monitoring of the whole chromosome loss event in a population and enables large-scale screening of this phenotype.

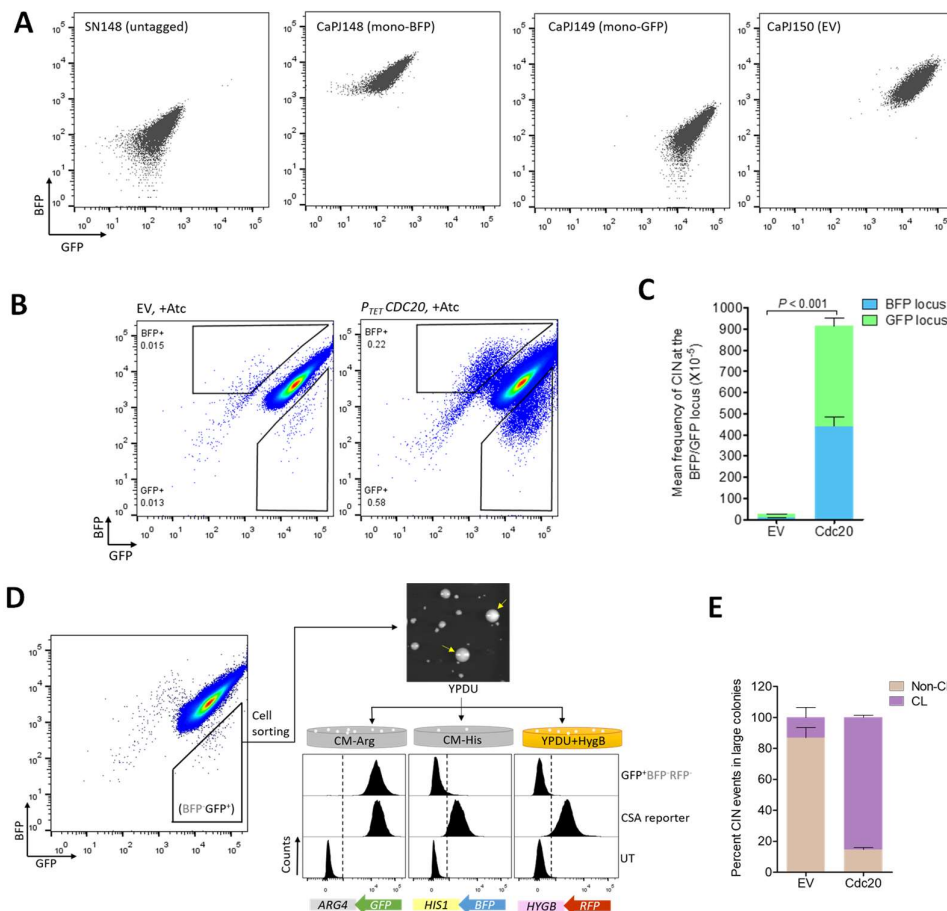


Figure 2.2. Functional validation of the CSA reporter. (A) Flow cytometric analysis of the BFP/GFP marker in various control strains as indicated. The strains were grown in YPDU medium overnight and analyzed by flow cytometry. Approximately 10,000 events are displayed. **(B)** Detection of chromosome instability in the *CDC20^{OE}* strain (CaPJ151). *Left*, a representative BFP/GFP density plot of EV in presence of anhydrotetracycline (Atc) (3 μ g/ml), an inducer of *P_{TET}* promoter. The proportion of BFP⁺GFP⁻ and BFP⁻GFP⁺ cells in the EV indicates the intrinsic instability of Ch4 in *C. albicans*. *Right*, a representative BFP/GFP

density plot of *CDC20^{OE}* strain in presence of Atc (3 $\mu\text{g/ml}$). (C) Quantitation of the mean frequency ($\times 10^{-5}$) of CIN at the BFP/GFP locus in EV (CaPJ150) and *CDC20^{OE}* strain (CaPJ151); $N=3$. Unpaired *t*-test, one-tailed, *P*-value shows a significant difference. (D) Schematic illustrating the workflow to differentiate CL from non-CL events. A representative flow cytometry density plot is shown as a reference. BFP⁺GFP⁺ cells were sorted and plated on YPDU agar. Large colonies (arrow marked in yellow) were tested for the presence of selectable markers, *ARG4*, *HIS1* and *HYGB* by replica plating, followed by flow cytometry analysis to monitor the presence of the associated fluorescent proteins (GFP, BFP and RFP). The fluorescence intensity profile of an *ARG4* resistant colony which had lost *HIS1* and *HYGB* (GFP⁺ BFP⁻RFP⁻) is shown as an example. The concomitant loss of *BFP-HIS1* and *RFP-HYGB* indicates that the entire Ch4B is lost. (E) Analysis of the marker genes, *ARG4*, *HIS1* and *HYGB* by replica plating BFP⁺GFP⁺ colonies of EV (CaPJ150) and *CDC20^{OE}* strain (CaPJ151); $N=3$ with ≥ 100 colonies for each *N*.

Generation and screening of *C. albicans* overexpression library to identify regulators of genome stability

Systematic gene overexpression emerges as an attractive avenue for performing large-scale genomics in *C. albicans*, a diploid ascomycete. To identify regulators of genome stability, we employed a recently developed collection of *C. albicans* overexpression plasmids (in collaboration with d'Enfert from Institut Pasteur and C. Munro from the University of Aberdeen). We individually transformed each of these overexpression plasmids into the CSA reporter strain (CEC5201, *P_{TDH3}GFP/BFP/RFP*) and successfully generated more than a thousand (1067) PCR confirmed *C. albicans* overexpression strains (Figure 2.3A, methods and appendix). Each of these strains, carrying a unique ORF under the *P_{TET}* promoter, could be induced for overexpression after anhydrotetracycline (Atc) or doxycycline (Dox) addition (Figure 2.3A). To identify regulators of genome stability, we carried out a primary screen with these 1067 overexpression strains by individually analyzing them for the loss of BFP/GFP signals by flow cytometry (Fig. 2.3 B). Our primary screening identified 23 candidate genes (out of 1067) whose overexpression resulted in ≥ 2 -fold increase in the BFP⁺GFP⁻ and BFP⁻GFP⁺ population relative to the EV (Table 2.1, 2.2, appendix). Next, we carried out a secondary screen with these 23 overexpression strains to revalidate the loss of BFP/GFP markers by flow cytometry (Fig. 2.3C). As genotoxic stress is intimately linked with polarized growth in *C. albicans* (Bachewich et al. 2005; Legrand et al. 2019), we microscopically examined the overexpression strains exhibiting higher instability at the BFP/GFP locus during secondary screening for any morphological transition (Fig. 2.3C). While overexpression of 17 genes (out of 23) could not reproduce the BFP/GFP loss

phenotype, overexpression of the six genes resulted in ≥ 2 -fold increase in the BFP⁺GFP⁻ or BFP⁻GFP⁺ population as compared to the EV, with three genes (out of 6) inducing polarized growth upon overexpression. These six genes, which we referred to as CSA genes, include *CSA1* (*CLB4*), *CSA2* (*ASE1*), *CSA3* (*KIP2*), *CSA4* (*MCM7*), *CSA5* (*BFA1*) and *CSA6* coded by *ORF19.1447* of unknown function (Fig. 2.3D).

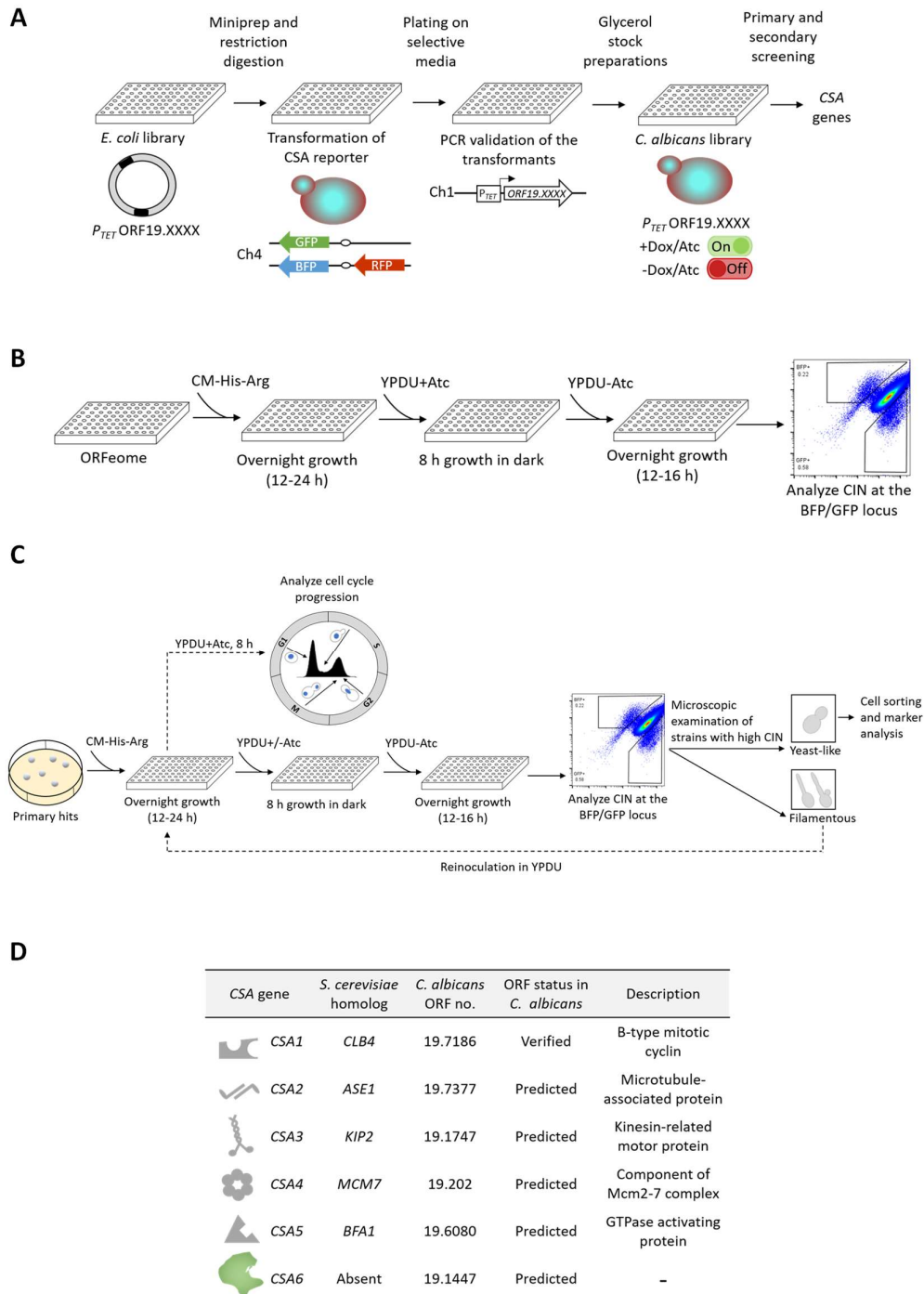


Figure 2.3. Primary and secondary screening of the *C. albicans* overexpression strains identifies six *CSA* genes. (A) Schematic depicting the strategy employed for identifying *CSA* genes in *C. albicans*. Briefly, a library of *C. albicans* overexpression strains, each carrying a unique ORF under the tetracycline promoter, P_{TET} , was generated using the *CSA* reporter (CEC5201) as the parent strain. The library was then analyzed by primary and secondary screening methods for CIN in *C. albicans* to identify *CSA* genes in this unicellular eukaryote. (B) Flow chart illustrating the steps of the primary screen. Briefly, overnight grown cells were induced for 8 h in presence of Atc (3 $\mu\text{g/ml}$), allowed to recover overnight in a rich medium without Atc, diluted in 1x PBS, and analyzed for BFP/GFP marker by flow cytometry ($\sim 10^6$ cells). Gates were defined for the BFP⁺GFP⁻ and BFP⁻GFP⁺ populations in the EV (CaPJ150) and applied to all other overexpression mutants (~ 1000). Mutants were selected if the frequency of CIN at the BFP/GFP locus was \geq two-fold higher than the frequency in the EV. (C) Flow diagram illustrating the steps of the secondary screen. The overexpression mutants identified from the primary screen (23 out of 1067) were induced for 8 h in presence or absence of Atc (3 $\mu\text{g/ml}$), allowed to recover overnight in a rich medium without Atc and analyzed for the loss of BFP and GFP by flow cytometry. Mutants were selected if they exhibited two-fold higher rate of CIN at the BFP/GFP locus in three biological replicates as compared to the EV and further analyzed for any morphological transition by microscopy. Overexpression mutants with yeast-like morphology were analyzed by cell sorting and marker analysis to determine the molecular mechanism (CL or non-CL) leading to CIN. Overexpression mutants exhibiting polarized growth were regrown, induced for 8 h in presence of Atc (3 $\mu\text{g/ml}$) and analyzed for cell cycle progression by microscopy or flow cytometry. (D) A brief overview of the *CSA* genes identified from the overexpression screen. Functional annotation of genes is based on the information available either in *Candida Genome Database* (www.candidagenome.org) or *Saccharomyces Genome Database* (www.yeastgenome.org) on August 1, 2021.

Table 2.1. Quantification of BFP/GFP loss frequency in EV

*Sample	Frequency of BFP ⁺ GFP ⁻ cells ($\times 10^{-5}$)	Frequency of BFP ⁻ GFP ⁺ cells ($\times 10^{-5}$)
1	7.14	19
2	7.52	24
3	13	16
4	5.7	24
5	6.69	20
6	7.75	15
7	24	16
8	18	15
9	15	22
10	13	20
11	15	21
12	24	19
13	7.8	21

14	15	22
15	14	15
16	11	14
17	15	13
18	20	16
19	14	15
20	22	20
21	18	25
22	15	21
Mean	14.02	18.77

*Samples indicate independently grown EV cultures

Table 2.2. BFP/GFP loss frequency in the primary hits

ORF no.	Orthologs in <i>S. cerevisiae</i>	Frequency of BFP ⁺ GFP ⁻ cells (x10 ⁻⁵)	Fold change	Frequency of BFP ⁺ GFP ⁺ cells (x10 ⁻⁵)	Fold change
19.1447	-	180	13.0	210	11.2
19.7186	<i>CLB4</i>	180	13.0	180	9.6
19.608	<i>BFA1</i>	140	10.0	190	10.2
19.3135	<i>UBX2</i>	120	8.6	45	2.4
19.202	<i>MCM7</i>	82	5.9	120	6.4
19.1048	<i>IFD6</i>	63	4.5	83	4.4
19.6588	<i>NBP2</i>	83	5.9	40	2.1
19.1601	<i>RPL3</i>	70	5.0	43	2.3
19.3437	-	72	5.1	37	2.0
19.1934	<i>HST3</i>	66	4.7	39	2.0
19.1542	<i>HEX3</i>	50	3.6	54	2.9
19.6778	<i>DRS2</i>	43	3.0	55	2.9
19.4153	<i>ULA1</i>	52	3.7	42	2.2
19.1396	<i>AGE2</i>	53	3.8	39	2.0
19.3349	<i>RPB2</i>	38	2.7	44	2.3
19.1747	<i>KIP2</i>	41	2.9	50	2.7
19.4979	<i>KNS1</i>	40	2.8	55	2.9
19.7377	<i>ASE1</i>	40	2.9	48	2.6
19.1999	-	33	2.3	44	2.3
19.3421.1	<i>ROX3</i>	35	2.5	47	2.5
19.6118	<i>DSS4</i>	38	2.7	39	2.1
19.4340.1	<i>SMX3</i>	33	2.4	39	2.1
19.5212	<i>CST9</i>	32	2.3	36	1.9

Molecular mechanisms underlying CIN in *CSA* overexpression mutants

Out of the six *CSA* genes, overexpression of three genes, namely, *CSA1^{CLB4}*, *CSA2^{ASE1}* and *CSA3^{KIP2}* caused little or no change in the morphology of *C. albicans* (Fig. 2.4A), but triggered CIN at the BFP/GFP locus, indicated by an expansion of the BFP⁺GFP⁻ and BFP⁻GFP⁺ population in the flow cytometry density plots (Figure 2.4B, C). To further dissect the molecular mechanisms leading to the loss of BFP/GFP signals in these mutants, we sorted BFP⁻GFP⁺ cells of these mutants and plated them for *GFP-ARG4*, *BFP-HIS1* and *RFP-HYGB* analysis, as described previously for the *CDC20^{OE}* mutant. We observed that a majority of the large BFP⁻GFP⁺ derived colonies of *CSA1^{CLB4}*, *CSA2^{ASE1}* and *CSA3^{KIP2}* overexpression mutants lost *BFP-HIS1* but retained *RFP-HYGB* and *GFP-ARG4* (Figure 2.4D) suggesting that localized genome instability events, rather than whole chromosome loss events, contributed to the high percentage of BFP⁻GFP⁺ cells in these mutants.

Overexpression of the remaining three genes, namely *CSA4^{MCM7}*, *CSA5^{BFA1}* and *CSA6*, drastically altered the morphology of the *C. albicans* cells by inducing polarized/filamentous growth (Fig. 2.4A). A connection between morphological switches and genotoxic stresses has been established in the polymorphic fungus *C. albicans*, wherein polarized growth is triggered in response to DNA damage or improper cell cycle regulation (Bachewich et al. 2005; Bensen et al. 2005; Roy et al. 2011; Thakur and Sanyal 2011; Thakur and Sanyal 2012). Flow cytometric analysis of cell cycle progression revealed that overexpression of *CSA4^{MCM7}*, *CSA5^{BFA1}* and *CSA6* shifted cells towards the 4N DNA content (Figure 2.4E). To further determine the cell cycle phase associated with the 4N shift, we compared nuclear segregation patterns (Hoechst staining for DNA and CENP-A/Cse4 localization for KT) and spindle dynamics (separation of Tub4 foci) in these overexpression mutants with those of the EV (Figure 2.4F). Our results suggested the 4N shift in *CSA4^{MCM7}* and *CSA6* overexpression mutants was a result of G2/M arrest, indicated by a high percentage of large-budded cells with unsegregated DNA mass and improperly separated SPBs (Figure 2.4F). In contrast, the 4N shift upon *CSA5^{BFA1}* overexpression was a consequence of late anaphase/telophase arrest, shown by an increased number of large-budded cells with segregated nuclei and SPBs (Figure 2.4F). Taken together, our results indicate that the polarized growth in *CSA4^{MCM7}*, *CSA5^{BFA1}* and *CSA6* overexpression mutants is a probable outcome of improper cell cycle progression.

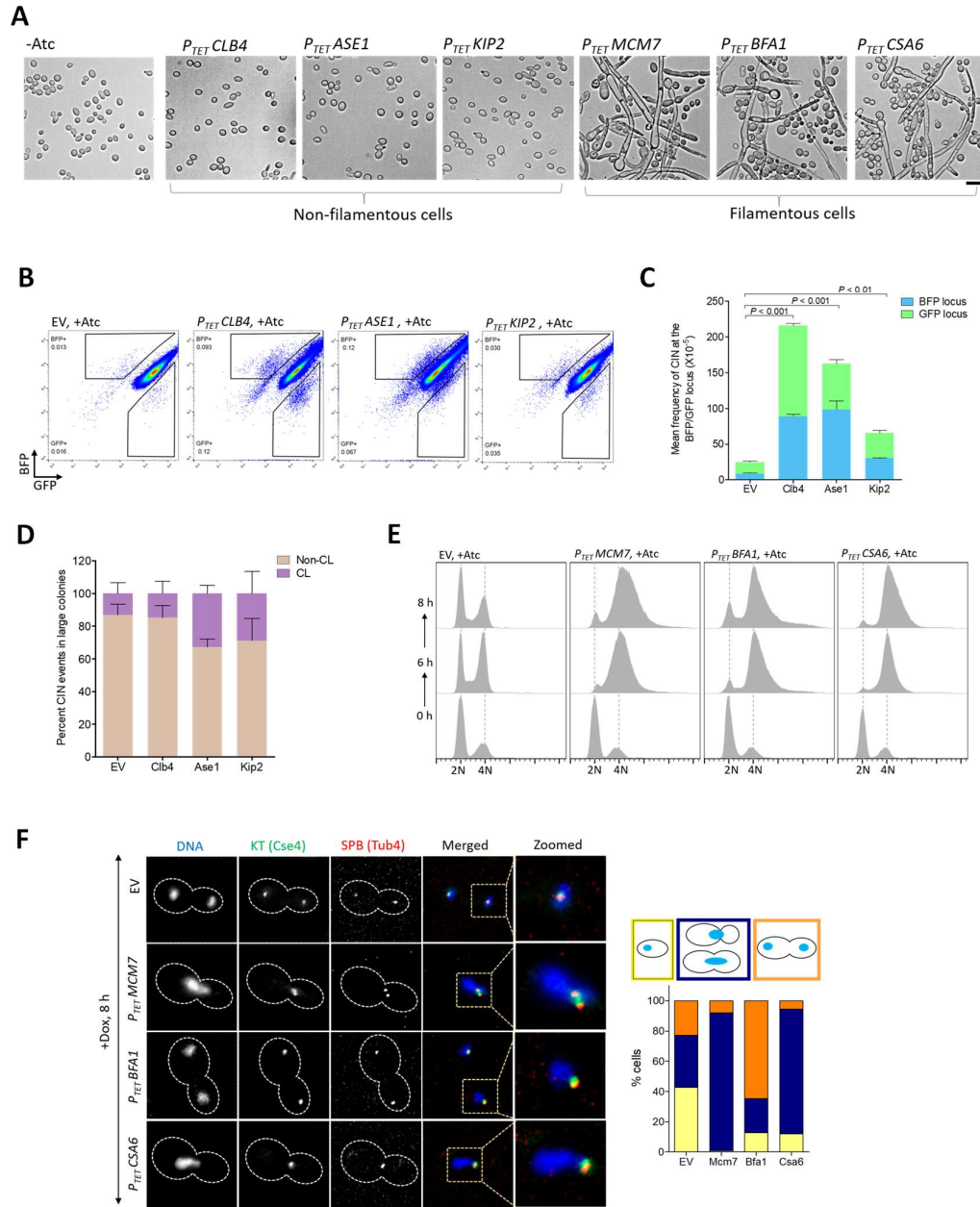


Figure 2.4 CIN associated with overexpression of CSA genes is regulated via distinct mechanisms. (A) Bright-field micrographs of the six overexpression strains, *CSA1^{CLB4}* (CaPJ152), *CSA2^{ASE1}* (CaPJ153), *CSA3^{KIP2}* (CaPJ154), *CSA4^{MCM7}* (CaPJ155), *CSA5^{BFA1}* (CaPJ156) and *CSA6* (CaPJ157), after 8 h of induction with Atc (3 μ g/ml) and overnight recovery in a rich medium without Atc. A representative image of an uninduced culture is shown as a reference (leftmost panel, -Atc). Scale bar, 10 μ m. (B) Representative flow cytometry density plots for BFP/GFP in *CSA1^{CLB4}* (CaPJ152), *CSA2^{ASE1}* (CaPJ153) and *CSA3^{KIP2}* (CaPJ154) overexpression strains, along with EV (CaPJ150), in presence of Atc (3 μ g/ml). (C) The mean frequency ($\times 10^{-5}$) of CIN at the BFP/GFP locus in EV (CaPJ150) versus *CSA1^{CLB4}* (CaPJ152), *CSA2^{ASE1}* (CaPJ153) and *CSA3^{KIP2}* (CaPJ154) overexpression

strains; $N=3$. Unpaired t -test, one-tailed, P -values show a significant difference. **(D)** Analysis of the marker genes, *ARG4*, *HIS1* and *HYGB* by replica plating in BFP-GFP⁺ colonies of EV (CaPJ150) and *CSA1*^{CLB4} (CaPJ152), *CSA2*^{ASE1} (CaPJ153) and *CSA3*^{KIP2} (CaPJ154) overexpression strains; $N=3$ with ≥ 100 colonies for each N . **(E)** Cell cycle analysis of EV (CaPJ160) and *CSA4*^{MCM7} (CaPJ165), *CSA5*^{BFA1} (CaPJ166) and *CSA6* (CaPJ167) overexpression strains; $N=2$. Briefly, overnight grown cells were induced for 8 h in presence of Atc (3 μ g/ml). Cells were harvested and ethanol-fixed, treated with RNase, stained with propidium iodide and analyzed by flow cytometry for DNA content at specific time intervals. **(F)** *Left*, representative micrographs showing nuclear segregation and mitotic spindle in EV (CaPJ160) and *CSA4*^{MCM7} (CaPJ165), *CSA5*^{BFA1} (CaPJ166) and *CSA6* (CaPJ167) overexpression strains, after 8 h of growth in presence of Dox (50 μ g/ml). The nuclear division was analyzed by both, Hoechst staining as well as by localization of a KT protein, Cse4-GFP. The spindle integrity was analyzed using Tub4-mCherry, an SPB protein, as a marker. Scale bar, 3 μ m. *Right*, quantitation of the cells with indicated phenotypes; $n \geq 100$ cells.

Two *CSA* genes, namely *CSA2*^{ASE1} and *CSA5*^{BFA1}, gave rise to similar overexpression phenotypes in both *S. cerevisiae* and *C. albicans* (Table 2.3). While phenotypes related to *CSA4*^{MCM7} and *CSA6* overexpression in *S. cerevisiae* or other related organisms remained unreported, the overexpression phenotypes of the remaining *CSA* genes were along the lines of their roles in cell cycle functioning, as reported in *S. cerevisiae* (Table 2.3, Figure 2.3D). Altogether, our results validated the role of *CSA* genes in regulating chromosome stability in *C. albicans*. While overexpression of either *CSA1*^{CLB4}, *CSA2*^{ASE1} or *CSA3*^{KIP2} induced CIN mostly through non-CL events, the effect of overexpressing either *CSA4*^{MCM7}, *CSA5*^{BFA1} or *CSA6* was so drastic that the *C. albicans* mutants were arrested at different cell cycle phases with the G2/M equivalent DNA content (4N) and thus were unable to complete the mitotic cell cycle.

Table 2.3. Overexpression phenotypes of *CSA* genes in *C. albicans* and *S. cerevisiae*

<i>CSA</i> gene	<i>C. albicans</i> ORF no.	<i>S. cerevisiae</i> homolog	Overexpression phenotype (<i>C. albicans</i>)	Overexpression phenotype (<i>S. cerevisiae</i>)	Reference
<i>CSA1</i>	19.7186	<i>CLB4</i>	Increased CIN involving non-CL events	Shift towards 2N (diploid) DNA content	(Sopko et al. 2006)
<i>CSA2</i>	19.7377	<i>ASE1</i>	Increased CIN involving non-CL events	i) CIN involving loss of an artificial chromosome fragment or rearrangements/	(Liu et al. 2008; Duffy et al. 2016)

				gene conversion events. ii) Spindle checkpoint dependent delay in entering anaphase upon HU treatment	
<i>CSA3</i>	19.1747	<i>KIP2</i>	Increased CIN involving non-CL events	Shift towards 2N (diploid) DNA content	(Sopko et al. 2006; Augustine et al. 2018)
<i>CSA4</i>	19.202	<i>MCM7</i>	Shift towards 4N (diploid) DNA content, G2/M arrest	NA	NA
<i>CSA5</i>	19.608	<i>BFA1</i>	Shift towards 4N (diploid) DNA content, anaphase arrest	Shift towards 2N (diploid) DNA content, Anaphase arrest	(Li 1999)
<i>CSA6</i>	19.1447	NA	Shift towards 4N (diploid) DNA content, G2/M arrest	NA	NA

NA, not available

Chapter 3

Results (Part II)

Csa6 is a spindle pole body localizing protein required for mitotic progression and mitotic exit in *C. albicans*

Csa6, a previously uncharacterized protein, as a key regulator of mitotic progression in *C. albicans*

Among the genes identified in the screen, Csa6 was the only protein with an unknown function and without any known homolog in *S. cerevisiae* (Figure 2.3D). Based on our findings thus far (Figure 2.4E, F), we hypothesized that Csa6 plays an important role in cell cycle regulation and genome stability. Therefore, we sought to identify the molecular pathways by which Csa6 performed its functions in *C. albicans*. We again made use of the inducible P_{TET} promoter system to generate a $CSA6^{OE}$ strain (CaPJ176, $P_{TET}CSA6$) in the wild-type (SN148) background of *C. albicans* (Figure 3.1A). Conditional overexpression of TAP-tagged Csa6 (CaPJ181, $P_{TET}CSA6-TAP$), in presence of Atc, was confirmed by western blot analysis (Figure 3.1B).

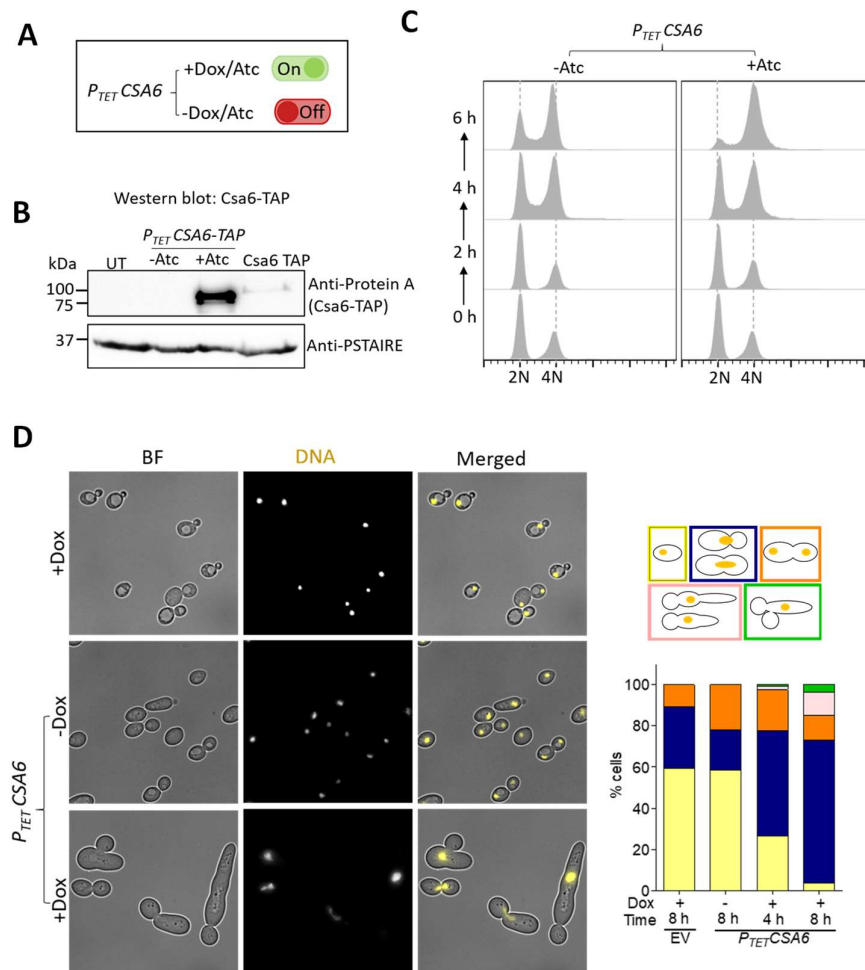


Fig. 3.1. Overexpression of Csa6 leads to G2/M arrest in *C. albicans*. (A) Atc/Dox-dependent functioning of the P_{TET} promoter system for conditional overexpression of $CSA6$. (B) Western blot analysis using anti-Protein A antibodies showed overexpression of $CSA6$ -

TAP from the P_{TET} promoter (CaPJ181), after 8 h induction in presence of Atc (3 $\mu\text{g/ml}$), in comparison to the uninduced culture (-Atc) or *CSA6-TAP* expression from its native promoter (CaPJ180); $N=2$. PSTAIRE was used as a loading control. UT, untagged control (SN148). **(C)** Flow cytometric analysis of cell cycle showing the cellular DNA content of *CSA6^{OE}* strain (CaPJ176) in presence or absence of Atc (3 $\mu\text{g/ml}$) at the indicated time intervals; $N=3$. **(D)** *Left*, microscopic images of Hoechst-stained EV (CaPJ170) and *CSA6^{OE}* strain (CaPJ176) after 8 h of growth under indicated conditions of Dox (50 $\mu\text{g/ml}$). BF, bright-field. Scale bar, 10 μm . *Right*, quantitation of different cell types at the indicated time-points; $n \geq 100$ cells.

The effect of *CSA6^{OE}* (CaPJ176, $P_{TET}CSA6$) on cell cycle functioning was then investigated by flow cytometric cell cycle analysis (Figure 3.1C) and microscopic examination of the nuclear division (Figure 3.1D). As observed previously (Figure 2.4E, F), *CSA6^{OE}* inhibited cell cycle progression in *C. albicans* by arresting cells in the G2/M phase, evidenced by the gradual accumulation of large-budded cells with unsegregated nuclei (Figure 3.1D), possessing 4N DNA content (Figure 3.1C). Some of these large-budded cells also underwent a morphological transition to an elongated bud or other complex multi-budded phenotypes (Figure 3.1D), indicating cell cycle arrest-mediated morphological switching (Bachewich et al. 2005) due to *CSA6^{OE}*. Strikingly, continuous upregulation of *Csa6* was toxic to the cells (Figure 3.2A) as nuclei failed to segregate in this mutant (Figure 3.1D).

Nuclear segregation during mitosis is facilitated by the formation of the mitotic spindle and its dynamic interactions with chromosomes via KTs. Thus, we sought to examine both the KT integrity and the mitotic spindle morphology in the *CSA6^{OE}* mutants. In *C. albicans*, the structural stability of the KT is a determinant of CENP-A/Cse4 stability wherein depletion of any of the essential KT proteins results in delocalization and degradation of the CENP-A/Cse4 by ubiquitin-mediated proteolysis (Thakur and Sanyal 2012). Fluorescence microscopy and western blot analysis confirmed that Cse4 was neither degraded nor delocalized from centromeric chromatin (Figure 3.2B, C) upon *CSA6^{OE}*. Next, we analyzed the spindle integrity in *CSA6^{OE}* mutants by tagging Tub4 (SPB) and Tub1 (MTs) with fluorescent proteins. Fluorescence microscopy analysis revealed that upon *CSA6^{OE}*, a large proportion (~73%) of the large-budded cells formed an unconventional rudimentary mitotic spindle structure, wherein it had a dot-like appearance as opposed to an elongated bipolar spindle structure in EV or uninduced (-Atc) samples (Figure 3.3). This suggests that nuclear segregation defects in *CSA6^{OE}* mutant cells are an attribute of aberrant mitotic spindle formation that might have led to the mitotic arrest.

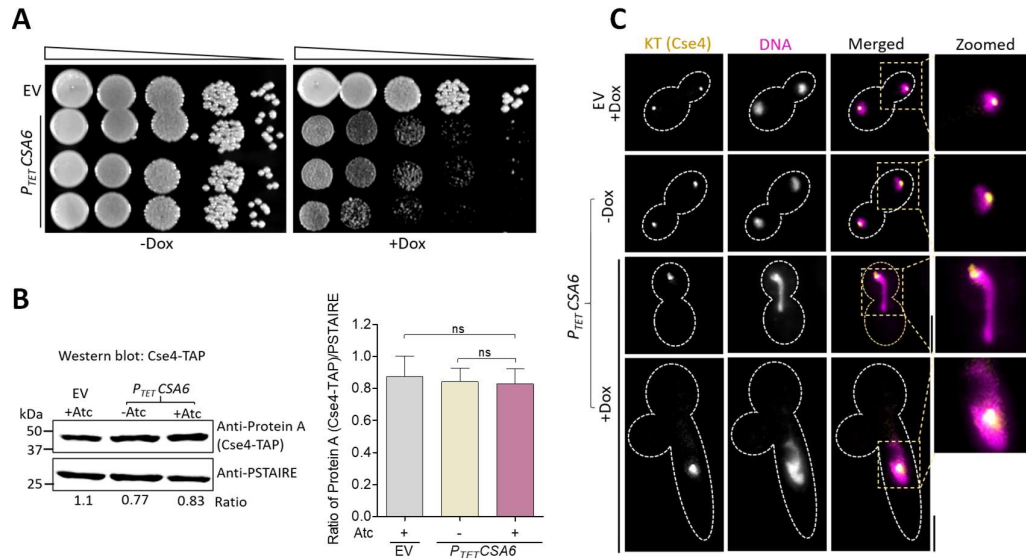


Figure 3.2. Overexpression of *CSA6* affects cell growth but does not perturb kinetochore integrity in *C. albicans*. (A) Ten-fold serial dilutions, starting from 10^5 cells each of EV (CaPJ170) or *CSA6*^{OE} strain (CaPJ176) were spotted on YPDU agar plates with or without Dox (50 μ g/ml) and incubated at 30°C for two days. (B) *Left*, immunoblot analysis of Cse4-TAP levels in EV (CaPJ173) and *CSA6*^{OE} mutant (CaPJ179) in presence or absence of Atc (3 μ g/ml) using anti-Protein A antibodies; $N=3$. PSTAIRE was used as a loading control. Cse4-TAP levels were normalized by calculating the ratio of Protein A/PSTAIRE. *Right*, Quantitation of the normalized Cse4-TAP levels; $N=3$. One-way ANOVA and Bonferroni posttest, P -values were non-significant (ns) (>0.05). (C) Localization of Cse4-GFP in *CSA6*^{OE} mutant (CaPJ183) and EV (CaPJ182), after 8 h of growth under indicated conditions of Dox (50 μ g/ml). The nucleus was stained with Hoechst dye for reference. Scale bar, 5 μ m.

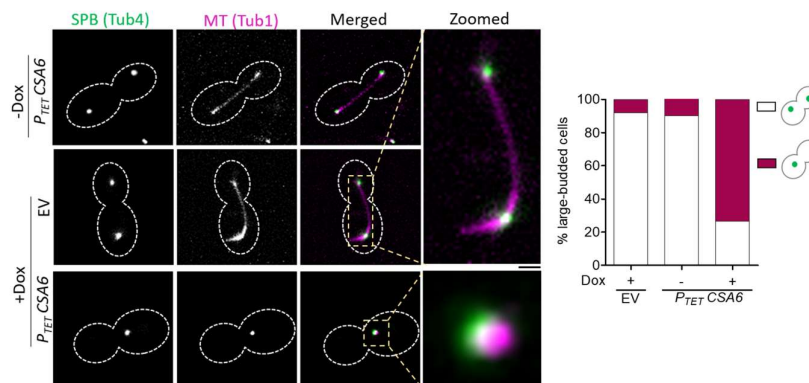


Figure 3.3. Overexpression of *Csa6* alters the morphology of the mitotic spindle. *Left*, representative micrographs of spindle morphology in the large-budded cells of EV (CaPJ172) and *CSA6*^{OE} strain (CaPJ178) after 8 h of growth under indicated conditions of Dox (50

$\mu\text{g/ml}$). SPBs and MTs are marked by Tub4-GFP and Tub1-mCherry, respectively. Scale bar, 1 μm . *Right*, the proportion of the large-budded cells with indicated SPB phenotypes; $n \geq 100$ cells.

SAC inactivation relieves the *CSA6* overexpression-induced G2/M arrest

During mitosis, surveillance mechanisms, including spindle assembly checkpoint (SAC) (Musacchio and Salmon 2007; Kops et al. 2020) and spindle positioning checkpoint (SPOC) (Caydasi and Pereira 2012; Scarfone and Piatti 2015) operate to maintain genome stability by delaying the metaphase-anaphase transition in response to improper chromosome-spindle attachments and spindle misorientation, respectively. We posit that the G2/M cell cycle arrest due to *CSA6*^{OE} in *C. albicans* could be a result of either SAC or SPOC activation. Hence, we decided to inactivate SAC and SPOC, individually, in the *CSA6*^{OE} strain by deleting the key spindle checkpoint genes *MAD2* (Thakur and Sanyal 2011) and *BUB2* (Bachewich et al. 2005), respectively. SAC inactivation in *CSA6*^{OE} mutant cells (Figure 3.4A) led to the emergence of unbudded cells with 2N DNA content (Figure 3.4B, C), indicating a bypass of the G2/M arrest caused by *CSA6*^{OE}.

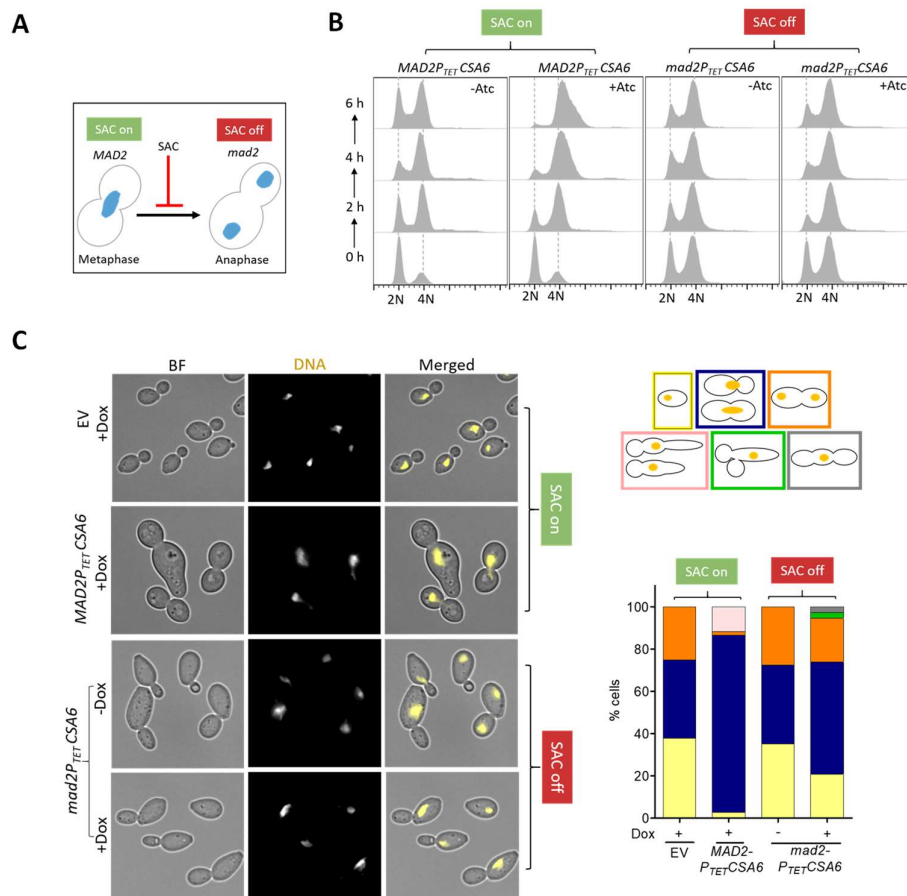


Figure 3.4 The G2/M cell cycle arrest in *CSA6^{OE}* mutant is mediated by Mad2. (A) The G2/M arrest posed by SAC in response to improper chromosome-spindle attachment is relieved in the absence of Mad2, allowing cells to transit from metaphase to anaphase. (B) Flow cytometric DNA content analysis in *MAD2CSA6^{OE}* strain (CaPJ176) and *mad2CSA6^{OE}* strain (CaPJ197) at the indicated times, in presence or absence of Atc (3 μ g/ml); $N=3$. (C) *Left*, microscopic images of EV (CaPJ170), *MAD2CSA6^{OE}* strain (CaPJ176) and *mad2CSA6^{OE}* strain (CaPJ197) following Hoechst staining, after 8 h of growth under indicated conditions of Dox (50 μ g/ml). Scale bar, 10 μ m. *Right*, quantitation of the indicated cell types; $n \geq 100$ cells.

We also observed a rescue of the growth defect in *CSA6^{OE}* mutant cells upon SAC inactivation (Figure 3.5A). Next, we sought to characterize the effect of SAC inactivation on the spindle integrity in *CSA6^{OE}* mutants. *CSA6^{OE}* resulted in the formation of an unconventional mitotic spindle (Figure 3.3) wherein it displayed a single focus of SPB (Tub4-GFP), colocalizing with a single focus of MTs (Tub1-mCherry).

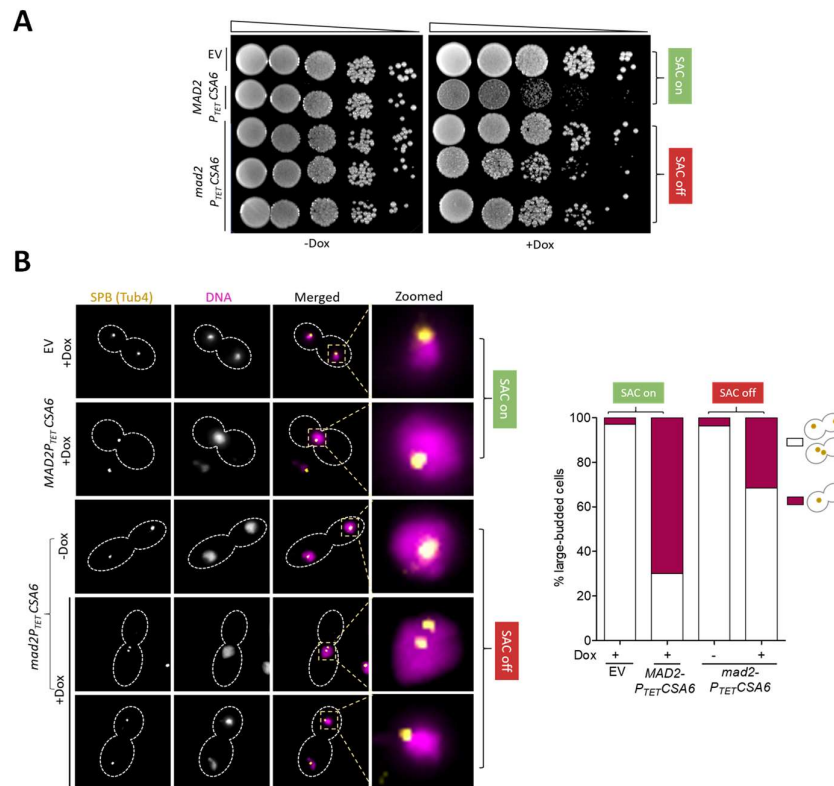


Figure 3.5 *CSA6^{OE}* associated G2/M arrest is relieved upon *mad2* deletion. (A) Spot dilution analysis of EV (CaPJ170), *MAD2CSA6^{OE}* strain (CaPJ176) and *mad2CSA6^{OE}* strain (CaPJ197). Ten-fold serial dilutions, starting from 10^5 cells, were spotted on YPDU agar plates with or without Dox (50 μ g/ml) and incubated at 30°C for two days. (B) *Left*,

localization patterns of Tub4-GFP in large-budded cells of EV (CaPJ171), *MAD2CSA6^{OE}* strain (CaPJ177) and *mad2CSA6^{OE}* strain (CaPJ198) after 8 h of growth under indicated conditions of Dox (50 μ g/ml). Hoechst staining was done to mark the nuclei. Scale bar, 3 μ m. *Right*, quantitation of the large-budded cells with the indicated Tub4 phenotypes; $n \geq 100$ cells.

We speculated two possibilities that may lead to the single focus of Tub4: a) a defect in SPB duplication or b) a delay in SPB separation. Fluorescence microscopy analysis revealed that SAC inactivation in *CSA6^{OE}* mutant drastically increased the percentage of large-budded cells (from ~30% to ~68%) with two separated SPB foci (Tub4-GFP) (Figure 3.5B). These results ruled out the possibility of an unduplicated SPB in *CSA6^{OE}* mutant cells and hinted at the importance of cellular Csa6 levels for proper SPB separation and chromosome segregation in *C. albicans*. We next determined the effect of inactivating SPOC in the cells overexpressing Csa6. For this, we generated a *CSA6^{OE}* strain (CaPJ200) using the *bub2* null mutant (CaPJ110) as the parent strain and monitored nuclear division following Hoechst staining. Strikingly, we did not observe a bypass of G2/M arrest in *CSA6^{OE}* mutant upon SPOC inactivation, indicated by a persistent population of large-budded cells with unsegregated nuclei (Figure 3.6). Altogether, our results demonstrate that overexpression of Csa6 leads to a Mad2-mediated metaphase arrest in *C. albicans*.

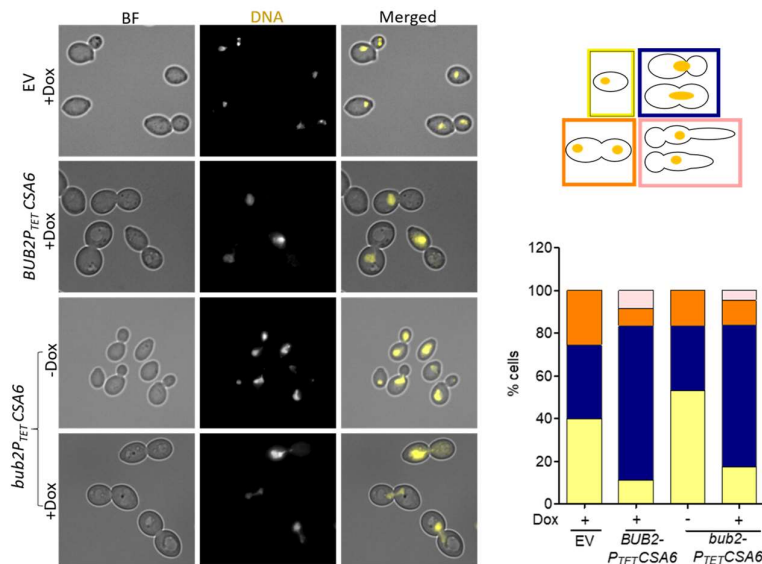


Figure 3.6 *CSA6^{OE}* associated G2/M arrest is not relieved upon *bub2* deletion. *Left*, representative images of Hoechst-stained EV (CaPJ170), *BUB2CSA6^{OE}* strain (CaPJ176) and

bub2CSA6^{OE} (CaPJ200) after 8 h of growth under indicated conditions of Dox (50 μ g/ml). Scale bar, 5 μ m. *Right*, percent cells with indicated cell types; $n \geq 100$ cells.

Csa6 regulates mitotic exit network and is essential for viability in *C. albicans*

To further gain insights into the biological function of Csa6, we sought to generate a promoter shut-down mutant of *csa6* (*CSA6^{PSD}*). For this, we deleted one of its alleles and placed the remaining one under the control of the *MET3* promoter (Care et al. 1999) which gets repressed in presence of methionine (M) and cysteine (C) (Figure 3.7A). Western blot analysis confirmed the depletion of TAP-tagged Csa6 in *CSA6^{PSD}* mutant within 6 h of growth under repressive conditions (Figure 3.7B). The inability of *CSA6^{PSD}* mutant to grow in non-permissive conditions confirmed the essentiality of Csa6 for viability in *C. albicans* (Figure 3.7C). Subsequently, we analyzed the cell cycle profile (Figure 3.7D) and nuclear division dynamics (Figure 3.7E) in *CSA6^{PSD}* strain after a specific period of incubation in either permissive or non-permissive conditions. Strikingly, Csa6 depletion, as opposed to its overexpression, resulted in cell cycle arrest at the late anaphase/telophase stage, indicated by an increasing proportion of large-budded cells, possessing segregated nuclei and 4N DNA content (Figure 3.7D, E). Additionally, we observed cells with more than two nuclei, elongated-budded cells and other complex phenotypes upon Csa6 depletion (Figure 3.7E).

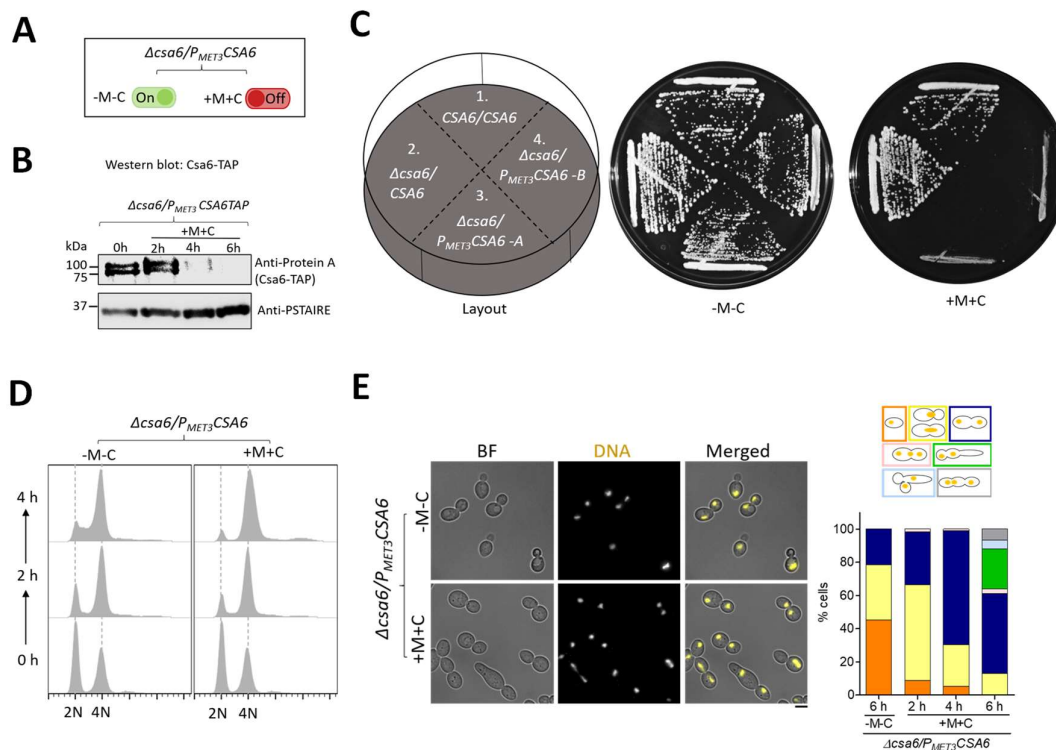


Figure 3.7. Csa6 depletion causes late anaphase/telophase arrest in *C. albicans*. (A) The *MET3* promoter system for depleting cellular levels of Csa6. The *MET3* promoter can be conditionally repressed in presence of methionine (M) and cysteine (C). (B) Western blot analysis using anti-Protein A antibodies revealed time dependent depletion of Csa6-TAP in *CSA6^{PSD}* strain (CaPJ212), grown under repressive conditions (YPDU + 5 mM M and 5 mM C) for indicated time interval; $N=2$. (C) Csa6 is essential for viability in *C. albicans*. Strains with indicated genotypes, (1) SN148, (2) CaPJ209, (3 and 4) CaPJ210 (two transformants) were streaked on agar plates with permissive (YPDU-M-C) or repressive (YPDU + 5 mM M and 5 mM C) media and incubated at 30°C for two days. (D) Cell cycle analysis of *CSA6^{PSD}* strain (CaPJ210) by flow cytometry under permissive (YPDU-M-C) and repressive conditions (YPDU + 5 mM M and 5 mM C) at the indicated time intervals; $N=3$. (E) *Left*, microscopic images of Hoechst stained *CSA6^{PSD}* strain (CaPJ210) grown under permissive (YPDU-M-C) or repressive (YPDU + 5 mM M and 5 mM C) conditions for 6 h. BF bright-field. Scale bar, 5 μ m. *Right*, quantitation of different cell types at the indicated time-points; $n \geq 100$ cells.

Although CENP-A/Cse4 remained localized to centromeres in *CSA6^{PSD}* mutant as revealed by the fluorescence microscopy (Figure 3.8A), an increase in the cellular levels of Cse4 was observed by western blot analysis (Figure 3.8B). The increase in Cse4 levels could be an outcome of Cse4 loading at anaphase in *C. albicans* (Shivaraju et al. 2012; Sreekumar et al. 2021). Finally, we analyzed the integrity of the mitotic spindle, as mentioned previously, in *CSA6^{PSD}* mutant. We noticed the mean length of the anaphase mitotic spindle in Csa6-depleted cells was significantly higher (~11 μ m) than that of the cells grown under permissive conditions (~6 μ m), indicating a spindle disassembly defect in *CSA6^{PSD}* mutant (Figure 3.9).

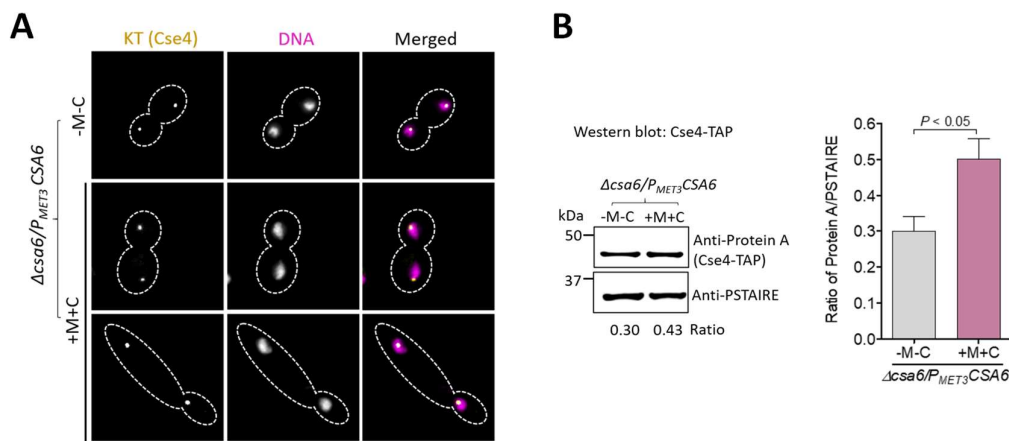


Figure 3.8. Csa6 depleted cells duplicate and segregate their nuclei. (B) Localization of Cse4-GFP in $CSA6^{PSD}$ strain (CaPJ213), after 6 h of growth in permissive (YPDU-M-C) or repressive (YPDU + 5 mM M and 5 mM C) conditions. Cse4-GFP colocalized with the nucleus, stained with Hoechst dye. Scale bar, 5 μm **(C)** *Left*, western blot analysis using anti-Protein A antibodies to compare Cse4-TAP levels in $CSA6^{PSD}$ strain (CaPJ214) when grown under permissive (YPDU-M-C) versus repressive (YPDU + 5 mM M and 5 mM C) conditions for 6 h; $N=3$. PSTAIRE was used as a loading control. Cse4-TAP levels were normalized by calculating the ratio of Protein A/PSTAIRE. *Right*, quantitation of the normalized Cse4 levels; $N=3$. Paired *t*-test, two-tailed, *P*-value shows a significant difference.

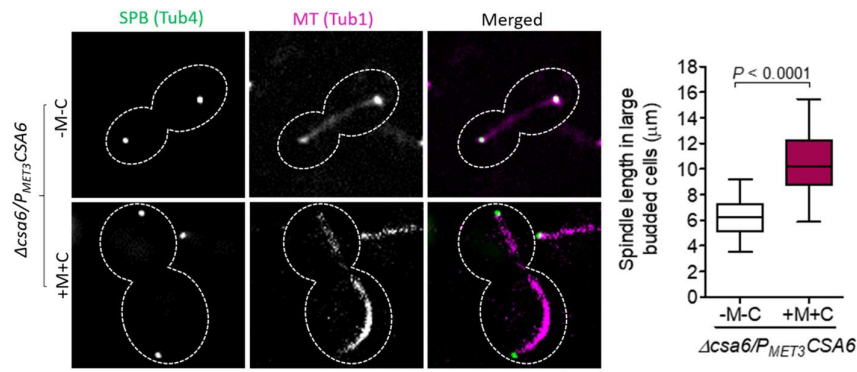


Figure 3.9 Csa6 depletion leads to hyper-extended mitotic spindle in *C. albicans*. *Left*, micrograph showing Tub4-GFP and Tub1-mCherry (representing mitotic spindle) in the large-budded cells of $CSA6^{PSD}$ strain (CaPJ211) after 6 h of growth under permissive (YPDU-M-C) or repressive (YPDU + 5 mM M and 5 mM C) conditions. Scale bar, 3 μm . *Right*, quantitation of the distance between the two SPBs, along the length of the MT (representing spindle length), in large-budded cells of $CSA6^{PSD}$ under permissive ($n=32$) or repressive ($n=52$) conditions. Paired *t*-test, one-tailed, *P*-value shows a significant difference.

A close link between anaphase arrest, hyper-elongated mitotic spindle and inactive mitotic exit network (MEN) have been established before (Surana et al. 1993; Liu et al. 1997; Bates 2018). Localized at the SPB, the MEN is a signaling cascade in *S. cerevisiae* that triggers cells to come out of the mitosis and proceed to cytokinesis (Figure 3.10A) (Hotz and Barral 2014). We speculated the anaphase arrest in $CSA6^{PSD}$ mutant could be a result of an inactive MEN signaling. To determine this, we sought to bypass the anaphase arrest associated with Csa6 depletion by overexpressing *SOLI*, the CDK inhibitor and Sic1 homolog in *C. albicans* (Atir-Lande et al. 2005) (Figure 3.10B), using the inducible P_{TET} system mentioned previously (Figure 3.10C). The conditional overexpression of Protein A-tagged Sol1 upon addition of Atc was verified by western blot analysis (Figure 3.10D). Strikingly, $SOLI^{OE}$ in

association with Csa6 depletion allowed cells to exit mitosis but not cytokinesis, as evidenced by the formation of chains of cells with >4N DNA content (Figure 3.10E, F).

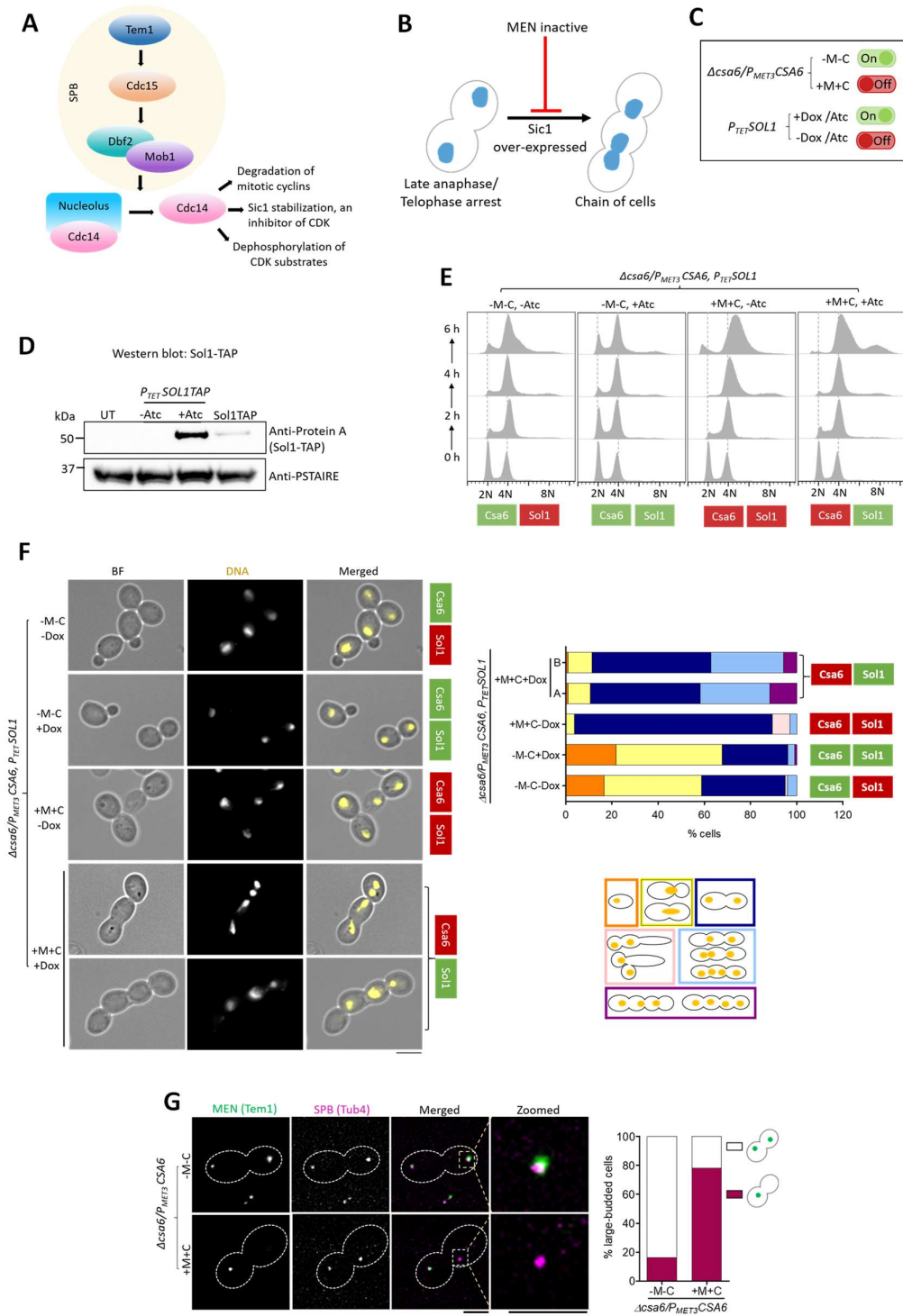


Figure 3.10. Csa6 is required for mitotic exit in *C. albicans*. (A) The MEN components in *S. cerevisiae*. At SPB, Nud1 acts as a scaffold. The ultimate target of the MEN is to activate Cdc14 phosphatase, which remains entrapped in the nucleolus in an inactive state until anaphase. Cdc14 release brings about mitotic exit and cytokinesis by promoting degradation of mitotic cyclins, inactivation of mitotic CDKs through Sic1 accumulation and dephosphorylation of the CDK substrates (Hotz and Barral 2014). (B) Inhibition of the MEN signaling prevents cells from exiting mitosis and arrests them at late anaphase/telophase. Bypass of cell cycle arrest due to the inactive MEN, viz. by overexpression of Sic1-a CDK inhibitor, often results in the chain of cells with multiple nuclei (Luca et al. 2001; Tamborini et al. 2018). (C) A combination of P_{TET} and P_{MET3} system to overexpress *C. albicans* homolog of Sic1, called *SOLI* (Sic one-like), in Csa6-depleted cells. The resulting strain, CaPJ215, can be conditionally induced for both, *SOLI* overexpression upon Atc/Dox addition and Csa6 depletion upon M/C addition. (D) Protein A western blot analysis showed increased levels of Sol1 (TAP-tagged) in *SOLI*^{OE} mutant (CaP217, $P_{TET}SOLI-TAP$) after 6 h induction in presence of Atc (3 μ g/ml) in comparison to the uninduced culture (-Atc) or *SOLI* expression from its native promoter (CaPJ216, *SOLI-TAP*); $N=2$. PSTAIRE was used as a loading control. UT, untagged control (SN148) (E) Flow cytometric analysis of cell cycle progression in CaPJ215 at indicated time intervals under various growth conditions, as indicated; $N=3$. Dox: 50 μ g/ml, M: 5 mM, C: 5 mM (F) *Left*, Hoechst staining of CaPJ215 after 6 h of growth under indicated conditions of Dox (50 μ g/ml), M (5 mM) and C (5 mM); $n \geq 100$ cells. BF bright-field. Scale bar, 5 μ m. *Right*, percent distribution of the indicated cell phenotypes; $n \geq 100$ cells. (G) *Left*, co-localization analysis of Tem1-GFP and Tub4-mCherry in large-budded cells of *CSA6*^{PSD} mutant (CaPJ218) under permissive (YPDU-M-C) or repressive conditions (YPDU + 5 mM M and 5 mM C). Scale bar, 3 μ m. *Right*, the proportion of the large-budded cells with indicated Tem1 phenotypes; $n \geq 100$ cells.

To further examine the role of Csa6 in mitotic exit, we analyzed the localization in *CSA6*^{PSD} mutant of a MEN component, Tem1, a GTPase that is known to initiate MEN signaling (Shirayama et al. 1994; Lee et al. 2001; Valerio-Santiago and Monje-Casas 2011; Milne et al. 2014). In *C. albicans*, Tem1 localizes to SPBs in a cell-cycle-regulated manner and is essential for viability (Milne et al. 2014). Fluorescence microscopy analysis revealed that while Tem1 localized to both the SPBs in anaphase under permissive conditions (Figure 3.10G) as observed earlier (Milne et al. 2014), a high percentage of Csa6 depleted cells (~78%) had Tem1 localized to only one of the two SPBs (Figure 3.10G), suggesting an important role of Csa6 in regulating mitotic exit in *C. albicans*. Altogether, our results demonstrate that Csa6 is essential for viability and required for mitotic exit in *C. albicans*.

Csa6 is an SPB-localizing protein, present in a subset of CUG-Ser clade species of fungi

To further comprehend the essential functions of Csa6 in mitosis, we sought to determine its subcellular localization. Epitope tagging of Csa6 with a fluorescent marker (mCherry) localized it close to the KT throughout the cell cycle in *C. albicans* (Figure 3.11A). The functionality of the mCherry-tagged Csa6 was determined by tagging the only copy of *CSA6* in a heterozygous null mutant (CaPJ209, *csa6/CSA6*) with mCherry. The resulting strain CaPJ117 (*csa6/CSA6-mCherry*) is viable and does not show any growth defect. In most unicellular fungi, often found proximal to the clustered KT, are the SPB complexes (Jin et al. 2000; Sanyal and Carbon 2002; Kitamura et al. 2007; Guin et al. 2020b). Although neither the SPB structure nor its composition is well characterized in *C. albicans*, the majority of the SPB proteins exhibit high sequence and structural conservation from yeast to humans (Lin et al. 2015). Hence, we re-examined Csa6 localization with two of the evolutionarily conserved SPB proteins, Tub4 and Spc110, in *C. albicans* (Lin et al. 2015; Lin et al. 2016) (Figure 3.11B). Our localization studies revealed that Csa6 constitutively localizes to the SPBs, close to the KTs, in *C. albicans*, further supporting Csa6's role in regulating mitotic spindle and mitotic exit in this ascomycete yeast.

Considering the essential roles played by the optimum levels of Csa6 in cell cycle progression, we were intrigued to examine its presence across various fungal species. Phylogenetic analysis using high confidence protein homology searches and synteny-based analysis indicated that Csa6 is exclusively present in a subset of species belonging to the CUG-Ser clade (Figure 3.12). To further elucidate the intra-species function and localization of Csa6, we decided to ectopically express Csa6 of another CUG-Ser clade species, *Candida dubliniensis* (CdCsa6) in *C. albicans*. *C. dubliniensis* is a human pathogenic budding yeast that shares a high degree of DNA sequence homology with *C. albicans* (Jackson et al. 2009). Upon protein sequence alignment, we found that CdCsa6 (*ORF Cd36_16290*) is 79% identical to Csa6 of *C. albicans* (CaCsa6) (Figure 3.13A). The ectopic expression of GFP-tagged CdCsa6 in *C. albicans* was carried out using the replicative plasmid pCdCsa6-GFP-ARS2 (Figure 3.13B), which contains the autonomously replicating sequence (ARS) of *C. albicans* (Chatterjee et al. 2016). Although unstable when present in an episomal form, ARS plasmids, upon spontaneous integration into the genome, can propagate stably over generations (Bijlani et al. 2019). Fluorescence microscopy of integrated pCdCsa6-GFP-ARS2 revealed that like CaCsa6, CdCsa6 is constitutively present at the SPBs in *C. albicans* (Figure 3.14A). We next asked if CdCsa6 can functionally complement CaCsa6. For this, we again ectopically expressed CdCsa6 in *CSA6^{PSD}* strain. Strikingly, the ectopic expression of

CdCsa6 rescued the growth defect associated with *CSA6*^{PSD} mutant under non-permissive conditions, indicating CdCsa6 can functionally complement CaCsa6 (Figure 3.14B). This suggests functional conservation of Csa6 among related *Candida* species belonging to the CUG-Ser clade.

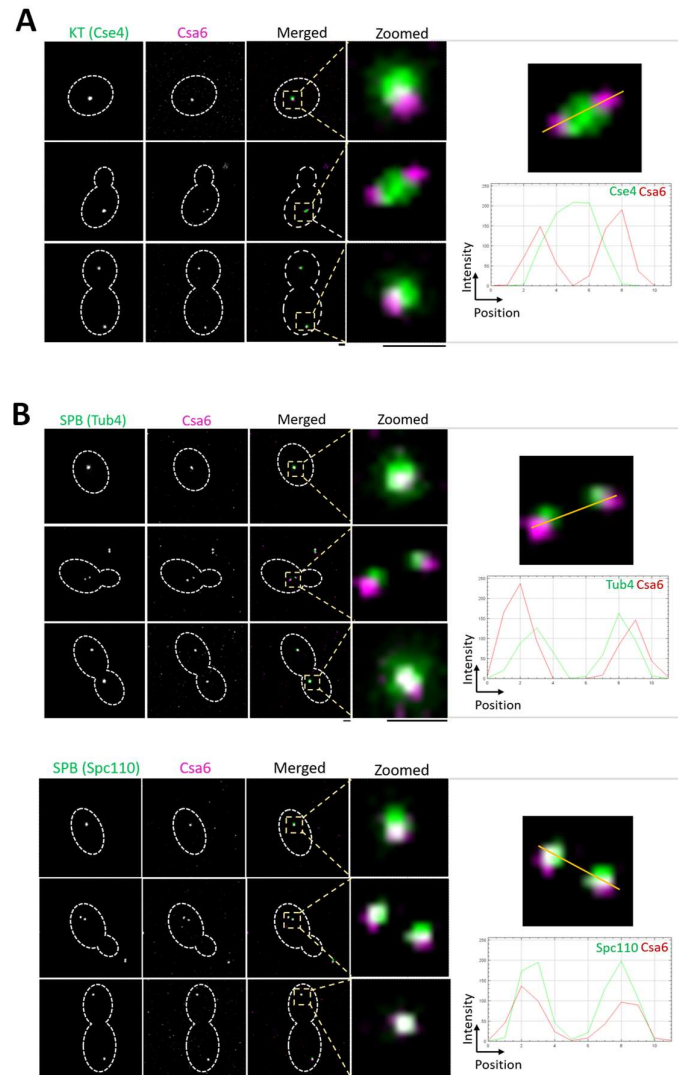


Figure 3.11. Csa6 is localized to the spindle pole bodies throughout the cell cycle in *C. albicans*. (A-B) *Left*, Micrographs comparing the sub-cellular localization of Csa6 with KT (Cse4) and SPB (Tub4 and Spc110) at various cell cycle stages. *Top*, Csa6-mCherry and Cse4-GFP (CaPJ119); *middle*, Csa6-mCherry and Tub4-GFP (CaPJ120), and *bottom*, Csa6m-Cherry and Spc110-GFP (CaPJ121). Scale bar, 1 μ m. *Right*, histogram plots showing the fluorescence intensity profile of Csa6-mCherry with Cse4-GFP (*top*), Tub4-GFP (*middle*) and Spc110-GFP (*bottom*) across the indicated lines.

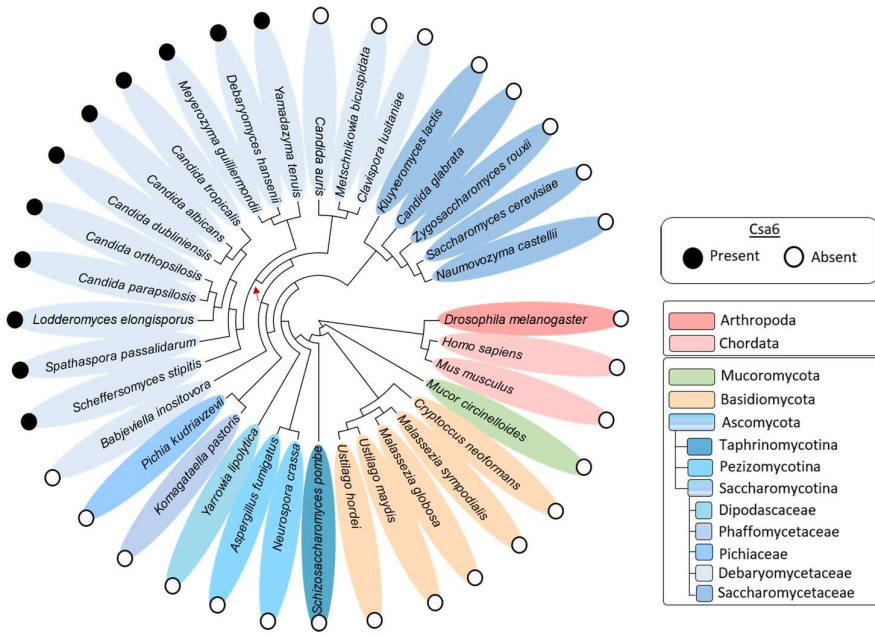


Figure 3.12. Restricted presence of Csa6 in CUG-Ser clade species. Phylogenetic tree showing the conservation of Csa6 across the mentioned species. The presence (filled circles) or absence (empty circles) of Csa6 in every species is marked. Each taxonomic rank is color-coded. The species mentioned under the family Debaryomycetaceae belong to the CUG-Ser clade in which the CUG codon is often translated as serine instead of leucine. The red arrow points to the CUG-Ser clade lineage that acquired Csa6. Searches for Csa6 homologs were carried out either in the *Candida Genome Database* (www.candidagenome.org) or NCBI nonredundant protein database (E value $\leq 10^{-2}$).

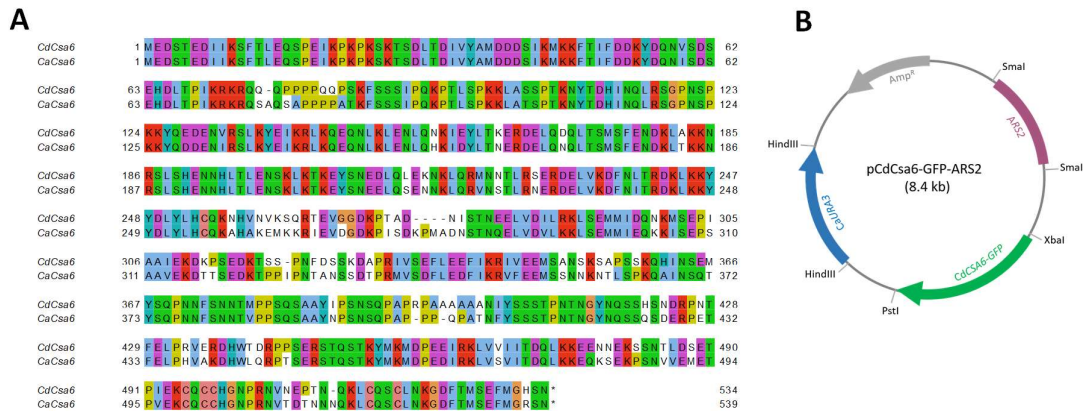


Figure 3.13. Conservation and ectopic expression of CdCsa6. (A) Pair-wise alignment of amino acid sequences of Csa6 proteins in *C. albicans* (CaCsa6) and *C. dubliniensis* (CdCsa6) by Clustal Omega, visualized using Jalview. (B) A vector map of pCdCsa6-GFP-ARS2 depicting the cloned sites of CaURA3, CaARS2 and CdCSA6-GFP. The CdCSA6-GFP

fragment contains the GFP tag, *CdCSA6* (*ORF Cd36_16290*) without the stop codon and the promoter region of *CdCSA6*.

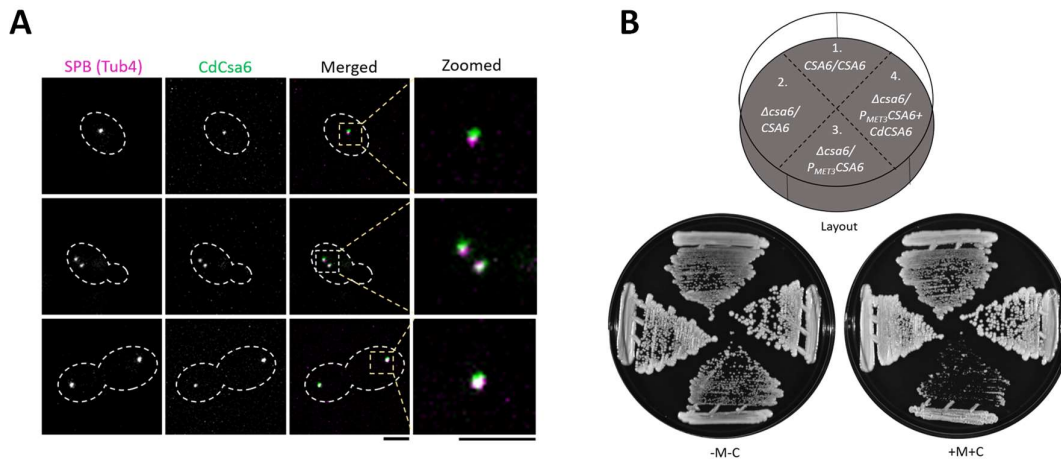


Figure 3.14. CdCsa6 localizes to the SPB and functionally complements CaCsa6. (A) Representative micrographs showing CdCsa6GFP localization at different cell cycle stages in CaPJ300. Tub4mCherry was used as an SPB marker. Scale bar, 3 μ m. **(B)** CdCsa6 functionally complements CaCsa6. Strains with indicated genotypes, (1) SN148, (2) CaPJ300, (3) CaPJ301 and (4) CaPJ302, were streaked on agar plates with permissive (YPDU-M-C) or repressive (YPDU + 5 mM M and 5 mM C) media and incubated at 30°C for two days.

Chapter 4

Discussion and future perspectives

In this study, we performed a large screen to identify genes that contribute to chromosome transmission in *C. albicans* by generating and analyzing a library of strains overexpressing more than a thousand genes (1067). Our screen identified six regulators of chromosome stability (CSA) including Csa6, a protein of unknown function (Figure 4.1). Molecular dissection of Csa6 function revealed its importance in cell cycle progression at least in two critical stages: metaphase-anaphase transition and mitotic exit. We further demonstrated that Csa6 is constitutively localized at SPBs, essential for viability, and alterations of its cellular level led to cell cycle arrest in *C. albicans*. Finally, subcellular localization and complementation analysis revealed functional conservation of Csa6 across the pathogenic *Candida* species.

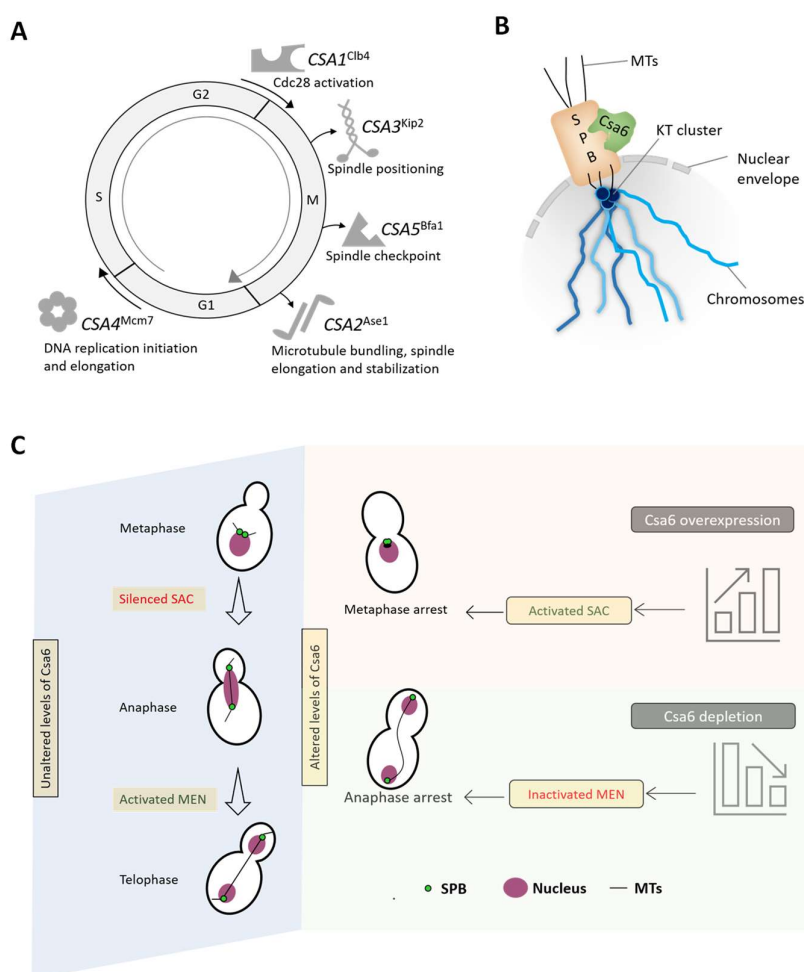


Figure 4.1. Csa6 levels are fine-tuned at various stages of the cell cycle to ensure both mitotic progression and mitotic exit in *C. albicans*. (A) A diagram illustrating the functions of the identified CSA genes except CSA6 in various phases and phase transitions of the cell

cycle. **(B)** Schematic depicting the approximate position of Csa6 with respect to SPB and KT. In *C. albicans*, SPBs and clustered KTs remain in close proximity throughout the cell cycle, while Csa6 remains constitutively localized to the SPBs. **(C)** A model summarizing the effects of overexpression or depletion of Csa6 in *C. albicans*. A wild-type cell with unperturbed Csa6 levels progresses through the mitotic cell cycle. Overexpression of *CSA6* alters the mitotic spindle dynamics which might lead to improper KT-MT attachments, prompting SAC activation and G2/M arrest. In contrast, decreased levels of Csa6 inhibit the MEN signaling pathway, probably by affecting Tem1 recruitment to the SPBs, resulting in cell cycle arrest at the anaphase stage.

The identification of two *CSA* genes, *CSA2^{ASE1}* and *CSA5^{BFA1}*, that were earlier reported as CIN genes (Stevenson et al. 2001; Duffy et al. 2016), further validates the power of the screening approach and the methods presented in this study. The respective overexpression phenotypes of these two genes in *C. albicans* were found to be similar to those in *S. cerevisiae*, suggesting that their functions might be conserved in these distantly related yeast species. In *S. cerevisiae*, Ase1 acts as an MT-bundling protein, required for spindle elongation and stabilization during anaphase (Pellman et al. 1995; Schuyler et al. 2003) (Figure 4.1A). Hence, increased CIN upon *ASE1* overexpression might be an outcome of premature spindle elongation and improper KT-microtubule attachments (Schuyler et al. 2003; Liu et al. 2008). Bfa1, on the other hand, is a key component of the Bub2-Bfa1 complex, involved in SPOC activation (Caydasi and Pereira 2012), and a negative regulator of mitotic exit (Wang et al. 2000) (Figure 4.1A). In *S. cerevisiae*, *BFA1* overexpression prevents Tem1 from interacting with its downstream effector protein Cdc15, thus inhibiting MEN signaling and arresting cells at the anaphase (Ro et al. 2002). In our screen, a B-type mitotic cyclin Clb4 (encoded by *CSA1*), and a kinesin-related motor protein Kip2 (encoded by *CSA3*) (Figure 4.1A), were found to increase CIN upon overexpression, primarily via non-CL events. *C. albicans* Clb4 acts as a negative regulator of polarized growth (Bensen et al. 2005) and is the functional homolog of *S. cerevisiae* Clb5 (Ofir and Kornitzer 2010), required for the entry into the S-phase (Schwob and Nasmyth 1993). Increased CIN upon *CSA1^{CLB4}* overexpression, is thus consistent with its role in S-phase initiation. The function of Kip2, however, is yet to be characterized in *C. albicans*. In *S. cerevisiae*, Kip2 functions as an MT polymerase (Hibbel et al. 2015), with its overexpression leading to hyperextended MTs and defects in SPB separation (Augustine et al. 2018). The associated CIN observed upon *CSA3^{KIP2}* overexpression in *C. albicans* is in line with its function during nuclear segregation.

Mcm7, another *CSA* gene (*CSA4*) identified in this study, is a component of the highly conserved Mcm2-7 helicase complex, essential for eukaryotic DNA replication initiation and elongation (Riera et al. 2017) (Figure 4.1A). While Mcm7 depletion arrests cells at S phase (Labib et al. 2000), the effect of *MCM7* overexpression on genomic integrity is comparatively less explored. Especially, several cancerous cells have been shown to overexpress Mcm7 (Ren et al. 2006; Toyokawa et al. 2011; Qiu et al. 2017), with its elevated levels increasing the chances of relapse and local invasions (Ren et al. 2006). In this study, we found that overexpression of *MCM7*, in contrast to Mcm7 depletion, arrested cells at G2/M stage. One possibility is increased Mcm7 levels interfered with DNA replication during the S phase, resulting in DNA damage or accumulation of single-stranded DNA, thus activating the *RAD9*-dependent cell cycle arrest at G2/M stage (Weinert and Hartwell 1988; Waterman et al. 2020). In a recent study from our laboratory, Mcm7 has been identified as a subunit of the kinetochore interactome in a basidiomycete yeast *Cryptococcus neoformans* (Sridhar et al. 2021). Another subunit of the Mcm2-7 complex, Mcm2, is involved in regulating the stability of centromeric chromatin in *C. albicans* (Sreekumar et al. 2021). Considering the growing evidence of the role of the Mcm2-7 complex beyond its canonical, well-established roles in DNA replication, the serendipitous identification of Mcm7 as a regulator of genome stability in our screen is striking.

We performed an in-depth analysis of *Csa6*, a novel regulator of cell cycle progression identified from our screen (Figure 4.1B, C). Our results revealed that overexpression of *CSA6* leads to an unconventional mitotic spindle formation and SAC-dependent G2/M cell cycle arrest in *C. albicans* (Figure 4.1C). While *mad2* deletion indicated that SPB duplication and separation of duplicated SPBs is unperturbed in *CSA6* overexpressing cells, what exactly triggered the activation of SAC in these cells remains to be determined. Recent studies on human cell lines have shown that failure in the timely separation of centrosomes promotes defective chromosome-MT attachments and may lead to lagging chromosomes lagging if left uncorrected by the cellular surveillance machinery (Silkworth et al. 2012; Zhang et al. 2012b; Nam et al. 2015) (Figure 4.2). Along the same lines, we posit that a delay in SPB separation, mediated by overexpression of *Csa6*, leads to increased instances of improper chromosome-MT attachments, leading to SAC activation and an indefinite arrest at the metaphase stage. Future studies on the SPB structure-function and composition in *C. albicans* should reveal how *Csa6* regulates SPB dynamics in this organism.

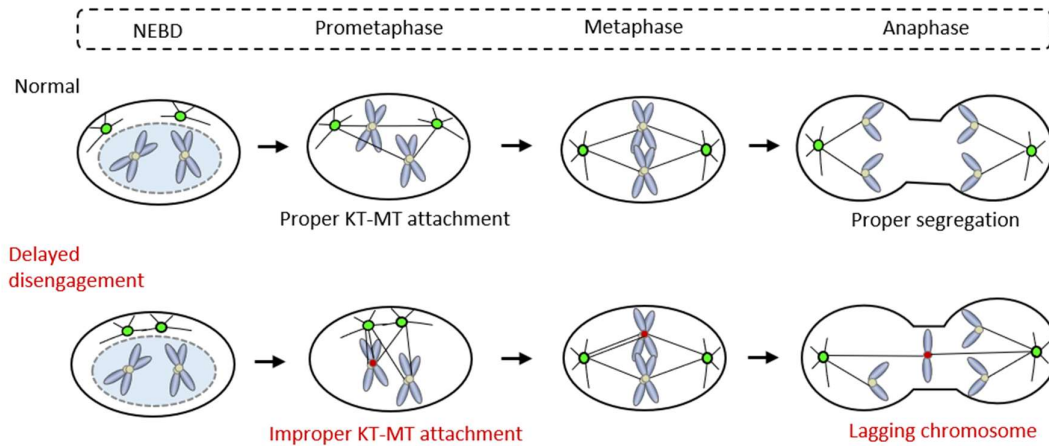


Figure 4.2. Proposed mechanisms by which aberrant centrosome dynamics can promote KT-MT misattachments. Normal centrosome dynamics promotes correct KT-MT attachments and faithful chromosome segregation. Delayed centrosome separation promotes misattachments in early metaphase because kinetochores are accessible to the MTs from the spindle poles in proximity. NEBD, nuclear envelope break-down. Centrosomes are marked in green. Erroneous KT-MT attachments are shown in red. Adapted and modified from (Nam et al. 2015).

In contrast to its overexpression, Csa6 depleted cells failed to exit mitosis and remained arrested at the late anaphase/telophase stage (Figure 4.1C). We further linked the mitotic exit failure in Csa6-depleted cells with the defective localization of Tem1, a protein appears upstream in the MEN signaling. While the hierarchy of MEN components, starting from the MEN scaffold Nud1, an SPB protein, to its ultimate effector Cdc14 is well established in *S. cerevisiae* (Hotz and Barral 2014), the existence of a similar hierarchy in *C. albicans* needs to be investigated (Figure 4.3). In addition, several lines of evidence suggest that MEN in *C. albicans* may function differently from *S. cerevisiae* (Figure 4.3): (a) *C. albicans* Dbf2 is required for proper nuclear segregation, actomyosin ring contraction, and cytokinesis (Gonzalez-Novo et al. 2009). (b) *C. albicans* Cdc14 is non-essential for viability with its deletion affecting cell separation (Clemente-Blanco et al. 2006). (c) Cdc14 is present in the nucleoplasm for the majority of the cell cycle in contrast to its nucleolar localization in *S. cerevisiae* (Clemente-Blanco et al. 2006). A recent study involving the identification of Cdc14 interactome in *C. albicans* (Kaneva et al. 2019) found only a subset of proteins (0.2%) as physical or genetic interactors in *S. cerevisiae* (Figure 4.4), suggesting the divergence of Cdc14 functions in *C. albicans*. Moreover, the counterpart of Cdc14 phosphatase in *C. albicans* is yet to be identified. Hence, further investigation on MEN functioning in *C.*

albicans is required to understand its divergence from *S. cerevisiae* and the mechanism by which Csa6 regulates mitotic exit in *C. albicans* and related species. Altogether, our results indicate that Csa6 has dual functions during cell cycle progression wherein it is first required during G2/M phase for proper assembly of the mitotic spindle and later during anaphase to exit from mitosis. In addition, the constitutive localization of Csa6 at SPBs strengthens the link between SPB-related functions and Csa6 in *C. albicans* (Figure 4.1B).

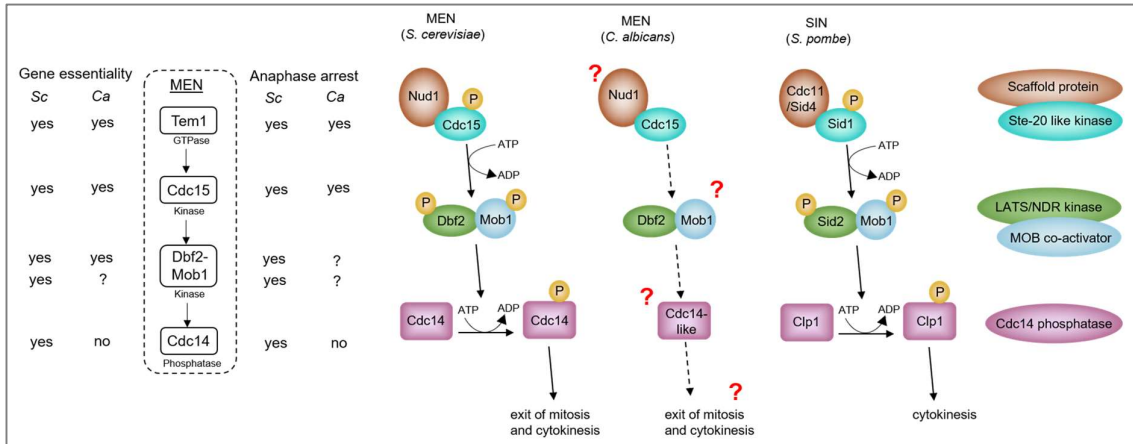


Figure 4.3 Comparison of the process of mitotic exit in yeast species. *Left*, cartoon depicting the gene essentiality and anaphase arrest associated with conditional or null mutants of MEN components in *S. cerevisiae* (*Sc*) and *C. albicans* (*Ca*). *Right*, conserved components of MEN and SIN in *S. cerevisiae* and *S. pombe*, respectively, are illustrated. A hypothetical model of MEN in *C. albicans* is shown. The hierarchy of MEN components in *C. albicans* (shown with dotted arrows) remains elusive. A yet unknown functional homolog of Cdc14 (Cdc14-like) in *C. albicans* is depicted in the model. Question marks highlight the proteins with no reported role in mitotic exit/cytokinesis. Phosphorylation marks are indicated by “P” in yellow. Adapted and modified from (Hergovich and Hemmings 2012).

Pre-RC activation and DNA Replication Cdc7 Dbf4* Orc1 Orc2 Orc3 Orc4 Orc5 Orc6 Orf19.2389 (Sid2) Orf19.6255 (Cdc9) Fkh2	DNA repair and DNA checkpoint Orf19.427 (Rif1) Rad52* Rad9 Orf19.4988 (Sae2) orf19.652 (yen1) Gin1 (MRC1) Exo1 Orf19.7060 orf19.6291 (Fun30)	Kinetochore attachment to microtubules DAM-DASH complex Dam1 Dad2 Dad3 Ask1 Duo1 Spc34 Spc19 CPC complex Ipl1 Orf19.6049 (Sli15) Orf19.643 (BIR1) NDC80 Complex Ndc80 Nuf2 Other MT-associated Orf19.4435 (Stu1) Stu2 Unknown Orfs localising to SPB Orf19.5491 Orf19.2684 Orf19.3091 Orf19.3296 Orf19.4101	Anaphase promotion and Mitotic exit Orf19.267 (Net1) Clb2(*) Orf19.6010 (Cdc5) Esp1* Dbf2 Cdc14 Orf19.3823 (ZDS1) orf2684 (Slk19)* APC (3) Orf19.1792 (Cdc16) Cdc27 Cdh1	Cytokinetic ring Mic1 Igg1 orf19.3535 (Csi2)	Cell separation CHT4 Ace2
---	--	---	--	--	--

Figure 4.4. Role of *C. albicans* Cdc14-interacting proteins in cell cycle. Depicted here are 55 known proteins (out of 126) identified in *C. albicans* Cdc14-interactome with the indicated functions (research from *S. cerevisiae* and *S. pombe*). Out of these 55 proteins, only 22 proteins, highlighted in black font or asterisks, have been identified as physical (17) or genetic (5) interactors of Cdc14, respectively, in *S. cerevisiae*. Adapted and modified from (Kaneva et al. 2019).

Alternatively, it is possible that being at SPBs, Csa6 indirectly regulates MT nucleation/growth and disassembly. This could explain the absence of long MTs in G2/M upon Csa6 overexpression. For instance, an increased level of Csa6 at the SPBs may interfere with the recruitment of a factor that promotes MT assembly. Likewise, the persistence of long MTs during anaphase upon Csa6 depletion may be supported by this hypothesis if the recruitment factor continues to promote MT assembly. The phylogenetic analysis of Csa6 revealed that it is only present in a group of fungal species, belonging to the CUG-Ser clade. Combined with its essential cell-cycle-related functions, it is intriguing to determine whether emergence of Csa6 is required to keep the pace of functional divergence in the regulatory mechanisms of cell cycle progression in these *Candida* species. While we demonstrated Csa6 of *C. dubliniensis* functionally complements Csa6 of *C. albicans*, whether Csa6 of distant species can also functionally complement CaCsa6 remains to be investigated. Analysis of Csa6 interactome at specific cell cycle stages, viz. metaphase or anaphase might unravel the underlying mechanisms by which Csa6 performs various essential functions in *C. albicans*. Structurally, the middle region of Csa6 is predicted to have the coiled-coil domain, built by two or more alpha-helices that are coiled together to form a supercoil (Figure 4.5).

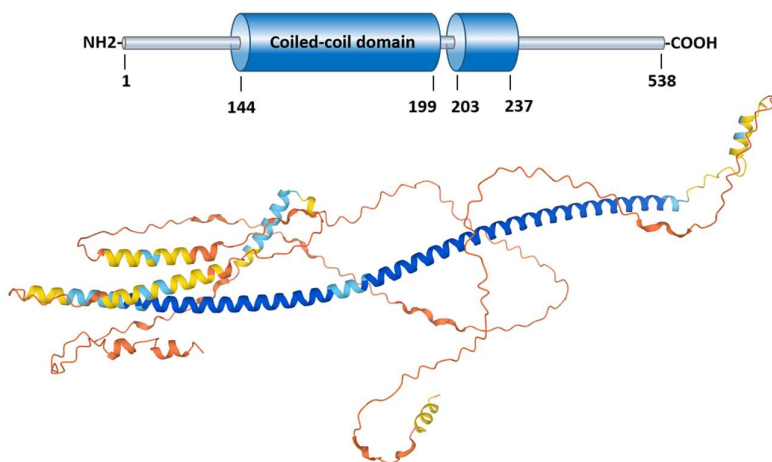


Figure 4.5 Predicted structural features of Csa6 in *C. albicans*. CaCsa6 is a 538-amino acid long protein, predicted to have coiled coil-domains or alpha-helices. The domains were predicted using HMMER (Potter et al. 2018) phmmer searches. The 3D structure was generated using AlphaFold Protein Structure Database (Tunyasuvunakool et al. 2021).

Future investigations involving perturbation of the Csa6 coiled-coil domain might shed some light on the stage-specific functions of Csa6 in *C. albicans*. A recent study showed that around 50 essential genes, including Csa6, are only present in a group of *Candida* species (see dataset 5 in (Segal et al. 2018)). Identification and functional characterization of these genes in the future will aid in developing clade-specific antifungal therapies (Segal et al. 2018). It is striking that although our screen successfully identified several genes including *ASE1*, *KIP2* and *BFA1* that are involved in spindle assembly, genes with direct functions in chromosome segregation such as *CSE4* or other KT-related proteins remain uncovered in the screen. Similarly, in a previous study by Loll-Krippleber et al (Loll-Krippleber et al. 2015), overexpression of several KT proteins were shown to cause no change in loss frequency of the BFP/GFP locus. It is possible that the regional centromeres of *C. albicans* harbour mechanisms to manage increased KT protein levels either through degradation of excess molecules or by their increased accumulation at the centromere as has been shown when Cse4 was overexpressed in *C. albicans* (Burrack et al. 2011). Additionally, we have analyzed only about a quarter of the total *C. albicans* ORFeome for their function in genome maintenance. Further screening of the remaining overexpression ORFs, that is in progress, is expected to reveal other factors/molecular pathways regulating genome stability in human fungal pathogens.

Chapter 5

Materials and methods

Strains, plasmids and primers

The list of all the yeast strains, primers and plasmids used in this study are mentioned in tables 5.1, 5.2 and 5.3, respectively. The *E. coli* library harbouring CIp10- P_{TET} -GTW derivatives was constructed in the TOP10 *ccdB^R* (Invitrogen) strain of *E. coli* (Chauvel et al. 2012). Other plasmids were propagated in *E. coli* strain DH5 α or XL-1 Blue.

Strain Construction

Construction of CSA reporter strain

The *RFP* was amplified by PCR using primers RFP-PstI-F and RFP-NheI-R from plasmid pNIM1R-RFP (Prieto et al. 2014). The PCR fragment was cloned into a TOPO®-TA vector (ThermoFisher), digested with PstI and NheI and cloned into the PstI and NheI sites of pTDH3-GFP-URA3 (Znaidi et al. 2018), yielding pTDH3-RFP-URA3. The *HYG B* gene was excised from pAU34-CaHygB (Basso et al. 2010) by BglII+XbaI digest and cloned into the BglII+XbaI double-digested pTDH3-RFP-URA3, to replace the *URA3* marker, yielding pCaTDH3-RFP-HygB. The plasmid pCaTDH3-RFP-HygB was finally modified by a NheI digest and Klenow treatment in order to shorten the extra sequence added at the 3' end because of the cloning steps. The desired $P_{TDH3-RFP-HygB}$ cassette was PCR amplified from plasmid pCaTDH3-RFP-HygB with oligonucleotides K7_BFP_GFP_Chr4_Right_F and RFP_Insertion_Chr4_Right_Reverse carrying sequences homologous to the genomic DNA located on the right arm of chromosome 4 (Ch4). The PCR product was then transformed in CEC3867 (Feri et al. 2016) yielding CEC5201.

Generation of a C. albicans overexpression strains collection

A library of *C. albicans* overexpression strains (1067) was generated in a high throughput manner using 96-well plates. Briefly, the *E. coli* cultures containing CIp10- P_{TET} -GTW derivatives (Legrand et al. 2018) were grown in 96-deep well plates containing LB or 2YT medium supplemented with ampicillin (50 or 100 μ g/ml). Plasmid miniprepations were carried out in 96-well plates using either Nucleospin™ 96 plasmid core kit (Machery-Nagel™) or the boiling lysis method (Harwood 1996). The quality of the isolated plasmids was randomly checked by ethidium-bromide staining following agarose gel electrophoresis.

The plasmids were then digested by either *StuI* (Anza™ 54 Eco147I) or *I-sceI* (NEB) depending on whether a *C. albicans* ORF contained a *StuI* recognition site (Chauvel et al. 2012). The digested plasmids were precipitated using 3M sodium acetate and 100% ethanol for transformation into the CSA reporter strain (CEC5201), which contains a pNIMX-encoded transactivator to promote the expression from the *TET* promoter (Chauvel et al. 2012). The *C. albicans* transformation was then carried out in 96 deep-well plates using the lithium acetate method, described previously (Walther and Wendland 2003). The *C. albicans* transformants were selected for prototrophy and screened by colony PCR using primers PJ88/PJ89 to confirm the integration of overexpression plasmid at the *RPS1* locus (Chauvel et al. 2012). The PCR positive transformants were grown in 96 deep-well plates containing YPDU and prepared for glycerol stocks.

Construction of C. albicans overexpression strains

StuI-digested or *I-SceI*-digested CIp10-*P_{TET}*-GTW derivatives were used to transform *C. albicans* strains in which the pNIMX transactivator cassette was integrated. The integration of pNIMX at the *ADH1* locus of *C. albicans* was carried out after digesting pNIMX with *KpnI* and *ApaI*, and confirming the transformants by PCR using primers PJ86/PJ87 (Chauvel et al. 2012). The *C. albicans* transformants harboring the overexpression plasmid at the *RPS1* locus were screened by PCR using primers PJ88 and 89.

C-terminal tagging of Tub4 with fluorescent proteins

GFP-tagged Tub4 strains were constructed by using the plasmid pTub4-GFP-His. Briefly, the 3' coding region of Tub4 without the stop codon was amplified from the *C. albicans* (SN148) genome using primers LS39FP/LS39RP and cloned into the *SacII* and *SpeI* sites of pBSGFP-His (Chatterjee et al. 2016). The resulting plasmid pTub4-GFP-His was confirmed using restriction analyses and transformed into the *C. albicans* strains after *PacI* digestion. The correct *C. albicans* transformants were screened by fluorescence microscopy.

Epitope tagging of Tub4 with mCherry was carried out using the plasmids pTub4-mCherry-Arg4 or pTub4-mCherry-Nat. To construct pTub4-mCherry-Arg4, the C-terminus of Tub4 was released from pTub4-GFP-His following digestion with *SacII* and *SpeI* and subsequently cloned into the *SacII* and *SpeI* sites of pRFP-Arg4 (Varshney and Sanyal 2019a). The *E. coli*

clones were confirmed by restriction analyses. The plasmid pTub4-mCherry-Arg4 was partially digested with PacI for transforming *C. albicans* strains. The transformants obtained were selected for prototrophy and screened by fluorescence microscopy. The plasmid pTub4-mCherry-Nat was constructed as follows: the mCherry coding gene was amplified from CaADH1pyEmRFP (Keppler-Ross et al. 2008) using the primers SR149/SR150 and cloned into the SpeI and SmaI sites of pBSNAT (Thakur and Sanyal 2013). The mCherry-NAT containing plasmid was then digested by SpeI and KpnI and the mCherry-NAT fragment was cloned into the SpeI and KpnI sites of pTub4-GFP-His. The resulting plasmid pTub4-mCherry-Nat was verified by restriction analyses and used to transform *C. albicans* strains after PacI digestion. The correct *C. albicans* transformants were screened by fluorescence microscopy.

C-terminal tagging of Tub1 with mCherry

The 3' coding region of Tub1 without the stop codon was amplified from *C. albicans* SN148 genome using the primer pairs PJ77/PJ88 and cloned into the SacII and SpeI sites of pRFP-Arg4 (Varshney and Sanyal 2019a). The resulting plasmid pTub1-mCherry-Arg4 was confirmed using restriction analyses and digested with XbaI for transforming the *C. albicans* strains. The correct *C. albicans* transformants were screened by fluorescence microscopy.

C-terminal tagging of Cse4 with TAP

CSE4 ORF (without the stop codon) along with the *TAP* tag was PCR amplified from the *C. albicans* strain CAKS102 (Mitra et al. 2014) using the primers NV241/NV242 and cloned into the SalI and ApaI sites of pMad2-2 (Thakur and Sanyal 2011). The desired plasmid pCse4-TAP-Leu was verified by restriction analyses and linearized by XhoI for transforming the *C. albicans* strains. The transformants were selected for prototrophy and confirmed by western blot analysis.

Construction of bub2 null mutant

Both the alleles of *BUB2* were deleted using the *SAT1* flipper cassette (pSFS2a) (Reuss et al. 2004). To delete the first allele, upstream (US) and downstream (DS) sequences of *BUB2* were amplified from the *C. albicans* SN148 genome using primers PJ110/PJ111 and

PJ112/PJ113, respectively. The US and DS sequences were then cloned in pSFS2a as KpnI/XhoI and SacII/SacI fragments, respectively, to obtain the plasmid pBub2del#1. The *E. coli* clones were verified using restriction analysis. The desired deletion cassette was transformed into the *C. albicans* strains after digesting pBub2del#1 with KpnI and SacI. The *C. albicans* transformants were screened for correct chromosomal integration by PCR using the primer pair PJ3/PJ116. The correct transformants were grown in YPM (1% yeast extract, 2% peptone, 2% maltose) medium supplemented with uridine (0.1 µg/ml) overnight and plated on YPMU agar to recycle the *SAT1* marker (Reuss et al. 2004). The single colonies obtained on YPMU agar were replica plated on YPDU and YPDU with nourseothricin (100 µg/ml). Nourseothricin-sensitive colonies, obtained as a result of *SAT1* recycling, were reconfirmed for *SAT1* eviction and *BUB2* first copy deletion by PCR using primers PJ110/PJ113 and selected for subsequent transformations to delete the remaining *BUB2* allele.

To delete the second allele of *BUB2*, the DS sequence of *BUB2* in pBub2del#1 was replaced with the 3' coding region of *BUB2*. For this, the 3' coding region of *BUB2* was amplified from the *C. albicans* SN148 genome using primers PJ114/PJ115 and cloned into the SacII and SacI sites of pBub2del#1. The resulting plasmid pBub2del#2 was verified using restriction analyses and was transformed into the *BUB2* heterozygous null strain after digesting pBub2del#2 with KpnI and SacI. The transformants obtained were grown in presence of Nourseothricin (100 µg/ml) and screened for the integration of pBub2del#2 deletion cassette by PCR using the primers PJ117/PJ118. The desired PCR positive transformants were reverified for *BUB2* first copy deletion using the primers PJ110/PJ113. The resulting nourseothricin-resistant *bub2* mutants were grown in YPMU overnight and plated on YPMU agar to recycle the *SAT1* marker (Reuss et al. 2004). The single colonies obtained on YPMU agar were replica plated on YPDU and YPDU with nourseothricin (100 µg/ml). Nourseothricin-sensitive colonies were selected for subsequent experiments.

Construction of csa6 conditional mutant

The first allele of *CSA6* (*ORF19.1447*) was deleted using the *SAT1* flipper cassette (pSFS2a) (Reuss et al. 2004) and the second allele was placed under the control of regulatable *MET3* promoter (Care et al. 1999). To delete the first allele, the US and DS sequences of *CSA6* were amplified from the *C. albicans* SN148 genome using primers PJ95/PJ96 and PJ97/PJ98,

respectively. The US and DS sequences were then cloned in pSFS2a as KpnI/XhoI and SacII/SacI fragments, respectively, to obtain the plasmid pCsa6del. The *E. coli* clones were confirmed using restriction analysis. The desired deletion cassette was transformed into *C. albicans* strains after digesting pCsa6del with KpnI and SacI. The *C. albicans* transformants were screened for correct chromosomal integration by PCR using the primer pair PJ3/PJ99. The correct transformants were grown in YPMU overnight and plated on YPMU agar to recycle the *SATI* marker (Reuss et al. 2004). Nourseothricin-sensitive colonies, obtained as a result of *SATI* recycling, were selected for subsequent transformations to inactivate the remaining wild-type allele of *CSA6*.

To replace the promoter of the second allele with the *MET3* promoter (Care et al. 1999), the 5' coding region of *CSA6* including the start codon was amplified from the *C. albicans* SN148 genome using primers PJ93/PJ94 and cloned into the BamHI and PstI sites of pCaDis (Care et al. 1999), generating the plasmid pCsa6-Met3-Ura. The *E. coli* clones were confirmed using restriction analyses. The plasmid pCsa6-Met3-Ura was linearized using BstBI and transformed into the *C. albicans* strains in which the first copy of *CSA6* was deleted. The resulting conditional mutants were screened for correct genomic integration by PCR using the primer pair PJ91/PJ95.

To generate the plasmid pCsa6-Met3-His, a *HIS1* fragment from pGFP-HIS (Chatterjee et al. 2016) was obtained after digesting pGFP-HIS with EcoRI and was cloned into the EcoRI site of p1447-Met3-His. The *E. coli* transformants were screened and validated by restriction analysis.

Epitope tagging of Csa6

The C-terminus of *CSA6* was tagged with either TAP or mCherry. To express TAP-tagged Csa6 from the native promoter or *MET3* promoter, the 3' coding region of *CSA6* without the stop codon was amplified from the *C. albicans* SN148 genome using the primer pair PJ108 (containing the BglIII restriction site) and PJ109 and cloned into the BamHI and PacI sites of pFA-TAP-*ARG4* (Lavoie et al. 2008). The *E. coli* clones were confirmed by both, restriction analyses and Sanger sequencing. The resulting plasmid p1447-TAP-Arg was linearized using BamHI for single-site integration into the *C. albicans* genome. The *C. albicans* transformants

were screened for correct genomic integration by PCR using the primer set NV34/TEJ13 and western blot analysis.

To express Csa6TAP from the P_{TET} promoter, a fragment containing the coding region of *CSA6* along with the *TAP* tag was amplified from CaPJ180 using primers PJ127/PJ128 and cloned into the EcoRV site of pCip10- P_{TET} -GTW (Chauvel et al. 2012). The resulting plasmid Cip10- P_{TET} -1447TAP was confirmed using restriction analyses and Sanger sequencing and was digested by StuI for transforming the *C. albicans* strains. The correct *C. albicans* transformants were screened by PCR using primers PJ88/PJ89 and western blot analyses.

To tag the C-terminus of Csa6 with mCherry, the 3' coding region of *CSA6* without the stop codon was amplified from the *C. albicans* SN148 genome using the primer pair TEJ1/TEJ2 and cloned into the SacII and SpeI sites of pRFP-Arg4 (Varshney and Sanyal 2019a). The *E. coli* clones were confirmed by both, restriction analyses and Sanger sequencing. The resulting plasmid pCsa6-mCherry-Arg was linearized using BstB1 for single-site integration into the *C. albicans* genome. The correct *C. albicans* transformants were confirmed by PCR using primers TEJ13/TEJ14 and analyzed by fluorescence microscopy.

Construction of SOL1 overexpression mutant

To overexpress Sol1, an extra copy of *SOL1* under the P_{TET} promoter was integrated at the *RPS1* locus (Chauvel et al. 2012). For this, the complete ORF sequence of *SOL1* including the start and the stop codon was PCR amplified from the *C. albicans* SN148 genome using primers PJ119/PJ120 and cloned into the EcoRV site of Cip10- P_{TET} -GTW (Chauvel et al. 2012) resulting in plasmid Cip10- P_{TET} -SOL1. The correct *E. coli* clones were screened using restriction analyses and verified by Sanger sequencing. The plasmid Cip10- P_{TET} -SOL1 can be linearized by StuI for *C. albicans* transformation. The *C. albicans* transformants were confirmed by PCR using primers PJ88/PJ89.

Epitope tagging of Sol1

The expression level of Sol1 from the native promoter and P_{TET} promoter was compared by tagging the C-terminus of *SOL1* with TAP. For TAP tagging Sol1 under its own promoter,

the 3' coding region of *SOL1* without the stop codon was amplified from the *C. albicans* SN148 genome using the primer pair PJ141/PJ142 and cloned into the BamHI and PacI sites of pFA-TAP-*His1* (Care et al. 1999). The *E. coli* clones were confirmed by both, restriction analyses and Sanger sequencing. The resulting plasmid pSol1-TAP-*His* was linearized using XbaI for single-site integration into the *C. albicans* genome. The *C. albicans* transformants were screened for correct genomic integration by PCR using the primer set PJ119/PJ128 and western blot analysis.

To express Sol1TAP from the P_{TET} promoter, a fragment containing the coding region of *SOL1* along with the *TAP* tag was amplified from CaPJ216 using primers PJ119/PJ128 and cloned into the EcoRV site of CIp10- P_{TET} -GTW (Chauvel et al. 2012). The resulting plasmid CIp10-PTET-SOL1TAP was confirmed using restriction analyses and Sanger sequencing. The plasmid CIp10-PTET-SOL1TAP was linearized by StuI for transforming the *C. albicans* strains and the transformants were screened by PCR using primers PJ88/PJ89 and western blot analyses.

Construction of GFP-tagged strains of Tem1 and Spc110

The C-terminus of Tem1 and Spc110 was tagged with GFP. For this, 3' coding region of Tem1 and Spc110 without the stop codon was amplified from *C. albicans* SN148 genome using the primer pairs PJ121/122 and PJ106/PJ107, respectively and cloned into the SacII and SpeI sites of pBSGFP-*His* (Chatterjee et al. 2016). The resulting plasmids (i) pTEM1-GFP-*His* was confirmed by both restriction analyses and Sanger sequencing (ii) pSpc110-GFP-*His* was validated by restriction analyses.

The plasmid pTEM1-GFP-*His* was propagated in the *dam*⁻/*dcm*⁻ strain of *E. coli* (C2925) obtained from NEB and digested with BclI for transforming the *C. albicans* strains. The correct *C. albicans* transformants were screened by PCR using primers PJ123/PJ124 and fluorescence microscopy.

The plasmid pSpc110-GFP-*His* was linearised with NheI or NsiI for single-site integration into the *C. albicans* genome. The *C. albicans* transformants were screened by fluorescence microscopy.

Expression of C. dubliniensis Csa6 in C. albicans

The C-terminus of *C. dubliniensis* Csa6 (*Cd36_16290*) was tagged with GFP and ectopically expressed in *C. albicans* using the plasmid pCdCsa6-GFP-ARS2. For this, complete ORF of *CdCSA6* (without the stop codon), along with its promoter region was PCR amplified from the genome of Cd36, a *C. dubliniensis* clinical isolate (Thakur and Sanyal 2013), using the primers VS5/Vs6. The GFP tag was amplified from pTub4-GFP-His using the primers VS7/Vs8. An overlap PCR of the two fragments was then set up using the primers VS5/Vs8. The resulting ~3.6 kb long fragment containing the GFP-tagged *C. dubliniensis* Csa6 under its own promoter was cloned into the XbaI and PstI sites of pARS2 (Chatterjee et al. 2016). The plasmid, pCdCsa6-GFP-ARS2, obtained was verified by restriction analyses and transformed into the *C. albicans* strains. The transformants were selected for prototrophy and screened by fluorescence microscopy. As ARS plasmids are highly unstable in *C. albicans*, we used the large transformant colonies, obtained as a result of an integrative transformation of pARS2 (Cannon et al. 1990) and retained the auxotrophic marker (*URA3*) even in the absence of any selection pressure, for all our assays.

Media and growth conditions

C. albicans strains were routinely grown at 30°C in YPD (1% yeast extract, 2% peptone, 2% dextrose) medium supplemented with uridine (0.1 µg/ml) or complete medium (CM, 2% dextrose, 1% yeast nitrogen base and auxotrophic supplements) with or without uridine (0.1 µg/ml) and amino acids such as histidine, arginine, leucine (0.1 µg/ml). Solid media were prepared by adding 2% agar. For the selection of transformants, nourseothricin and hygromycin B (hyg B) were used at a final concentration of 100 µg/ml and 800 µg/ml, respectively, in the YPDU medium.

Overexpression of genes from P_{TET} was achieved by the addition of anhydrotetracycline (Atc, 3 µg/ml) or doxycycline (Dox, 50 µg/ml) in YPDU medium at 30°C (Chauvel et al. 2012) in the dark as Atc and Dox are light-sensitive. The *CSA6^{PSD}* strains were grown at 30°C either in permissive (YPDU) or nonpermissive (YPDU + 5mM methionine (M) + 5mM cysteine (C)) conditions of the *MET3* promoter (Care et al. 1999; Sreekumar et al.). *E. coli* strains were cultured at 30°C or 37°C in Luria-Bertani (LB) medium or 2YT supplemented with ampicillin (50 µg/ml or 100 µg/ml), chloramphenicol (34 µg/ml), kanamycin (50 µg/ml) and

tetracycline (10 µg/ml). Solid media were prepared by adding 2% agar. Chemically competent *E. coli* cells were prepared according to Chung *et al* (Chung et al. 1989).

Flow cytometry analysis

Cultures of overexpression strains following 8 h of induction in YPDU+Atc and overnight recovery in the YPDU medium alone, were diluted in 1x phosphate-buffered saline (PBS) and analyzed (~10⁶ cells) for the BFP/GFP marker by flow cytometry (FACS Aria III, BD Biosciences) at a rate of 7000-10,000 events/s. We used 405- and 488-nm lasers to excite the BFP and GFP fluorophores and 450/40 and 530/30 filters to detect the BFP and GFP emission signals, respectively.

96-well plasmid miniprep by boiling lysis method

Overnight grown cultures of *E. coli* in 96-deep well plate were pelleted down at 3,500 rpm for 15 min and the supernatant was discarded. The pellet was resuspended in 110 µl of lysis buffer (100 µl STET solution consisting of 8% sucrose, 0.5% Triton®X-100, 10ml of 0.5M EDTA (pH 8), 1ml of 1M Tris HCl (pH 8) and 10 µl of 10mg/ml lysozyme) using mixmate or multichannel pipette. The plate was incubated in boiling water bath for 40-60 seconds. Cells were pelleted at 3,500 rpm for 40 min at 4°C. The pellet was discarded using a sterile toothpick. To the leftover supernatant, 150 µl of isopropanol was added using multichannel pipette and the plate was gently mixed using mixmate. The plate was incubated at -20°C for an hour. Next, the plate was spun down at 3,500 rpm for an hour at 4°C and the supernatant was discarded. The plate was allowed to air dry. Isolated DNA was resuspended in 50 µl of nuclease-free water. Quality of the plasmid DNA was checked following agarose gel electrophoresis and ethidium bromide staining.

***C. albicans* colony PCR**

A single colony of *C. albicans* was resuspended in 30 µl of 0.2% SDS in a microfuge tube. The tube was incubated in boiling water bath for 5 min. The tube was then spun down at 13,000 rpm, for a min. From the supernatant, 1 µl volume was used to set up the PCR reaction of 25 µl consisting of 1 µl 25% Triton®X-100.

Primary and secondary overexpression screening

To detect CIN at the BFP/GFP locus upon P_{TET} activation, overnight grown cultures of *C. albicans* overexpression strains were reinoculated in CM-His-Arg to ensure all cells contained *HIS1*-BFP or *ARG4*-GFP. To measure the loss of BFP/GFP in 96-well plates, a *CDC20^{OE}* mutant was used as a positive control. The primary selection of the overexpression mutants with increased BFP⁺GFP⁻ and BFP⁻GFP⁺ fractions of cell population was done by determining the BFP/GFP loss frequency in EV. For this, we analyzed the flow cytometry density plots for 22 independent cultures of EV using the FlowJo software (FlowJo X 10.0.7r2). We observed a similar profile for all the cultures. We then defined gates for the BFP⁺GFP⁻ and BFP⁻GFP⁺ fractions of cell population in one of the EV samples and applied these gates to the rest of EV samples. The mean frequency of BFP⁺GFP⁻ and BFP⁻GFP⁺ cells in EV were calculated (Table 2.1). Similar gates were applied to all 1067 overexpression strains analyzed for BFP/GFP markers and frequency of BFP⁺GFP⁻ and BFP⁻GFP⁺ cells for each strain were determined (appendix). The overexpression mutants, in which the BFP/GFP loss frequency was \geq two-fold higher than EV, were selected for further analysis (Table 2.2).

For secondary screening, the overexpression plasmids present in each of the overexpression strains, identified from the primary screen (23 out of 1067), were used to retransform the CSA reporter strain (CEC5201). The overexpression strains (23) were analyzed by flow cytometry to revalidate the loss of BFP/GFP signals. Overexpression strains displaying ≥ 2 -fold higher frequency of BFP⁺GFP⁻/BFP⁻GFP⁺ population than EV (6 out of 23) were monitored for any morphological transition by microscopy. As filamentous morphotype could distort the BFP/GFP loss analysis (Loll-Krippleber et al. 2015), we characterized the overexpression mutants exhibiting increased CIN at the BFP/GFP locus and filamentous growth (3 out of 6) by monitoring cell cycle progression. For this, we transformed the overexpression plasmids in CaPJ159 and analyzed the overexpression strains (*CSA4^{MCM7}*, *CSA5^{BFA1}* and *CSA6*) for DNA content, nuclear segregation and SPB separation. The 6 genes identified from the secondary screen were verified for the correct *C. albicans* ORF by Sanger sequencing using a common primer PJ90. During the secondary screening, we also cultured overexpression mutants in YPDU without Atc and observed no differences between EV and uninduced (-Atc) cultures in terms of morphology and the BFP/GFP loss frequency.

Cell sorting and marker analysis

Overnight grown cultures of EV and overexpression mutants (*CDC20*, *CSA1^{CLB4}*, *CSA2^{ASE1}* and *CSA3^{KIP2}*) were reinoculated in YPDU+Atc for 8 h and allowed to recover overnight in YPDU-Atc. The cultures were analyzed for BFP/GFP loss by flow cytometry followed by fluorescence-activated cell sorting (FACS) using a cell sorter (FACSAria III, BD Biosciences) at a rate of 10,000 events/s. Approximately fifteen hundred cells from the BFP⁻GFP⁺ populations were collected into 1.5-ml tubes containing 400 μ l YPDU and immediately plated onto YPDU agar plates. Upon incubation at 30°C for 2 days, both small and large colonies appeared, as was reported earlier (46). As most small colonies are expected to have undergone loss of the Ch4B haplotype (46), we carried out marker analysis in large colonies to characterize the molecular mechanisms underlying CIN in the overexpression mutants.

For marker analysis, we replica plated the large colonies along with the appropriate controls on CM-Arg, CM-His and YPDU+Hyg B (800 μ g/ml) and incubated the plates at 30°C for 2 days. The colonies from CM-Arg plates were then analyzed for BFP, GFP and RFP markers by flow cytometry. For this, overnight grown cultures in YPDU were diluted in 1 \times PBS and 5000-10,000 cells were analyzed (FACSAria III, BD Biosciences). We used 405-, 488- and 561 nm lasers to excite the BFP, GFP and RFP fluorophores and 450/40, 530/30, 582/15 filters to detect the BFP, GFP and RFP emission signals, respectively.

Cell cycle analysis

Overnight grown cultures of *C. albicans* were reinoculated at an OD₆₀₀ of 0.2 in different media (as described previously) and harvested at various time intervals post-inoculation (as mentioned previously). The overnight grown culture itself was taken as a 0 h control sample for all the experiments. Harvested samples were processed for propidium iodide (PI) staining as described before (Sanyal and Carbon 2002). Stained cells were diluted to the desired cell density in 1x PBS and analyzed ($\geq 30,000$ cells) by flow cytometry (FACSAria III, BD Biosciences) at a rate of 250-1000 events/s. The output was analyzed using the FlowJo software (FlowJo X 10.0.7r2). We used 561-nm laser to excite PI and 610/20 filter to detect its emission signals.

Fluorescence microscopy

For nuclear division analysis in untagged strains, the *C. albicans* cells were grown overnight. The next day, the cells were transferred into different media (as mentioned previously) with a starting O.D.₆₀₀ of 0.2, collected at various time intervals (as described previously) and fixed with formaldehyde (3.7%). Cells were pelleted and washed twice with 1xPBS, and Hoechst dye (50 ng/ml) was added to the cell suspension before imaging. Nuclear division in Cse4- and Tub4-tagged strains was analyzed as described above, except the cells were not fixed with formaldehyde. For Tem1 and mitotic spindle localization, overnight grown cultures were transferred to different media (as mentioned previously) with a starting O.D.₆₀₀ of 0.2 and were grown for 6 h or 8 h. Cells were then washed, resuspended in 1x PBS and imaged on a glass slide. Localization studies of each, CaCsa6, Tub4, Spc110 and CdCsa6 was carried out by washing the log phase grown cultures with 1x PBS (three times) followed by image acquisition.

The microscopy images were acquired using fluorescence microscope (Zeiss Axio Observer 7 equipped with Colibri 7 as the LED light source), 100x Plan Apochromat 1.4 NA objective, pco. edge 4.2 sCMOS. We used Zen 2.3 (blue edition) for image acquisition and controlling all hardware components. Filter set 92 HE with excitation 455–483 and 583–600 nm for GFP and mCherry, respectively, and corresponding emission was captured at 501–547 and 617–758 nm. Z sections were obtained at an interval of 300 nm. All the images were displayed after the maximum intensity projection using ImageJ. Image processing was done using ImageJ. We used the cell counter plugin of ImageJ to count various cell morphologies in different mutant strains. Images acquired in the mCherry channel were processed using the subtract background plugin of ImageJ for better visualization.

Protein preparation and western blotting

Approximately 3 O.D.₆₀₀ equivalent cells were taken, washed with water once and resuspended in 12.5% TCA (trichloroacetic acid) and incubated at -20°C overnight for precipitation. The cells were pelleted down and washed twice with ice-cold 80% acetone. The pellet was then allowed to air dry and finally resuspended in lysis buffer (0.1N NaOH and 1% SDS and 5xprotein loading dye). Samples were boiled at 95°C for 10 min and electrophoresed on a 10% SDS polyacrylamide gel. Gels were transferred to a nitrocellulose membrane by semi-dry method for 30 min at 25V and blocked for an hour in 5% non-fat milk in 1x PBS. Membranes were incubated with a 1:5000 dilution of rabbit anti-Protein A or

mouse anti-PSTAIRE in 2.5% non-fat milk in 1xPBS. Membranes were washed three times in 1x PBS-Tween (0.05%) and then exposed to a 1:10,000 dilution of either anti-mouse- or anti-rabbit-IgG horseradish peroxidase antibody in 2.5% non-fat milk in 1x PBS. Membranes were washed three times in 1x PBS-Tween (0.05%) and developed using chemiluminescence method.

Statistical analysis

Statistical significance of differences was calculated as mentioned in the figure legends with unpaired one-tailed *t*-test, paired one-tailed *t*-test, paired two-tailed *t*-test or one-way ANOVA with Bonferroni posttest. *P*-values ≥ 0.05 were considered as nonsignificant (n.s). Precise *P*-values of the corresponding figures are mentioned, if significant. All analyses were conducted using GraphPad Prism version Windows v5.00.

Table 5.1. Strains used in this study

Name (Description)	Genotype	Reference
SN148	<i>Δura3::imm434/Δura3::imm434</i> , <i>Δhis1::hisG/Δhis1::hisG</i> , <i>Δarg4::hisG/Δarg4::hisG</i> , <i>Δleu2::hisG/Δleu2::hisG</i>	(Noble and Johnson 2005)
YJB8675	<i>Δura3::imm434/Δura3::imm434</i> , <i>Δhis1::hisG/Δhis1::hisG</i> , <i>Δarg4::hisG/Δarg4::hisG</i> , <i>CSE4-GFPCSE4/CSE4</i>	(Joglekar et al. 2008)
J110	SN148 <i>mad2::ARG4/mad2::LEU2</i>	(Thakur and Sanyal 2011)
CEC3867	SN148 <i>Ca21ch4_C_albicans_SC5314:473390 to 476401Δ::PTDH3-GFP-ARG4/Ca21ch4_C_albicans_SC5314:47339</i>	(Feri et al. 2016)

	<i>0 to 476401Δ::PTDH3-BFP-HIS1, ADH1/adh1::PTDH3-cartTA-SAT1</i>	
CAKS102	SN148 <i>CSE4/CSE4-TAP::URA3</i>	(Mitra et al. 2014)
Cd36 (<i>C. dubliniensis</i> prototroph)	<i>URA3/URA3</i> (clinical isolate)	(Thakur and Sanyal 2013)
CEC5201 (CSA reporter)	CEC3867 <i>Ca22ch4_C_albicans_SC5314:1452840 to 1453029Δ::P_{TDH3}-RFP-Hyg^R/Ca22ch4_C_albicans_SC5314:1452840 to 1453029</i>	This study
CaPJ148 (Mono-BFP)	SN148 <i>Ca21ch4_C_albicans_SC5314:473390 to 476401Δ::PTDH3-BFP-HIS1/Ca21ch4_C_albicans_SC5314:473390 to 476401</i>	This study
CaPJ149 (Mono-GFP)	SN148 <i>Ca21ch4_C_albicans_SC5314:473390 to 476401Δ::PTDH3-GFP-ARG4/Ca21ch4_C_albicans_SC5314:473390 to 476401</i>	This study
CaPJ150 (EV in CSA reporter)	CEC5201 <i>RPS1/RPS1::PTET-GtwB-URA3</i>	This study
CaPJ151 (<i>CDC20^{OE}</i> in CSA reporter)	CEC5201 <i>RPS1/RPS1::PTET-CDC20-URA3</i>	This study
CaPJ152 (<i>CSA1^{CLB4}</i> overexpression in CSA reporter)	CEC5201 <i>RPS1/RPS1::PTET-CLB4-URA3</i>	This study
CaPJ153 (<i>CSA2^{ASE1}</i> overexpression in CSA reporter)	CEC5201 <i>RPS1/RPS1::PTET-ASE1-URA3</i>	This study
CaPJ154 (<i>CSA3^{KIP2}</i> overexpression in CSA reporter)	CEC5201 <i>RPS1/RPS1::PTET-KIP2-URA3</i>	This study
CaPJ155 (<i>CSA4^{MCM7}</i> overexpression in CSA reporter)	CEC5201 <i>RPS1/RPS1::PTET-MCM7-URA3</i>	This study

CaPJ156 (<i>CSA5^{BFAI}</i> overexpression in CSA reporter)	CEC5201 <i>RPS1/RPS1::PTET-BFAI-URA3</i>	This study
CaPJ157 (<i>CSA6^{OE}</i> in CSA reporter)	CEC5201 <i>RPS1/RPS1::PTET-CSA6-URA3</i>	This study
CaPJ158	YJB8675 <i>ADH1/adh1::PTDH3-cartTA-SAT1</i>	This study
CaPJ159	CaPJ158 <i>TUB4/TUB4-mCherry::ARG4</i>	This study
CaPJ160 (EV in <i>CSE4-GFP</i> , <i>TUB4-mCherry</i>)	CaPJ159 <i>RPS1/RPS1::PTET-GtwB-URA3</i>	This study
CaPJ165 (<i>CSA4^{MCM7}</i> overexpression in <i>CSE4-GFP</i> , <i>TUB4-mCherry</i>)	CaPJ159 <i>RPS1/RPS1::PTET-MCM7-URA3</i>	This study
CaPJ166 (<i>CSA5^{BFAI}</i> overexpression in <i>CSE4-GFP</i> , <i>TUB4-mCherry</i>)	CaPJ159 <i>RPS1/RPS1::PTET-BFAI-URA3</i>	This study
CaPJ167 (<i>CSA6^{OE}</i> in <i>CSE4-GFP</i> , <i>TUB4-mCherry</i>)	CaPJ159 <i>RPS1/RPS1::PTET-CSA6-URA3</i>	This study
CaPJ169	SN148 <i>ADH1/adh1::PTDH3-cartTA-SAT1</i>	This study
CaPJ180 (<i>CSA6-TAP</i>)	SN148 <i>CSA6/CSA6-TAP::ARG4</i>	This study
CaPJ181 (<i>PTETCSA6-TAP</i>)	CaPJ169 <i>RPS1/RPS1::PTET-CSA6-TAP-URA3</i>	This study
CaPJ170 (EV in SN148)	CaPJ169 <i>RPS1/RPS1::PTET-GtwB-URA3</i>	This study
CaPJ176 (<i>CSA6^{OE}</i> in SN148)	CaPJ169 <i>RPS1/RPS1::PTET-CSA6-URA3</i>	This study
CaPJ162	YJB8675 <i>TUB1/TUB1-mCherry::HIS1</i>	This study
CaPJ163	CaPJ162 <i>ADH1/adh1::PTDH3-cartTA-SAT1</i>	This study
CaPJ182 (EV in <i>CSE4-GFP</i>)	CaPJ163 <i>RPS1/RPS1::PTET-GtwB-URA3</i>	This study
CaPJ183 (<i>CSA6^{OE}</i> in <i>CSE4-GFP</i>)	CaPJ163 <i>RPS1/RPS1::PTET-CSA6-URA3</i>	This study
CaPJ173 (<i>CSE4-TAP</i> in EV)	CaPJ170 <i>CSE4/CSE4-TAP::LEU2</i>	This study
CaPJ179 (<i>CSE4-TAP</i> in <i>CSA6^{OE}</i>)	CaPJ176 <i>CSE4/CSE4-TAP::LEU2</i>	This study
CaPJ171 (EV in <i>TUB4-GFP</i>)	CaPJ170 <i>TUB4/TUB4-GFP::HIS1</i>	This study

CaPJ172 (EV in <i>TUB4-GFP</i> , <i>TUB1-mCherry</i>)	CaPJ170 <i>TUB4/TUB4-GFP::HIS1</i> , <i>TUB1/TUB1-mCherry::ARG4</i>	This study
CaPJ177 (<i>CSA6^{OE}</i> in <i>TUB4-GFP</i>)	CaPJ176 <i>TUB4/TUB4-GFP::HIS1</i>	This study
CaPJ178 (<i>CSA6^{OE}</i> in <i>TUB4-GFP</i> , <i>TUB1-mCherry</i>)	CaPJ177 <i>TUB1/TUB1-mCherry::ARG4</i>	This study
CaPJ196	CaJ110 <i>ADH1/adh1::PTDH3-cartTA-SAT1</i>	This study
CaPJ197 (<i>CSA6^{OE}</i> in <i>mad2</i>)	CaPJ196 <i>RPS1/RPS1::PTET-CSA6-URA3</i>	This study
CaPJ198 (<i>CSA6^{OE}</i> in <i>mad2</i> , <i>TUB4-GFP</i>)	CaPJ197 <i>TUB4/TUB4-GFP::HIS1</i>	This study
CaPJ109	SN148 <i>bub2::FRT/BUB2</i>	This study
CaPJ110	SN148 <i>bub2::FRT/ bub2::FRT</i>	This study
CaPJ199	CaPJ110 <i>ADH1/adh1::PTDH3-cartTA-SAT1</i>	This study
CaPJ200 (<i>CSA6^{OE}</i> in <i>bub2</i>)	CaPJ199 <i>RPS1/RPS1::PTET-CSA6-URA3</i>	This study
CaPJ209 (<i>CSA6</i> heterozygous null in SN148)	SN148 <i>csa6::FRT/CSA6</i>	This study
CaPJ210 (<i>CSA6^{PSD}</i> in SN148)	SN148 <i>csa6::FRT/MET3prCSA6::URA3</i>	This study
CaPJ212 (<i>P_{MET3}CSA6-TAP</i>)	SN148 <i>csa6::FRT/MET3prCSA6-TAP-ARG4::URA3</i>	This study
CaPJ113	YJB8675 <i>csa6::FRT/CSA6</i>	This study
CaPJ213 (<i>CSA6^{PSD}</i> in <i>CSE4-GFP</i>)	YJB8675 <i>csa6::FRT/MET3prCSA6::URA3</i>	This study
CaPJ214 (<i>CSE4-TAP</i> in <i>CSA6^{PSD}</i>)	CaPJ210 <i>CSE4/CSE4-TAP::LEU2</i>	This study
CaPJ211 (<i>CSA6^{PSD}</i> in <i>TUB4-GFP</i> , <i>TUB1-mCherry</i>)	CaPJ210, <i>TUB4/TUB4-GFP::HIS1</i> , <i>TUB1/TUB1-mCherry::ARG4</i>	This study
CaPJ216 (<i>SOL1-TAP</i>)	SN148 <i>SOL1/SOL1-TAP::HIS1</i>	This study
CaPJ217 (<i>P_{TET}SOL1-TAP</i>)	CaPJ169 <i>RPS1/RPS1::PTET-SOL1-TAP-URA3</i>	This study

CaPJ215 (<i>CSA6^{PSD}</i> in <i>SOL1^{OE}</i>)	SN148 <i>csa6::FRT/MET3prCSA6::HIS1</i> , <i>ADH1/adh1::PTDH3-cartTA-SAT1</i> , <i>RPS1/RPS1::PTET-SOL1-URA3</i>	This study
CaPJ218 (<i>TEM1-GFP</i> in <i>CSA6^{PSD}</i>)	SN148 <i>csa6::FRT/MET3prCSA6::URA3</i> , <i>TUB4/TUB4-mCherry::NAT</i> , <i>TEM1/TEM1-GFP::HIS1</i>	This study
CaPJ119 (<i>CSA6-mCherry</i> in <i>CSE4-GFP</i>)	YJB8675 <i>CSA6/CSA6-mCherry::ARG4</i>	This study
CaPJ117	SN148 <i>csa6::FRT/CSA6-mCherry::ARG4</i>	This study
CaPJ118	SN148 <i>CSA6/CSA6-mCherry::ARG4</i>	This study
CaPJ120 (<i>CSA6-mCherry</i> in <i>TUB4-GFP</i>)	CaPJ118 <i>TUB4/TUB4-GFP::HIS1</i>	This study
CaPJ121 (<i>CSA6-mCherry</i> in <i>SPC110-GFP</i>)	CaPJ118 <i>SPC110/SPC110-GFP::HIS1</i>	This study
CaPJ300	CaPJ209 <i>TUB4/TUB4-mCherry::ARG4</i> + <i>pCdCSA6-GFP-ARS2::URA3</i>	This study
CaPJ301	SN148 <i>csa6::FRT/MET3prCSA6::HIS1</i> , <i>TUB4/TUB4-mCherry::ARG4</i>	This study
CaPJ302	SN148 <i>csa6::FRT/MET3prCSA6::HIS1</i> , <i>TUB4/TUB4-mCherry::ARG4</i> + <i>pCdCSA6-GFP-ARS2::URA3</i>	This study

Table 5.2. Primers used in this study

Name	Sequence	Description
RFP-PstI-F	AAACCCctgcagAAAGATGGTTTCT AAAGGTG	RFP-HygB K7
RFP-NheI-R	CCCAAagctagcCATATTATTATCT TCAGAAG	RFP-HygB K7
K7-BFP-GFP-Ch4- Right-F	TATATATTTCTGGGCAATGCAGC AATTCTCGGATATCACCGAAAA AAAAGATCTTAGCGGGCACGAC ACGACTCTCTTGATATAAGCGA ATTTTCAGTATCAGGAAACAGCT <u>ATGACC</u>	Integration of the RFP- HygB K7 on the right arm of Chr4
RFP-Insertion-Ch4- Right-Reverse	TCTCTATACGAGTTAAGAGTAGT CTTACAATAGTCTATAGATAGA ATTTCAGACCTTTTTGTGTGGGT ATTGCCGAAATTCTTTTTCCAGA AGATGACGAGAGAAAATACCCG <u>TGACG</u>	Integration of the RFP- HygB K7 on the right arm of Chr4
PJ86	ACAAGCTTATTGAGTGACGAAA AGTC	Confirmation of pNIMX integration
PJ87	TTACGGGTTGTTAAACCTTCGA TTC	
PJ88	ATACTACTGAAAATTTCTGACT TTC	Confirmation of overexpression plasmid integration
PJ89	ATTACTATTTACAATCAAAGGTG GTC	
PJ90	ATCAACAAGTTTGTACAAA	Sequencing of overexpression plasmid
SR149	CgcACTAGTATGGTTTCAAAGG TGAAGAAG	Amplification of mCherry- coding gene
SR150	ggaCCCGGGACCCAGAAAGCATT CATCGCG	

LS39FP	TCCCCGCGGGATCGATATAAAA CTAATCGTGTTAG	C-term tagging of Tub4 with GFP/mCherry
LS39RP	GGACTAGTTATACCCATATCTGC ATCATCTATATTG	
PJ77	tataCCGCGGACTGTTCAATTAGTC GATTGGTGTC	C-term tagging of Tub1 with mCherry
PJ78	atatACTAGTATATTCTTCTTCTTC TTCAGGGAAAG	
NV241	TAA GGG CCC CCA GCT GCT ACT TCC TC	C-term tagging of Cse4 with TAP
NV242	acgc GTCGAC GGCCAATTATAAATGTGAAGGG	
PJ108	atatAGATCTAATAAGAATACGCT ATCTCC	C-term tagging of Csa6 with TAP
PJ109	atatTTAATTAAGTTAGAACGACC CATAAATTC	
NV34	GAGCACGTATTGGGTTTGC	Confirmation of TAP cassette integration
PJ127	atatGATATCATGGAAGATTCAAC TGAAGATATAATTA	Cloning of <i>CSA6TAP</i> under P_{TET}
PJ128	atatGATATCTCACTGATGATTCGC GTC	
PJ110	atatGGTACCAATGCTAGTAGGGT CTAGAC	Deletion cassette for <i>BUB2</i>
PJ111	atatCTCGAGTTTGTATCGGAAGG ATGTAG	
PJ112	atatCCGCGGATCAATTCTGCACA TGGTATG	
PJ113	atatGAGCTCTTGCCTAATAAGAC GCCAATTC	
PJ114	atatCCGCGGATATACGCTTTCCT TCG	

PJ115	atatGAGCTCAATTCTTTAGGAACT TTTCTATCG	
PJ116	AGTCTTGAACGAAAAAGTCTAG	
PJ3	CTATTCTCTAGAAAGTATAGGA ACTTC	Confirmation of pPSFS2a integration
PJ118	acgcctaacatatgtgaagtg	
PJ95	atatGGTACCAAGAAGCATGTGGT ATGAAGCAC	
PJ96	atatCTCGAGTTGTGTCGGTCTGTA CGTG	
PJ97	atatCCGCGGGTGGGTAGGTTACA CAGAGTC	Deletion cassette for <i>CSA6</i>
PJ98	atatGAGCTCTGGTCCACTACAAC CCCTTTTG	
PJ99	TGGCTGATATGGCTCATTG	
PJ93	atgtGGATCCATGGAAGATTCAAC TGAAGATATAATTA	Cloning of <i>CSA6</i> under <i>MET3</i>
PJ94	atctCTGCAGATTATATGCAGCAG ATTGAGAAGG	
PJ141	atatGGATCCATAACTCTTTCACGC AAGCTC	C-term tagging of <i>Sol1</i> with TAP
PJ142	atatTTAATTAATATATTATCAAAC GATAATCTCTTTGGTTTG	
PJ119	atatGATATCATGTCCTCTTCTAAT GATACACCATC	Cloning of <i>SOL1</i> under P_{TET}
PJ120	atatGATATCTTATATATTATCAAA CGATAATCTCTTTGGTTTG	
PJ121	atatCCGCGGACAAGAAAGTCTAC GCTAAATTC	
PJ122	atatACTAGTCTTATATATCAATAT GGGTTCCECCAC	C-term tagging of <i>Tem1</i> with GFP
PJ123	TGCTACCATTGGTCTCAAATGAT G	

PJ124	ccatacgcgaaagtagtg	Confirmation of GFP cassette integration
TEJ1	attaCCGCGGAATAAGAATACGCT ATCTCC	C-term tagging of Csa6 with mCherry
TEJ2	atgcACTAGTGTTAGAACGACCCA TAAATTC	
TEJ13	TCGAAGAAATGCTGTCC	
TEJ14	TCTTCTTCACCTTTTGAAACC	Confirmation of mCherry cassette integration
PJ106	atatCCGCGGAATTGAAGAAAGAG GTTCAAGAC	C-term tagging of Spc110 with GFP
PJ107	atatACTAGTATTGTATTTAAGTCT GGCCAC	
VS5	AGTCTCTAGACAAGTATTCAAC AATTTCTGTC	Ectopic expression of <i>C. dubliniensis</i> Csa6, tagged with GFP
VS6	GTGAAAAGTTCTTCTCCCTTACT CATATTGGAATGGCCCATAAATT CTG	
VS7	CAGAATTTATGGGCCATTCCAAT ATGAGTAAGGGAGSSGAACTTTT CAC	
VS8	AGTCCTGCAGGGGCATTTTATGA TGGAATGAATG	

Table 5.3. Plasmids used in this study

Name	Description	Reference
Cip10- <i>P_{TET}</i> -GTW derivatives	Overexpression plasmid collection	(Legrand et al. 2018)
pNIMX	Plasmid harbouring <i>P_{TET}</i> transactivator	(Chauvel et al. 2012)
pGFP-HIS	GFP-tagging plasmid	(Chatterjee et al. 2016)
pRFP-Arg4	mCherry-tagging plasmid	(Varshney and Sanyal 2019a)
pFA-TAP- <i>ARG4</i>	TAP-tagging plasmid	(Lavoie et al. 2008)
pFA-TAP- <i>HIS1</i>		
pSFS2a	Recyclable <i>SAT1</i> -flipper cassette	(Reuss et al. 2004)
pCaDis	Plasmid for promoter replacement with <i>MET3pr</i>	(Care et al. 1999)
pBSNAT	Plasmid used for cloning <i>NAT1</i>	(Thakur and Sanyal 2013)
pCaADH1-yEmRFP	Plasmid used for cloning mCherry	(Keppler-Ross et al. 2008)
pMad2-2	Plasmid used for cloning <i>CSE4-TAP</i> fragment	(Thakur and Sanyal 2011)
pNIM1R-RFP	Plasmid used for cloning RFP	(Prieto et al. 2014)
pTDH3-GFP-URA3	Plasmid used for generating the pTDH3-RFP-HygB plasmid	(Znaidi et al. 2018)
pAU34-CaHygB	Plasmid used for cloning HygB	(Basso et al. 2010)
pTub4-GFP-His	GFP-tagging plasmid for Tub4	This study
pTub4-mCherry-Arg4	mCherry-tagging plasmids for Tub4	This study
pTub4-mCherry-Nat		This study
pTub1-mCherry-Arg4	mCherry-tagging plasmid for Tub1	This study
pCse4-TAP-Leu	TAP-tagging plasmid for Cse4	This study
pCsa6-TAP-Arg	TAP-tagging plasmid for Csa6	This study
Cip10- <i>P_{TET}</i> -Csa6TAP	Overexpression plasmid for <i>CSA6-TAP</i>	This study

pBub2del#1	Deletion cassettes for <i>BUB2</i>	This study
pBub2del#2		This study
pCsa6del	Deletion cassette for <i>CSA6</i>	This study
pCsa6-Met3-Ura	Plasmids for promoter replacement of <i>CSA6</i> with <i>MET3</i>	This study
pCsa6-Met3-His		This study
CIp10- <i>P_{TET}</i> -SOL1	Overexpression plasmid for <i>SOL1</i>	This study
CIp10- <i>P_{TET}</i> -SOL1TAP	Overexpression plasmid for <i>SOL1-TAP</i>	This study
pTEM1-GFP-His	GFP-tagging plasmid for Tem1	This study
pCsa6-mCherry-Arg	mCherry-tagging plasmid for Csa6	This study
pSpcl10-GFP-His	GFP-tagging plasmid for Spcl10	This study
pCdCsa6-GFP-ARS2	Ectopic expression of GFP-tagged <i>C. dubliniensis</i> Csa6	This study

Chapter 6

References

- Adames NR, Cooper JA. 2000. Microtubule interactions with the cell cortex causing nuclear movements in *Saccharomyces cerevisiae*. *J Cell Biol* **149**: 863-874.
- Aguilera A, Gomez-Gonzalez B. 2008. Genome instability: a mechanistic view of its causes and consequences. *Nat Rev Genet* **9**: 204-217.
- Atir-Lande A, Gildor T, Kornitzer D. 2005. Role for the SCFDC4 ubiquitin ligase in *Candida albicans* morphogenesis. *Mol Biol Cell* **16**: 2772-2785.
- Augustine B, Chin CF, Yeong FM. 2018. Role of Kip2 during early mitosis - impact on spindle pole body separation and chromosome capture. *J Cell Sci* **131**.
- Bachewich C, Nantel A, Whiteway M. 2005. Cell cycle arrest during S or M phase generates polarized growth via distinct signals in *Candida albicans*. *Mol Microbiol* **57**: 942-959.
- Bardin AJ, Amon A. 2001. Men and sin: what's the difference? *Nat Rev Mol Cell Biol* **2**: 815-826.
- Barnum KJ, O'Connell MJ. 2014. Cell cycle regulation by checkpoints. *Methods Mol Biol* **1170**: 29-40.
- Basso LR, Jr., Bartiss A, Mao Y, Gast CE, Coelho PS, Snyder M, Wong B. 2010. Transformation of *Candida albicans* with a synthetic hygromycin B resistance gene. *Yeast* **27**: 1039-1048.
- Bates S. 2018. *Candida albicans* Cdc15 is essential for mitotic exit and cytokinesis. *Sci Rep* **8**: 8899.
- Baum M, Sanyal K, Mishra PK, Thaler N, Carbon J. 2006. Formation of functional centromeric chromatin is specified epigenetically in *Candida albicans*. *Proc Natl Acad Sci U S A* **103**: 14877-14882.
- Bell SP, Labib K. 2016. Chromosome Duplication in *Saccharomyces cerevisiae*. *Genetics* **203**: 1027-1067.
- Bennett RJ, Johnson AD. 2003. Completion of a parasexual cycle in *Candida albicans* by induced chromosome loss in tetraploid strains. *EMBO J* **22**: 2505-2515.
- Bensen ES, Clemente-Blanco A, Finley KR, Correa-Bordes J, Berman J. 2005. The mitotic cyclins Clb2p and Clb4p affect morphogenesis in *Candida albicans*. *Mol Biol Cell* **16**: 3387-3400.
- Berdal JE, Haagenen R, Ranheim T, Bjornholt JV. 2014. Nosocomial candidemia; risk factors and prognosis revisited; 11 years experience from a Norwegian secondary hospital. *PLoS One* **9**: e103916.
- Bijlani S, Thevandavakkam MA, Tsai HJ, Berman J. 2019. Autonomously Replicating Linear Plasmids That Facilitate the Analysis of Replication Origin Function in *Candida albicans*. *mSphere* **4**.
- Bloom J, Cross FR. 2007. Multiple levels of cyclin specificity in cell-cycle control. *Nat Rev Mol Cell Biol* **8**: 149-160.
- Bodakuntla S, Jijumon AS, Villablanca C, Gonzalez-Billault C, Janke C. 2019. Microtubule-Associated Proteins: Structuring the Cytoskeleton. *Trends Cell Biol* **29**: 804-819.
- Braun BR, Johnson AD. 1997. Control of filament formation in *Candida albicans* by the transcriptional repressor TUP1. *Science* **277**: 105-109.
- Brown GD, Denning DW, Gow NA, Levitz SM, Netea MG, White TC. 2012. Hidden killers: human fungal infections. *Sci Transl Med* **4**: 165rv113.
- Burrack LS, Applen SE, Berman J. 2011. The requirement for the Dam1 complex is dependent upon the number of kinetochore proteins and microtubules. *Curr Biol* **21**: 889-896.
- Burrack LS, Hutton HF, Matter KJ, Clancey SA, Liachko I, Plemmons AE, Saha A, Power EA, Turman B, Thevandavakkam MA et al. 2016. Neocentromeres Provide Chromosome Segregation Accuracy and Centromere Clustering to Multiple Loci along a *Candida albicans* Chromosome. *PLoS Genet* **12**: e1006317.
- Cannon RD, Jenkinson HF, Shepherd MG. 1990. Isolation and nucleotide sequence of an autonomously replicating sequence (ARS) element functional in *Candida albicans* and *Saccharomyces cerevisiae*. *Mol Gen Genet* **221**: 210-218.
- Care RS, Trevethick J, Binley KM, Sudbery PE. 1999. The MET3 promoter: a new tool for *Candida albicans* molecular genetics. *Mol Microbiol* **34**: 792-798.
- Carmena M, Pinson X, Platani M, Salloum Z, Xu Z, Clark A, Macisaac F, Ogawa H, Eggert U, Glover DM et al. 2012. The chromosomal passenger complex activates Polo kinase at centromeres. *PLoS Biol* **10**: e1001250.

- Cavanaugh AM, Jaspersen SL. 2017. Big Lessons from Little Yeast: Budding and Fission Yeast Centrosome Structure, Duplication, and Function. *Annu Rev Genet* **51**: 361-383.
- Caydasi AK, Ibrahim B, Pereira G. 2010. Monitoring spindle orientation: Spindle position checkpoint in charge. *Cell Div* **5**: 28.
- Caydasi AK, Pereira G. 2012. SPOC alert--when chromosomes get the wrong direction. *Exp Cell Res* **318**: 1421-1427.
- Chatterjee G, Sankaranarayanan SR, Guin K, Thattikota Y, Padmanabhan S, Siddharthan R, Sanyal K. 2016. Repeat-Associated Fission Yeast-Like Regional Centromeres in the Ascomycetous Budding Yeast *Candida tropicalis*. *PLoS Genet* **12**: e1005839.
- Chatterjee N, Walker GC. 2017. Mechanisms of DNA damage, repair, and mutagenesis. *Environ Mol Mutagen* **58**: 235-263.
- Chauvel M, Nesseir A, Cabral V, Znaidi S, Goyard S, Bachellier-Bassi S, Firon A, Legrand M, Diogo D, Naulleau C et al. 2012. A versatile overexpression strategy in the pathogenic yeast *Candida albicans*: identification of regulators of morphogenesis and fitness. *PLoS One* **7**: e45912.
- Chibana H, Beckerman JL, Magee PT. 2000. Fine-resolution physical mapping of genomic diversity in *Candida albicans*. *Genome Res* **10**: 1865-1877.
- Chibana H, Magee PT. 2009. The enigma of the major repeat sequence of *Candida albicans*. *Future Microbiol* **4**: 171-179.
- Chiou JG, Balasubramanian MK, Lew DJ. 2017. Cell Polarity in Yeast. *Annu Rev Cell Dev Biol* **33**: 77-101.
- Chung CT, Niemela SL, Miller RH. 1989. One-step preparation of competent *Escherichia coli*: transformation and storage of bacterial cells in the same solution. *Proc Natl Acad Sci U S A* **86**: 2172-2175.
- Clemente-Blanco A, Gonzalez-Novo A, Machin F, Caballero-Lima D, Aragon L, Sanchez M, de Aldana CR, Jimenez J, Correa-Bordes J. 2006. The Cdc14p phosphatase affects late cell-cycle events and morphogenesis in *Candida albicans*. *J Cell Sci* **119**: 1130-1143.
- Cortez D. 2015. Preventing replication fork collapse to maintain genome integrity. *DNA Repair (Amst)* **32**: 149-157.
- Daga RR, Chang F. 2005. Dynamic positioning of the fission yeast cell division plane. *Proc Natl Acad Sci U S A* **102**: 8228-8232.
- Daga RR, Yonetani A, Chang F. 2006. Asymmetric microtubule pushing forces in nuclear centering. *Curr Biol* **16**: 1544-1550.
- De Wulf P, McAinsh AD, Sorger PK. 2003. Hierarchical assembly of the budding yeast kinetochore from multiple subcomplexes. *Genes Dev* **17**: 2902-2921.
- Duffy S, Fam HK, Wang YK, Styles EB, Kim JH, Ang JS, Singh T, Larionov V, Shah SP, Andrews B et al. 2016. Overexpression screens identify conserved dosage chromosome instability genes in yeast and human cancer. *Proc Natl Acad Sci U S A* **113**: 9967-9976.
- Dunn MJ, Kinney GM, Washington PM, Berman J, Anderson MZ. 2018. Functional diversification accompanies gene family expansion of MED2 homologs in *Candida albicans*. *PLoS Genet* **14**: e1007326.
- Fachinetti D, Folco HD, Nechemia-Arbely Y, Valente LP, Nguyen K, Wong AJ, Zhu Q, Holland AJ, Desai A, Jansen LE et al. 2013. A two-step mechanism for epigenetic specification of centromere identity and function. *Nat Cell Biol* **15**: 1056-1066.
- Feri A, Loll-Krippléber R, Commere PH, Maufrais C, Sertour N, Schwartz K, Sherlock G, Bougnoux ME, d'Enfert C, Legrand M. 2016. Analysis of Repair Mechanisms following an Induced Double-Strand Break Uncovers Recessive Deleterious Alleles in the *Candida albicans* Diploid Genome. *mBio* **7**.
- Finkel JS, Mitchell AP. 2011. Genetic control of *Candida albicans* biofilm development. *Nat Rev Microbiol* **9**: 109-118.
- Finley KR, Berman J. 2005. Microtubules in *Candida albicans* hyphae drive nuclear dynamics and connect cell cycle progression to morphogenesis. *Eukaryot Cell* **4**: 1697-1711.

- Fitzpatrick DA, Logue ME, Stajich JE, Butler G. 2006. A fungal phylogeny based on 42 complete genomes derived from supertree and combined gene analysis. *BMC Evol Biol* **6**: 99.
- Forche A, Cromie G, Gerstein AC, Solis NV, Pisithkul T, Srida W, Jeffery E, Abbey D, Filler SG, Dudley AM et al. 2018. Rapid Phenotypic and Genotypic Diversification After Exposure to the Oral Host Niche in *Candida albicans*. *Genetics* **209**: 725-741.
- Forche A, Magee PT, Selmecki A, Berman J, May G. 2009. Evolution in *Candida albicans* populations during a single passage through a mouse host. *Genetics* **182**: 799-811.
- Fraschini R, Venturetti M, Chiroli E, Piatti S. 2008. The spindle position checkpoint: how to deal with spindle misalignment during asymmetric cell division in budding yeast. *Biochem Soc Trans* **36**: 416-420.
- Freire-Beneitez V, Price RJ, Tarrant D, Berman J, Buscaino A. 2016. *Candida albicans* repetitive elements display epigenetic diversity and plasticity. *Sci Rep* **6**: 22989.
- Friedman DZP, Schwartz IS. 2019. Emerging Fungal Infections: New Patients, New Patterns, and New Pathogens. *J Fungi (Basel)* **5**.
- Gonzalez-Novo A, Labrador L, Pablo-Hernando ME, Correa-Bordes J, Sanchez M, Jimenez J, Vazquez de Aldana CR. 2009. Dbf2 is essential for cytokinesis and correct mitotic spindle formation in *Candida albicans*. *Mol Microbiol* **72**: 1364-1378.
- Goodson HV, Jonasson EM. 2018. Microtubules and Microtubule-Associated Proteins. *Cold Spring Harb Perspect Biol* **10**.
- Guacci V, Hogan E, Koshland D. 1997. Centromere position in budding yeast: evidence for anaphase A. *Mol Biol Cell* **8**: 957-972.
- Guin K, Chen Y, Mishra R, Muzaki SRB, Thimmappa BC, O'Brien CE, Butler G, Sanyal A, Sanyal K. 2020a. Spatial inter-centromeric interactions facilitated the emergence of evolutionary new centromeres. *Elife* **9**.
- Guin K, Sreekumar L, Sanyal K. 2020b. Implications of the Evolutionary Trajectory of Centromeres in the Fungal Kingdom. *Annu Rev Microbiol* **74**: 835-853.
- Hartwell L, Nurse PM, Hunt RT. 2001. Milestones in cell division.
- Harwood AJ. 1996. The rapid boiling method for small-scale preparation of plasmid DNA. *Methods Mol Biol* **58**: 265-267.
- Hergovich A, Hemmings BA. 2012. Hippo signalling in the G2/M cell cycle phase: lessons learned from the yeast MEN and SIN pathways. *Semin Cell Dev Biol* **23**: 794-802.
- Hibbel A, Bogdanova A, Mahamdeh M, Jannasch A, Storch M, Schaffer E, Liakopoulos D, Howard J. 2015. Kinesin Kip2 enhances microtubule growth in vitro through length-dependent feedback on polymerization and catastrophe. *Elife* **4**.
- Hickman MA, Zeng G, Forche A, Hiraakawa MP, Abbey D, Harrison BD, Wang YM, Su CH, Bennett RJ, Wang Y et al. 2013. The 'obligate diploid' *Candida albicans* forms mating-competent haploids. *Nature* **494**: 55-59.
- Holmes AR, Tsao S, Ong SW, Lamping E, Niimi K, Monk BC, Niimi M, Kaneko A, Holland BR, Schmid J et al. 2006. Heterozygosity and functional allelic variation in the *Candida albicans* efflux pump genes CDR1 and CDR2. *Mol Microbiol* **62**: 170-186.
- Hotz M, Barral Y. 2014. The Mitotic Exit Network: new turns on old pathways. *Trends Cell Biol* **24**: 145-152.
- Hou H, Zhou Z, Wang Y, Wang J, Kallgren SP, Kurchuk T, Miller EA, Chang F, Jia S. 2012. Csi1 links centromeres to the nuclear envelope for centromere clustering. *J Cell Biol* **199**: 735-744.
- Howman EV, Fowler KJ, Newson AJ, Redward S, MacDonald AC, Kalitsis P, Choo KH. 2000. Early disruption of centromeric chromatin organization in centromere protein A (Cenpa) null mice. *Proc Natl Acad Sci U S A* **97**: 1148-1153.
- Huisman SM, Segal M. 2005. Cortical capture of microtubules and spindle polarity in budding yeast - where's the catch? *J Cell Sci* **118**: 463-471.

- Jackson AP, Gamble JA, Yeomans T, Moran GP, Saunders D, Harris D, Aslett M, Barrell JF, Butler G, Citiulo F et al. 2009. Comparative genomics of the fungal pathogens *Candida dubliniensis* and *Candida albicans*. *Genome Res* **19**: 2231-2244.
- Janke C, Ortiz J, Lechner J, Shevchenko A, Shevchenko A, Magiera MM, Schramm C, Schiebel E. 2001. The budding yeast proteins Spc24p and Spc25p interact with Ndc80p and Nuf2p at the kinetochore and are important for kinetochore clustering and checkpoint control. *EMBO J* **20**: 777-791.
- Jin QW, Fuchs J, Loidl J. 2000. Centromere clustering is a major determinant of yeast interphase nuclear organization. *J Cell Sci* **113 (Pt 11)**: 1903-1912.
- Joglekar AP, Bouck D, Finley K, Liu X, Wan Y, Berman J, He X, Salmon ED, Bloom KS. 2008. Molecular architecture of the kinetochore-microtubule attachment site is conserved between point and regional centromeres. *J Cell Biol* **181**: 587-594.
- Jones T, Federspiel NA, Chibana H, Dungan J, Kalman S, Magee BB, Newport G, Thorstenson YR, Agabian N, Magee PT et al. 2004. The diploid genome sequence of *Candida albicans*. *Proc Natl Acad Sci U S A* **101**: 7329-7334.
- Jordan MA, Wilson L. 2004. Microtubules as a target for anticancer drugs. *Nat Rev Cancer* **4**: 253-265.
- Juanes MA, Piatti S. 2016. The final cut: cell polarity meets cytokinesis at the bud neck in *S. cerevisiae*. *Cell Mol Life Sci* **73**: 3115-3136.
- Kaneva IN, Sudbery IM, Dickman MJ, Sudbery PE. 2019. Proteins that physically interact with the phosphatase Cdc14 in *Candida albicans* have diverse roles in the cell cycle. *Sci Rep* **9**: 6258.
- Keppler-Ross S, Noffz C, Dean N. 2008. A new purple fluorescent color marker for genetic studies in *Saccharomyces cerevisiae* and *Candida albicans*. *Genetics* **179**: 705-710.
- Ketel C, Wang HS, McClellan M, Bouchonville K, Selmecki A, Lahav T, Gerami-Nejad M, Berman J. 2009. Neocentromeres form efficiently at multiple possible loci in *Candida albicans*. *PLoS Genet* **5**: e1000400.
- Kitamura E, Tanaka K, Kitamura Y, Tanaka TU. 2007. Kinetochore microtubule interaction during S phase in *Saccharomyces cerevisiae*. *Genes Dev* **21**: 3319-3330.
- Kixmoeller K, Allu PK, Black BE. 2020. The centromere comes into focus: from CENP-A nucleosomes to kinetochore connections with the spindle. *Open Biol* **10**: 200051.
- Kollman JM, Merdes A, Mourey L, Agard DA. 2011. Microtubule nucleation by gamma-tubulin complexes. *Nat Rev Mol Cell Biol* **12**: 709-721.
- Kollman JM, Polka JK, Zelter A, Davis TN, Agard DA. 2010. Microtubule nucleating gamma-TuSC assembles structures with 13-fold microtubule-like symmetry. *Nature* **466**: 879-882.
- Kops G, Snel B, Tromer EC. 2020. Evolutionary Dynamics of the Spindle Assembly Checkpoint in Eukaryotes. *Curr Biol* **30**: R589-R602.
- Koren A, Tsai HJ, Tirosh I, Burrack LS, Barkai N, Berman J. 2010. Epigenetically-inherited centromere and neocentromere DNA replicates earliest in S-phase. *PLoS Genet* **6**: e1001068.
- Kursel LE, Malik HS. 2016. Centromeres. *Curr Biol* **26**: R487-R490.
- Labib K, Tercero JA, Diffley JF. 2000. Uninterrupted MCM2-7 function required for DNA replication fork progression. *Science* **288**: 1643-1647.
- Lampson MA, Renduchitala K, Khodjakov A, Kapoor TM. 2004. Correcting improper chromosome-spindle attachments during cell division. *Nat Cell Biol* **6**: 232-237.
- Lara-Gonzalez P, Westhorpe FG, Taylor SS. 2012. The spindle assembly checkpoint. *Curr Biol* **22**: R966-980.
- Lavoie H, Sellam A, Askew C, Nantel A, Whiteway M. 2008. A toolbox for epitope-tagging and genome-wide location analysis in *Candida albicans*. *BMC Genomics* **9**: 578.
- Lee SE, Frenz LM, Wells NJ, Johnson AL, Johnston LH. 2001. Order of function of the budding-yeast mitotic exit-network proteins Tem1, Cdc15, Mob1, Dbf2, and Cdc5. *Curr Biol* **11**: 784-788.

- Legrand M, Bachellier-Bassi S, Lee KK, Chaudhari Y, Tournu H, Arbogast L, Boyer H, Chauvel M, Cabral V, Maufrais C et al. 2018. Erratum: Generating genomic platforms to study *Candida albicans* pathogenesis. *Nucleic Acids Res* **46**: 8664.
- Legrand M, Chan CL, Jauert PA, Kirkpatrick DT. 2007. Role of DNA mismatch repair and double-strand break repair in genome stability and antifungal drug resistance in *Candida albicans*. *Eukaryot Cell* **6**: 2194-2205.
- Legrand M, Chan CL, Jauert PA, Kirkpatrick DT. 2011. The contribution of the S-phase checkpoint genes MEC1 and SGS1 to genome stability maintenance in *Candida albicans*. *Fungal Genet Biol* **48**: 823-830.
- Legrand M, Jaitly P, Feri A, d'Enfert C, Sanyal K. 2019. *Candida albicans*: An Emerging Yeast Model to Study Eukaryotic Genome Plasticity. *Trends Genet* **35**: 292-307.
- Lephart PR, Chibana H, Magee PT. 2005. Effect of the major repeat sequence on chromosome loss in *Candida albicans*. *Eukaryot Cell* **4**: 733-741.
- Li R. 1999. Bifurcation of the mitotic checkpoint pathway in budding yeast. *Proc Natl Acad Sci U S A* **96**: 4989-4994.
- Lin TC, Neuner A, Flemming D, Liu P, Chinen T, Jakle U, Arkowitz R, Schiebel E. 2016. MOZART1 and gamma-tubulin complex receptors are both required to turn gamma-TuSC into an active microtubule nucleation template. *J Cell Biol* **215**: 823-840.
- Lin TC, Neuner A, Schiebel E. 2015. Targeting of gamma-tubulin complexes to microtubule organizing centers: conservation and divergence. *Trends Cell Biol* **25**: 296-307.
- Liu H, Liang F, Jin F, Wang Y. 2008. The coordination of centromere replication, spindle formation, and kinetochore-microtubule interaction in budding yeast. *PLoS Genet* **4**: e1000262.
- Liu HY, Toyn JH, Chiang YC, Draper MP, Johnston LH, Denis CL. 1997. DBF2, a cell cycle-regulated protein kinase, is physically and functionally associated with the CCR4 transcriptional regulatory complex. *EMBO J* **16**: 5289-5298.
- Liu X, McLeod I, Anderson S, Yates JR, 3rd, He X. 2005. Molecular analysis of kinetochore architecture in fission yeast. *EMBO J* **24**: 2919-2930.
- Lo HJ, Kohler JR, DiDomenico B, Loebenberg D, Cacciapuoti A, Fink GR. 1997. Nonfilamentous *C. albicans* mutants are avirulent. *Cell* **90**: 939-949.
- Lockhart SR, Pujol C, Daniels KJ, Miller MG, Johnson AD, Pfaller MA, Soll DR. 2002. In *Candida albicans*, white-opaque switchers are homozygous for mating type. *Genetics* **162**: 737-745.
- Loll-Kripplbeber R, d'Enfert C, Feri A, Diogo D, Perin A, Marcet-Houben M, Bougnoux ME, Legrand M. 2014. A study of the DNA damage checkpoint in *Candida albicans*: uncoupling of the functions of Rad53 in DNA repair, cell cycle regulation and genotoxic stress-induced polarized growth. *Mol Microbiol* **91**: 452-471.
- Loll-Kripplbeber R, Feri A, Nguyen M, Maufrais C, Yansouni J, d'Enfert C, Legrand M. 2015. A FACS-optimized screen identifies regulators of genome stability in *Candida albicans*. *Eukaryot Cell* **14**: 311-322.
- Luca FC, Mody M, Kurischko C, Roof DM, Giddings TH, Winey M. 2001. *Saccharomyces cerevisiae* Mob1p is required for cytokinesis and mitotic exit. *Mol Cell Biol* **21**: 6972-6983.
- Magee BB, Magee PT. 2000. Induction of mating in *Candida albicans* by construction of MTL α and MTL α strains. *Science* **289**: 310-313.
- Magwene PM, Kayikci O, Granek JA, Reininga JM, Scholl Z, Murray D. 2011. Outcrossing, mitotic recombination, and life-history trade-offs shape genome evolution in *Saccharomyces cerevisiae*. *Proc Natl Acad Sci U S A* **108**: 1987-1992.
- Mahadevappa R, Neves H, Yuen SM, Bai Y, McCrudden CM, Yuen HF, Wen Q, Zhang SD, Kwok HF. 2017. The prognostic significance of Cdc6 and Cdt1 in breast cancer. *Sci Rep* **7**: 985.
- Mazouzi A, Velimezi G, Loizou JI. 2014. DNA replication stress: causes, resolution and disease. *Exp Cell Res* **329**: 85-93.
- McEachern MJ, Hicks JB. 1993. Unusually large telomeric repeats in the yeast *Candida albicans*. *Mol Cell Biol* **13**: 551-560.

- Mehrotra S, Mittra I. 2020. Origin of Genome Instability and Determinants of Mutational Landscape in Cancer Cells. *Genes (Basel)* **11**.
- Meitinger F, Palani S, Pereira G. 2012. The power of MEN in cytokinesis. *Cell Cycle* **11**: 219-228.
- Meraldi P, McAinsh AD, Rheinbay E, Sorger PK. 2006. Phylogenetic and structural analysis of centromeric DNA and kinetochore proteins. *Genome Biol* **7**: R23.
- Miki F, Kurabayashi A, Tange Y, Okazaki K, Shimanuki M, Niwa O. 2004. Two-hybrid search for proteins that interact with Sad1 and Kms1, two membrane-bound components of the spindle pole body in fission yeast. *Mol Genet Genomics* **270**: 449-461.
- Miller MG, Johnson AD. 2002. White-opaque switching in *Candida albicans* is controlled by mating-type locus homeodomain proteins and allows efficient mating. *Cell* **110**: 293-302.
- Milne SW, Cheetham J, Lloyd D, Shaw S, Moore K, Paszkiewicz KH, Aves SJ, Bates S. 2014. Role of *Candida albicans* Tem1 in mitotic exit and cytokinesis. *Fungal Genet Biol* **69**: 84-95.
- Mitra S, Gomez-Raja J, Larriba G, Dubey DD, Sanyal K. 2014. Rad51-Rad52 mediated maintenance of centromeric chromatin in *Candida albicans*. *PLoS Genet* **10**: e1004344.
- Morgan DO. 1997. Cyclin-dependent kinases: engines, clocks, and microprocessors. *Annu Rev Cell Dev Biol* **13**: 261-291.
- Musacchio A, Desai A. 2017. A Molecular View of Kinetochore Assembly and Function. *Biology (Basel)* **6**.
- Musacchio A, Salmon ED. 2007. The spindle-assembly checkpoint in space and time. *Nat Rev Mol Cell Biol* **8**: 379-393.
- Muzzey D, Schwartz K, Weissman JS, Sherlock G. 2013. Assembly of a phased diploid *Candida albicans* genome facilitates allele-specific measurements and provides a simple model for repeat and indel structure. *Genome Biol* **14**: R97.
- Nam HJ, Naylor RM, van Deursen JM. 2015. Centrosome dynamics as a source of chromosomal instability. *Trends Cell Biol* **25**: 65-73.
- Negrini S, Gorgoulis VG, Halazonetis TD. 2010. Genomic instability--an evolving hallmark of cancer. *Nat Rev Mol Cell Biol* **11**: 220-228.
- Noble SM, Gianetti BA, Witchley JN. 2017. *Candida albicans* cell-type switching and functional plasticity in the mammalian host. *Nat Rev Microbiol* **15**: 96-108.
- Noble SM, Johnson AD. 2005. Strains and strategies for large-scale gene deletion studies of the diploid human fungal pathogen *Candida albicans*. *Eukaryot Cell* **4**: 298-309.
- Ofir A, Kornitzer D. 2010. *Candida albicans* cyclin Clb4 carries S-phase cyclin activity. *Eukaryot Cell* **9**: 1311-1319.
- Pellman D, Bagget M, Tu YH, Fink GR, Tu H. 1995. Two microtubule-associated proteins required for anaphase spindle movement in *Saccharomyces cerevisiae*. *J Cell Biol* **130**: 1373-1385.
- Petr MA, Tulika T, Carmona-Marin LM, Scheibye-Knudsen M. 2020. Protecting the Aging Genome. *Trends Cell Biol* **30**: 117-132.
- Piel M, Tran PT. 2009. Cell shape and cell division in fission yeast. *Curr Biol* **19**: R823-827.
- Potapova TA, Zhu J, Li R. 2013. Aneuploidy and chromosomal instability: a vicious cycle driving cellular evolution and cancer genome chaos. *Cancer Metastasis Rev* **32**: 377-389.
- Potter SC, Luciani A, Eddy SR, Park Y, Lopez R, Finn RD. 2018. HMMER web server: 2018 update. *Nucleic Acids Res* **46**: W200-W204.
- Pray L. 2008. LH Hartwell's yeast: a model organism for studying somatic mutations and cancer. *Nature Education* **1**: 183.
- Prieto D, Roman E, Correia I, Pla J. 2014. The HOG pathway is critical for the colonization of the mouse gastrointestinal tract by *Candida albicans*. *PLoS One* **9**: e87128.
- Qiu YT, Wang WJ, Zhang B, Mei LL, Shi ZZ. 2017. MCM7 amplification and overexpression promote cell proliferation, colony formation and migration in esophageal squamous cell carcinoma by activating the AKT1/mTOR signaling pathway. *Oncol Rep* **37**: 3590-3596.

- Ren B, Yu G, Tseng GC, Cieply K, Gavel T, Nelson J, Michalopoulos G, Yu YP, Luo JH. 2006. MCM7 amplification and overexpression are associated with prostate cancer progression. *Oncogene* **25**: 1090-1098.
- Reuss O, Vik A, Kolter R, Morschhauser J. 2004. The SAT1 flipper, an optimized tool for gene disruption in *Candida albicans*. *Gene* **341**: 119-127.
- Richmond D, Rizkallah R, Liang F, Hurt MM, Wang Y. 2013. Slk19 clusters kinetochores and facilitates chromosome bipolar attachment. *Mol Biol Cell* **24**: 566-577.
- Riera A, Barbon M, Noguchi Y, Reuter LM, Schneider S, Speck C. 2017. From structure to mechanism—understanding initiation of DNA replication. *Genes Dev* **31**: 1073-1088.
- Ro HS, Song S, Lee KS. 2002. Bfa1 can regulate Tem1 function independently of Bub2 in the mitotic exit network of *Saccharomyces cerevisiae*. *Proc Natl Acad Sci U S A* **99**: 5436-5441.
- Rock JM, Amon A. 2009. The FEAR network. *Curr Biol* **19**: R1063-1068.
- Roy B, Burrack LS, Lone MA, Berman J, Sanyal K. 2011. CaMtw1, a member of the evolutionarily conserved Mis12 kinetochore protein family, is required for efficient inner kinetochore assembly in the pathogenic yeast *Candida albicans*. *Mol Microbiol* **80**: 14-32.
- Roy B, Varshney N, Yadav V, Sanyal K. 2013. The process of kinetochore assembly in yeasts. *FEMS Microbiol Lett* **338**: 107-117.
- Sachidanandam R, Weissman D, Schmidt SC, Kakol JM, Stein LD, Marth G, Sherry S, Mullikin JC, Mortimore BJ, Willey DL et al. 2001. A map of human genome sequence variation containing 1.42 million single nucleotide polymorphisms. *Nature* **409**: 928-933.
- Sanchez-Perez I, Renwick SJ, Crawley K, Karig I, Buck V, Meadows JC, Franco-Sanchez A, Fleig U, Toda T, Millar JB. 2005. The DASH complex and Klp5/Klp6 kinesin coordinate bipolar chromosome attachment in fission yeast. *EMBO J* **24**: 2931-2943.
- Sankaranarayanan SR, Ianiri G, Coelho MA, Reza MH, Thimmappa BC, Ganguly P, Vadnala RN, Sun S, Siddharthan R, Tellgren-Roth C et al. 2020. Loss of centromere function drives karyotype evolution in closely related *Malassezia* species. *Elife* **9**.
- Sanyal K, Baum M, Carbon J. 2004. Centromeric DNA sequences in the pathogenic yeast *Candida albicans* are all different and unique. *Proc Natl Acad Sci U S A* **101**: 11374-11379.
- Sanyal K, Carbon J. 2002. The CENP-A homolog CaCse4p in the pathogenic yeast *Candida albicans* is a centromere protein essential for chromosome transmission. *Proc Natl Acad Sci U S A* **99**: 12969-12974.
- Sau S, Sutradhar S, Paul R, Sinha P. 2014. Budding yeast kinetochore proteins, Chl4 and Ctf19, are required to maintain SPB-centromere proximity during G1 and late anaphase. *PLoS One* **9**: e101294.
- Saville SP, Lazzell AL, Monteagudo C, Lopez-Ribot JL. 2003. Engineered control of cell morphology in vivo reveals distinct roles for yeast and filamentous forms of *Candida albicans* during infection. *Eukaryot Cell* **2**: 1053-1060.
- Sawin KE, Tran PT. 2006. Cytoplasmic microtubule organization in fission yeast. *Yeast* **23**: 1001-1014.
- Scarfone I, Piatti S. 2015. Coupling spindle position with mitotic exit in budding yeast: The multifaceted role of the small GTPase Tem1. *Small GTPases* **6**: 196-201.
- Schar P. 2001. Spontaneous DNA damage, genome instability, and cancer—when DNA replication escapes control. *Cell* **104**: 329-332.
- Schleiden M. 1838. Beiträge zur phytogenesis, Arch. Anat. Physiol. Wiss Med.
- Schuyler SC, Liu JY, Pellman D. 2003. The molecular function of Ase1p: evidence for a MAP-dependent midzone-specific spindle matrix. Microtubule-associated proteins. *J Cell Biol* **160**: 517-528.
- Schwann T, Hünzeler F. 1910. *Mikroskopische Untersuchungen über die Ubereinstimmung in der Struktur und dem Wachstume der Tiere und Pflanzen*. W. Engelmann.
- Schwob E, Nasmyth K. 1993. CLB5 and CLB6, a new pair of B cyclins involved in DNA replication in *Saccharomyces cerevisiae*. *Genes Dev* **7**: 1160-1175.

- Segal ES, Gritsenko V, Levitan A, Yadav B, Dror N, Steenwyk JL, Silberberg Y, Mielich K, Rokas A, Gow NAR et al. 2018. Gene Essentiality Analyzed by In Vivo Transposon Mutagenesis and Machine Learning in a Stable Haploid Isolate of *Candida albicans*. *mBio* **9**.
- Selmecki A, Forche A, Berman J. 2006. Aneuploidy and isochromosome formation in drug-resistant *Candida albicans*. *Science* **313**: 367-370.
- Selmecki A, Forche A, Berman J. 2010. Genomic plasticity of the human fungal pathogen *Candida albicans*. *Eukaryot Cell* **9**: 991-1008.
- Selmecki A, Gerami-Nejad M, Paulson C, Forche A, Berman J. 2008. An isochromosome confers drug resistance in vivo by amplification of two genes, ERG11 and TAC1. *Mol Microbiol* **68**: 624-641.
- Shirayama M, Matsui Y, Toh EA. 1994. The yeast TEM1 gene, which encodes a GTP-binding protein, is involved in termination of M phase. *Mol Cell Biol* **14**: 7476-7482.
- Shivaraju M, Unruh JR, Slaughter BD, Mattingly M, Berman J, Gerton JL. 2012. Cell-cycle-coupled structural oscillation of centromeric nucleosomes in yeast. *Cell* **150**: 304-316.
- Silkworth WT, Nardi IK, Paul R, Mogilner A, Cimini D. 2012. Timing of centrosome separation is important for accurate chromosome segregation. *Mol Biol Cell* **23**: 401-411.
- Simanis V. 2015. Pombe's thirteen - control of fission yeast cell division by the septation initiation network. *J Cell Sci* **128**: 1465-1474.
- Sirbu BM, Cortez D. 2013. DNA damage response: three levels of DNA repair regulation. *Cold Spring Harb Perspect Biol* **5**: a012724.
- Skrzypek MS, Binkley J, Binkley G, Miyasato SR, Simison M, Sherlock G. 2017. The *Candida* Genome Database (CGD): incorporation of Assembly 22, systematic identifiers and visualization of high throughput sequencing data. *Nucleic Acids Res* **45**: D592-D596.
- Soll DR. 2002. *Candida* commensalism and virulence: the evolution of phenotypic plasticity. *Acta Trop* **81**: 101-110.
- Sopko R, Huang D, Preston N, Chua G, Papp B, Kafadar K, Snyder M, Oliver SG, Cyert M, Hughes TR et al. 2006. Mapping pathways and phenotypes by systematic gene overexpression. *Mol Cell* **21**: 319-330.
- Sreekumar L, Jaitly P, Chen Y, Thimmappa BC, Sanyal A, Sanyal K. 2019. Cis- and Trans-chromosomal Interactions Define Pericentric Boundaries in the Absence of Conventional Heterochromatin. *Genetics* **212**: 1121-1132.
- Sreekumar L, Kumari K, Guin K, Bakshi A, Varshney N, Thimmappa BC, Narlikar L, Padinhateeri R, Siddharthan R, Sanyal K. 2021. Orc4 spatiotemporally stabilizes centromeric chromatin. *Genome Res* **31**: 607-621.
- Sridhar S, Hori T, Nakagawa R, Fukagawa T, Sanyal K. 2021. Bridgin connects the outer kinetochore to centromeric chromatin. *Nat Commun* **12**: 146.
- Steenwyk JL, Phillips MA, Yang F, Date SS, Graham TR, Berman J, Hittinger CT, Rokas A. 2021. A gene coevolution network provides insight into eukaryotic cellular and genomic structure and function. *bioRxiv*.
- Stevenson LF, Kennedy BK, Harlow E. 2001. A large-scale overexpression screen in *Saccharomyces cerevisiae* identifies previously uncharacterized cell cycle genes. *Proc Natl Acad Sci U S A* **98**: 3946-3951.
- Surana U, Amon A, Dowzer C, McGrew J, Byers B, Nasmyth K. 1993. Destruction of the CDC28/CLB mitotic kinase is not required for the metaphase to anaphase transition in budding yeast. *EMBO J* **12**: 1969-1978.
- Takahashi K, Chen ES, Yanagida M. 2000. Requirement of Mis6 centromere connector for localizing a CENP-A-like protein in fission yeast. *Science* **288**: 2215-2219.
- Takeda DY, Dutta A. 2005. DNA replication and progression through S phase. *Oncogene* **24**: 2827-2843.

- Takeo S, Lake CM, Morais-de-Sa E, Sunkel CE, Hawley RS. 2011. Synaptonemal complex-dependent centromeric clustering and the initiation of synapsis in *Drosophila oocytes*. *Curr Biol* **21**: 1845-1851.
- Tamborrini D, Juanes MA, Ibanes S, Rancati G, Piatti S. 2018. Recruitment of the mitotic exit network to yeast centrosomes couples septin displacement to actomyosin constriction. *Nat Commun* **9**: 4308.
- Tanaka TU, Rachidi N, Janke C, Pereira G, Galova M, Schiebel E, Stark MJ, Nasmyth K. 2002. Evidence that the Ipl1-Sli15 (Aurora kinase-INCENP) complex promotes chromosome bi-orientation by altering kinetochore-spindle pole connections. *Cell* **108**: 317-329.
- Taylor AMR, Rothblum-Oviatt C, Ellis NA, Hickson ID, Meyer S, Crawford TO, Smogorzewska A, Pietrucha B, Weemaes C, Stewart GS. 2019. Chromosome instability syndromes. *Nat Rev Dis Primers* **5**: 64.
- Thakur J, Sanyal K. 2011. The essentiality of the fungus-specific Dam1 complex is correlated with a one-kinetochore-one-microtubule interaction present throughout the cell cycle, independent of the nature of a centromere. *Eukaryot Cell* **10**: 1295-1305.
- Thakur J, Sanyal K. 2012. A coordinated interdependent protein circuitry stabilizes the kinetochore ensemble to protect CENP-A in the human pathogenic yeast *Candida albicans*. *PLoS Genet* **8**: e1002661.
- Thakur J, Sanyal K. 2013. Efficient neocentromere formation is suppressed by gene conversion to maintain centromere function at native physical chromosomal loci in *Candida albicans*. *Genome Res* **23**: 638-652.
- Thomas G, Bain JM, Budge S, Brown AJP, Ames RM. 2020. Identifying *Candida albicans* Gene Networks Involved in Pathogenicity. *Front Genet* **11**: 375.
- Toyokawa G, Masuda K, Daigo Y, Cho HS, Yoshimatsu M, Takawa M, Hayami S, Maejima K, Chino M, Field HI et al. 2011. Minichromosome Maintenance Protein 7 is a potential therapeutic target in human cancer and a novel prognostic marker of non-small cell lung cancer. *Mol Cancer* **10**: 65.
- Tran PT, Marsh L, Doye V, Inoue S, Chang F. 2001. A mechanism for nuclear positioning in fission yeast based on microtubule pushing. *J Cell Biol* **153**: 397-411.
- Tsai HJ, Baller JA, Liachko I, Koren A, Burrack LS, Hickman MA, Thevandavakkam MA, Rusche LN, Berman J. 2014. Origin replication complex binding, nucleosome depletion patterns, and a primary sequence motif can predict origins of replication in a genome with epigenetic centromeres. *mBio* **5**: e01703-01714.
- Tso GHW, Reales-Calderon JA, Tan ASM, Sem X, Le GTT, Tan TG, Lai GC, Srinivasan KG, Yurieva M, Liao W et al. 2018. Experimental evolution of a fungal pathogen into a gut symbiont. *Science* **362**: 589-595.
- Tunyasuvunakool K, Adler J, Wu Z, Green T, Zielinski M, Zidek A, Bridgland A, Cowie A, Meyer C, Laydon A et al. 2021. Highly accurate protein structure prediction for the human proteome. *Nature* doi:10.1038/s41586-021-03828-1.
- Valerio-Santiago M, Monje-Casas F. 2011. Tem1 localization to the spindle pole bodies is essential for mitotic exit and impairs spindle checkpoint function. *J Cell Biol* **192**: 599-614.
- van het Hoog M, Rast TJ, Martchenko M, Grindle S, Dignard D, Hogues H, Cuomo C, Berriman M, Scherer S, Magee BB et al. 2007. Assembly of the *Candida albicans* genome into sixteen supercontigs aligned on the eight chromosomes. *Genome Biol* **8**: R52.
- van Jaarsveld RH, Kops G. 2016. Difference Makers: Chromosomal Instability versus Aneuploidy in Cancer. *Trends Cancer* **2**: 561-571.
- Varshney N, Sanyal K. 2019a. Aurora kinase Ipl1 facilitates bilobed distribution of clustered kinetochores to ensure error-free chromosome segregation in *Candida albicans*. *Mol Microbiol* **112**: 569-587.
- Varshney N, Sanyal K. 2019b. Nuclear migration in budding yeasts: position before division. *Curr Genet* **65**: 1341-1346.

- Vaziri C, Saxena S, Jeon Y, Lee C, Murata K, Machida Y, Wagle N, Hwang DS, Dutta A. 2003. A p53-dependent checkpoint pathway prevents rereplication. *Mol Cell* **11**: 997-1008.
- Walther A, Wendland J. 2003. An improved transformation protocol for the human fungal pathogen *Candida albicans*. *Curr Genet* **42**: 339-343.
- Wang Y, Hu F, Elledge SJ. 2000. The Bfa1/Bub2 GAP complex comprises a universal checkpoint required to prevent mitotic exit. *Curr Biol* **10**: 1379-1382.
- Waterman DP, Haber JE, Smolka MB. 2020. Checkpoint Responses to DNA Double-Strand Breaks. *Annu Rev Biochem* **89**: 103-133.
- Weinert TA, Hartwell LH. 1988. The RAD9 gene controls the cell cycle response to DNA damage in *Saccharomyces cerevisiae*. *Science* **241**: 317-322.
- Wijnen H, Landman A, Futcher B. 2002. The G(1) cyclin Cln3 promotes cell cycle entry via the transcription factor Swi6. *Mol Cell Biol* **22**: 4402-4418.
- Yurov YB, Vorsanova SG, Iourov IY. 2019. Chromosome Instability in the Neurodegenerating Brain. *Front Genet* **10**: 892.
- Zhang A, Petrov KO, Hyun ER, Liu Z, Gerber SA, Myers LC. 2012a. The Tlo proteins are stoichiometric components of *Candida albicans* mediator anchored via the Med3 subunit. *Eukaryot Cell* **11**: 874-884.
- Zhang Y, Foreman O, Wigle DA, Kosari F, Vasmataz G, Salisbury JL, van Deursen J, Galardy PJ. 2012b. USP44 regulates centrosome positioning to prevent aneuploidy and suppress tumorigenesis. *J Clin Invest* **122**: 4362-4374.
- Znaidi S, van Wijlick L, Hernandez-Cervantes A, Sertour N, Desseyn JL, Vincent F, Atanassova R, Gouyer V, Munro CA, Bachellier-Bassi S et al. 2018. Systematic gene overexpression in *Candida albicans* identifies a regulator of early adaptation to the mammalian gut. *Cell Microbiol* **20**: e12890.

Appendix

Results of the primary screen

ORF	Systematic name	Frequency of BFP⁺GFP⁻ cells (x10⁻⁵)	Frequency of BFP⁻GFP⁺ cells (x10⁻⁵)
19.2074	C2_00530W	6.5	4.3
19.2766	C4_02380W	7.2	62
19.3413	C6_01730W	8.5	54
19.4101	C2_06160W	9.3	5.5
19.5556	C6_02820W	7.3	6
19.67	C1_11330C	5	2.2
19.1821	C1_06290C	8.5	16
19.222	C2_08260W	7	6.1
19.3907	C5_04240C	5.8	16
19.3968	C5_04820W	8.6	17
19.4055	C5_05510C	10	11
19.4652	C4_01350W	6.7	3.6
19.6113	C1_00030C	7.9	4.5
19.4090.1	C2_09290W	9.4	3.6
19.670.2	C1_11320C	11	1.8
19.1008	CR_05270W	8.6	2.4
19.1778	C2_10040W	3.5	20
19.27	C3_02790W	9.9	31
19.3992	C5_05010W	6.5	19
19.4241	C5_02330W	13	24
19.5284	CR_05420W	4.4	3
19.533	CR_04430W	8.4	4
19.605	CR_07930C	4.7	2.6
19.7266	C1_14480W	5.4	2
19.741	C4_05120C	5.6	2.2
19.758	CR_10040W	8.4	1.6
19.1059	C1_04240C	7.9	22
19.1854	CR_06800C	6.8	24
19.2212	C2_07700C	7.8	20
19.3637	C2_08440W	8.6	6.4
19.4685	C4_01030W	4	3.7
19.517	CR_04290W	5.8	3.8
19.588	C5_00850C	3.3	2.5
19.6188	C3_07930C	4	2.3
19.7395	C3_06130W	4.5	21
19.596.2	CR_08010W	6.4	22
19.4132	C5_01420W	6.7	23
19.1482	C2_01710W	8.6	22
19.2061	C2_00670C	7.3	4.1
19.2645	C5_03340W	8	3.5
19.2704	C4_02910W	5.6	3.2
19.2992	C1_03010W	8.2	5.9
19.3748	CR_02230W	6.8	2.7
19.4146	C5_01510W	9	1.6

19.4509	C2_04430W	10	1.8
19.5606	C6_03190C	5.2	18
19.6062	C1_00460W	12	9.9
19.7271	C1_14530W	11	20
19.7348	C3_05670C	15	19
19.133	C6_01250W	10	4.1
19.1968	C5_01040W	7.2	4.9
19.3284	CR_00720W	11	5.2
19.5547	C6_02740W	7.1	4.3
19.5866	C3_04240C	8.4	1.7
19.6273	C1_06380C	7.7	1.1
19.6989	C3_05540C	5.8	1.8
19.7252	C1_14370W	7.8	42
19.728	CR_08850W	9.8	21
19.848	C2_03720W	8	28
19.934	C5_00550C	9.2	24
19.257	C3_02650W	13	6.2
19.2698	C4_02950C	8.2	6.2
19.6164	C3_00870W	8.6	3.8
19.6177	C3_07820W	6.7	3.3
19.6321	C6_00160W	6.8	3.8
19.653	CR_05000C	7.6	2.8
19.6575	C7_01530W	7.8	2.7
19.7188	C7_03920C	7.6	56
19.7603	CR_10280W	11	17
19.2754	C4_02480C	6.1	5.8
19.5503	C7_03740C	4.5	1.7
19.3016	C1_03240W	1.8	4.9
19.519	C7_02760W	3.5	6.6
19.5264	C1_12020W	4.9	8.3
19.544	CR_04540C	3.5	7.4
19.3113	C4_06960W	3.8	8.2
19.3528	C2_04960C	4.5	7.9
19.4143	C5_01480W	4.6	5.1
19.4623	C4_01710C	7.6	6.1
19.5308	C4_04020C	5.4	8.5
19.7007	C7_01060W	7.6	6.7
19.2483	C1_05680C	24	5.7
19.287	C4_06620C	3	7.3
19.3574	C2_05450C	3.1	5.5
19.4481	C1_04050C	3.2	4.2
19.5262	C1_12040W	4.2	6
19.6231	C1_06790C	5.9	5.8
19.6785	C3_07150C	10	9.2
19.1456	C2_01500W	6	8.9
19.2439	C1_06060C	4.9	7.7

19.392	C1_08470W	6.9	9.3
19.1136	C1_11800C	1.4	11
19.444	C1_05220C	3.7	10
19.4646	C4_01400W	3.1	7.8
19.6253	C1_06580W	3	7.3
19.7555	CR_09820C	6	9.9
19.909.1	C2_03210W	6.5	7.8
CAALFMP02	Mitochondrial gene	3.9	9.8
19.1349	C2_08340C	5.5	8.9
19.2283	C2_07260C	7.1	7.6
19.3134	C4_06750C	4.9	5.7
19.5666	C4_00390W	5	9.3
19.6897	C7_01130C	6.8	10
19.694	C3_03780W	7.1	13
19.7519	CR_00160C	2.3	3.7
19.3117	C4_06920C	11	8.8
19.3292	C1_01040W	9	11
19.3435	C6_01490C	7	5.7
19.397	C1_08520C	12	9.5
19.4439	C1_07290W	3.1	8.5
19.4522	C1_02030C	6.4	8.3
19.539	C3_00680C	3	5.1
19.725	C1_14350W	5.5	9
19.233.1	C3_02450W	4.4	7.7
19.1975	C5_00920W	7.1	5.7
19.2367	CR_06980W	20	6.4
19.2723	C4_02750W	5.8	4.7
19.3107	C4_07020C	11	5.7
19.3578	C2_05490W	3.2	6.8
19.3783	C4_04950W	19	7.2
19.515	CR_04270C	5.1	7.6
19.2018	C2_01060C	4.3	7.6
19.3533	C2_05020W	5.1	11
19.3712	CR_07830C	7.7	7.3
19.837	C2_03870W	6.8	12
19.2621	CR_07510W	8.2	6.6
19.2066.1	C2_00610C	32	7.2
19.1386	C2_09680W	3.9	5.2
19.4321	C5_02960C	5.1	5.7
19.4855	C1_09880C	3.9	10
19.5522	C6_02530C	7.4	4.7
19.6118	CR_07470W	38	39
19.836.1	C2_03880C	10	5
19.2125	C6_04420W	3.7	8.1
19.3294	C1_01060W	6.1	9.8
19.3925	C5_04390C	6.1	7.4

19.4185	C4_00580W	3.2	9
19.4311	C5_02890W	5.3	9.9
19.93	C6_00920W	4.8	9.2
19.4340.1	C5_03110C	33	39
19.2037	C2_00870W	6.5	10
19.2341	C1_10780C	15	8.7
19.6075	C1_00330C	7.9	8.9
19.1034	C1_03750W	7.5	8.9
19.3378	C4_03500C	3.7	5.5
19.422	C5_02140C	3.7	6
19.1352	C2_08310W	4.9	3.2
19.3271	CR_00840C	6.9	14
19.424	C1_05410C	5.3	10
19.4443	C1_07240W	5.4	9.1
19.4539	C1_01840C	4	5.7
19.5994	C3_05180W	2.6	6.6
19.6917	C7_01360C	3.6	5.9
19.7482	CR_00530W	2.1	3.7
19.2028	C2_00960C	2.5	7.3
19.24	C3_02500W	4	6.9
19.423	C1_05420W	3.4	7.1
19.4603	C4_01890C	8.5	12
19.5813	C2_02920W	5.2	9.5
19.647	C7_02390W	5.3	6.4
19.1681	C3_01620W	3.8	11
19.17	C3_01490W	4.6	7.5
19.3475	C6_02330W	20	8.3
19.2204.2	C2_07750W	3.8	6.2
19.6548	C7_01760C	5.8	4.8
19.679	C1_11230W	12	11
19.7097	C7_00250C	6.8	9
19.1448	C2_01430W	4.7	10
19.5402	C3_00590W	5.7	11
19.6196	C1_07080W	5.8	14
19.6246	C1_06650W	4.7	10
19.659	CR_09720W	7.9	13
19.6313.2	CR_04790W	14	11
19.275	C3_02840W	12	9.1
19.297	C3_03010C	8.9	27
19.334	C3_03370C	4.1	8.3
19.1552	C2_02320C	6.3	10
19.236	C3_02470C	5.9	7.7
19.39	C1_08450C	3.4	5.1
19.5063	C1_07900W	5.7	8.9
19.665	CR_05640C	4.8	11
19.7327	CR_09320C	6.4	9.6

19.735	C3_05710W	5.4	8.9
19.201	C2_09030W	7.4	8.1
19.1477	C2_01660C	8.9	14
19.4229	C5_02220C	57	3
19.1999	C2_01250W	33	44
19.2	C2_09040W	9.6	9.2
19.3087	C4_07180W	5.7	13
19.4566	C4_02240C	3.6	7
19.635	CR_04980C	5.6	7.5
19.1114	C5_03800W	6.8	10
19.3089	C4_07140W	6.9	11
19.3421.1	C6_01640W	35	47
19.5411	C3_00520W	8.6	12
19.3375	C4_03480C	5.2	8.4
19.3939	C5_04550W	26	8.01
19.4733	C1_08750W	20	9.31
19.6901	C7_01190W	21	13
19.2114	C2_00180C	15	11
19.3931	C5_04440C	46	11
19.4021	C5_05270C	17	11
19.4567	C4_02230C	19	7.74
19.465	C4_01370W	25	13
19.5364	C2_10810W	18	11
19.5973	C3_05030W	15	8.47
19.617	C3_07770C	27	14
19.1304	C4_03740W	19	10
19.232	C3_02440C	21	7.56
19.4864	C1_09980C	20	9.01
19.6341	C1_12810W	43	10
19.1043	C1_04110W	27	9.61
19.4112	C2_06080C	18	8.06
19.4537	C1_01860W	37	14
19.6284	CR_07660C	22	10
19.6445	CR_08690C	24	10
19.2089	C2_00420W	18	8.7
19.2468	C1_05830W	20	9.81
19.291	C3_02970C	17	12
19.2963	C1_02740C	19	7.64
19.4817	C1_09530W	19	8.23
19.1714	C3_01370C	21	12
19.2607	CR_02060W	21	10
19.4885	C1_10160W	24	7.89
19.6185	C3_07910W	20	9.19
19.7437	C3_06490W	19	10
19.3732	CR_02370W	23	11
19.4474	C1_03990W	11	13

19.4579	C4_02120W	23	8.33
19.7441	C3_06520C	19	7.09
19.778	C1_04680W	17	9.01
19.3504	C6_02070C	17	11
19.134	C7_03350C	17	14
19.1679	C3_01640C	12	11
19.1824	C1_06260W	11	11
19.4583	C4_02080W	18	12
19.5049	C1_07790C	20	9.49
19.6057	C1_00510W	17	12
19.6136	CR_07320C	17	12
19.7504	CR_00290W	19	10
19.1611	C3_02330C	18	10
19.3022	C1_03280W	13	14
19.715	C7_04230W	15	9.76
19.386	C1_08410C	15	9.99
19.5689	C5_00080C	24	9.58
19.6904	C7_01220W	17	11
19.4723	C1_08650C	15	8.93
19.544.1	CR_04550W	16	9.69
19.6582	C7_01470C	20	8.77
19.2381	CR_03410W	17	11
19.2726	C4_02720C	29	12
19.3293	C1_01050C	16	8.27
19.3676	C1_02190W	19	11
19.4952	C1_13250W	16	8.25
19.6948	C3_03710W	16	6.15
19.7015	C7_00990W	18	13
19.1637	C3_02090C	19	12
19.6588	C7_01410C	83	40
19.6637	CR_05750W	77	9.15
19.3861	CR_06080W	130	10
19.5472	C3_00040W	46	12
19.5611	C6_03240W	99	10
19.6923	C3_03930W	37	12
19.1048	C1_04140W	63	83
19.155	C2_04710C	48	14
19.1897	C2_07370W	32	15
19.2876	C4_06580W	72	9.22
19.3059	C1_03560C	31	29
19.5159	C7_03020C	110	18
19.5857	C3_04130W	49	11
19.6514	C7_02040C	160	10
19.1364	C2_09870W	25	10
19.1505	C2_01930C	63	13
19.243	C3_02540C	29	8.2

19.3929	C5_04420W	99	14
19.561	C6_03230W	67	11
19.6392	CR_08280W	56	12
19.2437	C1_06080C	25	8.4
19.324	CR_01140C	35	16
19.333	C1_01420C	40	6.2
19.3519	CR_05490W	71	7.22
19.5802	C2_03000C	41	15
19.1355	C2_09970C	68	17
19.2251	C2_06970W	78	12
19.5591	C6_03080C	37	13
19.7009	C7_01050W	50	9.22
19.1973	C5_00940C	33	11
19.364	C4_00020W	62	9.41
19.7643	CR_10600C	85	6.28
19.771	C1_04740W	50	9.16
19.1828	C1_06210W	35	7.56
19.3311	C1_01240W	49	9.01
19.4504	C2_04480W	47	8.73
19.4734	C1_08760W	53	11
19.5628	C6_03390W	75	13
19.5963	C3_04940W	24	9.64
19.6869	C2_05570C	74	7.73
19.1377	C2_09730C	64	7.9
19.2909	C4_06270C	96	6.5
19.2967	C1_02790W	100	10
19.4496	C2_04540C	96	10
19.4735	C1_08770W	62	10
19.5474	C3_00010C	66	11
19.5534	C6_02640C	73	17
19.5661	C4_00340W	79	11
19.6827	C3_06770W	100	8.12
19.71	C1_03690W	39	12
19.7296	CR_08990C	63	9.75
19.7411	C3_06220C	52	11
19.246	C1_05890W	58	13
19.3928	C5_04410C	4.97	4
19.567	C5_00690C	4.46	3.12
19.6899	C7_01170C	6.06	1.74
19.89	C6_00880W	9.6	4.27
19.2111	C2_00220C	7.71	0.231
19.468	C4_01090C	8.16	0.302
19.4844	C1_09790C	6.16	3.47
19.59	C1_05060W	5.21	2.84
19.7219	C1_14130W	4.54	2.87
19.1789.1	C4_05320W	5.38	0.922

19.2146	C6_04540C	11	4.22
19.3604	C2_08720W	8.8	0.969
19.5479	C2_06180C	16	9.96
19.568	C5_00700C	4.56	5.28
19.6068	C1_00400W	3.34	19
19.7088	C7_00330C	13	1.92
19.7231	C1_14220C	7.61	2.15
19.1095	C6_04360C	3.41	2.6
19.2127	C6_04430W	3.29	4.82
19.2799	C1_07460C	4.12	4.78
19.3457	C6_02170C	4.03	3.21
19.4293	C5_02730C	7.55	2.49
19.7297	CR_09010C	3.73	0.746
19.1156	C1_11630C	3.93	4.6
19.1911	C2_00100C	4.29	3.02
19.2262	C2_07070W	3.49	4.31
19.3438	C6_01460C	3.62	5.08
19.3873	CR_06180W	3.44	6.14
19.4121	C2_05990C	3.75	2.77
19.5764	C6_03890C	2.31	0.99
19.6082	C1_00210C	3.38	4.23
19.2344	C1_10740C	3.2	3.44
19.3127	C4_06820C	11	0.42
19.3365	C4_03380C	4.99	1.47
19.3583	C2_05530C	8.73	8.18
19.445	C1_05210C	8.2	2.01
19.4622	C4_01720C	4.92	1.58
19.5134	C7_03210W	4.23	3.91
19.5312	C4_04000W	3.62	3.45
19.6398	CR_08310C	8.63	29
19.657	C1_11450C	3.73	3.65
19.7391	C3_06090C	3.8	3.54
19.1167	C1_11530C	5.85	1.71
19.1682	C3_01610W	3.79	2.47
19.188	C2_07490W	6.53	7.02
19.2774	C4_02290W	10	13
19.3675	C1_02180W	10	9.29
19.3699	C7_02650W	11	8.72
19.5052	C1_07820W	14	8.08
19.767	C1_04770C	28	0.442
19.9	CR_07120C	11	6.41
19.5212	C2_05900W	32	36
19.1396	C2_09580W	53	39
19.4263	C5_02510C	14	5.23
19.554	CR_04630C	11	5.55
19.1515	C2_02010C	14	11

19.1639	C3_02070C	13	13
19.2166	C2_08190W	8.75	12
19.2835	CR_02770C	18	8.95
19.3115	C4_06940C	14	6.51
19.3151	C2_06710W	11	6.36
19.2309.2	C1_11060C	13	13
19.1461	C2_01540W	17	7.42
19.1601	C2_09430W	70	43
19.2735	C4_02640C	11	6.94
19.4177	C4_00650W	10	12
19.4414	C4_06040W	11	16
19.5413	C3_00500C	10	24
19.7203	C7_03790W	21	7.39
19.7539.1	CR_00040C	10	7.76
19.2257	C2_07010W	9.68	7.97
19.1053	C1_04190C	15	7.43
19.1617	C3_02290W	10	9.65
19.3643	C6_00810C	9.05	7.54
19.6052	C1_00560W	9.92	13
19.6344	C1_12780W	11	21
19.6524	C7_01970C	15	25
19.7095	C7_00270W	8.61	36
19.7422	C3_06370C	8.14	7.91
19.7522	CR_00130C	11	10
19.2107	C2_00260C	9.47	5.03
19.3793	C4_04860W	9.18	8.66
19.4731	C1_08730W	9.97	10
19.5714	C6_03490C	9.54	10
19.623	C1_06800W	7.34	6.16
19.6597	CR_09660W	11	6.64
19.7036	C7_00810W	29	14
19.732	CR_09220C	14	12
19.872	C2_03490C	9	11
19.2709	C4_02870C	11	14
19.3315	C1_01270W	11	16
19.7305	CR_09090C	17	25
19.7354	C3_05730C	17	11
19.2527	CR_01410C	14	24
19.3622	C2_08570W	21	11
19.363	C2_08480W	10	12
19.482	CR_04000W	9	14
19.4827	C1_09640W	13	21
19.6080	C1_00230C	140	190
19.69	C7_01180W	13	12
19.1773	C2_10080W	34	12
19.4015	C5_05220W	9	8

19.6982	C3_05440C	13	10
19.7567	CR_09930W	15	22
19.3123	C4_06870W	10	14
19.3848	CR_06010W	9	9
19.3914	C5_04290C	19	7
19.6784	C3_07160W	13	11
19.6908	C7_01280C	17	30
19.1665	C3_01810C	9	31
19.3333	C1_01470W	10	16
19.3572	C2_05400W	8	26
19.4809	C1_09460W	12	9
19.507	C1_07990C	14	12
19.6562	C7_01630W	11	10
19.7068	C7_00510W	17	10
19.3131	C4_06780C	17	12
19.378	C4_05000W	15	14
19.4606	C4_01870C	16	11
19.5537	C6_02670C	10	10
19.5572	C6_02940C	7	13
19.7495	CR_00380W	9	10
19.1362	C2_09890W	9	6
19.1543	C2_02250C	12	12
19.1948	C5_01220W	11	12
19.2591	CR_01920W	14	12
19.3198	C5_01770C	6	6
19.3476	C6_02340W	16	16
19.3705	CR_07770C	12	9
19.4007	C5_05150C	13	12
19.474	CR_03930C	13	9
19.5211	C2_05890C	8	12
19.1369	C2_09810C	12	11
19.3915	C5_04300C	12	10
19.4013	C5_05200C	14	14
19.5168	C7_02930C	24	17
19.7355	C3_05740C	13	14
19.854	C2_03640W	9	9
19.1299	C4_03790W	16	17
19.27	C2_06510W	7	7.9
19.3581	C2_05510C	13	12
19.5288	CR_05340C	12	9.1
19.7577	CR_10010C	20	12
19.118	C6_01110W	16	13
19.22	C2_07810W	17	12
19.4919	C1_12890W	18	10
19.5641	C4_00160C	9.5	8
19.5917	C3_04580C	11	13

19.618	C3_07850W	12	9
19.1589	C2_02630W	32	10
19.3554	C2_05250C	22	11
19.4595	C4_01970W	19	15
19.2324	C1_10930C	15	5.3
19.299	C1_02990C	15	13
19.4036	C5_05400W	14	7.6
19.5831	C2_02750C	14	11
19.5952	C3_04840C	12	12
19.6629	CR_05830C	10	7.9
19.3542	C2_05110W	24	10
19.6716	C3_07710W	19	8
19.278	C3_02870C	18	19
19.2923	C4_06140C	16	14
19.3158	C3_01190C	17	20
19.3758	C1_12580W	13	11
19.5933	C3_04730C	18	13
19.5989	C3_05150W	18	11
19.2982	C1_02910C	15	17
19.3945	C5_04610W	17	16
19.7648	CR_10640W	13	14
19.1754	C2_10260C	17	12
19.4117	C2_06030W	12	13
19.4589	C4_02040W	10	14
19.5418	C3_00470W	15	15
19.5457	C3_00160C	16	14
19.6209	C1_06980C	14	9
19.6905	C7_01230C	11	21
19.1536	C2_02200W	19	16
19.3045	C1_03440C	14	15
19.3281	CR_00750C	16	17
19.6531	C7_01900W	13	9
19.664	CR_05720W	11	17
19.1494	C2_01850W	17	11
19.6888	C2_05770W	14	25
19.1833	C1_10620W	16	14
19.3656	C6_00720C	13	14
19.4428	C1_07400C	13	15
19.5056	C1_07850C	13	12
19.6176	C3_07810C	21	25
19.6845	C1_04510W	17	12
19.2834	CR_02760C	12	15
19.4262	C5_02500C	14	12
19.4475	C1_04000C	13	11
19.481	CR_03990C	14	9
19.5282	C1_11850W	16	17

19.5499	C2_06350C	13	14
19.5672	C4_00430W	17	13
19.3054	C1_03520W	14	11
19.3447	C6_01370W	16	15
19.5205	C2_05820W	25	9.57
19.7313	CR_09170C	26	11
19.1553	C2_02340C	24	14
19.1759	C2_10220C	33	14
19.2343	C1_10760W	51	12
19.2558	CR_01670W	39	14
19.387	CR_06150C	47	14
19.3996	C5_05040W	58	14
19.4014	C5_05210W	74	16
19.4148	C5_01530C	120	16
19.4341	C5_03120W	24	10
19.5942	C3_04790W	20	8
19.6918	C7_01370W	34	12
19.7317	CR_09200C	19	15
19.19	C2_07360W	53	12
19.2137	C6_04510C	35	10
19.348	C6_02370C	33	15
19.2167	C2_08180C	35	17
19.2507	C3_01030W	37	13
19.3154	C3_01170W	37	11
19.542	CR_04510W	110	14
19.7593	CR_10170C	24	32
19.2044	C2_00800C	20	12
19.2326	C1_10910C	33	11
19.5535	C6_02650C	26	18
19.6229	C1_06810W	57	12
19.6404	CR_08370W	29	11
19.6884	C2_05730C	26	10
19.3567	C2_05360C	59	12
19.4265	C5_02530W	25	14
19.5117	C1_08360C	47	11
19.6639	CR_05730C	48	8
19.7186	C7_03940C	180	180
19.1789	C4_05310W	25	12
19.1934	C5_01340W	66	39
19.189	C2_07410W	48	10
19.245	C3_02560W	24	13
19.2494	C1_05610W	22	12
19.3218	C5_03940C	18	12
19.5043	C4_03880W	18	13
19.7081	C7_00390W	36	14
19.4284	C5_02670W	97	9.37

19.5859	C3_04160W	15	9.58
19.6781	C3_07200C	190	9.49
19.7094	C7_00280W	26	8.59
19.3	C3_03040W	29	6.59
19.3916	C5_04310W	13	9.52
19.4818	C1_09540W	29	16
19.4835	C1_09710C	20	8.83
19.5025	C1_13870W	37	8.04
19.511	C1_08310W	37	9.27
19.6152	CR_07200W	35	6.54
19.624	C1_06700W	30	7.01
19.2647	C5_03320C	35	10
19.4955	C1_13290W	22	8.25
19.5917.3	C3_04590W	16	10
19.7331	CR_09360W	21	11
19.922	C5_00660C	26	11
19.303	C1_03330C	12	11
19.4004	C5_05120W	40	8.15
19.5771	C6_03940C	25	5.22
19.651	CR_05020W	29	5.8
19.117	C6_01100W	13	8.9
19.3405	C6_01790C	12	11
19.3474	C6_02320C	31	7.62
19.4332	C5_03040W	15	8.62
19.4813	C1_09490C	23	8.46
19.5257	C1_12080W	19	6.74
19.1666	C3_01800C	13	8.09
19.4705	C4_00880W	12	11
19.4747	C1_08880W	7.91	6.72
19.4768	C1_09110W	13	8.25
19.4828	C1_09650W	15	9.16
19.686	C6_01950C	19	8.04
19.7624	CR_10470C	10	11
19.6559	C7_01650W	12	12
19.5692	C5_00060C	14	7.34
19.4153	C5_01590W	52	42
19.6755	C3_07360W	16	5.99
19.1978	C5_00890C	16	6.83
19.4223	C5_02170C	96	11
19.5558	C6_02840C	15	12
19.6234	C1_06760C	10	12
19.108	C6_04230W	12	13
19.1614	C3_02310W	16	11
19.1979	C5_00880C	22	12
19.5496	C2_06330C	8.52	8.06
19.6533	C7_01870W	14	8.65

19.412	C1_05530C	24	10
19.1069	C1_04330W	11	9.8
19.7364	C3_05840W	16	18
19.5362	C2_10780C	12	7.6
19.5368	C2_10850C	13	9.32
19.7468	CR_00630W	23	15
19.867	C2_03530W	11	6.78
19.1447	C2_01420C	180	210
19.156	C2_02380W	18	7.16
19.3667	C1_02100W	13	10
19.7512	CR_00220W	13	8.53
19.5575	C6_02970C	15	13
19.5722	C6_03550C	27	9.12
19.6408	CR_08420W	17	7.84
19.5954	C3_04870W	29	8.56
19.205	C2_00740C	8.4	9.67
19.3812	C4_04700W	14	10
19.482	C1_09570W	340	260
19.6099	C1_00110W	14	9.55
19.1233	C1_07710C	14	12
19.5416	C3_00490W	22	14
19.6017	C1_00880W	19	8.02
19.742	C4_05130C	13	9.7
19.7447	C3_06580W	13	11
19.1339	C7_03360W	15	10
19.3437	C6_01470W	72	37
19.4445	C1_07220W	12	10
19.4746	C1_08870C	19	11
19.4982	C1_13510C	18	26
19.6066	C1_00410C	13	9.55
19.131	C4_03680C	16	11
19.1476	C2_01650W	13	8.01
19.5046	C4_03900C	12	8.61
19.698	C3_05420W	10	13
19.745	C4_05150W	11	9.44
19.1325	C4_03540C	11	9.34
19.1619	C3_02260C	14	8.92
19.261	C3_02690C	8.94	7.82
19.2991	C1_03000W	8.43	10
19.7077	C7_00430W	9.81	8.51
19.3631	C2_08470C	12	12
19.6438	CR_08640C	12	9.76
19.3055	C1_03530W	7.1	9.5
19.1574	C2_02500W	14	9.42
19.1608	C3_02360C	8.53	8.63
19.3981	C5_04930C	12	10

19.4365	CR_03660C	8.86	13
19.5943	C3_04800C	6.66	9.52
19.71	C7_00230W	12	13
19.756	C1_04870W	12	9.97
19.204	C2_00840W	11	16
19.2728	C4_02700W	8.39	12
19.2971	C1_02830W	7.51	9.27
19.3192	C5_01820W	6.53	7.09
19.3803	C4_04770C	7.64	8.58
19.404	C5_05410C	8.29	7.08
19.469	CR_03900W	9.14	7.09
19.6592	CR_09700W	9.84	12
19.6951	C3_03680W	9.92	9.45
19.2449	C1_05970W	11	5.78
19.6045	C1_00610W	8.57	9.4
19.1534	C2_02180W	11	9.92
19.2882	C4_06530C	120	45
19.5001	C1_13640W	9.56	9.47
19.2573	CR_01760C	6.75	7.58
19.2633	CR_07730W	7.37	7
19.492	CR_04090C	9.46	9.64
19.504	C4_03850W	9.76	7.7
19.5548	C6_02750C	14	8.08
19.564	C4_00150C	10	5.65
19.7112	C7_00100W	9.46	14
19.7393	C3_06110C	13	7.81
19.207	C2_00570W	8.49	8.87
19.3135	C4_06740C	9.45	6.21
19.4675	C4_01150W	8.01	8.3
19.6749	C3_07410C	6.83	8.14
19.1033	C1_03760C	7.68	9.15
19.1793	C4_05350W	6.77	8.63
19.1863	C2_07620W	8.29	8.66
19.2847	CR_02890C	30	6.94
19.2987	C1_02960C	7.76	5.05
19.3669	C1_02120C	14	11
19.3974	C5_04880C	9.04	20
19.4777	C1_09190C	7.42	9.01
19.6003	C3_05250C	7.07	9.43
19.6981	C3_05430W	6.6	7.26
19.5007	C1_13700W	9.08	8.61
19.1715	C3_01360C	9.14	11
19.7058	C7_00610C	5.92	9.07
19.1832	C1_10610W	7.42	9.76
19.2084	C2_00450C	8.98	10
19.2347	C1_10720C	9.03	8.1

19.2506	C3_01020W	9.9	30
19.3412	C6_01740C	12	21
19.4246	C5_02380W	11	14
19.461	C4_01830C	8.47	11
19.4866	C1_10000C	9.05	9.7
19.1596	C4_03910W	8.34	15
19.2434	C1_06110C	8.26	24
19.4441	C1_07260C	7.93	27
19.3195	C5_01800C	6.06	23
19.3425	C6_01620W	11	17
19.6023	C1_00830W	9.54	6.45
19.7254	C1_14380C	9.24	12
19.7394	C3_06120C	10	12
19.6786	C3_07140C	10	15
19.1411	C4_04360W	10	24
19.2545	CR_01580C	7.68	8.14
19.4599	C4_01940W	8.27	14
19.4455	C1_07130C	10	16
19.1005	C1_10570C	11	13
19.1542	C2_02240C	50	54
19.3278	CR_00780C	19	12
19.6518	C7_02010C	14	9.11
19.2528	CR_01420W	28	17
19.4203	C6_00560W	12	14
19.5107	C1_08300W	12	16
19.7016	C7_00980W	10	19
19.4201	C6_00570C	23	14
19.5723	C6_03560W	12	12
19.2796	C1_07490C	18	11
19.1747	C2_10310C	41	50
19.7645	CR_10620C	20	11
19.795	C2_04250W	15	13
19.1609	C3_02350W	16	8.97
19.4979	C1_13470W	40	55
19.336	C1_01710W	12	12
19.5255	C1_12100C	17	15
19.6512	C7_02050C	18	14
19.6687	C7_03550C	15	14
19.4739	C1_08810C	20	12
19.5915	C3_04570C	15	9.84
19.7545	CR_00010C	16	10
19.2078	C2_00490W	17	9.85
19.4184	C4_00590C	13	11
19.4278	C5_02620C	14	13
19.5234	C1_12290C	10	14
19.671	C1_11310C	42	9.6

19.6952	C3_03670W	14	12
19.151	C2_04690C	13	15
19.368	C1_02230W	16	13
19.6783	C3_07170C	8.58	30
19.3152	C2_06700W	27	14
19.4239	C5_02310C	23	17
19.4337	C5_03080C	15	12
19.5017	C1_13800C	17	10
19.6119	CR_07460C	11	18
19.2319	C1_10970W	13	15
19.2867	C4_06650W	13	16
19.7392	C3_06100C	12	12
19.2938	C1_02490C	16	12
19.3773	C4_05060W	14	9.16
19.4326	C5_03010W	13	8.85
19.491	CR_04080C	20	9.25
19.5592	C6_03090W	22	12
19.578	C2_03150C	25	12
19.5031	C1_13930W	18	11
19.6187	C3_07920W	15	13
19.1743	C2_10350C	14	22
19.3672	C1_02150W	25	13
19.4222	C5_02160W	15	14
19.5429	C3_00380C	16	8.74
19.3444	C6_01400W	21	26
19.7193	C7_03890C	20	12
19.2443	C1_06020W	25	32
19.451	C2_04420W	11	15
19.3019	C1_03260W	16	9.4
19.755	CR_09780C	16	15
19.2312	C1_11020W	13	12
19.2973	C1_02850W	26	9.38
19.237	CR_06940W	13	14
19.2672	C4_03180W	18	9.36
19.1748	C2_10300C	17	15
19.1994	C2_01310W	15	12
19.7583	CR_10070C	18	11
19.976	C5_00210C	17	20
19.221	C2_07720C	23	10
19.3912	C5_04280C	19	7.79
19.6915	C7_01340W	14	13
19.6942	C3_03750C	12	12
19.1613	C3_02320W	18	12
19.4465	C1_03910C	17	13
19.1189	C6_00290W	30	8.96
19.3463	C6_02230W	27	7.88

19.3846	C4_04410C	15	9.84
19.5622	C6_03340C	24	11
19.652	CR_05010W	21	11
19.6525	C7_01960W	22	7.73
19.6782	C3_07180C	40	9.67
19.6534.2	C7_01850C	17	15
19.2615	CR_02150W	18	12
19.4	C5_05080W	30	13
19.4699	C4_00950C	19	9.61
19.921	C5_00670C	22	11
19.3077	C4_07230C	17	11
19.5799	C2_03020C	21	8.33
19.414	C1_05500W	7.6	13
19.5138	C7_03170W	8.08	23
19.7473	CR_00600C	8.53	30
19.3603	C2_08730W	9.47	24
19.4752	C1_08940C	10	13
19.5011	C1_13740W	6.58	20
19.1753	C2_10270W	11	29
19.3764	C1_12520W	8.65	22
19.591	C3_04540C	9.43	26
19.6208	C1_07000W	8.31	25
19.6648	CR_05660W	15	32
19.4315	C5_02910C	5.83	11
19.4775	C1_09170W	7.21	16
19.4829	C1_09660W	6.38	9.49
19.4932	C1_13060C	8.46	10
19.5155	C7_03060C	6.95	12
19.1254	C4_05690W	7.29	10
19.4068	C2_09100C	5.6	12
19.7376	C3_05950W	5.7	12
19.5071	C1_08000W	10	13
19.1112	C5_03820C	9.35	13
19.3399	C6_01850W	8.68	16
19.7041	C7_00780W	8.27	15
19.265	C5_03300C	9.69	12
19.427	C5_02570W	7.71	14
19.7119	C7_00050C	7.69	16
19.6432	CR_08590W	8.67	17
19.1687	C3_01560W	9.23	16
19.2551	CR_01620C	14	22
19.3999	C5_05070W	10	16
19.2559	CR_01680C	15	24
19.5704	C6_03440W	9.07	12
19.6742	C3_07460W	11	14
19.7105	C7_00180W	8.79	18

19.6812	C3_06890W	7.14	22
19.1289	C3_00820W	11	18
19.4312	C5_02900W	11	20
19.6155	C3_00830C	6.67	11
19.4575	C4_02160C	6.57	15
19.1323	C4_03560W	8.23	18
19.5209	C2_05850C	6.57	14
19.5059	C1_07880C	9.22	15
19.6921	C7_01400C	8.71	12
19.6244	C1_06670W	6.6	15
19.936	C5_00530W	8.04	14
19.431	C1_05340C	21	9.23
19.4535	C1_01880C	14	16
19.879	C2_03420C	13	16
19.274	C4_02590C	11	18
19.4151	C5_01570C	10	19
19.6706	C7_03490W	25	19
19.5439	C3_00300W	9.98	18
19.891	C2_03360W	9.64	19
19.1409	C4_04370C	9.85	16
19.2404	CR_03200C	8.64	15
19.6479	C7_02320W	6.96	18
19.3944	C5_04600C	11	17
19.202	C2_09020W	82	120
19.4931	C1_13030C	10	23
19.3185	C5_01870W	9.39	18
19.354	C2_05090W	11	15
19.1195	C6_00340C	8.47	13
19.4673	C4_01170C	9.68	14
19.5381	C3_00730W	15	15
19.6124	CR_07440W	12	18
19.1106	C5_03880C	14	19
19.2678	C4_03120C	26	15
19.6985	C3_05470W	9.02	22
19.7021	C7_00930W	13	12
19.7328	CR_09330C	10	15
19.5265	C1_12010C	17	16
19.1288	C3_00810C	12	16
19.6133	CR_07360W	13	9.68
19.7377	C3_05960W	40	48
19.6373	CR_08120C	14	9.15
19.7479	CR_00560W	14	8.9
19.338	C4_03510C	10	6.93
19.5991	C3_05160C	10	11
19.5788	C2_03100W	14	9.22
19.6356	C1_12670C	12	12

19.712	CR_06540W	18	26
19.775	C1_04700C	16	10
19.3761	C1_12550C	18	11
19.1823	C1_06270W	13	15
19.1718	C3_01330W	9.54	9.12
19.2563	CR_01700C	15	13
19.2903	C4_06340W	15	7.71
19.3753	CR_02190C	16	13
19.4273	C5_02590C	13	8.94
19.228	C2_07230C	18	9.37
19.5121	C2_08360C	14	7.57
19.761	CR_10340W	13	12
19.1509	C2_01970C	9.63	16
19.767	CR_10800C	14	13
19.642	CR_05120W	20	8.87
19.661	CR_09520C	29	12
19.217	C2_08140C	32	8.7
19.4732	C1_08740C	18	8.16
19.5798	C2_03030W	14	11
19.1607	C3_02370C	18	8.84
19.1795	C4_05370W	23	7.72
19.6345	C1_12770W	25	9.54
19.1285	C5_04050W	21	10
19.583	C2_02760W	42	16
19.5292	C4_04170C	26	13
19.4755	C1_08990C	21	11
19.759	C1_04830W	15	7.43
19.3467	C6_02260C	19	8.86
19.6008	C3_05290C	20	14
19.6348	C1_12740W	23	9.92
19.1244	C4_05600W	46	11
19.119	C6_00300C	21	7.56
19.6805	C3_06950W	21	15
19.2753	C4_02490W	21	8.93
19.5224	C1_12410C	24	11
19.6875	C2_05650W	20	10
19.167	C3_01750C	16	7.66
19.2364	CR_07010W	13	9.31
19.4899	C1_10290W	14	9.32
19.654	C7_01800C	15	8.48
19.6848	C1_04540C	14	8.46
19.999	C1_10550C	18	13
19.2143	C6_04530C	22	9.33
19.3556	C2_05270W	22	7.84
19.3815	C4_04660C	25	7.49
19.5426	C3_00400C	39	0.733

19.4432	C1_07380C	26	11
19.2792	C1_07520C	17	9.76
19.528	CR_04380C	25	9.72
19.5974	C3_05040C	17	8.33
19.2791	C1_07540C	21	11
19.3694	C1_02370C	15	8.86
19.5365	C2_10820C	21	12
19.1727	C3_01250W	20	7.86
19.751	CR_00260W	8.28	5.55
19.4937	C1_13110C	8.35	11
19.4945	C1_13170C	7.99	12
19.7011	C7_01030C	14	9.37
19.5391	C3_00660W	27	12
19.5281	C1_11860W	49	11
19.1672	C3_01720C	110	10
19.5068	C1_07970C	12	8.74
19.3279	CR_00760C	13	6.6
19.4242	C5_02340C	48	30
19.3349	C1_01590C	38	44
19.658	C1_11440C	12	7.87
19.5395	C3_00630W	140	8.11
19.262	C3_02700W	21	12
19.94	C5_00490C	13	21
19.4367	CR_03680C	17	10
19.6729	C3_07610W	13	8.66
19.1667	C3_01790C	91	5.44
19.7242	C1_14300C	22	9.74
19.6973	C3_05360C	25	3.93
19.1622	C3_02230C	15	7.74
19.2081	C2_00470W	15	7.56
19.4348	C5_03160W	14	7.98
19.6193	C1_07110W	36	10
19.209	C2_00410C	18	8.91
19.4136	C5_01460W	16	5.97
19.6217	C1_06930W	8.84	7.44
19.6789	C3_07110W	16	7.81
19.81	C2_04110W	12	6.36
19.3959	C5_04730C	28	8.54
19.4531	C1_01920W	40	18
19.7604	CR_10290C	30	7.62
19.6012	C1_00920W	16	9.22
19.643	CR_05100W	22	16
19.1133	C1_03710C	9.39	8.64
19.728	CR_07580C	38	13
19.6041	C1_00640C	19	7.98
19.2216	C2_07660W	17	15

19.239	C3_02490C	20	7.29
19.4435	C1_07360W	20	14
19.5804	C2_02990C	12	9.33
19.457	CR_05980W	12	11
19.7572	CR_09980W	13	14
19.2879	C4_06550C	20	9.67
19.6453	C7_02560W	8.83	8.93
19.3949	C5_04640C	8.22	9.53
19.738	C4_05100C	13	8.61
19.4924	C1_12950W	11	7.14
19.5095	C1_08180C	11	7
19.5162	C7_02990W	21	9.19
19.6778	C3_07230W	43	55
19.7451	C3_06620W	7.11	8.24
19.1166	C1_11540C	17	7.22
19.7475	CR_00590W	14	8.81
19.1648	C3_02000W	22	7.99
19.6926	C3_03890W	13	5.98
19.3767	C1_12490W	12	6.9
19.7402	C3_06300W	18	8.52
19.5387	C3_00700W	13	11
19.1573	C2_02490C	14	9.2
19.6871	C2_05580W	11	7.47
19.51	C1_04970W	11	6.28
19.6544	C7_01780W	10	8.03
19.964	C5_00300C	18	9.64
19.6317	CR_04740C	14	8.89
19.6818	C3_06830C	17	7.71
19.7342	CR_09470W	18	8.43
19.626	C1_06530C	13	9.23
19.3256	CR_01000C	13	8.41
19.4728	C1_08700W	14	6.79
19.906	C2_03240C	14	4.94
19.1777	C2_10050W	13	11
19.6396	CR_08300C	49	9.37
19.3765	C1_12510W	11	10
19.3297	C1_01090C	7.59	19
19.6715	C3_07720C	7.27	9.33
19.6663	C5_03540C	6.69	10
19.5589	C6_03070C	7.55	7.73
19.6949	C3_03700C	7.58	12
19.128	C5_04090C	7.32	11
19.462	C4_01740W	5.03	6.92
19.4654	C4_01330W	6.19	9.23
19.5876	C3_04330C	5.81	28
19.277	C4_02330C	9.09	15

19.994	C1_10510W	5.07	32
19.292	C4_06170C	8.09	17
19.449	C2_04600C	4.92	9.93
19.5669	C4_00410W	7.63	7.63
19.4952.1	C1_13260W	5.68	7.39
19.1057	C1_04220C	8.8	6.85
19.6315	CR_04770C	5.23	9.13
19.822	C2_04010C	6.67	8.31
19.4217	C5_02130W	5.43	10
19.493	C1_13020C	11	8.56
19.5142	C7_03130C	7	9.22
19.762	CR_10430C	10	10
19.4741	C1_08830C	9.61	8.45
19.287	C3_02940C	5.38	7.63
19.1691	C3_01540W	7.83	9.61
19.21	C2_06430C	5.63	6.97
19.3903	C5_04200W	6.52	8.61
19.443	C1_05230W	6.02	5.02
19.4044	C5_05450C	8.17	8.44
19.604	C1_00650C	13	8.7
19.6179	C3_07840C	9.84	12
19.5563	C6_02870W	5.7	8.96
19.703	C7_00860W	7.3	6.93
19.6864	C4_05250W	7.2	6.93
19.945	C5_00440C	6.41	9.75
19.251	C3_02610C	7.25	9.94
19.2568	CR_01730W	4.69	11
19.3366	C4_03390W	6.6	6.6
19.4677	C4_01130C	6.83	7.01
19.6237	C1_06730W	12	6.68
19.501	CR_04170W	6.63	12
19.826	C2_03980C	8.7	9.88
19.306	C3_03090W	8.18	5.82
19.4211	C6_00480C	9	9.63
19.6449	CR_08720W	6.11	9.03
19.6091	C1_00150C	9.94	8.65
19.1861	C2_07640W	6.67	11
19.2093	C2_00380C	11	13
19.4546	C1_01780C	8.64	8
19.84	C6_00830C	11	7.33
19.151	C2_01980C	4.3	7.29
19.4212	C6_00470C	8	28
19.3175	C5_01960C	6.74	11
19.839	C2_03830W	6.2	9.03
19.1002	C1_10560C	5.71	6.98
19.199	C2_01350C	8.14	7.86

19.3854	CR_06040W	10	6.88
19.3863	CR_06100C	6.33	6.96
19.4591	C4_02020W	7.16	7.9
19.4645	C4_01410W	19	10
19.455	C1_01750W	9.44	6.6
19.1835	C1_10640C	8.79	8.42
19.2473	C1_05780W	13	11
19.7492	CR_00400C	7.89	6.51
19.776	C1_04690C	12	24
19.3592	C2_08790W	8.29	9.76
19.7257	C1_14400C	6.8	8.37

LIST OF PUBLICATIONS

- 1.** Legrand M, **Jaitly P**, Feri A, d'Enfert C, Sanyal K. 2019. *Candida albicans*: An Emerging Yeast Model to Study Eukaryotic Genome Plasticity. *Trends in Genetics* 35: 292-307.
<https://doi.org/10.1016/j.tig.2019.01.005>
- 2.** Sreekumar L, **Jaitly P**, Chen Y, Thimmappa BC, Sanyal A, Sanyal K. 2019. Cis- and Trans-chromosomal Interactions Define Pericentric Boundaries in the Absence of Conventional Heterochromatin. *Genetics* 212: 1121-1132.
<https://doi.org/10.1534/genetics.119.302179>
- 3.** **Jaitly P**, Legrand M, Das A, Patel T, Chauvel M, d'Enfert, Sanyal K. 2021. A phylogenetically-restricted essential cell cycle progression factor in the human pathogen *Candida albicans*. *bioRxiv* 2021.09.23.461448.
<https://doi.org/10.1101/2021.09.23.461448>

Review

Candida albicans: An Emerging Yeast Model to Study Eukaryotic Genome Plasticity

Mélanie Legrand,¹ Priya Jaitly,² Adeline Feri,^{1,3,4} Christophe d'Enfert,^{1,*} and Kaustuv Sanyal^{2,*}

Saccharomyces cerevisiae and *Schizosaccharomyces pombe* have served as uncontested unicellular model organisms, as major discoveries made in the field of genome biology using yeast genetics have proved to be relevant from yeast to humans. The yeast *Candida albicans* has attracted much attention because of its ability to switch between a harmless commensal and a dreaded human pathogen. *C. albicans* bears unique features regarding its life cycle, genome structure, and dynamics, and their links to cell biology and adaptation to environmental challenges. Examples include a unique reproduction cycle with haploid, diploid, and tetraploid forms; a distinctive organisation of chromosome hallmarks; a highly dynamic genome, with extensive karyotypic variations, including aneuploidies, isochromosome formation, and loss-of-heterozygosity; and distinctive links between the response to DNA alterations and cell morphology. These features have made *C. albicans* emerge as a new and attractive unicellular model to study genome biology and dynamics in eukaryotes.

Candida albicans: A Model for Studying Genome Biology

Maintenance of genome integrity and the accuracy of DNA replication are at the core of cell function, survival, and propagation. Thus, deciphering the molecular mechanisms that underlie genome biology is of crucial importance, especially as they have relevance in numerous human diseases such as cancer but also because they underlie species evolution and adaptation. For more than 50 years, *Saccharomyces cerevisiae* (see Glossary) and *Schizosaccharomyces pombe* have served as uncontested yeast models for molecular understanding of the processes underlying eukaryotic genome biology [1–6]. Major discoveries in this field have benefited from the ‘awesome power of yeast genetics’ and proven to be relevant across eukaryotes. In addition, the ascomycetous yeast *Candida albicans* – a distantly related cousin of *S. cerevisiae* (Box 1) – has attracted considerable interest because of its dominant importance as a human pathogen. While normally a commensal of humans, *C. albicans* is also responsible for superficial infections – thrush, oropharyngeal candidiasis, vaginal candidiasis – in healthy individuals as well as disseminated infections in hospitalised patients that receive broad-spectrum antibiotic treatment and have debilitated immunity [7]. The investigation of putative *C. albicans* virulence factors, in particular the ability to alternate between yeast and filamentous forms; the exploration of *C. albicans* interactions with the host; and the search for new antifungal targets have been accompanied by the development of a molecular toolkit that allows gene function to be accurately characterised in this species (Box 1) [8–16]. Notably, this toolkit has enabled exploring other aspects in depth, especially the genome biology of *C. albicans*. A number of features distinguish *C. albicans* from other yeast species – a unique reproduction cycle where haploid, diploid, and tetraploid forms are observed; a distinctive organisation of chromosome hallmarks; a highly dynamic genome, with extensive karyotypic

Highlights

C. albicans is a major human pathogen, with features that distinguish it from other yeast species.

Rather than meiosis, ploidy reduction upon mating occurs by a parasexual process of concerted chromosome loss.

Centromeres have unique organisation and are epigenetically regulated. Neither centromeres nor the DNA replication origins share any common defining DNA sequence.

Loss-of-heterozygosity events are frequent and widespread in the genome of *C. albicans*.

The DNA damage response is coupled to morphogenetic shifts.

C. albicans emerges as a new unicellular model to study eukaryotic genome biology and dynamics.

¹Fungal Biology and Pathogenicity Unit, Department of Mycology, Institut Pasteur, INRA, Paris, France

²Molecular Mycology Laboratory, Molecular Biology and Genetics Unit, Jawaharlal Nehru Centre for Advanced Scientific Research, Bangalore, India

³Université Paris Diderot, Sorbonne Paris Cité, Cellule Pasteur, Paris, France

⁴Current address: Pathoquest, BioPark, 11 rue Watt, 75013 Paris, France

*Correspondence: christophe.denfert@pasteur.fr (C. d'Enfert) and sanyal@jncasr.ac.in (K. Sanyal).

variations, including chromosomal loss and gain, as well as rearrangements, **isochromosome** formation, segmental duplication, and loss-of-heterozygosity (LOH); and distinctive links between the response to DNA alterations and cell morphology (Figure 1, Key Figure). In this review, we highlight these unique features that have helped *C. albicans* emerge as a new unicellular model to study genome biology and its evolution.

Candida albicans: A Yeast Species with a Cryptic Reproduction Cycle

Sequencing of the *C. albicans* genome has revealed that this diploid species, long thought to be devoid of sex [17–20] is actually equipped with the majority of the genetic circuit required for sexual reproduction. Similar to mating type (**MAT**) loci in *S. cerevisiae*, mating type-like (**MTL**; Figure 2A) regions encoding the transcriptional regulators that control expression of mating specific genes [21] and elements of a functional pheromone response pathway exist in the *C. albicans* genome [22]. While many of the meiotic regulators from *S. cerevisiae* have counterparts in *C. albicans*, the latter lacks key meiotic components including **IME1**, the master switch for entry into the meiotic pathway in *S. cerevisiae*, and **SPO13**, which in *S. cerevisiae* is essential for proper execution of **meiosis I**. Existence of functional analogues of these genes in *C. albicans* is difficult to rule out as extensive sequence divergence may cause difficulty in their *in silico* identification. While **IME1** is essential for meiosis in a number of yeast species, strikingly, this gene is absent from many sexual species in the CTG clade, suggesting a possible clade-specific rewiring of the meiotic cycle (Box 1) [23]. In addition, the highly conserved pheromone response pathways were detected in nonmating species [23]. The apparent plasticity of mating and meiosis pathways in *Candida* species reinforces the fact that knowledge of gene products involved in sexual reproduction is insufficient to accurately predict the reproductive behaviour of an organism.

Hints from *in silico* data have fuelled the quest for evidence of mating and sexual reproduction in *C. albicans*. While engineered *C. albicans* strains homozygous for **MTL loci** are able to mate and form tetraploids both in laboratory conditions and in a mammalian host [24,25], meiosis remains to be demonstrated in *C. albicans*. Tetraploid cells revert to diploidy by undergoing a parasexual process of concerted chromosome loss [26–29]. The combination of mating and subsequent concerted chromosome loss that allows *C. albicans* to alternate between diploid and tetraploid (but also haploid and diploid) has been referred to as a **parasexual cycle** (Figure 2B). The apparent lack of conventional meiosis in *C. albicans* suggests that the function of meiotic genes may have diverged [22,23,30,31]. A classic example is Ndt80, the meiosis-specific transcription factor and a key modulator of progression of meiosis and sporulation in *S. cerevisiae*, that functionally diverged to participate in the biofilm pathway in *C. albicans* [32,33]. Similarly, Ume6, a key transcriptional regulator of early meiosis-specific genes in *S. cerevisiae*, has been rewired towards autophagy and hyphal growth regulation in *C. albicans* [30,34]. The latest example of such rewiring is Rme1; the function of which diverged from preventing meiosis by repressing **IME1** in *S. cerevisiae* to regulating chlamyospore formation in *C. albicans* (Hernandez-Cervantes *et al.*, personal communication).

Although we cannot rule out the possibility of *C. albicans* undergoing meiosis in conditions that have not been explored thus far, the hypothetical absence of meiosis does not prevent *C. albicans* from generating genetic and phenotypic diversity necessary for this opportunistic human pathogen to adapt to new environments. In addition to extensive shuffling of parental chromosomes resulting in new combinations of homologues, completion of the parasexual cycle often gives rise to aneuploid strains and is accompanied by recombination events between homologous chromosomes [35,36]. Unexpectedly, recombination events during the nonmeiotic parasexual cycle are dependent on the DNA double-strand break (DSB)

Glossary

- Candida albicans:** this ascomycetous yeast, normally a commensal of humans, is responsible for superficial infections in healthy individuals as well as disseminated infections in immunocompromised patients.
- Centromere (CEN):** an essential chromosomal element that facilitates sister chromatid separation via kinetochore formation during mitosis.
- CRISPR-Cas9:** Cas9 is an RNA-guided DNA endonuclease enzyme that associate with the CRISPR (clustered regularly interspaced short palindromic repeats) to target and cut specific sites in genomes. CRISPR-Cas9 can be exploited for genome editing in *C. albicans*.
- DNA replication origins (ORIs):** genetic elements bound by the origin recognition complex and where DNA replication initiates. In *C. albicans*, ORIs are categorized into arm ORIs and centromere ORIs.
- Experimental evolution:** use of laboratory experiments to study evolutionary dynamics in controlled conditions imposed by the experimenter.
- Gene flow:** transfer of genetic variation from one population to another.
- Heterozygosity:** presence of different alleles at one or more loci on homologous chromosomes in a diploid organism.
- Homologous recombination (HR):** pathway that repairs DSBs in DNA using a type of genetic recombination in which nucleotide sequences are exchanged between two identical DNA molecules.
- Homozygosis bias:** when one haplotype or even a part of it is never found in the homozygous state.
- IME1:** master regulator of meiosis. The **IME1** gene is required for expression of meiosis specific genes and sporulation and in *S. cerevisiae*.
- Isochromosome:** abnormal chromosome whereby two identical chromosome arms flank a centromere.
- Kinetochore:** large multiprotein complex that assembles on centromere DNA and serves as the chromosomal attachment site of the spindle microtubules.

inducing **Spo11**; the meiosis-specific endonuclease that initiates meiotic recombination in *S. cerevisiae* [35].

The majority of *C. albicans* isolates are found in the diploid state and diploidy is considered the preferred ploidy state of *C. albicans*. Nevertheless, nondiploid isolates have also been reported [37]. Changes in ploidy including haploidy, tetraploidy, or aneuploidy (primarily monosomy or trisomy) are thought to provide *C. albicans* with a rapid response to changing environments within the host [38]. Deviations from diploidy seem to harbour a fitness cost in the long term, as **experimental evolution** experiments using clinical and laboratory haploid, diploid, and polyploid *C. albicans* strains in complete medium and under nutrient-limited conditions have revealed that the stabilised genome nearly always reaches diploidy, a phenomenon termed as **ploidy drive** [39].

Large genomic changes, similar to the ones observed in products of *in vitro* parasexual genome reduction or long-term evolution experiments, are well tolerated by *C. albicans* and have been associated with acquisition of new phenotypic traits, such as drug resistance. Although population genetics approaches have recently confirmed the predominance of clonal reproduction in the *C. albicans* population [17,40,41], the work by Ropars and colleagues on genomes of 182 *C. albicans* isolates from diverse origins revealed the occurrence of **gene flow** in this population [42] (Figure 2C). These lines of evidence highlight the fact that parasexuality (or possibly sexuality) also occurs in nature and significantly contributes to *C. albicans* genetic and phenotypic diversities.

The *Candida albicans* Genome: An Organisational View

The essential elements of a eukaryotic chromosome – namely **centromeres**, **DNA replication origins**, and **telomeres** – have been identified in *C. albicans* (Figure 3). The centromere (CEN) is an essential chromosomal element that facilitates sister chromatid separation via **kinetochore** formation during mitosis. The CEN DNA sequences of *C. albicans* are 3–5 kb long and are all unique; devoid of any common sequence motif or repeat [43] (Figure 3A). The absence of a CEN-specific DNA sequence and the inability of the exogenously introduced CEN DNA to function as a native CEN suggest epigenetic regulation of CEN identity in *C. albicans* [44]. However, upon CEN deletion, **neocentromeres** are formed efficiently in *C. albicans*, mostly proximal and rarely distal to the native CEN [45–47]. Similar to the native CENs, neocentromeres also cluster in 3D with other functional CENs [47]. Gene conversion (GC) at the CENs can interchange the deleted CEN with the native CEN [45] and possibly explains the low frequency of SNPs across *C. albicans* CENs. Besides CEN clustering, structural integrity of the kinetochore is required for CEN function in *C. albicans*. Depletion of an essential kinetochore protein disrupts the integrity of the kinetochore architecture [48,49] and results in delocalisation and degradation of CENP-A [48] that forms centromeric chromatin.

DNA replication initiates from multiple discrete genetic loci – the DNA replication origins (*ORI*). Based on the location, *ORIs* in *C. albicans* are of two types [50]: (i) arm *ORIs*, which are located on the chromosomal arms; and (ii) centromeric *ORIs*, which are present on [51] or close to the CENs [52] (Figure 3B). While a subset of arm *ORIs* are defined by a 15-bp AC-rich consensus motif and a nucleosome-depleted pattern, centromeric *ORIs* are defined by epigenetic mechanisms [50] and replicate earliest in the genome [51]. The centromeric *ORIs* together with the **homologous recombination** (HR) proteins, Rad51 and Rad52, play a key role in loading CENP-A onto the CENs [52]. While replicating CEN DNA, the moving replication forks from CEN-proximal *ORIs* stall at CEN due to the presence of the kinetochore acting as a physical barrier [52]. The fork stalling accumulates single-stranded DNA that attracts HR proteins Rad51

Loss-of-heterozygosity (LOH):

genetic event resulting in the loss of one of the haplotype information in heterozygous diploid organisms.

MAT loci: mating-type or *MAT* locus harbours genes that control sexual reproduction in fungi.

Major repeat sequences (MRS): special feature of the *C. albicans* genome, consisting of a long tract of repetitive DNA, which is present on all chromosomes, except chromosome 3.

Meiosis: cell division that reduces the number of chromosomes by half.

MTL loci: mating type-like or *MTL* locus encodes transcription factors responsible for cellular identity in *C. albicans*.

Neocentromere: non-native centromere locus where a functional kinetochore assembles to allow chromosome segregation following disruption or inactivation of the native centromere.

Nondisjunction: failure of homologous chromosomes or sister chromatids to segregate equally in daughter cells during cell division.

Nonhomologous end joining (NHEJ): pathway that repairs DSBs in DNA by directly ligating the break ends without requirement for a homologous template.

Parasexual cycle: combination of mating and subsequent concerted chromosome loss that allows *C. albicans* to alternate between diploid and tetraploid (but also haploid and diploid).

Ploidy drive: process that brings an organism to its base ploidy level.

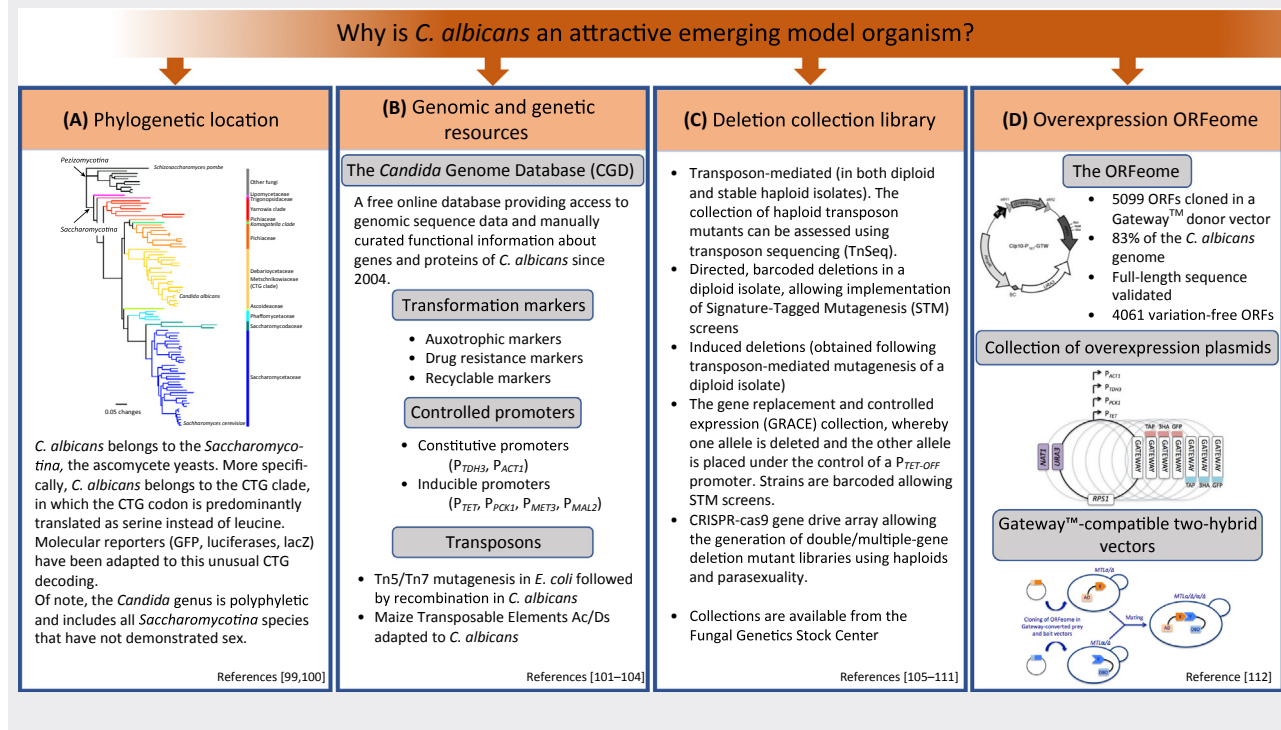
Saccharomyces cerevisiae: commonly known as baker's yeast or brewer's yeast, *S. cerevisiae* is a single-celled eukaryote that operates in a manner similar to a human cell and therefore is used as an important model organism in genetics and molecular biology.

Spo11: endonuclease that initiates meiotic recombination by catalysing the formation of double-strand breaks in DNA.

Telomeres: regions of repetitive nucleotide sequences located at the termini of a eukaryotic chromosome to ensure chromosome end replication and protection from degradation or end-to-end chromosome fusion.

Box 1. *Candida albicans*, an Alternative Yeast Model with an Extended and Adapted Molecular Genetics Toolkit

Because *C. albicans* decodes the CUG codon as serine instead of leucine and is predominantly a diploid, numerous tools have been adapted for genetic engineering of this species, allowing most molecular approaches to be developed in this species from insertional mutagenesis to gene tagging and two-hybrid screens as well as the production of mutant collections. The recent identification of stable haploids allows new approaches to be developed. CRISPR-cas9-based gene editing allows one-step generation of mutants in the diploid background, speeding up their construction [99–112].

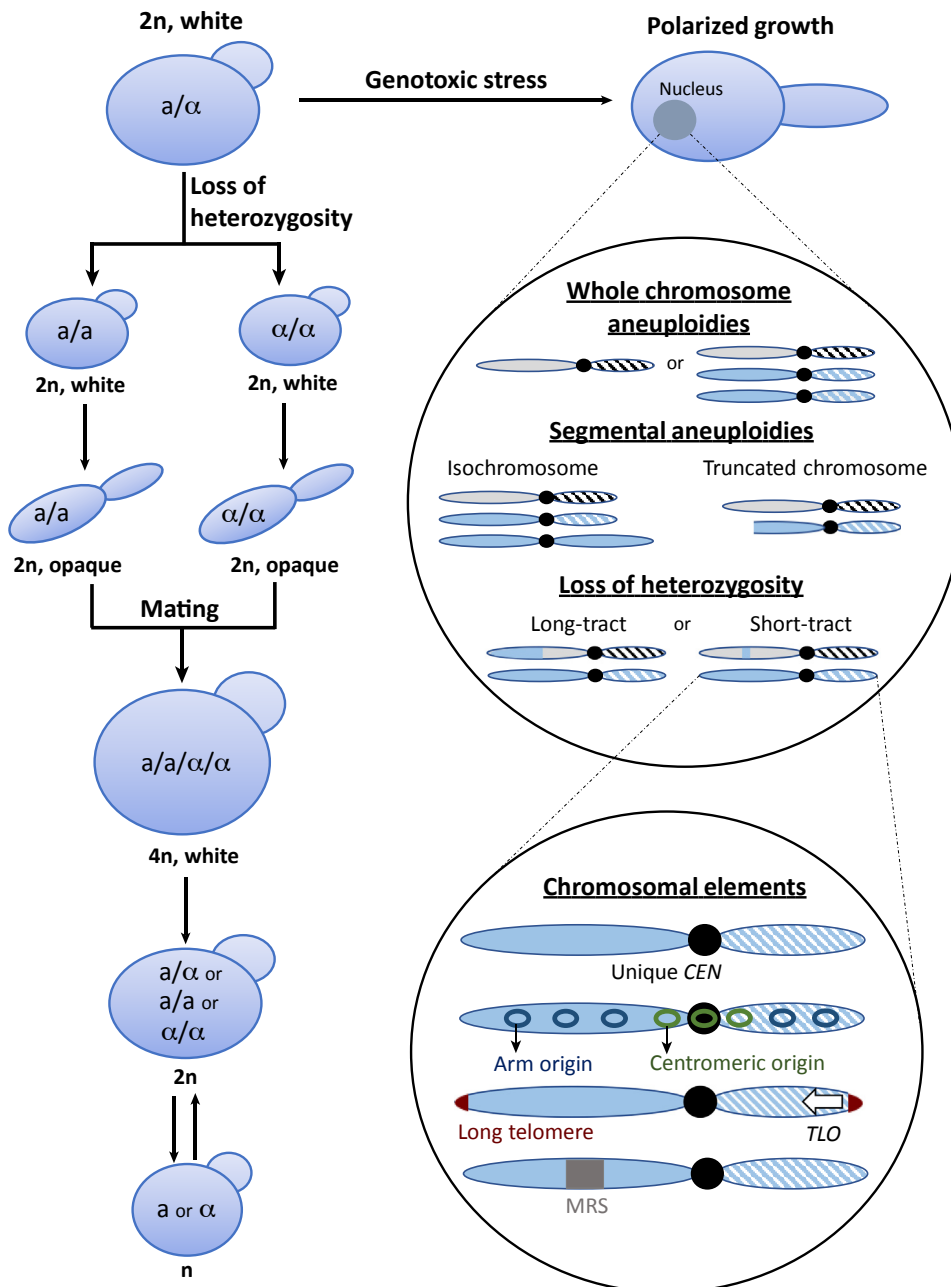


and Rad52, which are shown to interact with CENP-A in *C. albicans* [52]. As a consequence, CENP-A is deposited onto the CENs. Consistent with this, in a CEN-deleted strain, the neocentromere becomes the earliest replicating region [51].

A telomere, at the termini of a eukaryotic chromosome, ensures chromosome end replication and protects the chromosome from degradation or end-to-end chromosome fusion. *C. albicans* telomeres are unique in containing tandem copies of unusually long 23-bp repeating units [53] (Figure 3C). However, they are assembled into heterochromatin via the classical Sir2-mediated pathway [53,54]. The subtelomeric regions of *C. albicans* consist of the telomere-associated (*TLO*) family of genes, which encode for the subunits of the mediator complex; a crucial component for transcription initiation [55]. There are 15 *TLO* genes (including one pseudogene) in *C. albicans* but other non-*C. albicans* species have either one or two *TLO* genes [56]. In addition, overexpression of *TLO* genes in *C. albicans* influences many growth- and virulence-related properties [57]. The expansion in the number of *TLO* genes could thus explain the ability of *C. albicans* to adapt in various host niches.

A special feature of the *C. albicans* genome is the **major repeat sequence (MRS)**. The MRS is a long tract (10–100 kb) of repetitive DNA that is present on all chromosomes, except chromosome 3. Structurally, an MRS is composed of three subunits: the repetitive RPS

Key Figure

Major Defining Features of *Candida albicans* and Its Genome.

Trends in Genetics

Figure 1. *C. albicans* undergoes a unique haploid–diploid–tetraploid life cycle. A phenotypic switch from white to opaque form due to homozygosis of the *MTL* locus is the initial step of this cycle. Opaque cells of opposite mating-type then fuse together to form tetraploids. These tetraploids undergo a nonmeiotic parasexual cycle to return to the diploid state. Diploid (Figure legend continued on the bottom of the next page.)

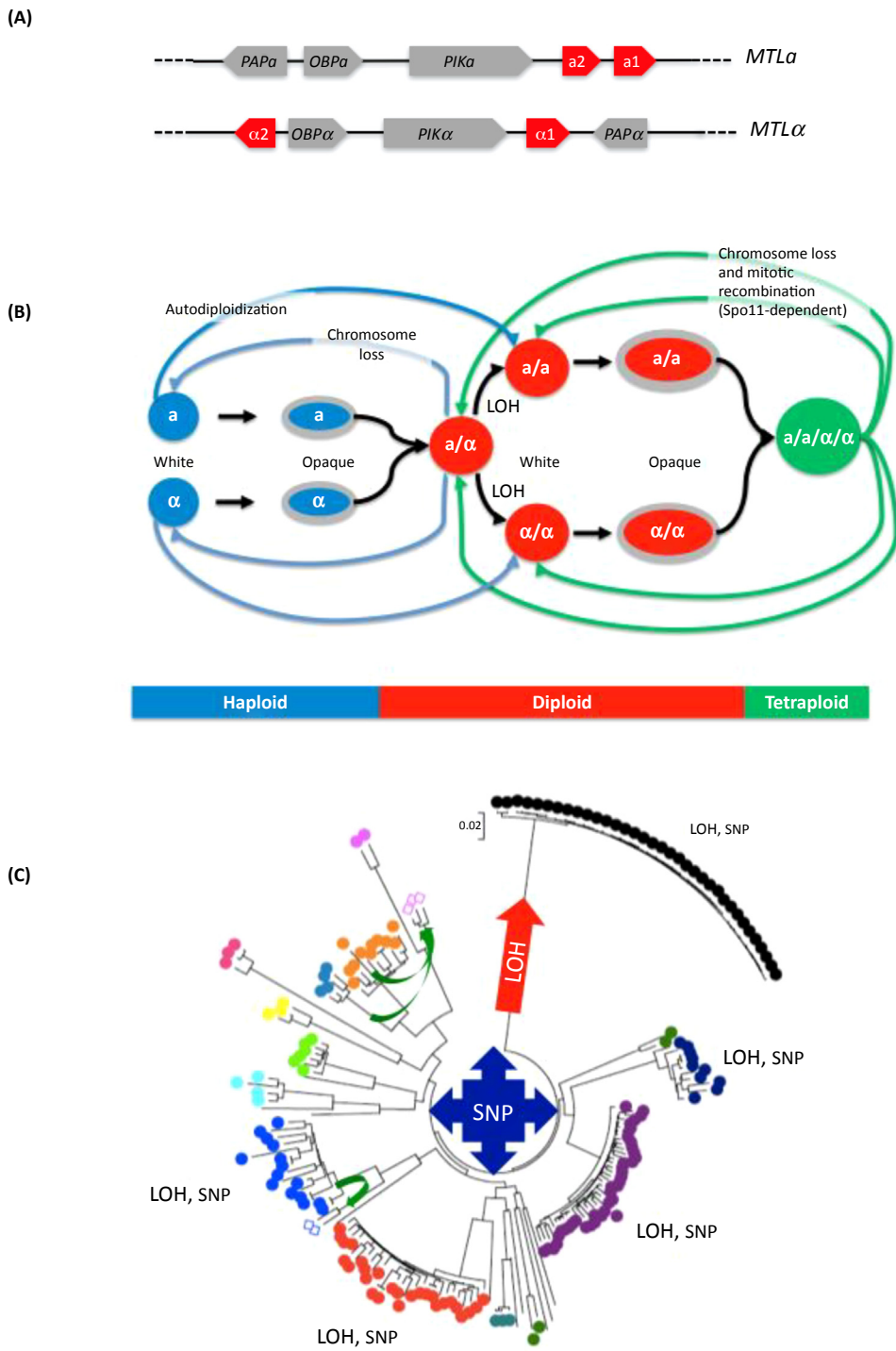
subunit flanked by nonrepetitive elements RB2 and HOK (Figure 3D). Chromosome 3 contains only the RB2 element without the RPS or HOK unit [58]. Surprisingly, the MRS, being a repetitive region, is not assembled into classical heterochromatin but carries marks of both euchromatin and heterochromatin [54]. The MRS covers about 3% of the total genome, yet its function remains elusive, except that it is considered to be a hotspot for genome rearrangements in *C. albicans* [59]. The MRS is a preferred site for chromosomal translocations [58], and the expansion and contraction of its RPS region give rise to chromosome length polymorphism [60]. Furthermore, the presence of the MRS affects the frequency of **nondisjunction**, whereby a homologue bearing a larger MRS is more likely to be lost at the time of chromosome segregation [59]. Thus, the MRS serves as an important means of generating karyotypic diversity in *C. albicans* and needs to be studied in greater detail for its function and origin.

***Candida albicans*, a Heterozygous Diploid with a Dynamic Genome**

Although genome variation has so far been explored primarily either in haploid or homozygous diploid genomes, it is now being tackled in diploid organisms having **heterozygosity**, with a hope of better understanding the genomics of adaptation in various environmental or host niches. Population genomics studies have revealed a number of aspects regarding heterozygosity in the *C. albicans* genome [19,42,61–63] (Figure 4A). Natural heterozygosity is observed across the *C. albicans* genome with an average rate of one SNP every 237–283 bases. By comparing a large number of strains, a higher level of heterozygosity is found to correlate with faster growth rates. These observations likely reflect the loss of alleles that influence fitness in strains that have undergone partial or complete homozygosis. Genome sequencing data have identified about 3600 open reading frames (ORFs) with high-confidence SNPs leading to changes in the amino acid sequence. In addition, SNPs found in regulatory regions, or even in ORFs, can also affect transcription levels and/or translation efficiency between the alleles [63]. Thus, extensive allelic differences may function to increase genetic and phenotypic diversity in an organism devoid of a true sexual cycle and contribute to the acquisition of new phenotypic traits such as drug resistance.

Population genomics studies in *C. albicans* have revealed that genome heterozygosity can vary from 48% to 89% – heterozygous and homozygous regions being defined as such based on the number of heterozygous SNPs within 5-kb windows [19,23,42,61]. The levels of heterozygosity are primarily influenced by large LOH events encompassing whole chromosomes or extending from a specific chromosomal locus to the telomere. These LOH events have been shown to be pervasive in *C. albicans* isolates and can be detected on all chromosomes. LOH can involve an entire chromosome upon chromosome loss due to chromosome nondisjunction during mitosis. Depletion of the centromeric histone H3, Cse4/CENP-A at centromeres has been reported in response to changes in ploidy and the environment, and is associated with chromosome instability [64]. The genome of *C. albicans* contains two homologous histone H2A-encoding genes, *HTA1* on chromosome 3 encoding Hta1p and *HTA2* on chromosome 1

C. albicans can become haploid or vice versa by chromosome loss and autodiploidisation, respectively. Several host factors or environmental stress can lead to karyotypic variations in *C. albicans*. The genome of *C. albicans* is remarkably plastic and can tolerate segmental aneuploidies, whole chromosome aneuploidies, and loss-of-heterozygosity events. Accumulation of such DNA alterations can be associated to polarised growth and drug resistance in *C. albicans*. Several chromosomal elements influence the organisation and stability of the *C. albicans* genome. These include centromeres (CEN), which are all unique and different in *C. albicans*; replication origins, which are of two types, arm origins and centromeric origins; telomeres, which are unusually long and associated with a family of telomere-associated genes (TLO); and the major repeat sequence (MRS), a feature unique to *C. albicans*.



Trends in Genetics

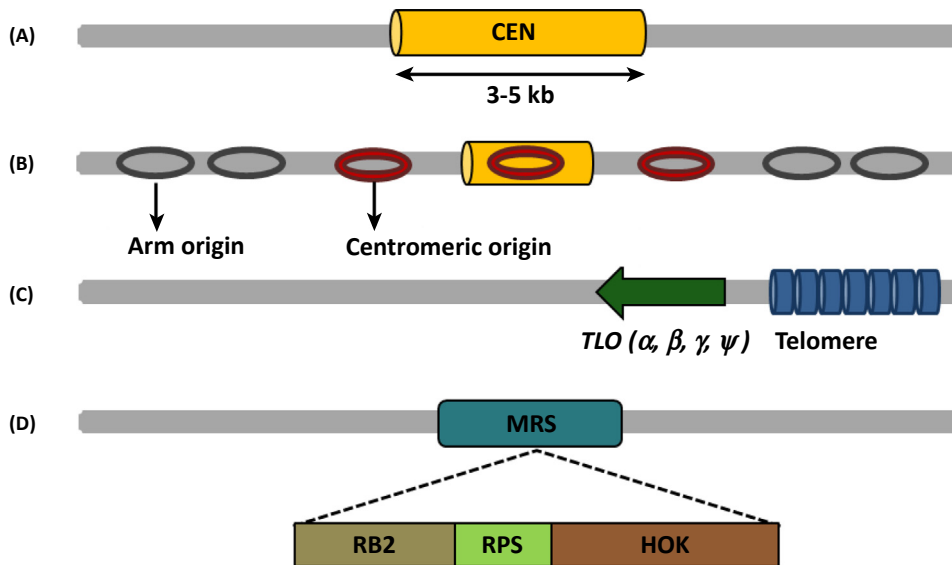
Figure 2. *Candida albicans* Mating Type, Parasexuality, and Population Structure. (A) Schematic of the *MTL α* and *MTL α* idiotypes. The genes encoding transcription factors responsible for cellular identity are shown in red, while the *OBP*, *PAP*, and *PIK* genes that are not involved in cellular identity but differ between the two idiotypes are shown in grey. (B) Schematic of the haploid–diploid–tetraploid life cycle of *C. albicans*. *C. albicans* is predominantly existing in the diploid (Figure legend continued on the bottom of the next page.)

encoding Hta2p. Unlike Hta2p, Hta1p has lost the conserved phosphorylation site for the Bub1 kinase, a key regulator of chromosome segregation, and has been shown to facilitate chromosome gain and loss events in *C. albicans* [64]. Another frequent cause of LOH is somatic HR used to repair DNA DSBs. DSBs are the consequence of DNA replication defects or R loop formation but can also arise due to external stresses [65]. The extent of the LOH event can reflect the molecular mechanisms involved in DSB repair in *C. albicans*. Short-range LOH can occur by GC without crossover and long-range LOH including whole chromosome arms can occur by either GC with crossover, break-induced replication (BIR), or mitotic crossover (MCO). If left unrepaired, a DSB may result in chromosome truncation or chromosome loss, characterized by LOH events that span an entire chromosome or an arm of it. Several tools have been developed to study LOH events in *C. albicans* (Box 2). They have in particular revealed that DNA DSBs are predominantly repaired by GC but other repair events such as BIR/MCO and GC with crossover (CO) can also be observed at a significant frequency [66]. They have also revealed that the frequency at which LOH events arise and the nature of these LOH are influenced by environmental parameters (see below).

A link between LOH, aneuploidy, and the elevation of antifungal resistance by studying drug-resistant *C. albicans* isolates has been precisely established (Figure 4B). Gain-of-function alleles of genes involved in the resistance to azole antifungals have been shown to be codominant with wild-type alleles and therefore high levels of resistance cannot be achieved in the presence of the wild-type allele. It is only upon homozygosity of the gain-of-function allele, as a result of LOH, that high levels of azole resistance can be achieved [67–69]. In addition, the appearance of aneuploidy and, in particular, the formation of an isochromosome composed of the two left arms of chromosome 5 is often associated with the acquisition of azole resistance [70]. Increased copy number of *ERG11* and *TAC1*, both located on the left arm of chromosome 5, accounts for the majority of drug resistance associated with the chromosome 5 isochromosome [71]. Large-scale genome changes have been characterized in *S. cerevisiae* as a means of adaptation in response to stress [72,73]. Similarly, *in vitro* exposure to oxidative stress, elevated temperature, and antifungal drugs [74,75], as well as passaging through an animal model of infection result in increased genomic rearrangements in *C. albicans* [76,77]. The large-scale changes described above provide *C. albicans* with the ability to rapidly generate genetic and phenotypic diversity within the host environment.

Although LOH events are frequent and widespread in the genome of *C. albicans*, several studies have observed that, for some chromosomes, one haplotype or even a part of it is never found in the homozygous state in the *C. albicans* laboratory strain SC5314. This homozygosity bias has been observed in haploids, in parasexual derivatives, and in *rad52* mutant derivatives [35,37,78]. These observations suggest that recessive lethal and deleterious alleles can be found in the heterozygous state in the genome of *C. albicans*. Several groups, including ours, have identified such recessive lethal or deleterious alleles on chromosome 3A and chromosome 4B [66,79]. Overall, consistent with clonal reproduction, *C. albicans* strains harbour

state with heterozygosity at the *MTL* locus. Homozygosity at the *MTL* locus allows occasional white–opaque phenotypic switching and more efficient mating between opaque cells. Transition from tetraploidy to diploidy or diploidy to haploidy is independent of meiosis and involves random concerted chromosome loss with the intermediate aneuploidy progeny cells. Haploids are shown in blue, diploids in red, and tetraploids in green. (C) Genome sequencing of 182 *C. albicans* isolates confirms a predominantly clonal population structure and reveals, for the first time, footprints of admixtures in two genetic clusters (green arrows), demonstrating the occurrence of (para)sexuality in the *C. albicans* natural environment. LOH (BIR/MCO and GC) is a major driver of intraclade evolution and major LOH events can result in the emergence of clusters with altered virulence/niche restriction, possibly due to pseudogenization [42]. Abbreviations: BIR, break-induced replication; GC, gene conversion; LOH, loss of heterozygosity; MCO, mitotic crossover.



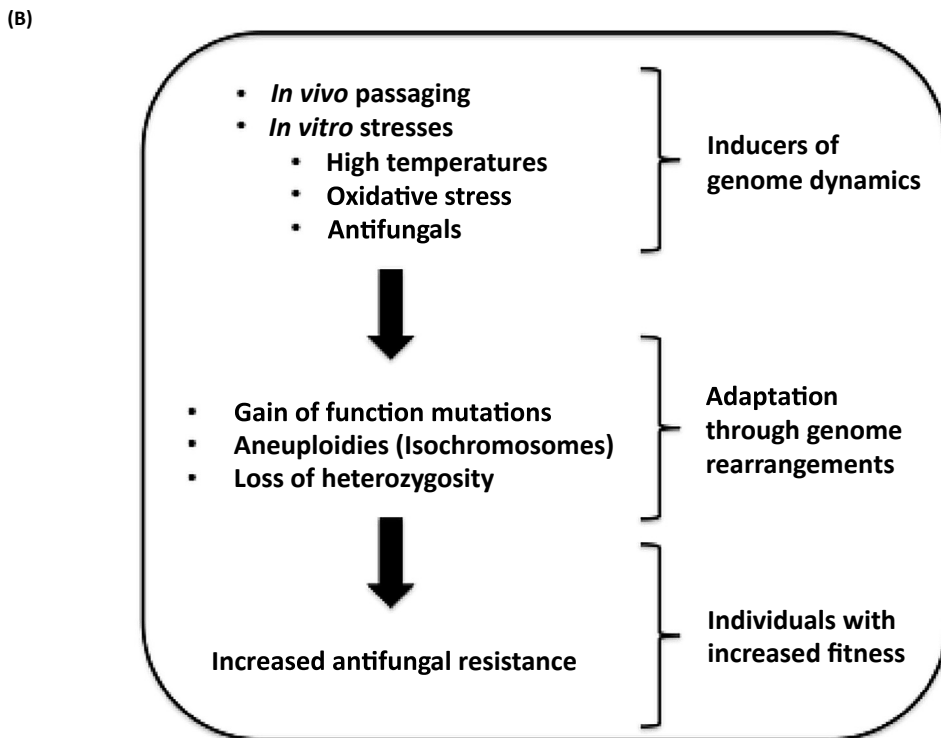
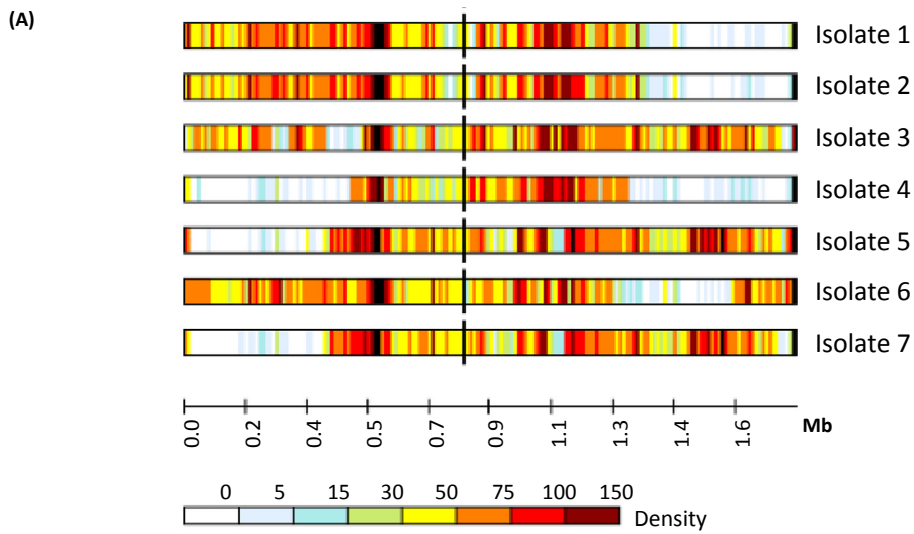
Trends in Genetics

Figure 3. Schematic of Essential Chromosomal Elements in *Candida albicans*. (A) A 3–5-kb long CENP-A-rich centromere (CEN) that lacks any common DNA sequence elements or pericentric repeats. The AT% of CEN regions is not significantly different from the rest of the genome and the CEN DNA sequence does not show any DNA methylation. The CEN function is dependent on the chromosomal context rather than DNA sequence, and thus epigenetically regulated. (B) DNA replication origins (*OR*s), identified as *ORC*-bound regions, are categorised into arm *OR*s and centromere *OR*s. Like centromeres, origins do not show any strong common DNA sequence motif. (C) Telomere repeats in *C. albicans* are unusually long and subtelomeric regions have an unusually high number of *TLO* genes in this organism. The high copy number of *TLO* genes in *C. albicans* is expected to be the result of subtelomeric recombination, mediated positively by *TLO* recombination element and negatively by *Sir2* [98]. (D) The *MRS*, which further consists of three sequence elements, namely, *RB2*, *RPS*, and *HOK*. The *RB2* (~6 kb) and *HOK* (~8 kb) elements are nonrepetitive sequences that occur only once per *MRS*, flanking the *RPS* element. The repeated sequence (*RPS*) is a ~2-kb-long repetitive sequence whose number can vary in an *MRS*. Each *RPS* unit carries an *SfiI* restriction enzyme site. *SfiI* mapping of the *C. albicans* genome served as a valuable tool to study chromosomal rearrangements before the whole genome sequence was available.

recessive lethal and deleterious alleles that constrain the outcome of LOH events. Although **homozygosity** of some alleles has been linked to fitness advantage in a specific host niche, overall genome-wide heterozygosity remains prevalent in the *C. albicans* population. For these reasons, the fate of cells having undergone LOH still needs to be addressed in *C. albicans*.

Specificities of DNA Repair Mechanisms in *Candida albicans*

DNA DSBs, where both strands of the double helix are severed, are the most serious forms of DNA damage. Indeed, failure to repair a DSB leads to loss of the CEN-lacking chromosome fragment, while improper repair of a DSB can lead to gross chromosomal rearrangements such as translocations, inversions, and deletions. Two major pathways of DSB repair are known: HR and **nonhomologous end joining (NHEJ)**. Characterisation of deletion mutants of genes involved in HR (*RAD52*, *RAD51*, *RAD59*, *RAD54*, and *RDH54*) have shown that HR plays a crucial role in DNA damage repair in *C. albicans* [78,80–83]. In contrast, the characterisation of mutants impaired for NHEJ has suggested that this process is not efficient in *C. albicans* [78,82]. Recent results on the mode of repair of **CRISPR-cas9**-induced DSBs are in agreement with this observation but suggest that NHEJ could occur in *C. albicans*, albeit rarely. Indeed, it has been shown that HR is the predominant repair pathway of CRISPR-Cas9-induced DSBs in *S. cerevisiae* and *C. albicans*, in contrast to other yeast species such as

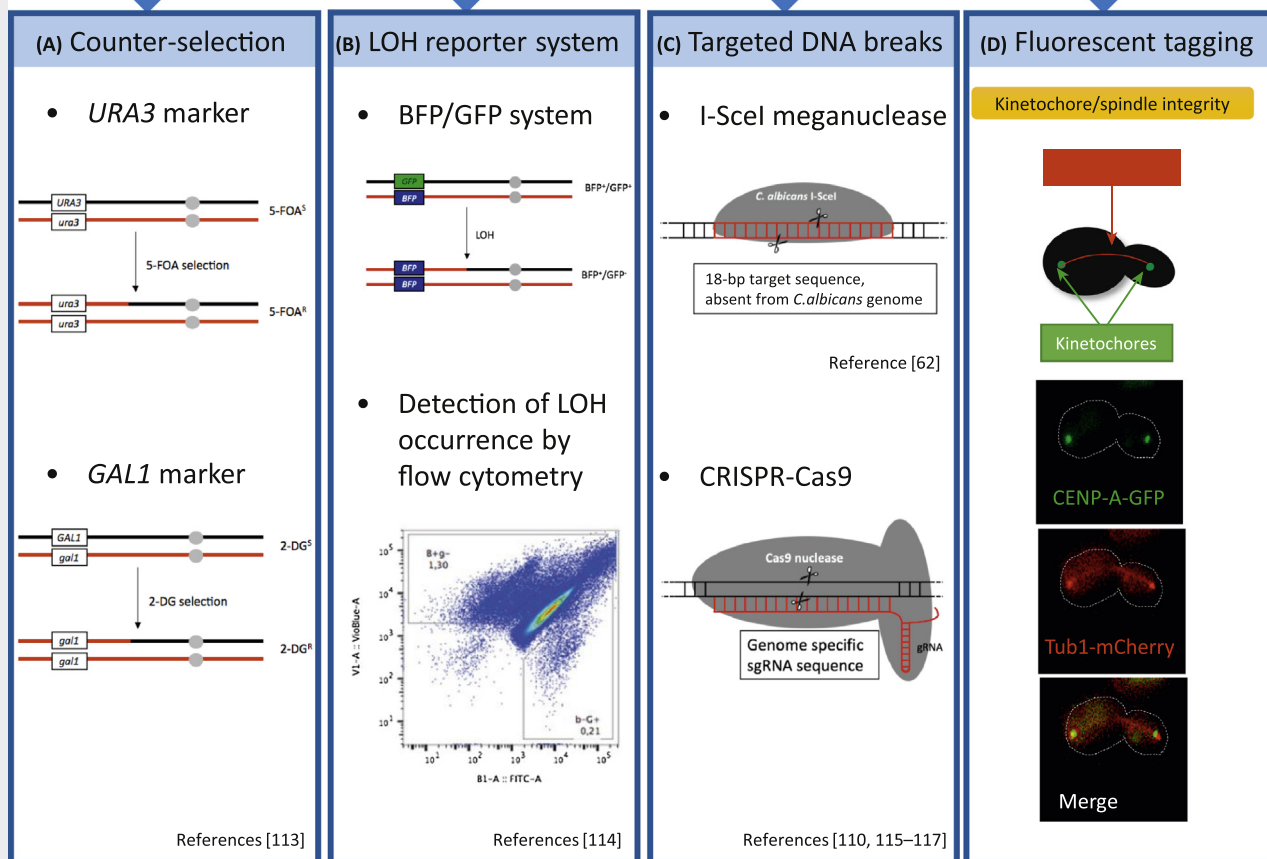


Trends in Genetics

Figure 4. Heterozygosity, LOH, Genome Dynamics, and Antifungal Resistance. (A) Heat map illustrating the density of heterozygous SNPs across chromosome 3 for seven sequenced isolates. Regions that have undergone LOH appear white and are most often extending towards the telomere, indicating that they are the result of either mitotic recombination, break-induced replication, or gene conversion with crossover. (B) Schematic view of the impact of environmental stresses on genome dynamics and adaptation in *C. albicans*. Abbreviation: LOH, loss-of-heterozygosity.

Box 2. A Molecular Toolkit to Study *Candida albicans* Genome Dynamics

Molecular tools have been developed and successfully used to identify and study genome dynamics in *C. albicans*. (A) Identification of LOH events using the *URA3* or *GAL1* markers. In strains that have been engineered to be heterozygous for the *URA3* or *GAL1* gene at a given locus, LOH at this locus leads to resistance to 5-fluoroorotic acid (5-FOA) or 2-deoxygalactose (2-DG), respectively. (B) Identification of LOH events using a combination of *GFP* (green fluorescent protein-coding gene) and *BFP* (blue fluorescent protein-coding gene). In strains that have been engineered to be heterozygous at a given locus through insertion of *GFP* on one chromosome and *BFP* on its homologue, LOH at this locus results in loss of one of the *FP* genes and therefore results in monofluorescence, which can be revealed by flow cytometry. The monofluorescent cells are localised in the side gates and the double fluorescent cells are found in the middle gate. (C) Genome editing systems have been developed in *C. albicans*. A DNA DSB-inducing system was developed through conditional expression of the *S. cerevisiae* I-SceI meganuclease in a *C. albicans* strain engineered to harbour a unique I-SceI cleavage site. Characterisation of repair events at this I-SceI site show that they almost always correspond to GC events but some instances of BIR/MCO or WCL were also observed, as well as combinations of independent events. A method based on the CRISPR/CRISPR-Cas9 system has emerged for genome editing in *C. albicans*. By combining several guiding RNAs, multiple sites can be targeted simultaneously allowing simultaneous editing of multiple chromosomal sites. (D) Live cell fluorescence imaging of chromosome segregation. CENP-A-GFP strains with Tub1-mCherry allows one to follow kinetochore integrity and spindle morphology [110,113–117].

Approaches to study genome dynamics in *C. albicans*

Candida glabrata and *Naumovia castelli* [84]. Moreover, while HR-defective *S. cerevisiae* mutants could still repair a CRISPR-Cas9-induced DSB in the absence of a repair template, likely via NHEJ, the same is not true in *C. albicans*, consistent with limited efficiency of NHEJ in this species [84]. Nevertheless, NHEJ is likely to occur in *C. albicans* as scars typical of this repair process have been reported at repaired CRISPR-Cas9-induced DSBs [85]. Notably, all of these studies have been performed in diploid isolates of *C. albicans* that are heterozygous at the *MTL* locus. In *S. cerevisiae*, NHEJ is downregulated in *a/α* diploid cells when compared with homozygous diploid or haploid cells only expressing *MATa* or *MATα*. This is shown to be accomplished by transcriptional repression of specific genes by the *a1/α2* repressor [86]. Therefore, NHEJ studies in *MTL* homozygous diploid cells or haploid cells should address the absence or presence of NHEJ in *C. albicans*.

Several studies have shown that treatment of *C. albicans* with DNA-damaging agents triggers polarized growth [87,88]. Mutants with altered expression of genes coding for proteins involved in DNA damage response and cell cycle regulation also display aberrant filamentous morphology [48,49,78,87,89–93] (Figure 5). Strikingly, these data suggest that genotoxic-stress-induced polarised growth involves but does not require the expression of hyphal-specific genes. It is possible that stress-induced polarised growth is different from standard hyphal growth. Another key aspect of DNA repair is the accessibility of the DNA lesion to the DNA repair machinery. Proteins involved in chromatin assembly and remodelling have been shown to be important for efficient DNA repair in *C. albicans* as they change chromatin structure and allow repair proteins to access damaged DNA through the acetylation of histone H4 [94]. Similarly, involvement of HR in the kinetochore assembly has been demonstrated in *C. albicans* [52]. In mammalian cells, acetylation of histone H4 has been shown to also play a critical role in directing changes both in chromatin organisation and in promoting recruitment of DSB repair proteins to sites of DNA damage [95]. Moreover, different chromatin signatures associated with HR or NHEJ repair have been recently defined [96]. It has also been demonstrated that, apart from rapidly accumulating DNA damage, *C. albicans* cells lacking the histone acetyltransferase Hat1 also switch from yeast-like to polarized growth [94]. Altogether, these data corroborate

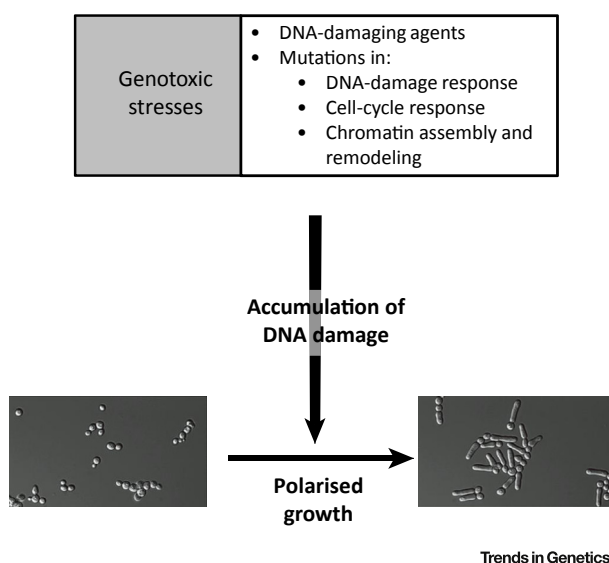


Figure 5. DNA-Damage-Induced Morphogenesis in *Candida albicans*. Schematic of the link between accumulation of DNA damage induced by various genotoxic stresses and polarised growth in *C. albicans*.

that perturbations of cell-cycle progression, a direct consequence of DNA damage, induce filamentous growth in *C. albicans*, in a manner dependent on the DNA damage/replication checkpoint kinase Rad53.

Concluding Remarks

In this review, we have highlighted some of the distinctive features uncovered from recent studies on the genome biology of *C. albicans* that make this yeast a model complementary to *S. cerevisiae* and *S. pombe*; two model species that are at the two extremes of yeast evolution. *C. albicans* exhibits specificities with respect to: (i) its life cycle whereby haploid, diploid, and tetraploid alternate through means of a meiosis-independent, recombinogenic parasexual cycle; (ii) chromosomal landmarks, especially the CENs that have unique organisation and epigenetic properties; (iii) an unusual genome plasticity, that frequently generates aneuploidies and LOH events; (iv) an almost obligate usage of HR for DSB repair; and (v) a coupling of the DNA damage response to morphogenetic shifts. A unique combination of these attributes in one organism allows investigators to address a variety of questions in genome biology that are not generally studied using the conventional yeast models. For instance, as most studies on recombination in *S. cerevisiae* and *S. pombe* employ laboratory haploid or homozygous diploid strains, little is known about the impact of heterozygosity on the biology of yeasts. Results from studies in *C. albicans* clearly demonstrate that heterozygosity is often advantageous, yet allows the propagation of recessive deleterious or lethal alleles that are detrimental upon homozygosis.

Despite changes in epidemiology, *C. albicans* remains responsible for a majority of yeast infections and the treatment of these infections is still a challenge in specific cases, such as systemic or recurrent vulvovaginal candidiasis. One of the key questions is whether *C. albicans* genome plasticity and hallmarks indeed contribute to making this species such an important pathogen. There is no doubt that LOH, ploidy changes, and isochromosome formation contribute to the elevation of antifungal resistance and treatment failure. Moreover, exposure of *C. albicans* to a variety of stresses – antifungals, oxidative stress, high temperature – has been shown to promote recombination events that could help *C. albicans* permanently adapt to changes in environment. Residence of *C. albicans* in animals including in healthy humans, whether as a commensal or pathogen, is accompanied by mutation and recombination events, predominantly short-range LOH (76; Sitterlé *et al.*, personal communication), that could not only reflect adaptation to the host but also help in repairing DNA alterations caused by constant exposure to DNA damaging agents (e.g., reactive oxygen species produced by immune cells). A recent study reports that a combination of mutations and LOH events acquired during serial passaging in the gastrointestinal tract of mice, where *C. albicans* does not normally reside, allows *C. albicans* to shift from a poor gastrointestinal commensal and harmful bloodstream-borne pathogen to an efficient commensal and poor systemic pathogen [97]. Therefore, the high genomic plasticity of *C. albicans* can bear long-term impact on its biology and gaining further insights into the genome biology of this species will certainly impact not only on our understanding of eukaryotic genome biology in general but also the mechanisms that make *C. albicans* such a successful opportunistic pathogen (see Outstanding Questions).

Acknowledgements

M.L., C.D., and K.S. are supported by a grant from the Indo French Centre for the Promotion of Advanced Research (CEFIPRA, Project no. 5703-2). Work in the laboratory of C.D. has been supported by the French Government's Investissement d'Avenir program (Laboratoire d'Excellence Integrative Biology of Emerging Infectious Diseases, ANR-10-LABX-62-IBED). A.F. was the recipient of a PhD. grant from INRA Jouy-en-Josas and Institut Pasteur. Work in the laboratory of K.S. is supported by grants from the Department of Biotechnology, Government of India (BT/PR13909/BRB/

Outstanding Questions

Is *C. albicans* completely devoid of meiosis?

How does Spo11 function during the parasexual cycle?

Can we utilise the parasexual cycle to understand recombination in organisms with cryptic meiosis?

Why is the MRS the hotspot for chromosomal rearrangements?

What is the contribution of the DNA sequence in replication origin and centromere function?

Is heterozygosity necessary for fitness of *C. albicans* in the host?

How is heterozygosity maintained in the largely clonal *C. albicans* population?

What are the mechanisms for tolerance of genome plasticity in *C. albicans*?

Is genome plasticity contributing to *C. albicans* success as a commensal and/or pathogen?

Is there an influence of the microbiota on *C. albicans* genome plasticity?

Is NHEJ active in *C. albicans*?

How is the link between DNA damage and cell polarity precisely established?

10/1432/2015; BT/PR14557/BRB/10/15529/2016; BT/HRD/35/01/03/2017) and a grant for Life Science Research, Education, and Training (BT/INF/22/SP27679/2018). P.J. and K.S. are also financially supported by an intramural Jawaharlar Nehru Centre for Advanced Scientific Research (JNCASR) grant.

References

- Botstein, D. and Fink, G.R. (1988) Yeast: an experimental organism for modern biology. *Science* 240, 1439–1443
- Cavanaugh, A.M. and Jaspersen, S.L. (2017) Big lessons from little yeast: budding and fission yeast centrosome structure, duplication, and function. *Annu. Rev. Genet.* 51, 361–383
- Fair, B.J. and Pleiss, J.A. (2017) The power of fission: yeast as a tool for understanding complex splicing. *Curr. Genet.* 63, 375–380
- Hinnebusch, A.G. and Johnston, M. (2011) YeastBook: an encyclopedia of the reference eukaryotic cell. *Genetics* 189, 683–684
- Noma, K.I. (2017) The yeast genomes in three dimensions: mechanisms and functions. *Annu. Rev. Genet.* 51, 23–44
- Nurse, P.M. (2002) Nobel Lecture: Cyclin dependent kinases and cell cycle control. *Biosci. Rep.* 22, 487–499
- Brown, G.D. et al. (2012) Hidden killers: human fungal infections. *Sci. Transl. Med.* 4, 165rv113
- Ene, I.V. and Bennett, R.J. (2014) The cryptic sexual strategies of human fungal pathogens. *Nat. Rev. Microbiol.* 12, 239–251
- Erwig, L.P. and Gow, N.A. (2016) Interactions of fungal pathogens with phagocytes. *Nat. Rev. Microbiol.* 14, 163–176
- Gow, N.A. et al. (2011) *Candida albicans* morphogenesis and host defence: discriminating invasion from colonization. *Nat. Rev. Microbiol.* 10, 112–122
- Lohse, M.B. et al. (2018) Development and regulation of single- and multi-species *Candida albicans* biofilms. *Nat. Rev. Microbiol.* 16, 19–31
- Netea, M.G. et al. (2015) Immune defence against *Candida* fungal infections. *Nat. Rev. Immunol.* 15, 630–642
- Noble, S.M. et al. (2017) *Candida albicans* cell-type switching and functional plasticity in the mammalian host. *Nat. Rev. Microbiol.* 15, 96–108
- Perfect, J.R. (2017) The antifungal pipeline: a reality check. *Nat. Rev. Drug Discov.* 16, 603–616
- Shapiro, R.S. et al. (2011) Regulatory circuitry governing fungal development, drug resistance, and disease. *Microbiol. Mol. Biol. Rev.* 75, 213–267
- Sudbery, P.E. (2011) Growth of *Candida albicans* hyphae. *Nat. Rev. Microbiol.* 9, 737–748
- Bougnoux, M.E. et al. (2008) Mating is rare within as well as between clades of the human pathogen *Candida albicans*. *Fungal. Genet. Biol.* 45, 221–231
- Graser, Y. et al. (1996) Molecular markers reveal that population structure of the human pathogen *Candida albicans* exhibits both clonality and recombination. *Proc. Natl. Acad. Sci. U. S. A.* 93, 12473–12477
- Jones, T. et al. (2004) The diploid genome sequence of *Candida albicans*. *Proc. Natl. Acad. Sci. U. S. A.* 101, 7329–7334
- Riggsby, W.S. et al. (1982) DNA content, kinetic complexity, and the ploidy question in *Candida albicans*. *Mol. Cell Biol.* 2, 853–862
- Hull, C.M. and Johnson, A.D. (1999) Identification of a mating type-like locus in the asexual pathogenic yeast *Candida albicans*. *Science* 285, 1271–1275
- Tzung, K.W. et al. (2001) Genomic evidence for a complete sexual cycle in *Candida albicans*. *Proc. Natl. Acad. Sci. U. S. A.* 98, 3249–3253
- Butler, G. et al. (2009) Evolution of pathogenicity and sexual reproduction in eight *Candida* genomes. *Nature* 459, 657–662
- Hull, C.M. et al. (2000) Evidence for mating of the asexual yeast *Candida albicans* in a mammalian host. *Science* 289, 307–310
- Magee, B.B. and Magee, P.T. (2000) Induction of mating in *Candida albicans* by construction of MTL α and MTL α strains. *Science* 289, 310–313
- Bennett, R.J. and Johnson, A.D. (2003) Completion of a parasexual cycle in *Candida albicans* by induced chromosome loss in tetraploid strains. *EMBO J.* 22, 2505–2515
- Dumitru, R. et al. (2007) *In vivo* and *in vitro* anaerobic mating in *Candida albicans*. *Eukaryot. Cell* 6, 465–472
- Lachke, S.A. et al. (2003) Skin facilitates *Candida albicans* mating. *Infect. Immun.* 71, 4970–4976
- Miller, M.G. and Johnson, A.D. (2002) White-opaque switching in *Candida albicans* is controlled by mating-type locus homeodomain proteins and allows efficient mating. *Cell* 110, 293–302
- Banerjee, M. et al. (2008) UME6, a novel filament-specific regulator of *Candida albicans* hyphal extension and virulence. *Mol. Biol. Cell* 19, 1354–1365
- Chen, C.G. et al. (2004) CaNdt80 is involved in drug resistance in *Candida albicans* by regulating CDR1. *Antimicrob. Agents Chemother.* 48, 4505–4512
- Nobile, C.J. et al. (2012) A recently evolved transcriptional network controls biofilm development in *Candida albicans*. *Cell* 148, 126–138
- Nocedal, I. et al. (2017) Gene regulatory network plasticity predates a switch in function of a conserved transcription regulator. *eLife* 6, e23250
- Bartholomew, C.R. et al. (2012) Ume6 transcription factor is part of a signaling cascade that regulates autophagy. *Proc. Natl. Acad. Sci. U. S. A.* 109, 11206–11210
- Forche, A. et al. (2008) The parasexual cycle in *Candida albicans* provides an alternative pathway to meiosis for the formation of recombinant strains. *PLoS Biol.* 6, e110
- Hickman, M.A. et al. (2015) Parasexual ploidy reduction drives population heterogeneity through random and transient aneuploidy in *Candida albicans*. *Genetics* 200, 781–794
- Hickman, M.A. et al. (2013) The ‘obligate diploid’ *Candida albicans* forms mating-competent haploids. *Nature* 494, 55–59
- Berman, J. (2016) Ploidy plasticity: a rapid and reversible strategy for adaptation to stress. *FEMS yeast research* 16,
- Gerstein, A.C. et al. (2017) Ploidy tug-of-war: Evolutionary and genetic environments influence the rate of ploidy drive in a human fungal pathogen. *Evolution* 71, 1025–1038
- Schmid, J. et al. (2016) Last hope for the doomed? Thoughts on the importance of a parasexual cycle for the yeast *Candida albicans*. *Curr. Genet.* 62, 81–85
- Zhang, N. et al. (2015) Selective advantages of a parasexual cycle for the yeast *Candida albicans*. *Genetics* 200, 1117–1132
- Ropars, J. et al. (2018) Gene flow contributes to diversification of the major fungal pathogen *Candida albicans*. *Nat. Commun.* 9, 2253
- Sanyal, K. et al. (2004) Centromeric DNA sequences in the pathogenic yeast *Candida albicans* are all different and unique. *Proc. Natl. Acad. Sci. U. S. A.* 101, 11374–11379
- Baum, M. et al. (2006) Formation of functional centromeric chromatin is specified epigenetically in *Candida albicans*. *Proc. Natl. Acad. Sci. U. S. A.* 103, 14877–14882
- Thakur, J. and Sanyal, K. (2013) Efficient neocentromere formation is suppressed by gene conversion to maintain centromere function at native physical chromosomal loci in *Candida albicans*. *Genome Res.* 23, 638–652
- Ketel, C. et al. (2009) Neocentromeres form efficiently at multiple possible loci in *Candida albicans*. *PLoS Genet.* 5, e1000400

47. Burrack, L.S. *et al.* (2016) Neocentromeres provide chromosome segregation accuracy and centromere clustering to multiple loci along a *Candida albicans* chromosome. *PLoS Genet.* 12, e1006317
48. Thakur, J. and Sanyal, K. (2012) A coordinated interdependent protein circuitry stabilizes the kinetochore ensemble to protect CENP-A in the human pathogenic yeast *Candida albicans*. *PLoS Genet.* 8, e1002661
49. Roy, B. *et al.* (2011) CaMtw1, a member of the evolutionarily conserved Mis12 kinetochore protein family, is required for efficient inner kinetochore assembly in the pathogenic yeast *Candida albicans*. *Mol. Microbiol.* 80, 14–32
50. Tsai, H.J. *et al.* (2014) Origin replication complex binding, nucleosome depletion patterns, and a primary sequence motif can predict origins of replication in a genome with epigenetic centromeres. *mBio* 5, e01703-01714
51. Koren, A. *et al.* (2010) Epigenetically-inherited centromere and neocentromere DNA replicates earliest in S-phase. *PLoS Genet.* 6, e1001068
52. Mitra, S. *et al.* (2014) Rad51-Rad52 mediated maintenance of centromeric chromatin in *Candida albicans*. *PLoS Genet.* 10, e1004344
53. McEachern, M.J. and Hicks, J.B. (1993) Unusually large telomeric repeats in the yeast *Candida albicans*. *Mol. Cell Biol.* 13, 551–560
54. Freire-Beneitez, V. *et al.* (2016) *Candida albicans* repetitive elements display epigenetic diversity and plasticity. *Sci Rep.* 6, 22989
55. Zhang, A. *et al.* (2012) The Tlo proteins are stoichiometric components of *Candida albicans* mediator anchored via the Med3 subunit. *Eukaryot. Cell* 11, 874–884
56. Jackson, A.P. *et al.* (2009) Comparative genomics of the fungal pathogens *Candida dubliniensis* and *Candida albicans*. *Genome Res.* 19, 2231–2244
57. Dunn, M.J. *et al.* (2018) Functional diversification accompanies gene family expansion of MED2 homologs in *Candida albicans*. *PLoS Genet.* 14, e1007326
58. Chibana, H. and Magee, P.T. (2009) The enigma of the major repeat sequence of *Candida albicans*. *Future Microbiol.* 4, 171–179
59. Lephart, P.R. *et al.* (2005) Effect of the major repeat sequence on chromosome loss in *Candida albicans*. *Eukaryot. Cell* 4, 733–741
60. Chibana, H. *et al.* (2000) Fine-resolution physical mapping of genomic diversity in *Candida albicans*. *Genome Res.* 10, 1865–1877
61. Hirakawa, M.P. *et al.* (2015) Genetic and phenotypic intra-species variation in *Candida albicans*. *Genome Res.* 25, 413–425
62. Muzzey, D. *et al.* (2013) Assembly of a phased diploid *Candida albicans* genome facilitates allele-specific measurements and provides a simple model for repeat and indel structure. *Genome Biol.* 14, R97
63. Muzzey, D. *et al.* (2014) Extensive and coordinated control of allele-specific expression by both transcription and translation in *Candida albicans*. *Genome Res.* 24, 963–973
64. Brimacombe, C.A. *et al.* (2018) Chromatin rewiring mediates programmed evolvability via aneuploidy. *bioRxiv*. In: <https://doi.org/10.1101/407841>
65. Chatterjee, N. and Walker, G.C. (2017) Mechanisms of DNA damage, repair, and mutagenesis. *Environ. Mol. Mutagen.* 58, 235–263
66. Feri, A. *et al.* (2016) Analysis of repair mechanisms following an induced double-strand break uncovers recessive deleterious alleles in the *Candida albicans* diploid genome. *mBio* 7, <http://dx.doi.org/10.1128/mBio.01109-16>
67. Coste, A. *et al.* (2007) Genotypic evolution of azole resistance mechanisms in sequential *Candida albicans* isolates. *Eukaryot. Cell* 6, 1889–1904
68. Ford, C.B. *et al.* (2015) The evolution of drug resistance in clinical isolates of *Candida albicans*. *eLife* 4, e00662
69. Morschhauser, J. *et al.* (2007) The transcription factor Mrr1p controls expression of the MDR1 efflux pump and mediates multidrug resistance in *Candida albicans*. *PLoS Pathog.* 3, e164
70. Selmecki, A. *et al.* (2006) Aneuploidy and isochromosome formation in drug-resistant *Candida albicans*. *Science* 313, 367–370
71. Selmecki, A. *et al.* (2008) An isochromosome confers drug resistance *in vivo* by amplification of two genes, ERG11 and TAC1. *Mol. Microbiol.* 68, 624–641
72. Chang, S.L. *et al.* (2013) Dynamic large-scale chromosomal rearrangements fuel rapid adaptation in yeast populations. *PLoS Genet.* 9, e1003232
73. Yona, A.H. *et al.* (2012) Chromosomal duplication is a transient evolutionary solution to stress. *Proc. Natl. Acad. Sci. U. S. A.* 109, 21010–21015
74. Forche, A. *et al.* (2011) Stress alters rates and types of loss of heterozygosity in *Candida albicans*. *mBio* 2, <http://dx.doi.org/10.1128/mBio.00129-11>
75. Harrison, B.D. *et al.* (2014) A tetraploid intermediate precedes aneuploid formation in yeasts exposed to fluconazole. *PLoS Biol.* 12, e1001815
76. Ene, I.V. *et al.* (2018) Global analysis of mutations driving microevolution of a heterozygous diploid fungal pathogen. *Proc. Natl. Acad. Sci. U. S. A.* 115, E8688–E8697
77. Forche, A. *et al.* (2018) Rapid phenotypic and genotypic diversification after exposure to the oral host niche in *Candida albicans*. *Genetics* 209, 725–741
78. Andaluz, E. *et al.* (2011) Rad52 function prevents chromosome loss and truncation in *Candida albicans*. *Mol. Microbiol.* 79, 1462–1482
79. Ciudad, T. *et al.* (2016) Phenotypic consequences of a spontaneous loss of heterozygosity in a common laboratory strain of *Candida albicans*. *Genetics* 203, 1161–1176
80. Bellido, A. *et al.* (2015) Genetic interactions among homologous recombination mutants in *Candida albicans*. *Fungal Genet. Biol.* 74, 10–20
81. Garcia-Prieto, F. *et al.* (2010) Role of the homologous recombination genes RAD51 and RAD59 in the resistance of *Candida albicans* to UV light, radiomimetic and anti-tumor compounds and oxidizing agents. *Fungal Genet. Biol.* 47, 433–445
82. Legrand, M. *et al.* (2007) Role of DNA mismatch repair and double-strand break repair in genome stability and antifungal drug resistance in *Candida albicans*. *Eukaryot. Cell* 6, 2194–2205
83. Legrand, M. *et al.* (2011) The contribution of the S-phase checkpoint genes MEC1 and SGS1 to genome stability maintenance in *Candida albicans*. *Fungal Genet. Biol.* 48, 823–830
84. Vyas, V.K. *et al.* (2018) New CRISPR mutagenesis strategies reveal variation in repair mechanisms among fungi. *mSphere* 3, In: <https://doi.org/10.1128/mSphere.00154-18>
85. Ng, H. and Dean, N. (2017) Dramatic improvement of CRISPR/Cas9 editing in *Candida albicans* by increased single guide RNA expression. *mSphere* 2, In: <https://doi.org/10.1128/mSphere.00385-16>
86. Valencia, M. *et al.* (2001) NEJ1 controls non-homologous end joining in *Saccharomyces cerevisiae*. *Nature* 414, 666–669
87. Bachewich, C. *et al.* (2005) Cell cycle arrest during S or M phase generates polarized growth via distinct signals in *Candida albicans*. *Mol. Microbiol.* 57, 942–959
88. da Silva Dantas, A. *et al.* (2010) Thioredoxin regulates multiple hydrogen peroxide-induced signaling pathways in *Candida albicans*. *Mol. Cell Biol.* 30, 4550–4563
89. Bachewich, C. and Whiteway, M. (2005) Cyclin Cln3p links G1 progression to hyphal and pseudohyphal development in *Candida albicans*. *Eukaryot. Cell* 4, 95–102
90. Bensen, E.S. *et al.* (2005) The mitotic cyclins Clb2p and Clb4p affect morphogenesis in *Candida albicans*. *Mol. Biol. Cell* 16, 3387–3400

91. Shi, Q.M. *et al.* (2007) Critical role of DNA checkpoints in mediating genotoxic-stress-induced filamentous growth in *Candida albicans*. *Mol. Biol. Cell* 18, 815–826
92. Thakur, J. and Sanyal, K. (2011) The essentiality of the fungus-specific Dam1 complex is correlated with a one-kinetochore-one-microtubule interaction present throughout the cell cycle, independent of the nature of a centromere. *Eukaryot. Cell* 10, 1295–1305
93. Loll-Kripplleber, R. *et al.* (2014) A study of the DNA damage checkpoint in *Candida albicans*: uncoupling of the functions of Rad53 in DNA repair, cell cycle regulation and genotoxic stress-induced polarized growth. *Mol. Microbiol.* 91, 452–471
94. Tscherner, M. *et al.* (2012) The histone acetyltransferase Hat1 facilitates DNA damage repair and morphogenesis in *Candida albicans*. *Mol. Microbiol.* 86, 1197–1214
95. Dhar, S. *et al.* (2017) The tale of a tail: histone H4 acetylation and the repair of DNA breaks. *Philos. Trans. R. Soc. Lond. B. Biol. Sci.* 372
96. Clouaire, T. *et al.* (2018) Comprehensive mapping of histone modifications at DNA double-strand breaks deciphers repair pathway chromatin signatures. *Mol. Cell.* 72, 250–262 e256
97. Tso, G.H.W. *et al.* (2018) Experimental evolution of a fungal pathogen into a gut symbiont. *Science* 362, 589–595
98. Freire-Beneitez, V. *et al.* (2016) Sir2 regulates stability of repetitive domains differentially in the human fungal pathogen *Candida albicans*. *Nucleic Acids Res.* 44, 9166–9179
99. Santos, M.A. *et al.* (2011) The genetic code of the fungal CTG clade. *C. R. Biol.* 334, 607–611
100. Shen, X.X. *et al.* (2016) Reconstructing the backbone of the Saccharomycotina yeast phylogeny using genome-scale data. *G3 (Bethesda)* 6, 3927–3939
101. Skrzypek, M.S. *et al.* (2018) Using the *Candida* genome database. *Methods Mol. Biol.* 1757, 31–47
102. Hernday, A.D. *et al.* (2010) Genetics and molecular biology in *Candida albicans*. *Methods Enzymol.* 470, 737–758
103. Xu, T. *et al.* (2011) Genome-wide transposon mutagenesis in *Saccharomyces cerevisiae* and *Candida albicans*. *Methods Mol. Biol.* 765, 207–224
104. Mielich, K. *et al.* (2018) Maize transposable elements Ac/Ds as insertion mutagenesis tools in *Candida albicans*. *G3 (Bethesda)* 8, 1139–1145
105. Roemer, T. *et al.* (2003) Large-scale essential gene identification in *Candida albicans* and applications to antifungal drug discovery. *Mol. Microbiol.* 50, 167–181
106. Xu, D. *et al.* (2007) Genome-wide fitness test and mechanism-of-action studies of inhibitory compounds in *Candida albicans*. *PLoS Pathog.* 3, e92
107. Nobile, C.J. and Mitchell, A.P. (2009) Large-scale gene disruption using the *UAU1* cassette. *Methods Mol. Biol.* 499, 175–194
108. Homann, O.R. *et al.* (2009) A phenotypic profile of the *Candida albicans* regulatory network. *PLoS Genet.* 5, e1000783
109. Noble, S.M. *et al.* (2010) Systematic screens of a *Candida albicans* homozygous deletion library decouple morphogenetic switching and pathogenicity. *Nat. Genet.* 42, 590–598
110. Shapiro, R.S. *et al.* (2018) A CRISPR-Cas9- based gene drive platform for genetic interaction analysis in *Candida albicans*. *Nat. Microbiol.* 3, 73–82
111. Segal, E.S. *et al.* (2018) Gene essentiality analyzed by *in vivo* transposon mutagenesis 658 and machine learning in a stable haploid isolate of *Candida albicans*. *mBio* 9, In: <https://doi.org/10.1128/mBio.02048-18>
112. Legrand, M. *et al.* (2018) Generating genomic platforms to study *Candida albicans* pathogenesis. *Nucleic Acids Res.* 46, 6935–6949
113. Forche, A. *et al.* (2003) A system for studying genetic changes in *Candida albicans* during infection. *Fungal. Genet. Biol.* 39, 38–50
114. Loll-Kripplleber, R. *et al.* (2015) A FACS-optimized screen identifies regulators of genome stability in *Candida albicans*. *Eukaryot. Cell* 14, 311–322
115. Vyas, V.K. *et al.* (2015) A *Candida albicans* CRISPR system permits genetic engineering of essential genes and gene families. *Science advances* 1, e1500248
116. Min, K. *et al.* (2016) *Candida albicans* gene deletion with a transient CRISPR-Cas9 system. *mSphere* 1, In: <https://doi.org/10.1128/mSphere.00130-16>
117. Nguyen, N. *et al.* (2017) An efficient, rapid, and recyclable system for CRISPR-mediated genome editing in *Candida albicans*. *mSphere* 2, In: <https://doi.org/10.1128/mSphereDirect.00149-17>

Cis- and *Trans*-chromosomal Interactions Define Pericentric Boundaries in the Absence of Conventional Heterochromatin

Lakshmi Sreekumar,* Priya Jaitly,* Yao Chen,† Bhagya C. Thimmappa,*¹ Amartya Sanyal,† and Kaustuv Sanyal*²

*Molecular Biology and Genetics Unit, Jawaharlal Nehru Centre for Advanced Scientific Research, Bangalore 560064, India and

†School of Biological Sciences, Nanyang Technological University, Singapore, Singapore 637551

ORCID IDs: 0000-0002-1849-4374 (L.S.); 0000-0002-1660-6416 (P.J.); 0000-0003-2708-8674 (Y.C.); 0000-0002-2109-4478 (A.S.); 0000-0002-6611-4073 (K.S.)

ABSTRACT The diploid budding yeast *Candida albicans* harbors unique CENPA-rich 3- to 5-kb regions that form the centromere (CEN) core on each of its eight chromosomes. The epigenetic nature of these CENs does not permit the stabilization of a functional kinetochore on an exogenously introduced CEN plasmid. The flexible nature of such centromeric chromatin is exemplified by the reversible silencing of a transgene upon its integration into the CENPA-bound region. The lack of a conventional heterochromatin machinery and the absence of defined boundaries of CENPA chromatin makes the process of CEN specification in this organism elusive. Additionally, upon native CEN deletion, *C. albicans* can efficiently activate neocentromeres proximal to the native CEN locus, hinting at the importance of CEN-proximal regions. In this study, we examine this CEN-proximity effect and identify factors for CEN specification in *C. albicans*. We exploit a counterselection assay to isolate cells that can silence a transgene when integrated into the CEN-flanking regions. We show that the frequency of reversible silencing of the transgene decreases from the central core of *CEN7* to its peripheral regions. Using publicly available *C. albicans* high-throughput chromosome conformation capture data, we identify a 25-kb region centering on the CENPA-bound core that acts as CEN-flanking compact chromatin (CFCC). *Cis-* and *trans*-chromosomal interactions associated with the CFCC spatially segregates it from bulk chromatin. We further show that neocentromere activation on chromosome 7 occurs within this specified region. Hence, this study identifies a specialized CEN-proximal domain that specifies and restricts the centromeric activity to a unique region.

KEYWORDS centromere; CENPA; Hi-C; *Candida albicans*; neocentromere

In a majority of eukaryotes, centromere (CEN) specification is fulfilled by the assembly of the histone H3 variant, CENPA, and subsequent kinetochore stabilization. In most fungal species, CENs extend over to a region on every chromosome, ranging in sizes from 3 to 300 kb (Friedman and Freitag 2017), which are categorized as short regional or long re-

gional CENs. The CENs in the *Candida* species are one of the most well-studied short regional CENs. *Candida albicans* has unique 3–5 kb CENPA-bound CEN DNA (Sanyal *et al.* 2004), as does *C. dubliniensis* (Padmanabhan *et al.* 2008) and *C. lusitanae* (Kapoor *et al.* 2015). On the other hand, the 10- to 11-kb CENs in *C. tropicalis* consist of a 2- to 5-kb central core flanked by inverted repeats (Chatterjee *et al.* 2016). The 40- to 110-kb-long regional CENs of *Schizosaccharomyces pombe* contain a 10- to 14-kb-long CENPA-bound region flanked by outer pericentric repeats (Clarke *et al.* 1986). The filamentous yeast *Neurospora crassa* harbors 150–300 kb of heterochromatic CENPA-rich DNA (Smith *et al.* 2011). Among the basidiomycetes, *Cryptococcus neoformans* contain 27–65 kb of transposon-rich CENPA-bound DNA sequences (Yadav *et al.* 2018). Evidently, regional CENs in fungi do not

Copyright © 2019 by the Genetics Society of America

doi: <https://doi.org/10.1534/genetics.119.302179>

Manuscript received April 4, 2019; accepted for publication May 22, 2019; published Early Online May 29, 2019.

Supplemental material available at FigShare: <https://doi.org/10.25386/genetics.8197388>.

¹Present address: Department of Biochemistry, Robert-Cedergren Centre for Bioinformatics and Genomics, University of Montreal, Montreal, QC H3T1J4, Canada.

²Corresponding author: Molecular Mycology Laboratory, Molecular Biology and Genetics Unit, Jawaharlal Nehru Centre for Advanced Scientific Research, Jakkur Post, Bangalore 560064, India. E-mail: sanyal@jncasr.ac.in

entirely depend on conserved DNA elements for kinetochore binding, and therefore have been proposed as excellent models to study epigenetically regulated metazoan CENs.

The centromeric chromatin is different from bulk chromatin and is epigenetically specified in most regional CENs (Sullivan and Karpen 2004). While the core CEN and adjacent pericentric regions are poorly transcribed, pervasive levels of transcription at fungal CENs are known to influence CEN activity (Choi *et al.* 2011; Ohkuni and Kitagawa 2011; Ling and Yuen 2019). Even though CENPA limits its localization on a chromosome, the functional region required for chromosome segregation is much larger and involves pericentric regions. This is largely exemplified in *S. pombe* minichromosomes, which are stabilized in the presence of an outer pericentric repeat in addition to the central core (Baum *et al.* 1994). Centric and pericentric chromatin differ notably in fungal systems. In *S. pombe*, H3 nucleosomes are nearly absent from the CENPA-rich central core (Thakur *et al.* 2015). RNA interference (RNAi)-directed heterochromatin assembly at the outer repeat mediates targeting of CENPA by Clr4-mediated dimethylation at H3K9 (Volpe *et al.* 2002; Folco *et al.* 2008; Allshire and Ekwall 2015). These features are shared in *C. neoformans*, where the extensively methylated CEN DNA is enriched with H3K9me2 and maintained with the help of the RNAi machinery (Yadav *et al.* 2018). In contrast, the CENPA-bound regions in *N. crassa* have heterochromatic properties containing H3K9me3 nucleosomes and 5-methylcytosine (5mC) (Smith *et al.* 2011). Their pericentric regions are 5- to 20-kb long and enriched in H3K4me3 and 5mC (Smith *et al.* 2011; Friedman and Freitag 2017). All known variants of fungal CEN chromatin in regional CENs are more similar to heterochromatin than euchromatin, largely owing to the presence of silencing histone marks and components of RNAi machinery (Friedman and Freitag 2017). Intriguingly, the pericentric boundaries are often not well defined in organisms having short regional CENs, as features like pericentric repeats, associated histone marks, or RNAi machinery are either lacking or cryptic.

One of the hallmarks of the epigenetic control at CENs is the reversible silencing of a transgene positioned within the CENPA-binding region. Transgenes inserted at the central core and outer repeats of the *S. pombe* CENs undergo transcriptional silencing that are clonally inherited. Compared to the outer repeats that are highly heterochromatinized, transgene silencing within the CENPA-bound central core is relatively unstable, resulting in variegated expression (Allshire *et al.* 1994; Karpen and Allshire 1997; Allshire and Ekwall 2015). Hence, transgene silencing is an effective screen employed to study centric and pericentric heterochromatin properties. The epigenetic regulation of CENs has also been demonstrated by neocentromere formation. First observed in humans to rescue acentric fragments (Voullaire *et al.* 1993), neocentromeres are activated at ectopic loci when the native

CEN is inactivated. Therefore, neocentromeres are an aid to study *de novo* CEN formation mechanisms. Neocentromeres are formed at CEN-proximal loci in *Drosophila* (Maggert and Karpen 2001) and chicken cells (Shang *et al.* 2013). The assembly of ectopic CENPA as a “CENPA-rich zone” or “CENPA cloud” surrounding the endogenous CEN and proximity of neocentromere hotspots to the native CEN in these organisms indicates that CENPA is peppered on CEN-adjacent loci and can get rapidly incorporated into the CEN upon eviction (Fukagawa and Earnshaw 2014). Also, the site of neocentromere activation is found to be incompatible with transcription (Scott and Sullivan 2014). These epigenetic mechanisms ensure stable propagation of active CENs across generations.

CENs cluster next to the spindle pole bodies throughout the cell cycle in budding yeast species including *Saccharomyces cerevisiae* (Jin *et al.* 2000; Haase *et al.* 2013) and several species of *Candida* (Sanyal and Carbon 2002; Padmanabhan *et al.* 2008; Burrack *et al.* 2016; Chatterjee *et al.* 2016). Clustered centromeric regions were shown to be in physical proximity by a genome-wide chromosomal interaction study in *S. cerevisiae*, giving rise to physical interactions between different CENs (Duan *et al.* 2010). High-throughput chromosome conformation capture (Hi-C) and related studies in *S. cerevisiae* have revealed chromosome substructures in which domains with similar contact probabilities have higher interactions than the ones that interact due to random diffusion (Tjong *et al.* 2012; Eser *et al.* 2017). Recently, chromosome conformation capture-on-chip (4C) analysis in vertebrates revealed that clustered CENs are present in a compact chromatin environment (Nishimura *et al.* 2018). The neocentromeres in these cells were commonly associated with specific heterochromatin-rich regions in the three-dimensional (3D) nuclear space. Hence, the 3D architecture of the chromosome, its scaffolds, and its associated chromatin within the nucleus provide the spatial cues required to specify CEN location.

Nonrepetitive CENs serve as excellent models to study characterization of centromeric chromatin. In *C. albicans*, every CEN harbors a unique CEN DNA sequence (Sanyal *et al.* 2004), each of which cannot stabilize a CEN plasmid (Sanyal *et al.* 2004; Baum *et al.* 2006). The activation of neocentromeres at hotspots proximal to the native CEN location (Thakur and Sanyal 2013) and presence of CEN-proximal replication origins (Koren *et al.* 2010; Mitra *et al.* 2014) indicate the prominent role of CEN-proximal or pericentric regions for CEN function. Moreover, there is no functional evidence for the existence of a pericentric boundary element to restrict CENPA in *C. albicans*, as seen in the case of CENs in *S. pombe* (Karpen and Allshire 1997; Allshire and Ekwall 2015). Unlike *S. pombe*, the genome of *C. albicans* does not encode an HP1/Swi6-like protein, an H3K9 methyltransferase like Clr4, and components of a fully functional RNAi machinery (Freire-Benítez *et al.* 2016). There is no evidence of DNA methylation at the CEN DNA in *C. albicans* (Baum *et al.* 2006; Mishra *et al.* 2011). The reversible silencing of the

expression of a marker gene, *URA3*, captured by 5-Fluoroorotic acid (5-FOA) counterselection, has been observed upon its integration into the CENPA-binding region of the CEN in *C. albicans*, giving it a transcriptionally flexible status (Thakur and Sanyal 2013). These features make it difficult to determine the exact molecular cues for positioning CENPA to form centromeric chromatin in this organism.

In the present study, we attempt to identify factors that determine CEN formation within a confined territory of the 3D nuclear space. We do so by combining a transgene silencing assay on chromosome 7 (Chr7) with analysis of published Hi-C data to decipher pericentromeric chromatin boundaries in *C. albicans* and map CEN-flanking compact chromatin (CFCC). This CFCC acts as the pericentromere, spatially segregating CENs from bulk chromatin and favoring neocentromere formation.

Materials and Methods

Construction of *URA3* integration strains

To construct the individual *URA3* integration cassettes, long primer pairs were designed (Supplemental Material, Table S5). Briefly, 70-bp regions both upstream and downstream of the site of integration were incorporated in the primers as overhangs. For all the integrations (except the L3 and R2 loci), the 1.4-kb *URA3* gene was amplified from the plasmid pUC19-*URA3* (Mitra *et al.* 2014) using the aforementioned primers. The integration corresponding to L3 was constructed using an *MluI*-digested plasmid pFA-*URA3*-I-*SceI*-TS-Orf 19.6524/25. The integration corresponding to R2 was constructed using an *MluI*-digested plasmid pFA-*URA3*-I-*SceI*-TS-Orf 19.6520/22. The PCR and digestion products were used to independently transform J200 (Thakur and Sanyal 2013). The transformants were selected on complete medium (CM) lacking uridine (CM-Uri) and confirmed by PCR. For the *CEN7* deletion experiments, integration cassettes corresponding to L4 and R4 loci were transformed in 8675 (Joglekar *et al.* 2008) and confirmed by PCR. Three independent transformants of each integration type were used for the assays. All the distances of individual *URA3* insertions are indicated with respect to the midpoint of *CEN7* which has been taken as Ca21Chr7_427262.

Construction of *Mtw1*-Protein A-expressing strains

To tag an endogenous copy of *MTW1* with Protein A, the *MTW1*-TAP fragment was amplified from CAKS13 (Roy *et al.* 2011) using primers listed in Table S5. This fragment was then cloned as a *NotI*/*SpeI* fragment in pBS-NAT to obtain the plasmid pMTW1-TAP(NAT). The neocentromere strains LSK446, LSK459 (5-FOA sensitive) and LSK450, LSK465 (5-FOA resistant) were transformed with pMTW1-TAP(NAT) fragment to obtain the strains LSK469/LSK470/LSK473/LSK474 (5-FOA sensitive) and LSK471/LSK472/LSK475/LSK476 (5-FOA resistant) (Table S4). All strains

were confirmed by Western blot using anti-Protein A antibodies (catalogue no. P3775; Sigma, St. Louis, MO).

Construction of the *CEN7*-deleted strains (*CaCEN7*)

To delete one copy of *CEN7*, a cassette was constructed as follows. A 1.4-kb fragment containing a 66-bp upstream sequence (Ca21Chr7 424413–424472) and a 70-bp downstream sequence (Ca21Chr7 428994–429053) of *CEN7* and a marker gene (*CaHIS1*) were amplified from pBS-HIS using specific primers (Table S5). The PCR product was used to transform the 5-FOA-resistant isolates from the strains LSK443 and LSK456 and their corresponding 5-FOA-sensitive isolates. The transformants were selected on CM lacking histidine (CM-His) and screened by PCR. Transformants in the *cis*-orientation, where *URA3* and *HIS1* are present on the same homolog, were screened by Southern hybridization (Southern 1975).

Media and growth conditions

All strains of *C. albicans* where *URA3* was integrated into Chr7 and Chr5 were propagated in YPD (1% yeast extract, 2% peptone, 2% dextrose) with uridine (YPDU), unless otherwise specified. All transformation experiments were done in YPDU using standard methods (Mitra *et al.* 2014). The auxotrophs were selected on appropriate selection media, as mentioned previously. For the 5-FOA sensitivity assays, CM with 2% agar was supplemented with 1 mg/ml 5-FOA (catalogue no. F5013; Sigma). Strains with neocentromeres were grown in YPDU.

Silencing assay

Each of the *URA3* integrants was grown in YPDU overnight. The cells were spun down, washed, and ~1 million cells from three independent transformants of each kind of integration were plated on CM+5-FOA. The plates were incubated at 30° for 72 hr. A total of 100 colonies from each plate were patched on CM-Uri and YPDU. These were simultaneously patched on CM-His and CM-Arg plates to detect events such as loss of the marker gene *URA3* or whole chromosome loss. The colonies showing growth in CM-Uri were counted and the percentage of reversible silencing was determined. For the *CEN7::URA3* strains, we plated ~150 colonies on 5-FOA and analyzed ~70 of them.

Chromatin immunoprecipitation (ChIP) and quantitative PCR (qPCR) analysis

A single colony of *C. albicans* was inoculated into 50 ml YPDU and grown until log phase. Crosslinking was done for 15 min (for CENPA) or 30 min (for *Mtw1*) using formaldehyde to a final concentration of 1% and cells were quenched using 0.135 mM glycine for 5 min at room temperature. Quenched cells were incubated in a reducing environment in the presence of 9.5 ml distilled water and 0.5 ml β-mercaptoethanol (catalogue no. MB041; HiMedia). The rest of the protocol from Yadav *et al.* (2018) was then followed. Finally, the

DNA pellet was resuspended in 20 μ l MilliQ water. All three samples (I, +, -) were subjected to PCR reactions. The input and immunoprecipitation (IP) DNA were diluted appropriately and quantitative PCR (qPCR) reactions were set up using primers listed in Table S5. CENPA/Mtw1 enrichment was determined by the percentage input method using the formula: $100 \times 2^{(\text{adjusted Ct input} - \text{adjusted Ct IP})}$. Here, the adjusted Ct is the dilution factor (\log_2 of dilution factor) subtracted from the Ct value of the input or IP. Three technical replicates were taken for qPCR analysis and SEM was calculated. To determine statistical significance of test regions with the noncentromeric control *LEU2*, two-way ANOVA was used. Multiple comparisons were performed using Bonferonni post-tests with the following *P*-values: *** $P < 0.001$, ** $P < 0.01$, NS $P > 0.05$. Final values for ChIP-qPCR were plotted using GraphPad Prism 5.0.

ChIP-sequencing analysis

For the CENPA ChIP-sequencing (ChIP-seq), immunoprecipitated DNA and the corresponding DNA from whole-cell extracts from strains LSK450 and LSK465 were quantified using Qubit before proceeding for library preparation. An amount of 5 ng ChIP or total DNA was used to prepare sequencing libraries using NEBNext Ultra DNA Library Prep Kit for Illumina (New England Biolabs, Beverly, MA). The library quality and quantity were checked using Qubit HS DNA Assay Kits (Thermo Fisher Scientific, Waltham, MA) and Bioanalyzer High Sensitivity DNA Analysis kits (Agilent Technologies, Santa Clara, CA), respectively. The libraries that passed quality control were sequenced on Illumina HiSeq 2500 (Illumina, San Diego, CA). The HiSeq Rapid Cluster Kit and SBS Kit v2 were used to generate 50-bp paired end reads. The reads were independently aligned onto the *C. albicans* SC5314 reference genome (v. 21) and a genome with an altered version of Chr7 using the bowtie2 (v. 2.3.2) aligner. These processed BAM files were processed further using MACS2 for identification of peaks (Zhang *et al.* 2008). These peaks were annotated with the *C. albicans* SC5314 reference and altered assembly annotation files. Visualization of the aligned reads (BAM files) on the reference genome was performed using Integrative Genome Viewer (IGV; <https://software.broadinstitute.org/software/igv/>).

Hi-C analysis

For the generation of the Hi-C contact probability matrix, *C. albicans* Hi-C data were analyzed using the hiclib package (<http://mirnylab.bitbucket.org/hiclib/>) (Imakaev *et al.* 2012). First, 2×80 -bp paired end reads were iteratively aligned to the *C. albicans* genome assembly 21 (Ca21) using Bowtie2 (Langmead and Salzberg 2012) with the *-very-sensitive* option. The alignment started from first 20 bases from 5' end, with an increment of 5 bases in subsequent iterations. Aligned read pairs were then assigned to *Sau3AI* restriction fragments. The fragment filtering steps subsequently removed

self-circles, dangling ends, and PCR duplicates, and all the unique valid pairs were used for the generation of the interaction matrix (with bin size of 2 kb or otherwise specified). Bin filtering steps included removal of bins with <50% sequence information in the genome assembly and removal of 1% bins with the lowest summation. Diagonal bins were excluded from further downstream analysis. Iterative bin bias correction was then performed on the genome-wide interaction matrix. The contact probability matrix (C_{ij}) was generated from the normalized interaction matrix (I_{ij}) where each value C_{ij} (representing probability of contacts between bin *i* and bin *j*) was calculated by the formula provided below:

$$C_{ij} = \frac{I_{ij} * n}{\sum_{i=1}^n \sum_{j=1}^n I_{ij}}$$

where *n* represents the total number of bins in the matrix.

For the plotting of *trans*-interactions, the distribution of all *trans*-contact probabilities (excluding 0 values) was plotted from interchromosomal regions of the genome-wide matrix. The mean *trans*-contact probability between all eight CENs was also calculated. Mann-Whitney *U* tests were then used to statistically compare interactions between CENs and *trans*-interactions of bulk chromatin.

For the plotting of distance-dependent contact probability curves, all *cis*-contact probabilities (excluding zero values) were taken from the genome-wide matrix as well as pericentric or control regions. The pericentric region was defined as bins containing a CEN plus 10 kb each of upstream and downstream sequence. For every chromosome, a noncentromeric control region was chosen, which had the same size as the pericentric region and was equidistant from the CEN. The mean contact probability between pairs of loci separated by a given genomic distance was calculated for each region (pericentric, control, and genome wide). Mann-Whitney *U* tests were then performed to estimate if the distributions of contact probabilities at a given distance were significantly different between regions.

Similarly, the distribution of distance-dependent contact probabilities at each distance in the pericentric region was generated and Mann-Whitney *U* tests were conducted to estimate if the distributions of contact probabilities between two adjacent genomic distances were significantly different.

For the plotting of the 3C profile, the contact probabilities between CEN and *cis*-regions were plotted using a single row containing the anchor (centromeric) bin from the chromosome-wide matrix.

Data availability

The sequencing data used in the study have been submitted to the National Center for Biotechnology Information (NCBI) under the BioProject accession number PRJNA477284. The Hi-C data were downloaded from the NCBI BioProject (accession: PRJNA308106). Strains and plasmids are available on request. Supplemental material available at FigShare: <https://doi.org/10.25386/genetics.8197388>.

Results

Frequency of reversible silencing of a transgene decreases from the CENPA-bound core CEN region to its periphery in *C. albicans*

The transgene *URA3* gets reversibly silenced when it is integrated into the CENPA-bound central core of *C. albicans* (Thakur and Sanyal 2013). 5-FOA is a toxin that kills cells that express *URA3* (Boeke *et al.* 1987). The cells that reversibly silence *URA3* grow both on CM-Uri and CM+5-FOA and switch between an epigenetically bistable on and off expression state and are termed as 5-FOA resistant. The Ura-positive cells that do not show reversible silencing remain 5-FOA sensitive. We used this principle to examine the expression profile of *URA3* at CEN-proximal regions in *C. albicans*.

We inserted the 1.4-kb *URA3* gene into each of the 10 different *CEN7*-proximal loci independently in the strain J200, which has differentially marked homologs of Chr7 (Sanyal *et al.* 2004) (Figure 1A and Table S1). We also integrated *URA3* into a *CEN7*-distal (far-*CEN7*) locus and a *CEN5*-proximal locus. We plated ~1 million cells of each *URA3* integrant type on CM+5-FOA plates and obtained ~100 5-FOA-resistant colonies (see *Materials and Methods*). These were replica plated on CM-Uri (Figure 1B). We specifically scored for colonies that grew both on CM-Uri and CM+5-FOA plates as those cells indicated reversible silencing of *URA3* (Table 1). We also monitored the frequency of chromosome loss/gene conversion events of *URA3* in these strains by examining the simultaneous loss of two markers on Chr7, *ARG4* and *URA3* or *HIS1* and *URA3* (Figure 1B and Table S2). This was done to ensure that the 5-FOA-resistant colonies obtained from the assay retained the *URA3* gene along with *HIS1* and *ARG4*. The chromosome loss assay using two unlinked markers indicated that all the *URA3* integrants exhibited loss rates comparable to the wild-type frequencies. With the exception of the L5 and far-*CEN7* *URA3* integrants, we could obtain 5-FOA-resistant colonies in all other integrants, suggesting silencing of *URA3* at the corresponding locus.

We observed a steep decline in the percentage of colonies showing reversible silencing of *URA3* (the ratio of the number of 5-FOA-resistant colonies that grow on CM-Uri and the total number of 5-FOA-resistant colonies analyzed) from the *CEN7* core to its periphery (Figure 1C). It must be noted here that, in every step of the plating assays, we proceeded with only those 5-FOA-resistant colonies that grew well on CM-Uri and CM+5-FOA. This suggests that *URA3* was not mutated or inactivated at any point, which otherwise would have yielded a lawn of colonies on CM+5-FOA and a complete absence of growth on CM-Uri. These sets of experiments strongly indicate that transcriptional silencing of a reporter gene is observed outside the central core of *CEN7* but is confined to a defined region. In addition, the frequency of reversible silencing of the transgene is a function of the radial distance from

the CEN, due to fewer numbers of reversibly silenced colonies being obtained from the peripheral insertions.

CENPA-bound core CEN and the pericentromeres encompass a 25-kb CFCC domain

CENs in *C. albicans* are clustered to form a CENPA-rich zone (Thakur and Sanyal 2013). Consistent with this, the interchromosomal Hi-C heatmaps of wild-type *C. albicans* are interspersed with conspicuous punctate areas which signify physical contacts between CENs (Burrack *et al.* 2016). Using the same data set, we investigated the distribution of all non-zero contact probabilities from the interchromosomal (*trans*) contact matrix. We found that the mean interactions between CENs of different chromosomes were significantly higher relative to the mean *trans*-interactions of bulk chromatin ($P = 3.47 \times 10^{-90}$; Mann-Whitney *U* test) (Figure 2A). To examine the intrachromosomal (*cis*) interactions in pericentric regions, we generated distance-dependent contact probability curves by averaging pairwise interaction data at different linear genomic distances. At any given distance, the mean *cis*-contact probability of loci in pericentric regions was significantly higher than the mean *cis*-interaction of bulk chromatin (Figure 2B). Consistently, noncentromeric control regions showed similar distance-dependent contact probabilities as all *cis*-interactions but they were significantly lower than those in the pericentric regions (except at a 24-kb distance, possibly due to small sample size). This observation was corroborated by analysis of subtraction matrices (pericentric region – a randomly-selected control region on Chr7) (Figure S1). Hence, the core CENs of *C. albicans* strongly interact with a CEN-proximal region in *cis*, forming a compact chromatin environment that is distinct from bulk chromatin.

We then sought to find the boundaries of the pericentric regions within which loci interact with each other at high frequencies. It is well known that the contact probability shows an inverse relationship with an increase in the genomic distance (Dekker *et al.* 2002). When we plotted the distribution of contact probabilities in pericentric regions at different genomic distances, we found that this distribution is significantly different at each increment until it reaches a 10-kb distance from the core CEN region (Figure 2C). From this point, distribution of contact probabilities remains at a low level (mostly without any statistically significant difference) irrespective of any increase in the genomic distance (Figure 2C). Thus, we honed in on a pericentric region centering on the core CEN that exhibits high *cis*-contacts with any locus within 10 kb of sequence, flanking it upstream or downstream. In the case of Chr7, the 3C profile of *CEN7* indicated a 25-kb region centering on *CEN7* that has the compact chromatin feature (Figure 2D). A similar observation was noted for *CEN2* (Figure 2E). The clear trend of an exponential decay in reversible silencing of *URA3* correlated with the decay of contact probabilities between *CEN7* and its neighboring *cis*-region. Hence, using a combination of the transgene silencing assay and Hi-C interaction analysis, we define an ~25-kb

Table 1 Frequency of reversible silencing of *URA3*-integrated strains

Integration type	Transformant no.	No. of reversibly silenced colonies/total no. of 5-FOA colonies analyzed	Percentage reversible silencing of <i>URA3</i> (%5-FOA ^R <i>URI</i> ⁺ <i>HIS</i> ⁺ <i>ARG</i> ⁺)
L5	1	0/107	ND
	2	0/73	ND
	3	0/95	ND
L4	1	1/116	0.862
	2	0/103	ND
	3	1/117	0.854
L3	1	1/86	1.162
	2	2/96	2.083
	3	2/98	2.04
L2	1	1/97	1.03
	2	3/117	2.564
	3	0/100	ND
L1	1	11/110	10
	2	23/158	14.556
	3	5/160	3.125
<i>CEN7::URA3/CEN7</i>	J151	72/74	97.297
	J153	46/61	78.688
	J154	75/79	94.936
R1	1	99/101	98.019
	2	58/58	100
	3	71/78	91.025
R2	1	2/118	1.694
	2	1/111	0.9
	3	1/100	1
R3	1	1/111	0.9
	2	1/108	0.925
	3	1/88	1.136
R4	1	3/97	3.09
	2	1/96	1.04
	3	2/101	1.98
R5	1	1/138	0.724
	2	2/157	1.273
	3	0/100	ND
far- <i>CEN7</i>	1	0/200	ND
	2	0/200	ND
	3	0/205	ND
<i>CEN5</i> int	1	4/98	4.08
	2	2/114	1.75
	3	0/89	ND

ND, not detected.

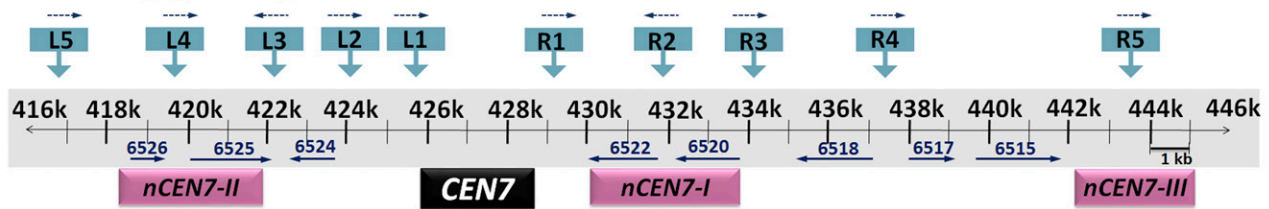
region centering on the CENPA-bound core CEN region as the pericentromeres displaying the CFCC domain in *C. albicans*.

Neocentromeres in *C. albicans* are activated within the pericentric boundaries

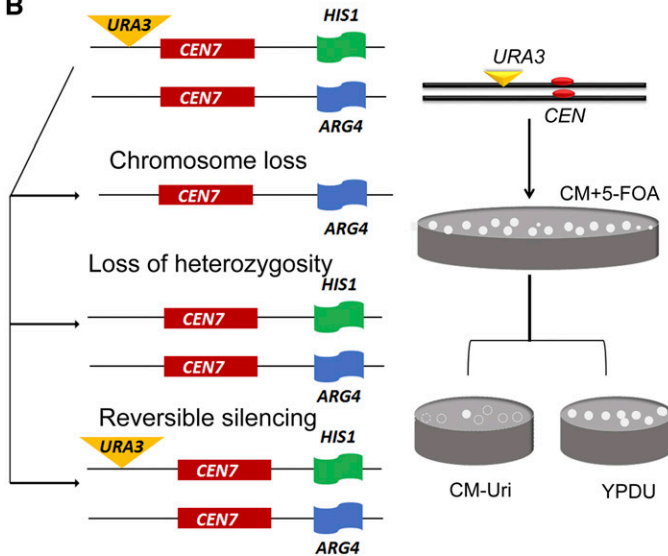
Pericentromeres of Chr7 and Chr5 house genomic loci-like neocentromere hotspots and DNA replication origins (Thakur and Sanyal 2013; Mitra *et al.* 2014). In *C. albicans*, neocentromeres are shown to be activated primarily at CEN-proximal loci, irrespective of the length of the CEN DNA deleted (Thakur and Sanyal 2013). There are four neocentromere hotspots mapped on Chr7 so far: *nCEN7-I*, *nCEN7-II*, *nCEN7-III*, and *nCEN7-IV* (Thakur and Sanyal 2013). These regions do not share any DNA sequence similarity, leaving proximity to native CEN as the only known neocentromere determinant so far.

We posed the question as to why these hotspots are the favored regions for neocentromere activation. To address this, we repeated the transgene silencing assay by integrating *URA3* at the R4 and L4 loci in the strain 8675 (*CSE4-GFP-CSE4/CSE4*) (Joglekar *et al.* 2008) and obtained 5-FOA-resistant colonies as mentioned previously. In the same strains, we deleted the native *CEN7* sequence (4.5-kb CENPA-rich region) using *HIS1* to obtain LSK443 (*L4/L4::URA3*) and LSK456 (*R4/R4::URA3*) (Table S2). We designed a Southern hybridization (Southern 1975) strategy to screen for colonies where *URA3* and *HIS1* were present on the same homolog of Chr7 (Figure S2). We wanted to examine the site of kinetochore assembly in these *CEN7*-deletion transformants. ChIP-qPCR analysis using anti-GFP antibodies showed that CENPA assembled at *URA3* and neighboring regions in the *CEN7*-deleted strains (Figure 3, A and B, top; Figure S3, A and B,

A Ca21Chr7_C_albicans_SC5314



B



C

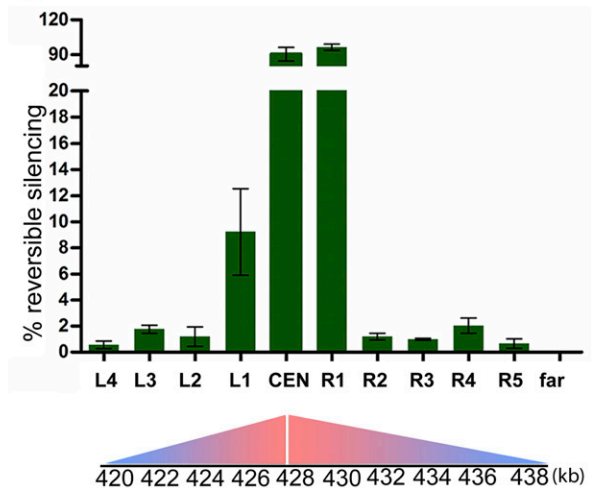


Figure 1 Frequency of reversible silencing of a transgene decreases from the CENPA-bound core CEN region to its periphery in *C. albicans*. (A) Schematic of the ~30-kb region on Chr7 (coordinates 416000–446000) spanning *CEN7* shows individual *URA3* integration sites (↓) and their identities (L1, R1, etc.). Previously mapped neocentromere hotspots (*nCEN7-I*, *nCEN7-II*, *nCEN7-III*) are also shown. Arrowheads and numbers above them indicate positions and identities of the open reading frames, respectively. Strains are listed in Table S4. (B) Schematic of the probable ways of obtaining Ura-negative derivatives (5-FOA-resistant cells) from a Ura-positive strain. (Left) The parent Ura-positive strain is a *URA3* integrant in the strain RM1000AH which is heterozygous for both *ARG4* and *HIS1*. (Right) The assay strategy used to screen reversibly silenced colonies derived from the *URA3* integrants using 5-FOA. (C) A decline in the percentage of reversibly silenced colonies from mid-*CEN7* (CEN) to the pericentric integrants (L4, L3...R5, far) was observed with increasing distance from the core CEN (top). The phase exponential decay curve is color coded and coordinates for the respective insertions have been depicted below (bottom).

top). We also examined the localization of an independent kinetochore protein, the Mis12 homolog in *C. albicans*, Mtw1 (Roy *et al.* 2011). ChIP-qPCR analysis using anti-Protein A antibodies revealed an overlapping binding pattern of Mtw1 with CENPA (Figure 3B, bottom; Figure S3B, bottom). We performed CENPA ChIP-qPCR analysis in the corresponding 5-FOA-sensitive derivatives (which expressed *URA3*) and found that neocentromeres were activated at the hotspot *nCEN7-II*, instead of at the *URA3* locus (Figure S3D). CENPA ChIP-seq in the strains LSK450 and LSK465 revealed two new hotspots, *URA3nCEN7-I* (Figure S3C) and *URA3nCEN7-II* (Figure 3C), respectively, on Chr7 (Table S3). Hence, we identified two new neocentromeres on Chr7 in this organism when a region is kept transcriptionally less permissive. These experiments strongly suggest that strains with the same genotype but varying expression levels of a transgene at pericentromeres can activate neocentromeres at different loci. This activation is restricted to the 25-kb pericentric CFCC that

we identified in this study. Within this CFCC, a transcription desert site can be a potential neocentromere.

Discussion

In this study, we map a 25-kb region spanning the CENPA-bound CEN core and its flanking regions on Chr7 in *C. albicans*, where the phenomenon of reversible silencing of a transgene, *URA3*, could be observed. We also demonstrate that this region forms a CFCC by stronger *cis*-interactions with neighboring sequences. In addition, *trans*-interactions among centromeric sequences also help cluster the CENs to provide a 3D nuclear space that we refer to as the CENPA-rich zone, possibly to facilitate epigenetic inheritance of CENPA chromatin. This is further evidenced by following the patterns of neocentromere activation on Chr7 in this study.

Using CENPA ChIP-seq analysis, we previously proposed the presence of the CENPA-rich zone around the clustered CENs (Thakur and Sanyal 2013), which we revisited in this

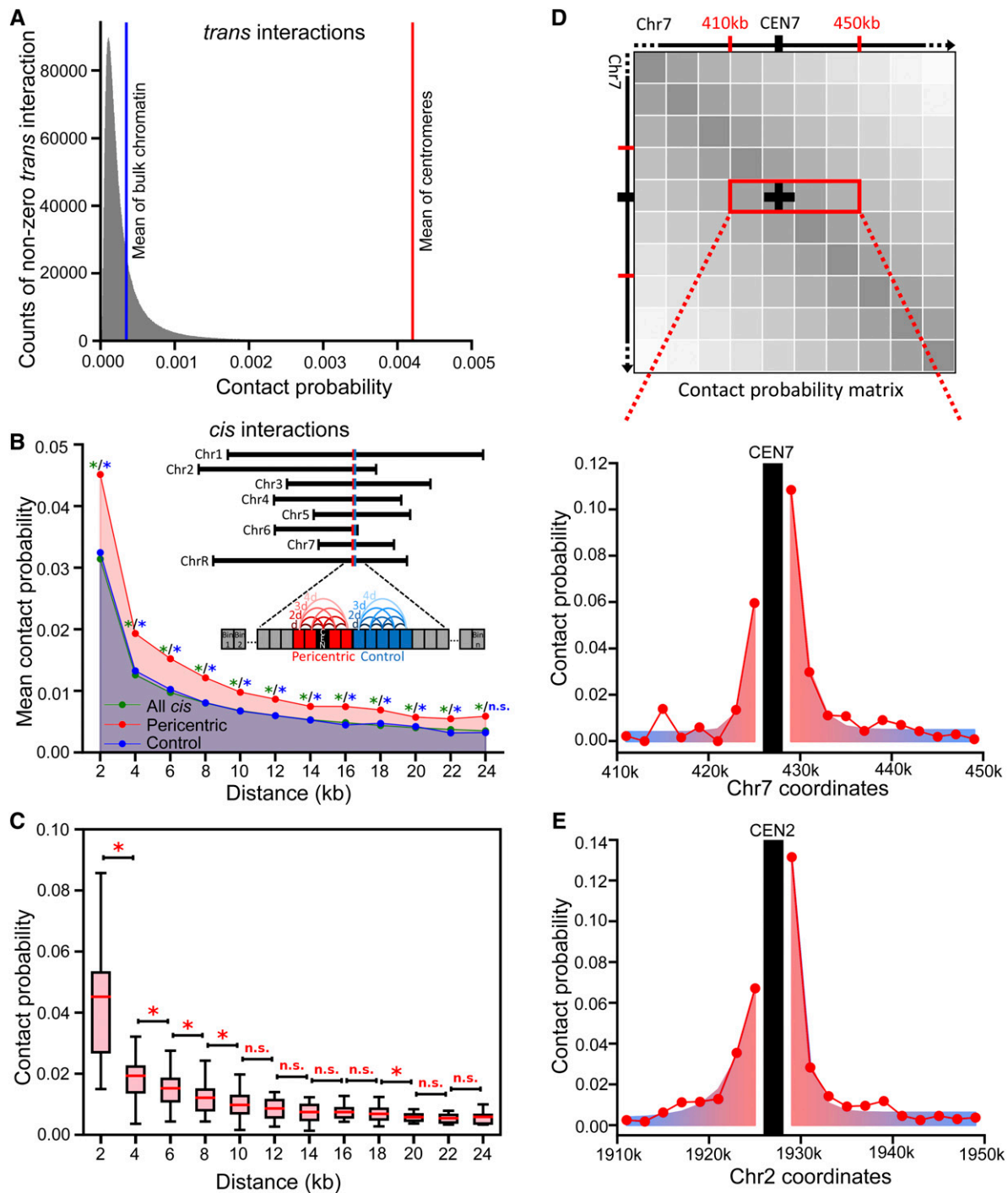


Figure 2 CENs in *C. albicans* are flanked by pericentric chromatin spanning ~25 kb, centering on the CENPA-rich core CEN region. (A) Distribution of *trans*-contact probabilities (nonzero values) plotted from wild-type *C. albicans* Hi-C data (Burrack *et al.* 2016). The blue vertical line shows the mean value. The red vertical line shows the mean contact probability between CENs. (B) The mean contact probability was calculated as a function of the genomic distance for genome-wide *cis*-interactions (green) and interactions within pericentric (red) and noncentromeric control (blue) regions. (Inset) Cartoon representation of binned *C. albicans* chromosomes depicting the interactions within pericentric regions (red bins) centering on the centromeric bin (black bin) as well as noncentromeric/pericentric control regions (blue bins). (C) Box-plot showing the distribution of contact probabilities at each genomic distance in pericentric regions, defined in B. Mean contact probabilities were shown by a red line inside each box. (D) The cartoon depicts a Hi-C heatmap showing the position of *CEN7* (black bar) (top). The 3C profile describing the *cis*-interactions of *CEN7* (anchor bin) was generated from the chromosome-wide contact probability matrix (red box). The 3C profile of the *CEN7* bin (Chr7:426000–428000; black bar) showing contact probabilities (red dots) between *CEN7* and its neighboring bins on Chr7 (Chr7:410000–450000) (bottom). (E) The 3C profile of the *CEN2* bin (Chr2:1926000–1928000; black bar) showing contact probabilities (red dots) between *CEN2* and its neighboring bins on Chr2 (Chr2:1910000–1950000). * $P < 0.05$ (Mann–Whitney U test).

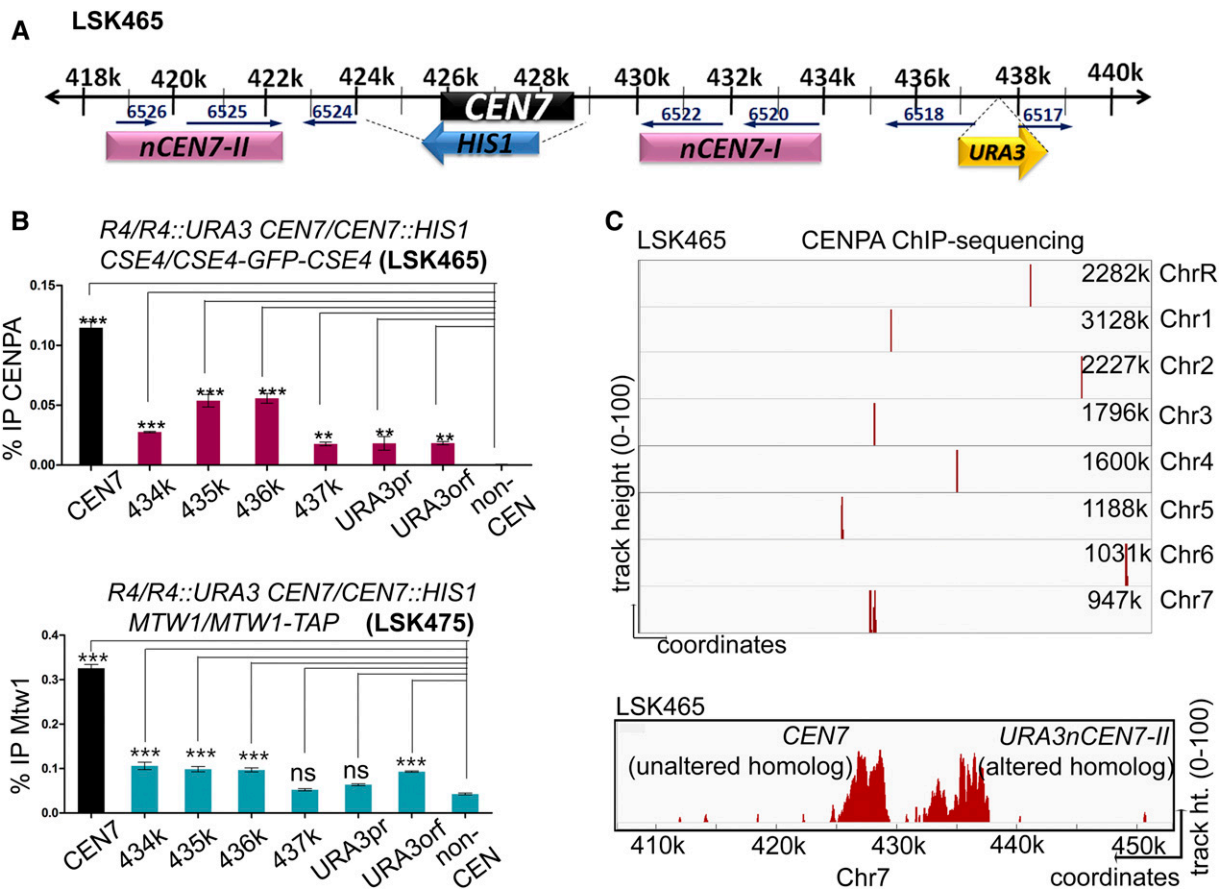


Figure 3 Neocentromeres in *C. albicans* are activated within the pericentromeres. (A) In the diploid *C. albicans*, only one homolog of Chr7 where *CEN7* (Ca21Chr7 424475–428994) has been replaced by *HIS1* in a *URA3* integrant strain, LSK465, is shown. (B) Relative enrichment of CENPA at native *CEN7* on the unaltered homolog (black) and at neocentromere *URA3nCEN7-II* (red) in the 5-FOA-resistant strain LSK465 (top). Relative enrichment of Mtw1 at *CEN7* (black) and *URA3nCEN7-II* (blue) at the native CEN (427k) in the strain LSK475 (bottom). Relative enrichment values of CENPA and Mtw1 indicate that the neocentromere formed on the altered homolog (*URA3nCEN7-II*) was mapped to a region surrounding the integration locus (Ca21Chr7 435078–440387); error bars indicate SEM. ns $P > 0.05$, ** $P < 0.01$, *** $P < 0.001$. (C) ChIP-seq using anti-GFP (CENPA) antibodies in the strain LSK465 reveals a single peak on all chromosomes, except Chr7 which shows two closely spaced peaks (top). Chr7 shows a combination of two peaks, the one at *CEN7* (left) is of the unaltered homolog, the one at *URA3nCEN7-II* (right) is of the altered homolog (bottom). A 50-kb region harboring *CEN7* depicts the track height (using IGV) on the y-axis and coordinates on the x-axis.

study. We had proposed that the local concentration of CENPA at and around the CENs is higher than in the rest of the genome. We previously demonstrated that preexisting CENPA molecules are required for epigenetic inheritance of CEN function in *C. albicans* (Baum *et al.* 2006). In this study, we hypothesize that the miniscule levels of CENPA at the pericentromeres, which may be undetectable by less-sensitive methods like ChIP-seq, is important to activate a neocentromere at CEN-proximal regions in the absence of the native CEN. A previous attempt to characterize the pericentromeres in *C. albicans* claimed that a pericentric insertion of *URA3* imposes a weak transcriptional repression (Freire-Benítez *et al.* 2016). These assays were based on growth phenotypes and qRT-PCR analysis, making them less sensitive. The silencing assay that we have employed in this study is a way to score for such rare events when the CEN can relocate to an ectopic locus. It enabled us to isolate and amplify a clonally inherited population of cells that can switch the transcriptional status of

a transgene. It has previously been demonstrated that when *URA3* is integrated into the CENPA-bound central core of *CEN7*, a fivefold decrease in *URA3* transcript levels was observed on growth in 5-FOA as compared to CM-Uri (Thakur and Sanyal 2013). Therefore, we can correlate the *URA3* transcript levels to CENPA binding at *URA3* in the pericentric insertions, although it is relatively unknown whether CENPA can silence transcription or whether a transcriptionally inert region stabilizes CENPA at the CENs in *C. albicans*. The reversible silencing seen at the *S. pombe* central core is because of its flexible CENPA domain (Allshire *et al.* 1994; Karpen and Allshire 1997; Allshire and Ekwall 2015). Unlike *S. pombe*, in our study, we define a pericentromere that is more transcriptionally permissible than the CENPA-rich core region in *C. albicans*.

The acquisition of centromeric properties on acentric DNA fragments have been studied extensively in metazoan CENs (Maggert and Karpen 2001). DNA fragments juxtaposed to

an active CEN gives rise to a neocentromere, the activity of which was found to be stable when the native CEN was removed (Maggert and Karpen 2001). This proximity effect of the endogenous CEN supports the spreading of CEN activity and identity, which helps in the epigenetic inheritance of CEN chromatin. In *C. albicans*, a previous study reported the deletion of the endogenous *CEN5* with *URA3* yielding two distinct classes of transformants forming neocentromeres: the proximal neocentromere and the distal neocentromere (Ketel *et al.* 2009). The proximal neocentromere harbored CENPA at *URA3*, resulting in silencing of its expression. Additionally, a Hi-C analysis in *C. albicans* (Burrack *et al.* 2016) revealed that neocentromeres on Chr5 cluster close to the endogenous CEN locus, implying that formation of a neocentromere leads to reorganization of the 3D architecture of the nucleus so that different chromosomal loci closely contact regions on other chromosomes. However, in the present study and in a previous study from our group (Thakur and Sanyal 2013), we could primarily detect proximal neocentromeres when *CEN7*, *CEN5*, and *CEN1* were deleted. Hence, proximity to the endogenous location is an important criterion for neocentromere activation. We claim that this proximity effect is enclosed within a 25-kb CFCC on Chr7 because of the closely interacting CENPA-occupied chromatin which we identify in the study.

An impending question in this direction is what restricts CENPA chromatin to a 3- to 5-kb unique DNA sequence on every chromosome in *C. albicans*? There must be a genetic or epigenetic element that restricts its localization. In *S. pombe*, a transfer RNA boundary element prevents CENPA from spreading to adjoining euchromatic sites (Scott *et al.* 2006). In *Drosophila melanogaster*, this function is performed by the flanking heterochromatin and repetitive DNA elements (Maggert and Karpen 2001). In the absence of obvious DNA sequence cues and a canonical heterochromatin machinery, we propose that the CFCC defined in this study encloses the CEN activity and hotspots for neocentromere activation. Additionally, the site of neocentromere formation, which remains fairly elusive in this organism, can now be explained in the context of an atypical pericentric region within which flexible CENPA positioning is permitted.

The lack of a conventional heterochromatin machinery has been observed in *S. cerevisiae* (Drinnenberg *et al.* 2009), where pericentric cohesion is maintained by the presence of topological adjusters like cohesin, condensin, and topoisomerase II (Bloom 2014). Even the regional CENs in *C. lusitanae* do not harbor any flanking heterochromatin, show a reduced rate of transgene silencing, and have methylation marks at H3K79 and H3R2 at the central core (Kapoor *et al.* 2015). It would be intriguing to examine cohesin localization at the pericentromeres in *C. albicans*. Transgene silencing assays and Hi-C analyses of all chromosomes will help establish the universality of the results obtained for Chr7 in this study. Additionally, Hi-C analysis of the strains forming neocentromeres obtained from the reversibly silenced colonies

will also reveal if the *cis*- and *trans*-chromosomal interactions are conserved in *C. albicans*.

Acknowledgments

The plasmids pFA-URA3-I-SceI-TS-Orf 19.6524/25 and pFA-URA3-I-SceI-TS-Orf 19.6520/22 were a kind gift from Christophe D'Enfert, Institut Pasteur, Paris. This work was supported by the Council of Scientific and Industrial Research, Government of India [grant number 09/733(0178)/2012-EMR-I to L.S.], and the Tata Innovation Fellowship, Department of Biotechnology, Government of India (to K.S.). P.J. and B.T were supported from the intramural funding from JNCASR. This work is also supported by a Department of Biotechnology grant in Life Science Research, Education and Training at Jawaharlal Nehru Centre for Advanced Scientific Research (BT/INF/22/SP27679/2018). A.S. is supported by Nanyang Technological University's Nanyang Assistant Professorship grant and Singapore Ministry of Education Academic Research Fund Tier 1 grant (RG46/16).

Literature Cited

- Allshire, R. C., and K. Ekwall, 2015 Epigenetic regulation of chromatin states in *Schizosaccharomyces pombe*. *Cold Spring Harb. Perspect. Biol.* 7: a018770. <https://doi.org/10.1101/cshperspect.a018770>
- Allshire, R. C., J. P. Javerzat, N. J. Redhead, and G. Cranston, 1994 Position effect variegation at fission yeast centromeres. *Cell* 76: 157–169. [https://doi.org/10.1016/0092-8674\(94\)90180-5](https://doi.org/10.1016/0092-8674(94)90180-5)
- Baum, M., V. K. Ngan, and L. Clarke, 1994 The centromeric K-type repeat and the central core are together sufficient to establish a functional *Schizosaccharomyces pombe* centromere. *Mol. Biol. Cell* 5: 747–761. <https://doi.org/10.1091/mbc.5.7.747>
- Baum, M., K. Sanyal, P. K. Mishra, N. Thaler, and J. Carbon, 2006 Formation of functional centromeric chromatin is specified epigenetically in *Candida albicans*. *Proc. Natl. Acad. Sci. USA* 103: 14877–14882. <https://doi.org/10.1073/pnas.0606958103>
- Bloom, K. S., 2014 Centromeric heterochromatin: the primordial segregation machine. *Annu. Rev. Genet.* 48: 457–484. <https://doi.org/10.1146/annurev-genet-120213-092033>
- Boeke, J. D., J. Trueheart, G. Natsoulis, and G. R. Fink, 1987 5-Fluoroorotic acid as a selective agent in yeast molecular genetics. *Methods Enzymol.* 154: 164–175. [https://doi.org/10.1016/0076-6879\(87\)54076-9](https://doi.org/10.1016/0076-6879(87)54076-9)
- Burrack, L. S., H. F. Hutton, K. J. Matter, S. A. Clancey, I. Liachko *et al.*, 2016 Neocentromeres provide chromosome segregation accuracy and centromere clustering to multiple loci along a *Candida albicans* chromosome. *PLoS Genet.* 12: e1006317. <https://doi.org/10.1371/journal.pgen.1006317>
- Chatterjee, G., S. R. Sankaranarayanan, K. Guin, Y. Thattikota, S. Padmanabhan *et al.*, 2016 Repeat-associated fission yeast-like regional centromeres in the ascomycetous budding yeast *Candida tropicalis*. *PLoS Genet.* 12: e1005839. <https://doi.org/10.1371/journal.pgen.1005839>
- Choi, E. S., A. Stralfors, A. G. Castillo, M. Durand-Dubief, K. Ekwall *et al.*, 2011 Identification of noncoding transcripts from within CENP-A chromatin at fission yeast centromeres. *J. Biol. Chem.* 286: 23600–23607. <https://doi.org/10.1074/jbc.M111.228510>

- Clarke, L., H. Amstutz, B. Fishel, and J. Carbon, 1986 Analysis of centromeric DNA in the fission yeast *Schizosaccharomyces pombe*. *Proc. Natl. Acad. Sci. USA* 83: 8253–8257. <https://doi.org/10.1073/pnas.83.21.8253>
- Dekker, J., K. Rippe, M. Dekker, and N. Kleckner, 2002 Capturing chromosome conformation. *Science* 295: 1306–1311. <https://doi.org/10.1126/science.1067799>
- Drinnenberg, I. A., D. E. Weinberg, K. T. Xie, J. P. Mower, K. H. Wolfe *et al.*, 2009 RNAi in budding yeast. *Science* 326: 544–550. <https://doi.org/10.1126/science.1176945>
- Duan, Z., M. Andronescu, K. Schutz, S. McIlwain, Y. J. Kim *et al.*, 2010 A three-dimensional model of the yeast genome. *Nature* 465: 363–367. <https://doi.org/10.1038/nature08973>
- Eser, U., D. Chandler-Brown, F. Ay, A. F. Straight, Z. Duan *et al.*, 2017 Form and function of topologically associating genomic domains in budding yeast. *Proc. Natl. Acad. Sci. USA* 114: E3061–E3070. <https://doi.org/10.1073/pnas.1612256114>
- Folco, H. D., A. L. Pidoux, T. Urano, and R. C. Allshire, 2008 Heterochromatin and RNAi are required to establish CENP-A chromatin at centromeres. *Science* 319: 94–97. <https://doi.org/10.1126/science.1150944>
- Freire-Benítez, V., R. J. Price, and A. Buscaino, 2016 The chromatin of *Candida albicans* pericentromeres bears features of both euchromatin and heterochromatin. *Front. Microbiol.* 7: 759. <https://doi.org/10.3389/fmicb.2016.00759>
- Friedman, S., and M. Freitag, 2017 Centromeromorphology of fungi. *Prog. Mol. Subcell. Biol.* 56: 85–109. https://doi.org/10.1007/978-3-319-58592-5_4
- Fukagawa, T., and W. C. Earnshaw, 2014 The centromere: chromatin foundation for the kinetochore machinery. *Dev. Cell* 30: 496–508. <https://doi.org/10.1016/j.devcel.2014.08.016>
- Haase, J., P. K. Mishra, A. Stephens, R. Haggerty, C. Quammen *et al.*, 2013 A 3D map of the yeast kinetochore reveals the presence of core and accessory centromere-specific histone. *Curr. Biol.* 23: 1939–1944. <https://doi.org/10.1016/j.cub.2013.07.083>
- Imakaev, M., G. Fudenberg, R. P. McCord, N. Naumova, A. Goloborodko *et al.*, 2012 Iterative correction of Hi-C data reveals hallmarks of chromosome organization. *Nat. Methods* 9: 999–1003. <https://doi.org/10.1038/nmeth.2148>
- Jin, Q. W., J. Fuchs, and J. Loidl, 2000 Centromere clustering is a major determinant of yeast interphase nuclear organization. *J. Cell Sci.* 113: 1903–1912.
- Joglekar, A. P., D. Bouck, K. Finley, X. Liu, Y. Wan *et al.*, 2008 Molecular architecture of the kinetochore-microtubule attachment site is conserved between point and regional centromeres. *J. Cell Biol.* 181: 587–594. <https://doi.org/10.1083/jcb.200803027>
- Kapoor, S., L. Zhu, C. Froyd, T. Liu, and L. N. Rusche, 2015 Regional centromeres in the yeast *Candida lusitanae* lack pericentromeric heterochromatin. *Proc. Natl. Acad. Sci. USA* 112: 12139–12144. <https://doi.org/10.1073/pnas.1508749112>
- Karpen, G. H., and R. C. Allshire, 1997 The case for epigenetic effects on centromere identity and function. *Trends Genet.* 13: 489–496. [https://doi.org/10.1016/S0168-9525\(97\)01298-5](https://doi.org/10.1016/S0168-9525(97)01298-5)
- Ketel, C., H. S. Wang, M. McClellan, K. Bouchonville, A. Selmecki *et al.*, 2009 Neocentromeres form efficiently at multiple possible loci in *Candida albicans*. *PLoS Genet.* 5: e1000400. <https://doi.org/10.1371/journal.pgen.1000400>
- Koren, A., H. J. Tsai, I. Tirosh, L. S. Burrack, N. Barkai *et al.*, 2010 Epigenetically-inherited centromere and neocentromere DNA replicates earliest in S-phase. *PLoS Genet.* 6: e1001068 [corrigenda: *PLoS Genet.* 7 (2011)]. <https://doi.org/10.1371/journal.pgen.1001068>
- Langmead, B., and S. L. Salzberg, 2012 Fast gapped-read alignment with Bowtie 2. *Nat. Methods* 9: 357–359. <https://doi.org/10.1038/nmeth.1923>
- Ling, Y. H., and K. W. Y. Yuen, 2019 Point centromere activity requires an optimal level of centromeric noncoding RNA. *Proc. Natl. Acad. Sci. USA* 116: 6270–6279. <https://doi.org/10.1073/pnas.1821384116>
- Maggert, K. A., and G. H. Karpen, 2001 The activation of a neocentromere in *Drosophila* requires proximity to an endogenous centromere. *Genetics* 158: 1615–1628.
- Mishra, P. K., M. Baum, and J. Carbon, 2011 DNA methylation regulates phenotype-dependent transcriptional activity in *Candida albicans*. *Proc. Natl. Acad. Sci. USA* 108: 11965–11970. <https://doi.org/10.1073/pnas.1109631108>
- Mitra, S., J. Gomez-Raja, G. Larriba, D. D. Dubey, and K. Sanyal, 2014 Rad51-Rad52 mediated maintenance of centromeric chromatin in *Candida albicans*. *PLoS Genet.* 10: e1004344. <https://doi.org/10.1371/journal.pgen.1004344>
- Nishimura, K., M. Komiya, T. Hori, T. Itoh, and T. Fukagawa, 2018 3D genomic architecture reveals that neocentromeres associate with heterochromatin regions. *J. Cell Biol.* 218: 134–149. <https://doi.org/10.1083/jcb.201805003>
- Ohkuni, K., and K. Kitagawa, 2011 Endogenous transcription at the centromere facilitates centromere activity in budding yeast. *Curr. Biol.* 21: 1695–1703. <https://doi.org/10.1016/j.cub.2011.08.056>
- Padmanabhan, S., J. Thakur, R. Siddharthan, and K. Sanyal, 2008 Rapid evolution of Cse4p-rich centromeric DNA sequences in closely related pathogenic yeasts, *Candida albicans* and *Candida dubliniensis*. *Proc. Natl. Acad. Sci. USA* 105: 19797–19802. <https://doi.org/10.1073/pnas.0809770105>
- Roy, B., L. S. Burrack, M. A. Lone, J. Berman, and K. Sanyal, 2011 CaMtw1, a member of the evolutionarily conserved Mis12 kinetochore protein family, is required for efficient inner kinetochore assembly in the pathogenic yeast *Candida albicans*. *Mol. Microbiol.* 80: 14–32. <https://doi.org/10.1111/j.1365-2958.2011.07558.x>
- Sanyal, K., and J. Carbon, 2002 The CENP-A homolog CaCse4p in the pathogenic yeast *Candida albicans* is a centromere protein essential for chromosome transmission. *Proc. Natl. Acad. Sci. USA* 99: 12969–12974. <https://doi.org/10.1073/pnas.162488299>
- Sanyal, K., M. Baum, and J. Carbon, 2004 Centromeric DNA sequences in the pathogenic yeast *Candida albicans* are all different and unique. *Proc. Natl. Acad. Sci. USA* 101: 11374–11379. <https://doi.org/10.1073/pnas.0404318101>
- Scott, K. C., and B. A. Sullivan, 2014 Neocentromeres: a place for everything and everything in its place. *Trends Genet.* 30: 66–74. <https://doi.org/10.1016/j.tig.2013.11.003>
- Scott, K. C., S. L. Merrett, and H. F. Willard, 2006 A heterochromatin barrier partitions the fission yeast centromere into discrete chromatin domains. *Curr. Biol.* 16: 119–129. <https://doi.org/10.1016/j.cub.2005.11.065>
- Shang, W. H., T. Hori, N. M. Martins, A. Toyoda, S. Misu *et al.*, 2013 Chromosome engineering allows the efficient isolation of vertebrate neocentromeres. *Dev. Cell* 24: 635–648. <https://doi.org/10.1016/j.devcel.2013.02.009>
- Smith, K. M., P. A. Phatale, C. M. Sullivan, K. R. Pomraning, and M. Freitag, 2011 Heterochromatin is required for normal distribution of *Neurospora crassa* CenH3. *Mol. Cell Biol.* 31: 2528–2542. <https://doi.org/10.1128/MCB.01285-10>
- Southern, E. M., 1975 Detection of specific sequences among DNA fragments separated by gel electrophoresis. *J. Mol. Biol.* 98: 503–517. [https://doi.org/10.1016/S0022-2836\(75\)80083-0](https://doi.org/10.1016/S0022-2836(75)80083-0)
- Sullivan, B. A., and G. H. Karpen, 2004 Centromeric chromatin exhibits a histone modification pattern that is distinct from both euchromatin and heterochromatin. *Nat. Struct. Mol. Biol.* 11: 1076–1083. <https://doi.org/10.1038/nsmb845>
- Thakur, J., and K. Sanyal, 2013 Efficient neocentromere formation is suppressed by gene conversion to maintain centromere function at

- native physical chromosomal loci in *Candida albicans*. *Genome Res.* 23: 638–652. <https://doi.org/10.1101/gr.141614.112>
- Thakur, J., P. B. Talbert, and S. Henikoff, 2015 Inner kinetochore protein interactions with regional centromeres of fission yeast. *Genetics* 201: 543–561. <https://doi.org/10.1534/genetics.115.179788>
- Tjong, H., K. Gong, L. Chen, and F. Alber, 2012 Physical tethering and volume exclusion determine higher-order genome organization in budding yeast. *Genome Res.* 22: 1295–1305. <https://doi.org/10.1101/gr.129437.111>
- Volpe, T. A., C. Kidner, I. M. Hall, G. Teng, S. I. Grewal *et al.*, 2002 Regulation of heterochromatic silencing and histone H3 lysine-9 methylation by RNAi. *Science* 297: 1833–1837. <https://doi.org/10.1126/science.1074973>
- Voullaire, L. E., H. R. Slater, V. Petrovic, and K. H. Choo, 1993 A functional marker centromere with no detectable alpha-satellite, satellite III, or CENP-B protein: activation of a latent centromere? *Am. J. Hum. Genet.* 52: 1153–1163.
- Yadav, V., S. Sun, R. B. Billmyre, B. C. Thimmappa, T. Shea *et al.*, 2018 RNAi is a critical determinant of centromere evolution in closely related fungi. *Proc. Natl. Acad. Sci. USA* 115: 3108–3113. <https://doi.org/10.1073/pnas.1713725115>
- Zhang, Y., T. Liu, C. A. Meyer, J. Eeckhoutte, D. S. Johnson *et al.*, 2008 Model-based analysis of ChIP-Seq (MACS). *Genome Biol.* 9: R137. <https://doi.org/10.1186/gb-2008-9-9-r137>

Communicating editor: J. Bateman

33 **Abstract**

34

35 Chromosomal instability in fungal pathogens caused by cell division errors is associated with
36 antifungal drug resistance. To identify mechanisms underlying such instability and to uncover
37 new potential antifungal targets, we conducted an overexpression screen monitoring chromosomal
38 stability in the human fungal pathogen *Candida albicans*. Analysis of ~1000 genes uncovered six
39 chromosomal stability (*CSA*) genes, five of which are related to cell division genes in other
40 organisms. The sixth gene, *CSA6*, is selectively present in the CUG-Ser clade species that
41 includes *C. albicans* and other human fungal pathogens. The protein encoded by *CSA6* localizes
42 to the spindle pole bodies, is required for exit from mitosis, and induces a checkpoint-dependent
43 metaphase arrest upon overexpression. Together, *Csa6* defines an essential CUG-Ser fungal
44 clade-specific cell cycle progression factor, highlighting the existence of phylogenetically-
45 restricted cell division genes which may serve as potential unique therapeutic targets.

46

47 **Teaser**

48

49 *Csa6* is essential for mitotic progression and mitotic exit in the human fungal pathogen *Candida*
50 *albicans*.

51

52

53

54

55

56

57

58

59

60

61

62

63

64

65

66

67 **Introduction**

68

69 Cell division is a fundamental aspect of all living organisms, required to support growth,
70 reproduction and replenishment of dead or damaged cells. The primary objective of cell division
71 is to ensure genome stability by preserving and transferring the genetic material with high-fidelity
72 into progeny. Genome stability is achieved by proper execution of key cell cycle events such as
73 chromosome duplication at the S phase followed by equal segregation of the duplicated
74 chromosomes at the M phase. In addition, various cell cycle checkpoints monitor the integrity and
75 fidelity of cell cycle events in response to an error or any damage until rectified or repaired.
76 Failure of any of the error-correcting mechanisms can introduce genetic alterations, causing
77 genomic instability in progeny. Genome instability can occur as a consequence of either point
78 mutations, insertions or deletions of bases in specific genes and/or gain, loss or rearrangements of
79 chromosomes, collectively referred to as chromosome instability (CIN) (1). CIN has been
80 intimately associated with aneuploidy (2) and is one of the potential drivers of human genetic and
81 neurodegenerative disorders (3, 4), aging (5) and several cancers (6). While considered harmful
82 for a cell or an organism, CIN may also contribute to generating variations and help in driving
83 evolution, especially in unicellular primarily asexual eukaryotes (7, 8).

84

85 The current understanding of the mechanisms underlying genome stability has evolved through
86 studies in a range of biological systems from unicellular yeasts to more complex metazoa
87 including humans. These studies highlighted concerted actions of genes involved in (a) high-
88 fidelity DNA replication and DNA damage repair, (b) efficient segregation of chromosomes and
89 (c) error-correcting cellular surveillance machinery (9, 10) in maintenance and inheritance of a
90 stable genome. In recent years, large-scale screenings of loss-of-function (11), reduction-of-
91 function (12) and overexpression (13-16) mutant collections in the budding yeast *Saccharomyces*
92 *cerevisiae* have appended the list of genome stability-regulators by identifying uncharacterized
93 proteins as well as known proteins with functions in other cellular processes. However,
94 considering the vast diversity of the chromosomal segregation mechanisms in eukaryotes, it is
95 conceivable that many genes involved in genome maintenance are yet to be discovered and
96 require additional screens in a wide range of organisms for their identification. While perturbation
97 of a candidate gene's function to decipher its role in a cellular pathway has been a classical
98 strategy in biological research, screening of strain collections aids in uncovering molecular
99 players and cellular pathways in an unbiased manner.

100

101 The ascomycetous yeast *Candida albicans* is emerging as an attractive unicellular model for
102 studying eukaryotic genome biology (17). *C. albicans*, a commensal of both the gastrointestinal
103 and genital tracts, remains the most frequently isolated fungal species worldwide from the
104 patients diagnosed with candidemia or other nosocomial *Candida* infections (18, 19). The diploid
105 genome of *C. albicans* shows remarkable plasticity in terms of ploidy, single nucleotide
106 polymorphism (SNP), loss of heterozygosity (LOH), copy number variations, and CIN events (17,
107 20). Although LOH can be detected on all the chromosomes of *C. albicans*, the presence of
108 recessive lethal or deleterious alleles on some haplotypes (17), prevents one of the haplotypes or
109 even a part of it from existing in the homozygous state. In particular, this homozygous bias has
110 been observed for chromosomes R (ChR), 2 (Ch2), 4 (Ch4), 6 (Ch6) and 7 (Ch7) (21, 22). LOH
111 and aneuploidy-driven CIN has serious phenotypic consequences in *C. albicans* such as
112 conferring resistance to antifungals (23-28) or help *C. albicans* adapt to different host niches (29-
113 31). Whether genome plasticity is contributing to the success of *C. albicans* as a commensal
114 or/and a dreaded pathogen of humans, remains an enigma (17). Nevertheless, with increasing
115 instances of *Candida* infections and emerging antifungal resistance, there is an immediate need to
116 identify novel fungus-specific molecular targets that may aid the development of antifungal
117 therapies. In addition, the remarkable ability of *C. albicans* to tolerate CIN in the form of whole
118 chromosome loss, isochromosome formation, chromosome truncation, or mitotic crossing-over
119 (17, 20, 32) raises intriguing questions on the functioning of genome stability-regulators in this
120 fungal pathogen.

121
122 Of utmost importance to maintain genomic integrity, is the efficient and error-free segregation of
123 the replicated chromosomes. In most eukaryotes including *C. albicans*, the assembly of a
124 macromolecular protein complex, called the kinetochore (KT), on CENP-A (Cse4 in budding
125 yeasts) containing centromeric chromatin mediates chromosome segregation during mitosis (33-
126 35). The KT acts as a bridge between a chromosome and the connecting microtubules (MTs),
127 emanating from the spindle pole bodies (SPBs), the functional homolog of centrosomes in
128 mammals (36). The subsequent attachment of sister KTs to opposite spindle poles then promotes
129 the formation of a bipolar mitotic spindle that drives the separation of the duplicated
130 chromosomes during anaphase (37), after which cells exit mitosis and undergo cytokinesis (38-
131 40). In *C. albicans*, KT proteins remain clustered throughout the cell cycle and are shown to be
132 essential for viability and mitotic progression (33, 41, 42). In addition, genes involved in
133 homologous recombination, such as *MRE11* and *RAD50*, and DNA damage checkpoint pathway,
134 including *MEC1*, *RAD53* and *DUNI*, are required to prevent genome instability in *C. albicans*

135 (43-45). Strikingly, aberrant expression of proteins involved in DNA damage response or cell
136 division triggers morphological transition to a unique polarized, filamentous growth in *C.*
137 *albicans* (17). A recent screen, using a collection of 124 over-expression strains, has identified
138 three additional genes, namely, *CDC20*, *BIMI*, and *RAD51*, with a role in genome maintenance as
139 indicated by increased LOH-driven CIN upon overexpression in *C. albicans* (46). Currently, only
140 a minor fraction of the *C. albicans* gene armamentarium has been evaluated for their roles in
141 genome stability. Systematic approaches are thus needed to exhaustively define the drivers of *C.*
142 *albicans* genome maintenance and outline species-specific processes as well as commonalities
143 with other eukaryotes.

144
145 Here, we describe a large-scale screen aimed at identifying regulators of genome stability in a
146 clinically relevant fungal model system. Our screen, involving ~20% of the *C. albicans*
147 ORFeome, has identified Csa6, a yet unknown player of genome stability, as a critical regulator
148 of cell cycle progression in *C. albicans*. Overall, this is the first-ever report of such a screen at this
149 scale in *C. albicans* and provides a framework for identifying regulators of eukaryotic genome
150 stability, some of which may serve as new targets for therapeutic interventions of fungal
151 infections.

152

153 **Results**

154

155 **A reporter system for monitoring chromosome stability in *C. albicans***

156

157 To understand the molecular mechanisms underlying genome instability in a fungal pathogen, we
158 developed a reporter system in *C. albicans* in which whole chromosome loss can be distinguished
159 from other events such as break-induced replication, gene conversion, chromosome truncation or
160 mitotic crossing over (22, 46). In our prior work, a loss-of-heterozygosity (LOH) reporter strain
161 was developed for use in *C. albicans* (22, 46). In this strain *GFP* and *BFP* genes, linked to *ARG4*
162 and *HIS1* auxotrophic markers, respectively, are integrated at the same intergenic locus on the left
163 arms of chromosome 4A (Ch4A) and chromosome 4B (Ch4B), respectively (Fig. 1A, S1A) (22).
164 Consequently, cells express both GFP and BFP as analyzed by flow cytometry and are
165 prototrophic for *ARG4* and *HIS1* genes, unless a chromosome instability (CIN) event causes loss
166 of one of the two loci (Fig. 1A, B) (22). To differentiate whole chromosome loss from other
167 events that may lead to loss of one of the two reporter loci, we modified the LOH reporter strain
168 by integrating a red fluorescent protein (RFP) reporter gene, associated with the hygromycin B

169 (hyg B) resistance marker, on the right arm of Ch4B (Fig. 1A, S1A). The RFP reporter insertion is
170 sufficiently distant from the BFP locus that loss of both BFP and RFP signal (and of their linked
171 auxotrophic/resistance markers) is indicative of loss of Ch4B, rather than a localized event
172 causing loss of the *BFP-HIS1* reporter insertion (Fig. 1A, S1A). Notably, while loss of Ch4A
173 cannot be tolerated due to the presence of recessive lethal alleles on Ch4B (22), loss of Ch4B
174 leads to formation of small colonies that mature into larger colonies following duplication of
175 Ch4A (46). Thus, the absence of both *BFP-HIS1* and *RFP-HYG B* but continued presence of
176 *GFP-ARG4* in the modified reporter strain, which we named as chromosome stability (CSA)
177 reporter, enables us monitor loss of Ch4B in a population. The fluorescence intensity profile of
178 GFP, BFP and RFP in the CSA reporter was validated by flow cytometry (Fig. S1B). To
179 functionally validate the CSA reporter system, we employed overexpression of *CDC20*, a gene
180 important for anaphase onset, activation of spindle assembly checkpoint and whose
181 overexpression is known to cause whole chromosome loss in *C. albicans* (46). We analyzed the
182 BFP/GFP density plots in various control strains (Fig. S1C) and monitored the loss of BFP/GFP
183 signal in cells overexpressing *CDC20* (*CDC20^{OE}*) by flow cytometry. As reported earlier (46), the
184 *CDC20^{OE}* strain displayed a higher population of BFP⁺GFP⁻ and BFP⁻GFP⁺ cells as compared to
185 the empty vector (EV) control indicating increased CIN in the *CDC20^{OE}* mutant (Fig. S1D, E).
186 Next, we isolated BFP⁻GFP⁺ cells of EV and *CDC20^{OE}* using flow cytometry and plated them for
187 subsequent analysis of auxotrophic/resistance markers (Fig. S1F). As noted above, upon
188 incubation of the sorted BFP⁻GFP⁺ cells, we observed the appearance of both small and large
189 colonies (Fig. S1F). Small colonies have been previously shown to be the result of loss of Chr4B
190 homolog and are predicted to be a consequence of Ch4A monosomy, eventually yielding large
191 colonies upon reduplication of Ch4A (46). We, therefore, performed the marker analysis on large
192 colonies and found that 85% of the BFP⁻GFP⁺ derived colonies of *CDC20^{OE}* mutant
193 concomitantly lost both *HIS1* and *HYG B* but retained *ARG4* (Fig. S1G) suggesting the loss of
194 Ch4B homolog; flow cytometry analysis further confirmed the loss of BFP and RFP signals in
195 these colonies. The remaining 15% of colonies retained *GFP-ARG4* and *RFP-HYG B* but not
196 *BFP-HIS1* (Fig. S1G) indicating that more localized events including gene conversion, rather
197 than whole chromosome loss, were responsible for loss of the BFP signals in these cells. The
198 above data indicate that the CSA reporter system that we engineered enables precise monitoring
199 of the whole chromosome loss event in a population and enables large-scale screening of this
200 phenotype.

201

202 **Medium-throughput screening of *C. albicans* overexpression strains identifies regulators of** 203 **genome stability**

204
205 Systematic gene overexpression is an attractive approach for performing large-scale functional
206 genomic analysis in *C. albicans*, a diploid ascomycete. Using a recently developed collection of
207 *C. albicans* inducible overexpression plasmids (Chauvel et al., manuscript in preparation) and the
208 CSA reporter strain described above, we generated a library of 1067 *C. albicans* inducible
209 overexpression strains. Each of these strains, carrying a unique ORF under control of the P_{TET}
210 promoter, could be induced for overexpression after anhydrotetracycline (Atc) or doxycycline
211 (Dox) addition (Fig. 1C) (46, 47). To identify regulators of genome stability, we carried out a
212 primary screen with these 1067 overexpression strains by individually analyzing them for the loss
213 of BFP/GFP signals by flow cytometry (Fig. 1C, S2A, Dataset 1). Our primary screening
214 identified 23 candidate genes (out of 1067) whose overexpression resulted in ≥ 2 -fold increase in
215 the BFP⁺GFP⁻ and BFP⁻GFP⁺ population relative to the EV (Table S1, S2). Next, we carried out a
216 secondary screen with these 23 overexpression strains to revalidate the loss of BFP/GFP markers
217 by flow cytometry (Fig. 1C, S2B). As genotoxic stress is intimately linked with polarized growth
218 in *C. albicans* (17, 48), we microscopically examined the overexpression strains exhibiting higher
219 instability at the BFP/GFP locus during secondary screening for any morphological transition
220 (Fig. 1C, S2B). While overexpression of 17 genes (out of 23) could not reproduce the BFP/GFP
221 loss phenotype, overexpression of the six genes resulted in ≥ 2 -fold increase in the BFP⁺GFP⁻ or
222 BFP⁻GFP⁺ population as compared to the EV, with three genes (out of 6) inducing polarized
223 growth upon overexpression (Fig. S3A, B). These six genes, which we referred to as CSA genes,
224 include *CSA1* (*CLB4*), *CSA2* (*ASE1*), *CSA3* (*KIP2*), *CSA4* (*MCM7*), *CSA5* (*BFA1*) and *CSA6*
225 coded by *ORF19.1447* of unknown function (Fig. 1D).

226 227 **Molecular mechanisms underlying CIN in CSA overexpression mutants**

228
229 Out of the six CSA genes, overexpression of three genes, namely, *CSA1*^{*CLB4*}, *CSA2*^{*ASE1*} and
230 *CSA3*^{*KIP2*} caused little or no change in the morphology of *C. albicans* (Fig. S3A), but triggered
231 CIN at the BFP/GFP locus, indicated by an expansion of the BFP⁺GFP⁻ and BFP⁻GFP⁺ population
232 in the flow cytometry density plots (Fig. S3B, C). To further dissect the molecular mechanisms
233 leading to the loss of BFP/GFP signals in these mutants, we sorted BFP⁻GFP⁺ cells of these
234 mutants and plated them for *GFP-ARG4*, *BFP-HIS1* and *RFP-HYG B* analysis, as described
235 previously for the *CDC20*^{*OE*} mutant. We observed that a majority of the large BFP⁻GFP⁺ derived

236 colonies of *CSA1^{CLB4}*, *CSA2^{ASE1}* and *CSA3^{KIP2}* overexpression mutants lost *BFP-HIS1* but retained
237 *RFP-HYG B* and *GFP-ARG4* (Fig. **S3D**), suggesting that localized genome instability events,
238 rather than whole chromosome loss events, contributed to the high percentage of BFP-GFP⁺ cells
239 in these mutants.

240
241 Overexpression of the remaining three genes, namely *CSA4^{MCM7}*, *CSA5^{BFA1}* and *CSA6*, drastically
242 altered the morphology of the *C. albicans* cells by inducing polarized/filamentous growth (Fig.
243 **S3A**). A connection between morphological switches and genotoxic stresses has been established
244 in the polymorphic fungus *C. albicans*, wherein polarized growth is triggered in response to
245 improper cell cycle regulation (41, 42, 48-50). Flow cytometric analysis of cell cycle progression
246 revealed that overexpression of *CSA4^{MCM7}*, *CSA5^{BFA1}* and *CSA6* shifted cells towards the 4N DNA
247 content (Fig. **S3E**). To further determine the cell cycle phase associated with the 4N shift, we
248 compared nuclear segregation patterns (Hoechst staining for DNA and CENP-A/Cse4 localization
249 for KT) and spindle dynamics (separation of Tub4 foci) in these overexpression mutants with
250 those of the EV control (Fig. **S3F**). Our results suggested the 4N shift in *CSA4^{MCM7}* and *CSA6*
251 overexpression mutants was a result of G2/M arrest, indicated by a high percentage of large-
252 budded cells with unsegregated DNA mass and improperly separated SPBs (Fig. **S3F**). In
253 contrast, the 4N shift upon *CSA5^{BFA1}* overexpression was a consequence of late anaphase/telophase
254 arrest, shown by an increased number of large-budded cells with segregated nuclei and SPBs (Fig.
255 **S3F**). Taken together, our results indicate that the polarized growth in each of *CSA4^{MCM7}*,
256 *CSA5^{BFA1}* and *CSA6* overexpression mutants is a probable outcome of improper cell cycle
257 progression.

258
259 Two *CSA* genes, namely *CSA2^{ASE1}* and *CSA5^{BFA1}*, gave rise to similar overexpression phenotypes
260 in both *S. cerevisiae* and *C. albicans* (**Table 1**). While phenotypes related to *CSA4^{MCM7}* and *CSA6*
261 overexpression in *S. cerevisiae* or other related organisms remained unreported, the
262 overexpression phenotypes of the remaining *CSA* genes were along the lines of their roles in cell
263 cycle functioning, as reported in *S. cerevisiae* (**Table 1**, Fig. **1D**). Altogether, our results validated
264 the role of *CSA* genes in regulating genome stability in *C. albicans*. While overexpression of
265 either *CSA1^{CLB4}*, *CSA2^{ASE1}* or *CSA3^{KIP2}* induced CIN mostly through non-chromosomal loss
266 events, the effect of overexpression of either *CSA4^{MCM7}*, *CSA5^{BFA1}* or *CSA6* was so drastic that the
267 *C. albicans* mutants were arrested at different cell cycle phases with G2/M equivalent DNA
268 content (4N) and thus were unable to complete the mitotic cell cycle.

269

Csa6 is an SPB-localizing protein, present across a subset of CUG-Ser clade fungal species

Among the genes identified in the screen, Csa6 was the only protein without any detectable homolog in *S. cerevisiae* (Fig. 1D). This intrigued us to examine its presence across various other fungi. Phylogenetic analysis using high confidence protein homology searches and synteny-based analysis indicated that Csa6 is exclusively present in a subset of fungal species belonging to the CUG-Ser clade (Fig. 2A). Strikingly, in all these species, Csa6 was predicted to have a central coiled-coil domain (Fig. 2B). Epitope tagging of Csa6 with a fluorescent marker (mCherry) localized it close to the KT throughout the cell cycle in *C. albicans* (Fig. 2C). In most unicellular fungi, often found proximal to the clustered KTs, are the SPB complexes (33, 35, 51, 52). Although neither the SPB structure nor its composition is well characterized in *C. albicans*, the majority of the SPB proteins exhibit high sequence and structural conservation from yeast to humans (53). Hence, we re-examined Csa6 localization with two of the evolutionarily conserved SPB proteins, Tub4 and Spc110, in *C. albicans* (53, 54) (Fig. 2D, E). These results showed that Csa6 constitutively localizes to the SPBs, close to the KTs, in cycling yeast cells of *C. albicans* (Fig. 2D, E).

Csa6, a previously uncharacterized protein, as a key regulator of mitotic progression in *C. albicans*

While roles of Csa6 have not been investigated before, based on our findings thus far (Fig. S3E, F), we hypothesized that Csa6 plays an important function in cell cycle regulation and genome stability in *C. albicans*. We sought to identify the molecular pathways by which Csa6 performed its functions in *C. albicans*. We again made use of the inducible P_{TET} promoter system to generate a *CSA6*^{OE} strain (CaPJ176, $P_{TET}CSA6$) in the wild-type (SN148) background of *C. albicans* (Fig. 3A). Conditional overexpression of TAP-tagged Csa6 (CaPJ181, $P_{TET}CSA6-TAP$), in presence of Atc, was confirmed by western blot analysis (Fig. 3B). The effect of *CSA6*^{OE} (CaPJ176, $P_{TET}CSA6$) on cell cycle functioning was then investigated by flow cytometric cell cycle analysis (Fig. 3C) and microscopic examination of the nuclear division (Fig. 3D). As observed previously (Fig. S3E, F), *CSA6*^{OE} inhibited cell cycle progression in *C. albicans* by arresting cells in the G2/M phase, evidenced by the gradual accumulation of large-budded cells with unsegregated nuclei (Fig. 3D), possessing 4N DNA content (Fig. 3C). Some of these large-budded cells also underwent a morphological transition to an elongated bud or other complex multi-budded phenotypes (Fig. 3D), indicating cell cycle arrest-mediated morphological switching (48) due to

304 *CSA6^{OE}*. Strikingly, continuous upregulation of Csa6 was toxic to the cells (Fig. **S4A**) as nuclei
305 failed to segregate in this mutant (Fig. **3D**).

306

307 Nuclear segregation during mitosis is facilitated by the formation of the mitotic spindle and its
308 dynamic interactions with chromosomes via KTs. Thus, we sought to examine both the KT
309 integrity and the mitotic spindle morphology in the *CSA6^{OE}* mutants. In *C. albicans*, the structural
310 stability of the KT is a determinant of CENP-A/Cse4 stability wherein depletion of any of the
311 essential KT proteins results in delocalization and degradation of the CENP-A/Cse4 by ubiquitin-
312 mediated proteolysis (50). Fluorescence microscopy and western blot analysis confirmed that
313 Cse4 was neither delocalized (Fig. **S4B**) nor degraded from centromeric chromatin (Fig. **S4C**)
314 upon *CSA6^{OE}*. Next, we analyzed the spindle integrity in *CSA6^{OE}* mutants by tagging Tub4 (SPB)
315 and Tub1 (MTs) with fluorescent proteins. Fluorescence microscopy analysis revealed that a large
316 proportion (~73%) of the large-budded cells formed an unconventional rudimentary mitotic
317 spindle structure upon *CSA6^{OE}*, wherein it had a dot-like appearance as opposed to an elongated
318 bipolar rod-like spindle structure in EV or uninduced (-Atc) strains (Fig. **3E**). This suggests that
319 nuclear segregation defects in *CSA6^{OE}* mutant cells are an attribute of aberrant mitotic spindle
320 formation that might have led to the mitotic arrest.

321

322 During mitosis, surveillance mechanisms, including spindle assembly checkpoint (SAC) (55, 56)
323 and spindle positioning checkpoint (SPOC) (57, 58) operate to maintain genome stability by
324 delaying the metaphase-anaphase transition in response to improper chromosome-spindle
325 attachments and spindle misorientation, respectively. We posit that the G2/M cell cycle arrest due
326 to *CSA6^{OE}* in *C. albicans* could be a result of either SAC or SPOC activation. Hence, we decided
327 to inactivate SAC and SPOC, individually, in the *CSA6^{OE}* strain by deleting the key spindle
328 checkpoint genes *MAD2* (41) and *BUB2* (48), respectively. SAC inactivation in *CSA6^{OE}* mutant
329 cells (Fig. **4A**) led to the emergence of unbudded cells with 2N DNA content (Fig. **4B, C**),
330 indicating a bypass of the G2/M arrest caused by *CSA6^{OE}*. Consequently, we also observed a
331 partial rescue of the growth defect in *CSA6^{OE}* mutant cells (Fig. **S5A**). Next, we sought to
332 characterize the effect of SAC inactivation on the spindle integrity in *CSA6^{OE}* mutants. *CSA6^{OE}*
333 resulted in the formation of an unconventional mitotic spindle (Fig. **3E**) wherein it displayed a
334 single focus of SPB (Tub4-GFP), colocalizing with a single focus of MTs (Tub1-mCherry). We
335 speculated two possibilities that may lead to the single focus of Tub4: a) a defect in the process of
336 SPB duplication or b) a delay in the separation of duplicated SPBs. Fluorescence microscopy
337 analysis revealed that SAC inactivation in *CSA6^{OE}* mutant drastically increased the percentage of

338 large-budded cells (from ~30% to ~68%) with two separated SPB foci (Tub4-GFP) (Fig. **S5B**).
339 These results ruled out the possibility of an unduplicated SPB in *CSA6^{OE}* mutant cells and hinted
340 at the importance of cellular Csa6 levels for proper SPB separation and chromosome segregation
341 in *C. albicans*.

342
343 We next determined the effect of inactivating SPOC in the cells overexpressing Csa6. For this, we
344 generated a *CSA6^{OE}* strain (CaPJ200) using the *bub2* null mutant (CaPJ110) as the parent strain
345 and monitored nuclear division following Hoechst staining. Strikingly, we did not observe a
346 bypass of G2/M arrest in *CSA6^{OE}* mutant upon SPOC inactivation, indicated by a persistent
347 population of large-budded cells with unsegregated nuclei (Fig. **S5C**). Altogether, our results
348 demonstrate that overexpression of Csa6 leads to a Mad2-mediated metaphase arrest due to a
349 malformed spindle in *C. albicans*.

350

351 **Csa6 regulates mitotic exit network and is essential for viability in *C. albicans***

352

353 To further gain insights into the biological function of Csa6, we sought to generate a promoter
354 shut-down mutant of *csa6* (*CSA6^{PSD}*). For this, we deleted one of its alleles and placed the
355 remaining one under the control of the *MET3* promoter (59) which gets repressed in presence of
356 methionine (Met/M) and cysteine (Cys/C) (Fig. **5A**). Western blot analysis confirmed the
357 depletion of TAP-tagged Csa6 in *CSA6^{PSD}* mutant within 6 h of growth under repressive
358 conditions (Fig. **5B**). The inability of *CSA6^{PSD}* mutant to grow in non-permissive conditions
359 confirmed the essentiality of Csa6 for viability in *C. albicans* (Fig. **5C**). Subsequently, we
360 analyzed the cell cycle profile (Fig. **5D**) and nuclear division dynamics (Fig. **5E**) in the *CSA6^{PSD}*
361 strain after a specific period of incubation in either permissive or non-permissive conditions.
362 Strikingly, Csa6 depletion, as opposed to its overexpression, resulted in cell cycle arrest at the late
363 anaphase/telophase stage, indicated by an increasing proportion of large-budded cells, possessing
364 segregated nuclei and 4N DNA content (Fig. **5D, E**). Additionally, we observed cells with more
365 than two nuclei, elongated-budded cells and other complex phenotypes upon Csa6 depletion (Fig.
366 **5E**). While CENP-A/Cse4 remained localized to centromeres in *CSA6^{PSD}* mutant as revealed by
367 the fluorescence microscopy (Fig. **S6A**), an increase in the cellular levels of Cse4 was observed in
368 *CSA6^{PSD}* mutant by western blot analysis (Fig. **S6B**). The increase in Cse4 levels could be an
369 outcome of Cse4 loading at anaphase in *C. albicans* (60, 61). Finally, we analyzed the integrity of
370 the mitotic spindle, as mentioned previously, in *CSA6^{PSD}* mutant. We noticed the mean length of
371 the anaphase mitotic spindle in Csa6-depleted cells was significantly higher (~11 μ m) than that of

372 the cells grown under permissive conditions (~6 μm), indicating a spindle disassembly defect in
373 *CSA6^{PSD}* mutant (Fig. 5F).

374
375 A close link between anaphase arrest, hyper-elongated mitotic spindle and inactive mitotic exit
376 network (MEN) have been established before (40, 62, 63). Localized at the SPB, the MEN is a
377 signaling cascade in *S. cerevisiae* that triggers cells to come out of mitosis and proceed to
378 cytokinesis (Fig. 6A) (64). We speculated the anaphase arrest in *CSA6^{PSD}* mutant could be a result
379 of an inactive MEN signaling. To determine this, we sought to bypass the anaphase arrest
380 associated with Csa6 depletion by overexpressing *SOLI*, the CDK inhibitor and Sic1 homolog in
381 *C. albicans* (65) (Fig. 6B), using the inducible P_{TET} system mentioned previously (Fig. 6C). The
382 conditional overexpression of Protein A-tagged Sol1 upon addition of Atc was verified by
383 western blot analysis (Fig. 6D). Strikingly, *SOLI^{OE}* in association with Csa6 depletion allowed
384 cells to exit mitosis but not cytokinesis, as evidenced by the formation of chains of cells with >4N
385 DNA content (Fig. 6E, F). To further examine the role of Csa6 in mitotic exit, we analyzed the
386 localization of a MEN component, Tem1, a GTPase that is known to initiate MEN signaling (39,
387 66-68). In *C. albicans*, Tem1 localizes to SPBs in a cell-cycle-regulated manner and is essential
388 for viability (39). Fluorescence microscopy revealed that while Tem1 is localized to both the
389 SPBs in anaphase under permissive conditions (Fig. 6G) as observed earlier (39), a high
390 percentage of Csa6-depleted cells (~78%) had Tem1 localized to only one of the two SPBs (Fig.
391 6G), suggesting an important role of Csa6 in regulating mitotic exit in *C. albicans*. Altogether,
392 our results demonstrate that Csa6 is required for mitotic exit and thus essential for viability in *C.*
393 *albicans*.

395 **Csa6 of *Candida dubliniensis* functionally complements Csa6 of *C. albicans***

396
397 To further elucidate the intra-species function and localization of Csa6, we decided to ectopically
398 express Csa6 of another CUG-Ser clade species, *Candida dubliniensis* (CdCsa6) in *C. albicans*.
399 *C. dubliniensis* is a human pathogenic budding yeast that shares a high degree of DNA sequence
400 homology with *C. albicans*, and possesses unique and different centromere DNA sequences on
401 each of its eight chromosomes (69, 70). Upon protein sequence alignment, we found that CdCsa6
402 (*ORF Cd36_16290*) is 79% identical to Csa6 of *C. albicans* (CaCsa6) (Fig. 7A). The ectopic
403 expression of GFP-tagged CdCsa6 in *C. albicans* was carried out using the replicative plasmid
404 pCdCsa6-GFP-ARS2 (Fig. 7B), which contains the autonomously replicating sequence (ARS) of
405 *C. albicans* (71). Although unstable when present in an episomal form, ARS plasmids, upon

406 spontaneous integration into the genome, can propagate stably over generations (72).
407 Fluorescence microscopy of integrated pCdCsa6-GFP-ARS2 revealed that similar to CaCsa6,
408 CdCsa6 localizes constitutively to the SPBs in *C. albicans* (Fig. 7C), further supporting Csa6's
409 evolutionarily conserved role in regulating mitotic spindle and mitotic exit in *C. albicans*. We
410 next asked if CdCsa6 can functionally complement CaCsa6. For this, we ectopically expressed
411 CdCsa6 in *CSA6^{PSD}* strain. Strikingly, the ectopic expression of CdCsa6 rescued the growth defect
412 associated with *CSA6^{PSD}* mutant under non-permissive conditions, indicating CdCsa6 can
413 functionally complement CaCsa6 (Fig. 7D). This suggests functional conservation of Csa6 among
414 related *Candida* species belonging to the CUG-Ser clade.

415

416 Discussion

417

418 In this study, we carried out an extensive screen to identify genes that contribute to genome
419 stability in *C. albicans* by generating and analyzing a library of more than a thousand
420 overexpression strains. Our screen identified six regulators of chromosome stability including
421 Csa6, a protein of unknown function. Molecular dissection of Csa6 function revealed its
422 importance in cell cycle progression at least in two critical stages, metaphase-anaphase transition
423 and mitotic exit. We further demonstrated that Csa6 is constitutively localized to the SPBs,
424 essential for viability, and alterations of its cellular level leads to cell cycle arrest in *C. albicans*.
425 Finally, subcellular localization and complementation analysis revealed functional conservation
426 of Csa6 across the pathogenic *Candida* species.

427

428 The identification of two *CSA* genes, *CSA2^{ASE1}* and *CSA5^{BFA1}*, that were earlier reported as CIN
429 genes (13, 14), further validates the power of the screening approach and the methods presented
430 in this study. The respective overexpression phenotypes of these two genes in *C. albicans* were
431 found to be similar to those in *S. cerevisiae*, suggesting that their functions might be conserved in
432 these distantly related yeast species. In *S. cerevisiae*, Ase1 acts as an MT-bundling protein,
433 required for spindle elongation and stabilization during anaphase (73, 74) (Fig. 8A). Hence,
434 increased CIN upon *ASE1* overexpression might be an outcome of premature spindle elongation
435 and improper KT-microtubule attachments (74, 75). Bfa1, on the other hand, is a key component
436 of the Bub2-Bfa1 complex, involved in SPOC activation (57), and a negative regulator of mitotic
437 exit (76) (Fig. 8A). In *S. cerevisiae*, *BFA1* overexpression prevents Tem1 from interacting with its
438 downstream effector protein Cdc15, thus inhibiting MEN signaling and arresting cells at the
439 anaphase (77). In our screen, a B-type mitotic cyclin Clb4 (*CSA1*), and a kinesin-related motor

440 protein Kip2 (*CSA3*) (Fig. **8A**), were found to increase CIN upon overexpression, primarily via
441 non-chromosomal loss events. *C. albicans* Clb4 acts as a negative regulator of polarized growth
442 (49) and is the functional homolog of *S. cerevisiae* Clb5 (78), required for the entry into the S-
443 phase (79). Increased CIN upon *CSA1^{CLB4}* overexpression, is thus consistent with its role in S-
444 phase initiation. The function of Kip2, however, is yet to be characterized in *C. albicans*. In *S.*
445 *cerevisiae*, Kip2 functions as an MT polymerase (80), with its overexpression leading to
446 hyperextended MTs and defects in SPB separation (81). The associated CIN observed upon
447 *CSA3^{KIP2}* overexpression in *C. albicans* is in line with its function in nuclear segregation.

448
449 Mcm7, another *CSA* gene (*CSA4*) identified in this study, is a component of the highly conserved
450 Mcm2-7 helicase complex, essential for eukaryotic DNA replication initiation and elongation (82)
451 (Fig. **8A**). While Mcm7 depletion arrests cells at S phase (83), the effect of *MCM7*
452 overexpression on genomic integrity is comparatively less explored. Especially, several cancerous
453 cells have been shown to overexpress Mcm7 (84-86), with its elevated levels increasing the
454 chances of relapse and local invasions (84). In this study, we found that overexpression of *MCM7*,
455 in contrast to Mcm7 depletion, arrested cells at the G2/M stage. One possibility is increased
456 Mcm7 levels interfered with DNA replication during the S phase, resulting in DNA damage or
457 accumulation of single-stranded DNA, thus activating the *RAD9*-dependent cell cycle arrest at the
458 G2/M stage (87, 88). In a recent study from our laboratory, Mcm7 has been identified as a subunit
459 of the kinetochore interactome in a basidiomycete yeast *Cryptococcus neoformans* (89). Another
460 subunit of the Mcm2-7 complex, Mcm2, is involved in regulating the stability of centromeric
461 chromatin in *C. albicans* (61). Considering the growing evidence of the role of Mcm2-7 subunits
462 beyond their canonical, well-established roles in DNA replication, the serendipitous identification
463 of Mcm7 as a regulator of genome stability in our screen is striking.

464
465 We performed an in-depth analysis of *Csa6*, a novel regulator of cell cycle progression identified
466 from our screen (Fig. **8B, C**). Our results revealed that overexpression of *CSA6* leads to an
467 unconventional mitotic spindle formation and SAC-dependent G2/M cell cycle arrest (Fig. **8C**) in
468 *C. albicans*. While *mad2* deletion indicated that SPB duplication and separation of duplicated
469 SPBs is unperturbed in *CSA6* overexpressing cells, what exactly triggered the activation of SAC
470 in these cells remains to be determined. Recent studies on human cell lines have shown that
471 failure in the timely separation of the centrosomes promotes defective chromosome-MT
472 attachments and may lead to chromosome lagging if left uncorrected by the cellular surveillance
473 machinery (90-92). Along the same lines, we posit that a delay in SPB separation, mediated by

474 overexpression of Csa6, leads to increased instances of improper chromosome-MT attachments,
475 leading to SAC activation and an indefinite arrest at the metaphase stage. Future studies on the
476 SPB structure-function and composition in *C. albicans* should reveal how Csa6 regulates SPB
477 dynamics in this organism.

478
479 In contrast to its overexpression, Csa6 depleted cells failed to exit mitosis and remained arrested
480 at the late anaphase/telophase stage (Fig. **8C**). We further linked the mitotic exit failure in Csa6
481 depleted cells with the defective localization of Tem1, an upstream MEN protein. While the
482 hierarchy of MEN components, starting from the MEN scaffold Nud1, an SPB protein, to its
483 ultimate effector Cdc14 is well established in *S. cerevisiae* (64), the existence of a similar
484 hierarchy in *C. albicans* needs to be investigated. In addition, several lines of evidence suggest
485 that MEN in *C. albicans* may function differently from *S. cerevisiae*: (a) Unlike *S. cerevisiae*, *C.*
486 *albicans* Cdc14 is non-essential for viability with its deletion affecting cell separation (93). (b)
487 Cdc14 is present in the nucleoplasm for the majority of the cell cycle in contrast to its nucleolar
488 localization in *S. cerevisiae* (93). (c) *C. albicans* Dbf2 is required for proper nuclear segregation,
489 actomyosin ring contraction, and cytokinesis (38). A recent study involving the identification of
490 Cdc14 interactome in *C. albicans* (94) found only a subset of proteins (0.2%) as physical or
491 genetic interactors in *S. cerevisiae*, suggesting the divergence of Cdc14 functions in *C. albicans*.
492 Hence, further investigations of MEN functioning in *C. albicans* are required to understand its
493 divergence from *S. cerevisiae* and the mechanism by which Csa6 regulates mitotic exit in *C.*
494 *albicans* and related species. Altogether, our results indicate that Csa6 has dual functions during
495 cell cycle progression wherein it is first required during the G2/M phase for proper assembly of
496 the mitotic spindle and then later during anaphase to exit the cells from mitosis. In addition, the
497 constitutive localization of Csa6 to the SPBs strengthens the link between SPB-related functions
498 and Csa6 in *C. albicans* (Fig. **8B, C**).

499
500 The phylogenetic analysis of Csa6 revealed that it is only present in a group of fungal species,
501 belonging to the CUG-Ser clade. Combined with its essential cell-cycle-related functions, it is
502 intriguing to determine whether emergence of Csa6 is required to keep the pace of functional
503 divergence in the regulatory mechanisms of cell cycle progression in these *Candida* species.
504 While we demonstrated Csa6 of *C. dubliniensis* functionally complements Csa6 of *C. albicans*,
505 whether Csa6 of distant species can also functionally complement CaCsa6 remains to be
506 investigated. A recent study shows that around 50 essential genes, including Csa6, are only
507 present in a group of *Candida* species (see Dataset 5 in (95)). Identification and functional

508 characterization of these genes in the future will aid in developing clade-specific antifungal
509 therapies (95). In this study, we have analyzed only a part of the *C. albicans* ORFeome for their
510 roles in genome maintenance. Further screening of the remaining overexpression ORFs will
511 provide a complete network of the molecular pathways regulating genome stability in human
512 fungal pathogens.

514 **Materials and Methods**

516 **1. Strains, plasmids and primers.** Information related to strains, plasmids and primers used in
517 this study is available in the supplementary material.

519 **2. Media and growth conditions.** *C. albicans* strains were routinely grown at 30°C in YPD (1%
520 yeast extract, 2% peptone, 2% dextrose) medium supplemented with uridine (0.1 µg/ml) or
521 complete medium (CM, 2% dextrose, 1% yeast nitrogen base and auxotrophic supplements) with
522 or without uridine (0.1 µg/ml) and amino acids such as histidine, arginine, leucine (0.1 µg/ml).
523 Solid media were prepared by adding 2% agar. For the selection of transformants, nourseothricin
524 and hygromycin B (hyg B) were used at a final concentration of 100 µg/ml and 800 µg/ml,
525 respectively, in the YPDU medium.

527 Overexpression of genes from the tetracycline inducible promoter (P_{TET}) was achieved by the
528 addition of anhydrotetracycline (Atc, 3 µg/ml) or doxycycline (Dox, 50 µg/ml) in YPDU medium
529 at 30°C (47) in the dark as Atc and Dox are light-sensitive. The *CSA6^{PSD}* strains were grown at
530 30°C either in permissive (YPDU) or nonpermissive (YPDU + 5mM methionine (M) + 5mM
531 cysteine (C)) conditions of the *MET3* promoter (59, 61). *E. coli* strains were cultured at 30°C or
532 37°C in Luria-Bertani (LB) medium or 2YT supplemented with ampicillin (50 µg/ml or 100
533 µg/ml), chloramphenicol (34 µg/ml), kanamycin (50 µg/ml) and tetracycline (10 µg/ml). Solid
534 media were prepared by adding 2% agar. Chemically competent *E. coli* cells were prepared
535 according to Chung *et al* (96).

537 **3. Flow cytometry analysis.** Cultures of overexpression strains following 8 h of induction in
538 YPDU+Atc and overnight recovery in the YPDU medium alone, were diluted in 1x phosphate-
539 buffered saline (PBS) and analyzed (~10⁶ cells) for the BFP/GFP marker by flow cytometry
540 (FACSAria III, BD Biosciences) at a rate of 7000-10,000 events/s. We used 405- and 488-nm

541 lasers to excite the BFP and GFP fluorophores and 450/40 and 530/30 filters to detect the BFP
542 and GFP emission signals, respectively.

543

544 **4. Primary and secondary overexpression screening.** To detect CIN at the BFP/GFP locus
545 upon P_{TET} activation, overnight grown cultures of *C. albicans* overexpression strains were
546 reinoculated in CM-His-Arg to ensure all cells contained *BFP-HIS1* or *GFP-ARG4*. To measure
547 the loss of BFP/GFP signals in 96-well plates, a *CDC20^{OE}* mutant was used as a positive control.
548 The primary selection of the overexpression mutants with increased BFP⁺GFP⁻ and BFP⁻GFP⁺
549 cells was done by determining the BFP/GFP loss frequency in EV. For this, we analyzed the flow
550 cytometry density plots for 22 independent cultures of EV using the FlowJo software (FlowJo X
551 10.0.7r2). We observed a similar profile for all the cultures. We then defined gates for the
552 BFP⁺GFP⁻ and BFP⁻GFP⁺ fractions of cell population in one of the EV samples and applied these
553 gates to the rest of EV samples. The mean frequency of BFP⁺GFP⁻ and BFP⁻GFP⁺ cells in EV was
554 calculated (Table S1). Similar gates were applied to all 1067 overexpression strains analyzed for
555 BFP/GFP markers and the frequency of BFP⁺GFP⁻ and BFP⁻GFP⁺ cells for each strain was
556 determined (Dataset 1). The overexpression mutants, in which the BFP/GFP loss frequency was
557 ≥ 2 -fold than EV, were selected for further analysis (Table S2).

558

559 For secondary screening, the overexpression plasmids present in each of the overexpression
560 strains, identified from the primary screen (23 out of 1067), were used to retransform the CSA
561 reporter strain (CEC5201). The overexpression strains (23) were analyzed by flow cytometry to
562 revalidate the loss of BFP/GFP signals. Overexpression strains displaying ≥ 2 -fold higher
563 frequency of BFP⁺GFP⁻ /BFP⁻GFP⁺ population than EV (6 out of 23) were monitored for any
564 morphological transition by microscopy. As filamentous morphotype could distort the BFP/GFP
565 loss analysis (46), we characterized the overexpression mutants exhibiting increased CIN at the
566 BFP/GFP locus and filamentous growth (3 out of 6) by monitoring cell cycle progression. For
567 this, we transformed the overexpression plasmids in CaPJ159 and analyzed the overexpression
568 strains (*CSA4^{MCM7}*, *CSA5^{BFA1}* and *CSA6*) for DNA content, nuclear segregation and SPB
569 separation. The 6 genes identified from the secondary screen were verified for the correct *C.*
570 *albicans* ORF by Sanger sequencing using a common primer PJ90. During the secondary
571 screening, we also cultured overexpression mutants in YPDU without Atc and observed no
572 differences between EV and uninduced (-Atc) cultures in terms of morphology and the BFP/GFP
573 loss frequency.

574

575 **5. Cell sorting and marker analysis following a CIN event.** Overnight grown cultures of EV
576 and overexpression mutants (*CDC20*, *CSA1*^{CLB4}, *CSA2*^{ASE1} and *CSA3*^{KIP2}) were reinoculated in
577 YPDU+Atc for 8 h and allowed to recover overnight in YPDU-Atc. The cultures were analyzed
578 for BFP/GFP loss by flow cytometry followed by fluorescence-activated cell sorting (FACS)
579 using a cell sorter (FACSARIA III, BD Biosciences) at a rate of 10,000 events/s. Approximately
580 1500 cells from the BFP⁻GFP⁺ population were collected into 1.5-ml tubes containing 400 µl
581 YPDU and immediately plated onto YPDU agar plates. Upon incubation at 30°C for 2 days, both
582 small and large colonies appeared, as reported earlier (46). As most small colonies are expected to
583 have undergone loss of the Ch4B haplotype (46), we analyzed auxotrophic/resistance markers of
584 large colonies to characterize the molecular mechanisms underlying CIN in the overexpression
585 mutants.

586
587 For marker analysis, we replica plated the large colonies along with the appropriate control strains
588 on CM-Arg, CM-His and YPDU+hyg B (800 µg/ml) and incubated the plates at 30°C for 2 days.
589 The colonies from CM-Arg plates were then analyzed for BFP, GFP and RFP markers by flow
590 cytometry. For this, overnight grown cultures in YPDU were diluted in 1x PBS and 5000-10,000
591 cells were analyzed (FACSARIA III, BD Biosciences). We used 405-, 488- and 561 nm lasers to
592 excite the BFP, GFP and RFP fluorophores and 450/40, 530/30, 582/15 filters to detect the BFP,
593 GFP and RFP emission signals, respectively.

594
595 **6. Cell cycle analysis.** Overnight grown cultures of *C. albicans* were reinoculated at an OD₆₀₀ of
596 0.2 in different media (as described previously) and harvested at various time intervals post-
597 inoculation (as mentioned previously). The overnight grown culture itself was taken as a control
598 sample (0 h) for all the experiments. Harvested samples were processed for propidium iodide (PI)
599 staining as described before (33). Stained cells were diluted to the desired cell density in 1x PBS
600 and analyzed (≥30, 000 cells) by flow cytometry (FACSARIA III, BD Biosciences) at a rate of
601 250-1000 events/s. The output was analyzed using the FLOWJO software. We used 561-nm laser
602 to excite PI and 610/20 filter to detect its emission signals.

603
604 **7. Fluorescence microscopy.** For nuclear division analysis in untagged strains, the *C. albicans*
605 cells were grown overnight. The next day, the cells were transferred into different media (as
606 mentioned previously) with a starting O.D.₆₀₀ of 0.2, collected at various time intervals (as
607 described previously) and fixed with formaldehyde (3.7%). Cells were pelleted and washed thrice
608 with 1x PBS, and Hoechst dye (50 ng/ml) was added to the cell suspension before imaging.

609 Nuclear division in Cse4-and Tub4-tagged strains was analyzed as described above, except the
610 cells were not fixed with formaldehyde. For Tem1 and mitotic spindle localization, overnight
611 grown cultures were transferred to different media (as mentioned previously) with a starting
612 O.D.₆₀₀ of 0.2 and were grown for 6 h or 8 h. Cells were then washed, resuspended in 1x PBS and
613 imaged on a glass slide. Localization studies of each, CaCsa6, Tub4, Spc110 and CdCsa6 was
614 carried out by washing the log phase grown cultures with 1x PBS (three times) followed by image
615 acquisition.

616
617 The microscopy images were acquired using fluorescence microscope (Zeiss Axio Observer 7
618 equipped with Colibri 7 as the LED light source), 100x Plan Apochromat 1.4 NA objective, pco.
619 edge 4.2 sCMOS. We used Zen 2.3 (blue edition) for image acquisition and controlling all
620 hardware components. Filter set 92 HE with excitation 455–483 and 583–600 nm for GFP and
621 mCherry, respectively, and corresponding emission was captured at 501–547 and 617–758 nm. Z
622 sections were obtained at an interval of 300 nm. All the images were displayed after the maximum
623 intensity projection using ImageJ. Image processing was done using ImageJ. We used the cell
624 counter plugin of ImageJ to count various cell morphologies in different mutant strains. Images
625 acquired in the mCherry channel were processed using the subtract background plugin of ImageJ
626 for better visualization.

627
628 **8. Protein preparation and western blotting.** Approximately 3 O.D.₆₀₀ equivalent cells were
629 taken, washed with water once and resuspended in 12.5% TCA (trichloroacetic acid) and
630 incubated at -20°C overnight for precipitation. The cells were pelleted down and washed twice
631 with ice-cold 80% acetone. The pellet was then allowed to air dry and finally resuspended in lysis
632 buffer (0.1N NaOH and 1% SDS and 5xprotein loading dye). Samples were boiled at 95°C for 5-
633 10 min and electrophoresed on a 10% SDS polyacrylamide gel. Gels were transferred to a
634 nitrocellulose membrane by semi-dry method for 30 min at 25V and blocked for an hour in 5%
635 non-fat milk in 1x PBS. Membranes were incubated with a 1:5000 dilution of rabbit anti-Protein
636 A or mouse anti-PSTAIRES in 2.5% non-fat milk in 1x PBS. Membranes were washed three times
637 in 1x PBS-Tween (0.05%) and then exposed to a 1:10,000 dilution of either anti-mouse- or anti-
638 rabbit-IgG horseradish peroxidase antibody in 2.5% non-fat milk in 1x PBS. Membranes were
639 washed three times in 1x PBS-Tween (0.05%) and developed using chemiluminescence method.

640
641 **9. Statistical analysis.** Statistical significance of differences was calculated as mentioned in the
642 figure legends with unpaired one-tailed *t*-test, paired one-tailed *t*-test, paired two-tailed *t*-test or

643 one-way ANOVA with Bonferroni posttest. P -values ≥ 0.05 were considered as nonsignificant
644 (n.s.). P -values of the corresponding figures are mentioned, if significant. All analyses were
645 conducted using GraphPad Prism version Windows v5.00.

646

647 **References**

648

- 649 1. A. Aguilera, B. Gomez-Gonzalez, Genome instability: a mechanistic view of its causes
650 and consequences. *Nat. Rev. Genet.* **9**, 204-217 (2008).
- 651 2. T. A. Potapova, J. Zhu, R. Li, Aneuploidy and chromosomal instability: a vicious cycle
652 driving cellular evolution and cancer genome chaos. *Cancer Metastasis Rev.* **32**, 377-389
653 (2013).
- 654 3. Y. B. Yurov, S. G. Vorsanova, I. Y. Iourov, Chromosome Instability in the
655 Neurodegenerating Brain. *Front. Genet.* **10**, 892 (2019).
- 656 4. A. M. R. Taylor, C. Rothblum-Oviatt, N. A. Ellis, I. D. Hickson, S. Meyer, T. O.
657 Crawford, A. Smogorzewska, B. Pietrucha, C. Weemaes, G. S. Stewart, Chromosome
658 instability syndromes. *Nat. Rev. Dis. Primers* **5**, 64 (2019).
- 659 5. M. A. Petr, T. Tulika, L. M. Carmona-Marin, M. Scheibye-Knudsen, Protecting the Aging
660 Genome. *Trends Cell Biol.* **30**, 117-132 (2020).
- 661 6. S. Negrini, V. G. Gorgoulis, T. D. Halazonetis, Genomic instability--an evolving hallmark
662 of cancer. *Nat. Rev. Mol. Cell Biol.* **11**, 220-228 (2010).
- 663 7. K. Guin, Y. Chen, R. Mishra, S. R. B. Muzaki, B. C. Thimmappa, C. E. O'Brien, G.
664 Butler, A. Sanyal, K. Sanyal, Spatial inter-centromeric interactions facilitated the
665 emergence of evolutionary new centromeres. *Elife* **9**, (2020).
- 666 8. S. R. Sankaranarayanan, G. Ianiri, M. A. Coelho, M. H. Reza, B. C. Thimmappa, P.
667 Ganguly, R. N. Vadnala, S. Sun, R. Siddharthan, C. Tellgren-Roth, T. L. J. Dawson, J.
668 Heitman, K. Sanyal, Loss of centromere function drives karyotype evolution in closely
669 related *Malassezia* species. *Elife* **9**, (2020).
- 670 9. A. Aguilera, T. Garcia-Muse, Causes of genome instability. *Annu. Rev. Genet.* **47**, 1-32
671 (2013).
- 672 10. M. S. Levine, A. J. Holland, The impact of mitotic errors on cell proliferation and
673 tumorigenesis. *Genes Dev.* **32**, 620-638 (2018).
- 674 11. K. W. Yuen, C. D. Warren, O. Chen, T. Kwok, P. Hieter, F. A. Spencer, Systematic
675 genome instability screens in yeast and their potential relevance to cancer. *Proc. Natl.*
676 *Acad. Sci. U S A* **104**, 3925-3930 (2007).

- 677 12. P. C. Stirling, M. S. Bloom, T. Solanki-Patil, S. Smith, P. Sipahimalani, Z. Li, M. Kofoed,
678 S. Ben-Aroya, K. Myung, P. Hieter, The complete spectrum of yeast chromosome
679 instability genes identifies candidate CIN cancer genes and functional roles for ASTRA
680 complex components. *PLoS Genet.* **7**, e1002057 (2011).
- 681 13. L. F. Stevenson, B. K. Kennedy, E. Harlow, A large-scale overexpression screen in
682 *Saccharomyces cerevisiae* identifies previously uncharacterized cell cycle genes. *Proc.*
683 *Natl. Acad. Sci. U S A* **98**, 3946-3951 (2001).
- 684 14. S. Duffy, H. K. Fam, Y. K. Wang, E. B. Styles, J. H. Kim, J. S. Ang, T. Singh, V.
685 Larionov, S. P. Shah, B. Andrews, C. F. Boerkoel, P. Hieter, Overexpression screens
686 identify conserved dosage chromosome instability genes in yeast and human cancer. *Proc.*
687 *Natl. Acad. Sci. U S A* **113**, 9967-9976 (2016).
- 688 15. C. Espinet, M. A. de la Torre, M. Aldea, E. Herrero, An efficient method to isolate yeast
689 genes causing overexpression-mediated growth arrest. *Yeast* **11**, 25-32 (1995).
- 690 16. R. Akada, J. Yamamoto, I. Yamashita, Screening and identification of yeast sequences
691 that cause growth inhibition when overexpressed. *Mol. Gen. Genet.* **254**, 267-274 (1997).
- 692 17. M. Legrand, P. Jaitly, A. Feri, C. d'Enfert, K. Sanyal, *Candida albicans*: An Emerging
693 Yeast Model to Study Eukaryotic Genome Plasticity. *Trends Genet.* **35**, 292-307 (2019).
- 694 18. G. D. Brown, D. W. Denning, N. A. Gow, S. M. Levitz, M. G. Netea, T. C. White, Hidden
695 killers: human fungal infections. *Sci. Transl. Med.* **4**, 165rv113 (2012).
- 696 19. D. Z. P. Friedman, I. S. Schwartz, Emerging Fungal Infections: New Patients, New
697 Patterns, and New Pathogens. *J. Fungi (Basel)* **5**, (2019).
- 698 20. A. Selmecki, A. Forche, J. Berman, Genomic plasticity of the human fungal pathogen
699 *Candida albicans*. *Eukaryot. Cell* **9**, 991-1008 (2010).
- 700 21. A. Forche, K. Alby, D. Schaefer, A. D. Johnson, J. Berman, R. J. Bennett, The parasexual
701 cycle in *Candida albicans* provides an alternative pathway to meiosis for the formation of
702 recombinant strains. *PLoS Biol.* **6**, e110 (2008).
- 703 22. A. Feri, R. Loll-Krippelber, P. H. Commere, C. Maufrais, N. Sertour, K. Schwartz, G.
704 Sherlock, M. E. Bougnoux, C. d'Enfert, M. Legrand, Analysis of Repair Mechanisms
705 following an Induced Double-Strand Break Uncovers Recessive Deleterious Alleles in the
706 *Candida albicans* Diploid Genome. *mBio* **7**, (2016).
- 707 23. A. Selmecki, M. Gerami-Nejad, C. Paulson, A. Forche, J. Berman, An isochromosome
708 confers drug resistance in vivo by amplification of two genes, ERG11 and TAC1. *Mol.*
709 *Microbiol.* **68**, 624-641 (2008).

- 710 24. N. Dunkel, J. Blass, P. D. Rogers, J. Morschhauser, Mutations in the multi-drug resistance
711 regulator MRR1, followed by loss of heterozygosity, are the main cause of MDR1
712 overexpression in fluconazole-resistant *Candida albicans* strains. *Mol. Microbiol.* **69**, 827-
713 840 (2008).
- 714 25. A. M. Selmecki, K. Dulmage, L. E. Cowen, J. B. Anderson, J. Berman, Acquisition of
715 aneuploidy provides increased fitness during the evolution of antifungal drug resistance.
716 *PLoS Genet.* **5**, e1000705 (2009).
- 717 26. C. B. Ford, J. M. Funt, D. Abbey, L. Issi, C. Guiducci, D. A. Martinez, T. Delorey, B. Y.
718 Li, T. C. White, C. Cuomo, R. P. Rao, J. Berman, D. A. Thompson, A. Regev, The
719 evolution of drug resistance in clinical isolates of *Candida albicans*. *Elife* **4**, e00662
720 (2015).
- 721 27. A. Selmecki, A. Forche, J. Berman, Aneuploidy and isochromosome formation in drug-
722 resistant *Candida albicans*. *Science* **313**, 367-370 (2006).
- 723 28. A. Coste, V. Turner, F. Ischer, J. Morschhauser, A. Forche, A. Selmecki, J. Berman, J.
724 Bille, D. Sanglard, A mutation in Tac1p, a transcription factor regulating CDR1 and
725 CDR2, is coupled with loss of heterozygosity at chromosome 5 to mediate antifungal
726 resistance in *Candida albicans*. *Genetics* **172**, 2139-2156 (2006).
- 727 29. A. Forche, G. Cromie, A. C. Gerstein, N. V. Solis, T. Pisithkul, W. Srifa, E. Jeffery, D.
728 Abbey, S. G. Filler, A. M. Dudley, J. Berman, Rapid Phenotypic and Genotypic
729 Diversification After Exposure to the Oral Host Niche in *Candida albicans*. *Genetics* **209**,
730 725-741 (2018).
- 731 30. G. H. W. Tso, J. A. Reales-Calderon, A. S. M. Tan, X. Sem, G. T. T. Le, T. G. Tan, G. C.
732 Lai, K. G. Srinivasan, M. Yurieva, W. Liao, M. Poidinger, F. Zolezzi, G. Rancati, N.
733 Pavelka, Experimental evolution of a fungal pathogen into a gut symbiont. *Science* **362**,
734 589-595 (2018).
- 735 31. A. Forche, P. T. Magee, A. Selmecki, J. Berman, G. May, Evolution in *Candida albicans*
736 populations during a single passage through a mouse host. *Genetics* **182**, 799-811 (2009).
- 737 32. R. J. Bennett, A. Forche, J. Berman, Rapid mechanisms for generating genome diversity:
738 whole ploidy shifts, aneuploidy, and loss of heterozygosity. *Cold Spring Harb. Perspect.*
739 *Med.* **4**, (2014).
- 740 33. K. Sanyal, J. Carbon, The CENP-A homolog CaCse4p in the pathogenic yeast *Candida*
741 *albicans* is a centromere protein essential for chromosome transmission. *Proc. Natl. Acad.*
742 *Sci. U S A* **99**, 12969-12974 (2002).

- 743 34. K. Sanyal, M. Baum, J. Carbon, Centromeric DNA sequences in the pathogenic yeast
744 *Candida albicans* are all different and unique. *Proc. Natl. Acad. Sci. U S A* **101**, 11374-
745 11379 (2004).
- 746 35. K. Guin, L. Sreekumar, K. Sanyal, Implications of the Evolutionary Trajectory of
747 Centromeres in the Fungal Kingdom. *Annu. Rev. Microbiol.* **74**, 835-853 (2020).
- 748 36. A. Musacchio, A. Desai, A Molecular View of Kinetochore Assembly and Function.
749 *Biology (Basel)* **6**, (2017).
- 750 37. N. Varshney, K. Sanyal, Nuclear migration in budding yeasts: position before division.
751 *Curr. Genet.* **65**, 1341-1346 (2019).
- 752 38. A. Gonzalez-Novo, L. Labrador, M. E. Pablo-Hernando, J. Correa-Bordes, M. Sanchez, J.
753 Jimenez, C. R. Vazquez de Aldana, Dbf2 is essential for cytokinesis and correct mitotic
754 spindle formation in *Candida albicans*. *Mol. Microbiol.* **72**, 1364-1378 (2009).
- 755 39. S. W. Milne, J. Cheetham, D. Lloyd, S. Shaw, K. Moore, K. H. Paszkiewicz, S. J. Aves, S.
756 Bates, Role of *Candida albicans* Tem1 in mitotic exit and cytokinesis. *Fungal Genet. Biol.*
757 **69**, 84-95 (2014).
- 758 40. S. Bates, *Candida albicans* Cdc15 is essential for mitotic exit and cytokinesis. *Sci. Rep.* **8**,
759 8899 (2018).
- 760 41. J. Thakur, K. Sanyal, The essentiality of the fungus-specific Dam1 complex is correlated
761 with a one-kinetochore-one-microtubule interaction present throughout the cell cycle,
762 independent of the nature of a centromere. *Eukaryot. Cell* **10**, 1295-1305 (2011).
- 763 42. B. Roy, L. S. Burrack, M. A. Lone, J. Berman, K. Sanyal, CaMtw1, a member of the
764 evolutionarily conserved Mis12 kinetochore protein family, is required for efficient inner
765 kinetochore assembly in the pathogenic yeast *Candida albicans*. *Mol. Microbiol.* **80**, 14-
766 32 (2011).
- 767 43. M. Legrand, C. L. Chan, P. A. Jauert, D. T. Kirkpatrick, Role of DNA mismatch repair
768 and double-strand break repair in genome stability and antifungal drug resistance in
769 *Candida albicans*. *Eukaryot. Cell* **6**, 2194-2205 (2007).
- 770 44. M. Legrand, C. L. Chan, P. A. Jauert, D. T. Kirkpatrick, The contribution of the S-phase
771 checkpoint genes MEC1 and SGS1 to genome stability maintenance in *Candida albicans*.
772 *Fungal Genet. Biol.* **48**, 823-830 (2011).
- 773 45. R. Loll-Krippelber, C. d'Enfert, A. Feri, D. Diogo, A. Perin, M. Marcet-Houben, M. E.
774 Bougnoux, M. Legrand, A study of the DNA damage checkpoint in *Candida albicans*:
775 uncoupling of the functions of Rad53 in DNA repair, cell cycle regulation and genotoxic
776 stress-induced polarized growth. *Mol. Microbiol.* **91**, 452-471 (2014).

- 777 46. R. Loll-Krippleber, A. Feri, M. Nguyen, C. Maufrais, J. Yansouni, C. d'Enfert, M.
778 Legrand, A FACS-optimized screen identifies regulators of genome stability in *Candida*
779 *albicans*. *Eukaryot. Cell* **14**, 311-322 (2015).
- 780 47. M. Chauvel, A. Nesseir, V. Cabral, S. Znaidi, S. Goyard, S. Bachellier-Bassi, A. Firon, M.
781 Legrand, D. Diogo, C. Naulleau, T. Rossignol, C. d'Enfert, A versatile overexpression
782 strategy in the pathogenic yeast *Candida albicans*: identification of regulators of
783 morphogenesis and fitness. *PLoS One* **7**, e45912 (2012).
- 784 48. C. Bachewich, A. Nantel, M. Whiteway, Cell cycle arrest during S or M phase generates
785 polarized growth via distinct signals in *Candida albicans*. *Mol. Microbiol.* **57**, 942-959
786 (2005).
- 787 49. E. S. Bensen, A. Clemente-Blanco, K. R. Finley, J. Correa-Bordes, J. Berman, The mitotic
788 cyclins Clb2p and Clb4p affect morphogenesis in *Candida albicans*. *Mol. Biol. Cell* **16**,
789 3387-3400 (2005).
- 790 50. J. Thakur, K. Sanyal, A coordinated interdependent protein circuitry stabilizes the
791 kinetochore ensemble to protect CENP-A in the human pathogenic yeast *Candida*
792 *albicans*. *PLoS Genet.* **8**, e1002661 (2012).
- 793 51. E. Kitamura, K. Tanaka, Y. Kitamura, T. U. Tanaka, Kinetochore microtubule interaction
794 during S phase in *Saccharomyces cerevisiae*. *Genes Dev* **21**, 3319-3330 (2007).
- 795 52. Q. W. Jin, J. Fuchs, J. Loidl, Centromere clustering is a major determinant of yeast
796 interphase nuclear organization. *J. Cell Sci.* **113 (Pt 11)**, 1903-1912 (2000).
- 797 53. T. C. Lin, A. Neuner, E. Schiebel, Targeting of gamma-tubulin complexes to microtubule
798 organizing centers: conservation and divergence. *Trends Cell Biol.* **25**, 296-307 (2015).
- 799 54. T. C. Lin, A. Neuner, D. Flemming, P. Liu, T. Chinen, U. Jakle, R. Arkowitz, E. Schiebel,
800 MOZART1 and gamma-tubulin complex receptors are both required to turn gamma-TuSC
801 into an active microtubule nucleation template. *J. Cell Biol* **215**, 823-840 (2016).
- 802 55. A. Musacchio, E. D. Salmon, The spindle-assembly checkpoint in space and time. *Nat Rev*
803 *Mol Cell Biol* **8**, 379-393 (2007).
- 804 56. G. Kops, B. Snel, E. C. Tromer, Evolutionary Dynamics of the Spindle Assembly
805 Checkpoint in Eukaryotes. *Curr. Biol.* **30**, R589-R602 (2020).
- 806 57. A. K. Caydasi, G. Pereira, SPOC alert--when chromosomes get the wrong direction. *Exp.*
807 *Cell Res.* **318**, 1421-1427 (2012).
- 808 58. I. Scarfone, S. Piatti, Coupling spindle position with mitotic exit in budding yeast: The
809 multifaceted role of the small GTPase Tem1. *Small GTPases* **6**, 196-201 (2015).

- 810 59. R. S. Care, J. Trevethick, K. M. Binley, P. E. Sudbery, The MET3 promoter: a new tool
811 for *Candida albicans* molecular genetics. *Mol. Microbiol.* **34**, 792-798 (1999).
- 812 60. M. Shivaraju, J. R. Unruh, B. D. Slaughter, M. Mattingly, J. Berman, J. L. Gerton, Cell-
813 cycle-coupled structural oscillation of centromeric nucleosomes in yeast. *Cell* **150**, 304-
814 316 (2012).
- 815 61. L. Sreekumar, K. Kumari, K. Guin, A. Bakshi, N. Varshney, B. C. Thimmappa, L.
816 Narlikar, R. Padinhateeri, R. Siddharthan, K. Sanyal, Orc4 spatiotemporally stabilizes
817 centromeric chromatin. *Genome Res.* **31**, 607-621 (2021).
- 818 62. H. Y. Liu, J. H. Toyn, Y. C. Chiang, M. P. Draper, L. H. Johnston, C. L. Denis, DBF2, a
819 cell cycle-regulated protein kinase, is physically and functionally associated with the
820 CCR4 transcriptional regulatory complex. *EMBO J.* **16**, 5289-5298 (1997).
- 821 63. U. Surana, A. Amon, C. Dowzer, J. McGrew, B. Byers, K. Nasmyth, Destruction of the
822 CDC28/CLB mitotic kinase is not required for the metaphase to anaphase transition in
823 budding yeast. *EMBO J.* **12**, 1969-1978 (1993).
- 824 64. M. Hotz, Y. Barral, The Mitotic Exit Network: new turns on old pathways. *Trends Cell*
825 *Biol.* **24**, 145-152 (2014).
- 826 65. A. Atir-Lande, T. Gildor, D. Kornitzer, Role for the SCFCDC4 ubiquitin ligase in
827 *Candida albicans* morphogenesis. *Mol. Biol. Cell* **16**, 2772-2785 (2005).
- 828 66. M. Shirayama, Y. Matsui, E. A. Toh, The yeast TEM1 gene, which encodes a GTP-
829 binding protein, is involved in termination of M phase. *Mol. Cell Biol.* **14**, 7476-7482
830 (1994).
- 831 67. M. Valerio-Santiago, F. Monje-Casas, Tem1 localization to the spindle pole bodies is
832 essential for mitotic exit and impairs spindle checkpoint function. *J. Cell Biol.* **192**, 599-
833 614 (2011).
- 834 68. S. E. Lee, L. M. Frenz, N. J. Wells, A. L. Johnson, L. H. Johnston, Order of function of
835 the budding-yeast mitotic exit-network proteins Tem1, Cdc15, Mob1, Dbf2, and Cdc5.
836 *Curr. Biol.* **11**, 784-788 (2001).
- 837 69. A. P. Jackson, J. A. Gamble, T. Yeomans, G. P. Moran, D. Saunders, D. Harris, M. Aslett,
838 J. F. Barrell, G. Butler, F. Citiulo, D. C. Coleman, P. W. de Groot, T. J. Goodwin, M. A.
839 Quail, J. McQuillan, C. A. Munro, A. Pain, R. T. Poulter, M. A. Rajandream, H. Renauld,
840 M. J. Spiering, A. Tivey, N. A. Gow, B. Barrell, D. J. Sullivan, M. Berriman, Comparative
841 genomics of the fungal pathogens *Candida dubliniensis* and *Candida albicans*. *Genome*
842 *Res.* **19**, 2231-2244 (2009).

- 843 70. S. Padmanabhan, J. Thakur, R. Siddharthan, K. Sanyal, Rapid evolution of Cse4p-rich
844 centromeric DNA sequences in closely related pathogenic yeasts, *Candida albicans* and
845 *Candida dubliniensis*. *Proc. Natl. Acad. Sci. U S A* **105**, 19797-19802 (2008).
- 846 71. G. Chatterjee, S. R. Sankaranarayanan, K. Guin, Y. Thattikota, S. Padmanabhan, R.
847 Siddharthan, K. Sanyal, Repeat-Associated Fission Yeast-Like Regional Centromeres in
848 the Ascomycetous Budding Yeast *Candida tropicalis*. *PLoS Genet.* **12**, e1005839 (2016).
- 849 72. S. Bijlani, M. A. Thevandavakkam, H. J. Tsai, J. Berman, Autonomously Replicating
850 Linear Plasmids That Facilitate the Analysis of Replication Origin Function in *Candida*
851 *albicans*. *mSphere* **4**, (2019).
- 852 73. D. Pellman, M. Bagget, Y. H. Tu, G. R. Fink, H. Tu, Two microtubule-associated proteins
853 required for anaphase spindle movement in *Saccharomyces cerevisiae*. *J. Cell Biol.* **130**,
854 1373-1385 (1995).
- 855 74. S. C. Schuyler, J. Y. Liu, D. Pellman, The molecular function of Ase1p: evidence for a
856 MAP-dependent midzone-specific spindle matrix. Microtubule-associated proteins. *J. Cell*
857 *Biol.* **160**, 517-528 (2003).
- 858 75. H. Liu, F. Liang, F. Jin, Y. Wang, The coordination of centromere replication, spindle
859 formation, and kinetochore-microtubule interaction in budding yeast. *PLoS Genet.* **4**,
860 e1000262 (2008).
- 861 76. Y. Wang, F. Hu, S. J. Elledge, The Bfa1/Bub2 GAP complex comprises a universal
862 checkpoint required to prevent mitotic exit. *Curr. Biol.* **10**, 1379-1382 (2000).
- 863 77. H. S. Ro, S. Song, K. S. Lee, Bfa1 can regulate Tem1 function independently of Bub2 in
864 the mitotic exit network of *Saccharomyces cerevisiae*. *Proc. Natl. Acad. Sci. U S A* **99**,
865 5436-5441 (2002).
- 866 78. A. Ofir, D. Kornitzer, *Candida albicans* cyclin Clb4 carries S-phase cyclin activity.
867 *Eukaryot. Cell* **9**, 1311-1319 (2010).
- 868 79. E. Schwob, K. Nasmyth, CLB5 and CLB6, a new pair of B cyclins involved in DNA
869 replication in *Saccharomyces cerevisiae*. *Genes Dev.* **7**, 1160-1175 (1993).
- 870 80. A. Hibbel, A. Bogdanova, M. Mahamdeh, A. Jannasch, M. Storch, E. Schaffer, D.
871 Liakopoulos, J. Howard, Kinesin Kip2 enhances microtubule growth in vitro through
872 length-dependent feedback on polymerization and catastrophe. *Elife* **4**, (2015).
- 873 81. B. Augustine, C. F. Chin, F. M. Yeong, Role of Kip2 during early mitosis - impact on
874 spindle pole body separation and chromosome capture. *J. Cell Sci.* **131**, (2018).

- 875 82. A. Riera, M. Barbon, Y. Noguchi, L. M. Reuter, S. Schneider, C. Speck, From structure to
876 mechanism-understanding initiation of DNA replication. *Genes Dev.* **31**, 1073-1088
877 (2017).
- 878 83. K. Labib, J. A. Tercero, J. F. Diffley, Uninterrupted MCM2-7 function required for DNA
879 replication fork progression. *Science* **288**, 1643-1647 (2000).
- 880 84. B. Ren, G. Yu, G. C. Tseng, K. Cieply, T. Gavel, J. Nelson, G. Michalopoulos, Y. P. Yu,
881 J. H. Luo, MCM7 amplification and overexpression are associated with prostate cancer
882 progression. *Oncogene* **25**, 1090-1098 (2006).
- 883 85. G. Toyokawa, K. Masuda, Y. Daigo, H. S. Cho, M. Yoshimatsu, M. Takawa, S. Hayami,
884 K. Maejima, M. Chino, H. I. Field, D. E. Neal, E. Tsuchiya, B. A. Ponder, Y. Maehara, Y.
885 Nakamura, R. Hamamoto, Minichromosome Maintenance Protein 7 is a potential
886 therapeutic target in human cancer and a novel prognostic marker of non-small cell lung
887 cancer. *Mol. Cancer* **10**, 65 (2011).
- 888 86. Y. T. Qiu, W. J. Wang, B. Zhang, L. L. Mei, Z. Z. Shi, MCM7 amplification and
889 overexpression promote cell proliferation, colony formation and migration in esophageal
890 squamous cell carcinoma by activating the AKT1/mTOR signaling pathway. *Oncol. Rep.*
891 **37**, 3590-3596 (2017).
- 892 87. T. A. Weinert, L. H. Hartwell, The RAD9 gene controls the cell cycle response to DNA
893 damage in *Saccharomyces cerevisiae*. *Science* **241**, 317-322 (1988).
- 894 88. D. P. Waterman, J. E. Haber, M. B. Smolka, Checkpoint Responses to DNA Double-
895 Strand Breaks. *Annu. Rev. Biochem.* **89**, 103-133 (2020).
- 896 89. S. Sridhar, T. Hori, R. Nakagawa, T. Fukagawa, K. Sanyal, Bridgin connects the outer
897 kinetochore to centromeric chromatin. *Nat. Commun.* **12**, 146 (2021).
- 898 90. Y. Zhang, O. Foreman, D. A. Wigle, F. Kosari, G. Vasmatazis, J. L. Salisbury, J. van
899 Deursen, P. J. Galardy, USP44 regulates centrosome positioning to prevent aneuploidy
900 and suppress tumorigenesis. *J. Clin. Invest.* **122**, 4362-4374 (2012).
- 901 91. W. T. Silkworth, I. K. Nardi, R. Paul, A. Mogilner, D. Cimini, Timing of centrosome
902 separation is important for accurate chromosome segregation. *Mol. Biol. Cell* **23**, 401-411
903 (2012).
- 904 92. H. J. Nam, R. M. Naylor, J. M. van Deursen, Centrosome dynamics as a source of
905 chromosomal instability. *Trends Cell Biol.* **25**, 65-73 (2015).
- 906 93. A. Clemente-Blanco, A. Gonzalez-Novo, F. Machin, D. Caballero-Lima, L. Aragon, M.
907 Sanchez, C. R. de Aldana, J. Jimenez, J. Correa-Bordes, The Cdc14p phosphatase affects

- 908 late cell-cycle events and morphogenesis in *Candida albicans*. *J. Cell Sci.* **119**, 1130-1143
909 (2006).
- 910 94. I. N. Kaneva, I. M. Sudbery, M. J. Dickman, P. E. Sudbery, Proteins that physically
911 interact with the phosphatase Cdc14 in *Candida albicans* have diverse roles in the cell
912 cycle. *Sci. Rep.* **9**, 6258 (2019).
- 913 95. E. S. Segal, V. Gritsenko, A. Levitan, B. Yadav, N. Dror, J. L. Steenwyk, Y. Silberberg,
914 K. Mielich, A. Rokas, N. A. R. Gow, R. Kunze, R. Sharan, J. Berman, Gene Essentiality
915 Analyzed by In Vivo Transposon Mutagenesis and Machine Learning in a Stable Haploid
916 Isolate of *Candida albicans*. *mBio* **9**, (2018).
- 917 96. C. T. Chung, S. L. Niemela, R. H. Miller, One-step preparation of competent *Escherichia*
918 *coli*: transformation and storage of bacterial cells in the same solution. *Proc. Natl. Acad.*
919 *Sci. U S A* **86**, 2172-2175 (1989).
- 920 97. S. C. Potter, A. Luciani, S. R. Eddy, Y. Park, R. Lopez, R. D. Finn, HMMER web server:
921 2018 update. *Nucleic Acids Res.* **46**, W200-W204 (2018).
- 922 98. F. C. Luca, M. Mody, C. Kurischko, D. M. Roof, T. H. Giddings, M. Winey,
923 *Saccharomyces cerevisiae* Mob1p is required for cytokinesis and mitotic exit. *Mol. Cell*
924 *Biol.* **21**, 6972-6983 (2001).
- 925 99. D. Tamborrini, M. A. Juanes, S. Ibanes, G. Rancati, S. Piatti, Recruitment of the mitotic
926 exit network to yeast centrosomes couples septin displacement to actomyosin constriction.
927 *Nat. Commun.* **9**, 4308 (2018).
- 928 100. R. Sopko, D. Huang, N. Preston, G. Chua, B. Papp, K. Kafadar, M. Snyder, S. G. Oliver,
929 M. Cyert, T. R. Hughes, C. Boone, B. Andrews, Mapping pathways and phenotypes by
930 systematic gene overexpression. *Mol. Cell* **21**, 319-330 (2006).
- 931 101. R. Li, Bifurcation of the mitotic checkpoint pathway in budding yeast. *Proc. Natl. Acad.*
932 *Sci. U S A* **96**, 4989-4994 (1999).

933

934 **Acknowledgments**

935

936 We thank members of the Sanyal and d'Enfert laboratories for their valuable suggestions and
937 constructive criticism. We thank the Munro group at University of Aberdeen and Mazel group at
938 Institut Pasteur for their contribution to the establishment of overexpression plasmids that were
939 used in this study, a work that will be reported elsewhere. We thank Dr. Arshad Desai for critical
940 reading of the manuscript. We thank N. Varshney for constructing the plasmid pCse4-TAP-Leu.
941 We thank L. Sreekumar for constructing pTub4-GFP-His cassette. Special thanks to K. Guin for

942 sharing the raw files to generate the phylogenetic tree. We thank V. Sood and A. Das for
943 generating the plasmid pCdCsa6-GFP-ARS2. We thank A.S. Amrutha for generating the strains
944 CaPJ300 and CaPJ301. We acknowledge N. Nala at the flow cytometry facility, JNCASR, for
945 assisting flow cytometry and cell sorting experiments. The establishment of overexpression
946 plasmids was supported by the Wellcome Trust [088858/Z/09/Z to CD]. This work was supported
947 by a grant from the Indo French Centre for the promotion of Advanced Research (CEFIPRA,
948 Project no. 5703-2). CEFIPRA also aided in the travel of PJ, KS and CD between the Sanyal and
949 d'Enfert laboratories. PJ acknowledges intramural funding from JNCASR. AD and TP were
950 supported by the CEFIPRA grant. K.S. acknowledges the financial support of JC Bose National
951 Fellowship (Science and Engineering Research Board, Govt. of India, JCB/2020/000021) and
952 intramural funding from JNCASR.

953

954 **Funding**

955

956 Indo French Centre for the promotion of Advanced Research (CEFIPRA, Project no. 5703-2).

957 Jawaharlal Nehru Centre for Advanced Scientific Research.

958 JC Bose National Fellowship (Science and Engineering Research Board, Govt. of India,

959 JCB/2020/000021).

960 The Wellcome Trust (088858/Z/09/Z).

961 Institut Pasteur.

962 Institut national de la recherche pour l'agriculture, l'alimentation et l'environnement (INRAE).

963

964 **Author contributions:**

965 Conceptualization: KS, CD, PJ, ML

966 Methodology: ML, PJ, AD, TP, MC

967 Investigation: PJ, AD, TP, ML

968 Supervision: KS, CD, ML

969 Writing—original draft: PJ, KS

970 Writing—review & editing: PJ, KS, CD, ML

971

972 **Competing interests:** The authors declare no competing interests.

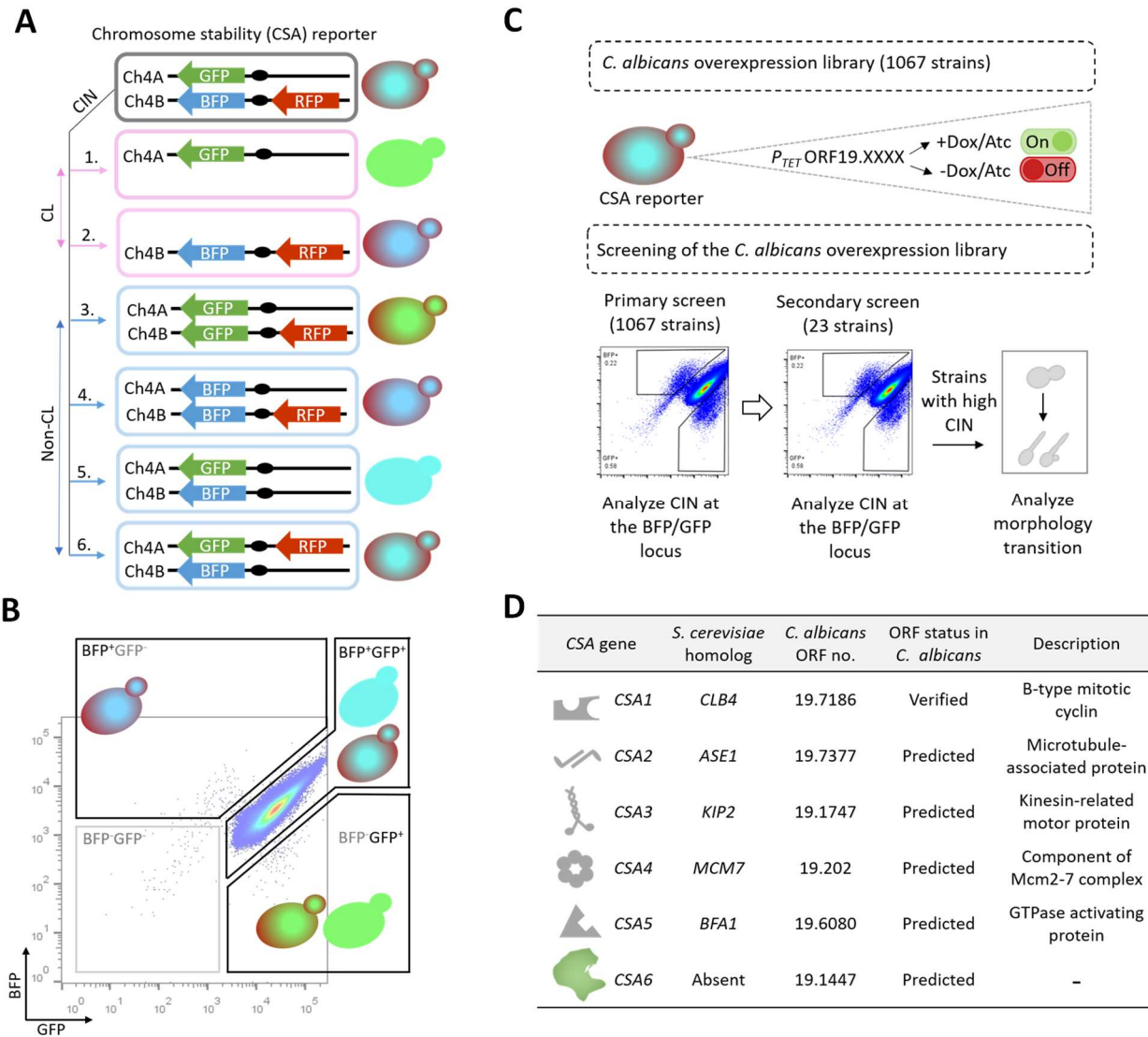
973

974 **Data and materials availability:** All data are available in the main text or supplementary

975 materials.

976 **Figure 1**

977



978

979

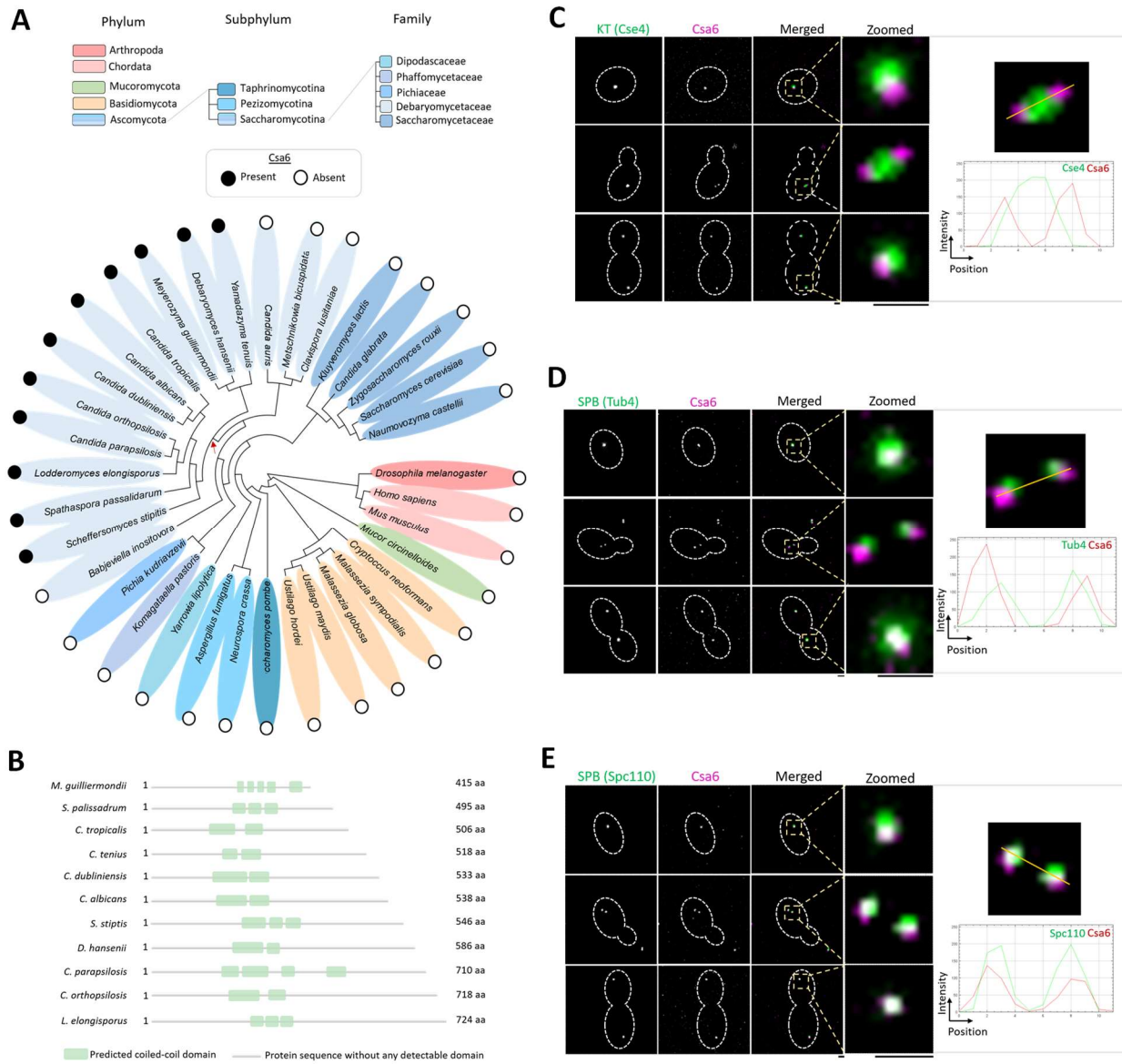
980 **Fig. 1. A medium-throughput protein overexpression screen identifies a set of CSA genes in**
 981 ***C. albicans*. (A)** Possible outcomes of CIN at the BFP/GFP and RFP loci. 1-4, CIN at the BFP or
 982 GFP locus, because of either chromosome loss (CL) or non-CL events such as break-induced
 983 replication, gene conversion, chromosome truncation or mitotic crossing over, will lead to the
 984 expression of either GFP or BFP expressing genes. CIN due to CL can be specifically identified
 985 by the concomitant loss of BFP and RFP, as shown in 1. 5 and 6, cells undergoing non-CL events
 986 at the RFP locus will continue to express BFP and GFP. (B) Flow cytometric analysis of the
 987 BFP/GFP density profile of empty vector (EV) (CaPJ150) containing BFP, GFP and RFP genes.
 988 Majority of the cells are positive for both BFP and GFP (BFP⁺GFP⁺). A minor fraction of the

989 population had lost either one of the markers (BFP⁺GFP⁻ or BFP⁻GFP⁺) or both the markers (BFP⁻
990 GFP⁻), indicating spontaneous instability of this locus (46). Approximately 1 million events are
991 displayed. **(C)** Pictorial representation of the screening strategy employed for identifying *CSA*
992 genes in *C. albicans*. Briefly, a library of *C. albicans* overexpression strains (1067), each carrying
993 a unique ORF under the tetracycline-inducible promoter, P_{TET}, was generated using the *CSA*
994 reporter (CEC5201) as the parent strain. The library was then analyzed by primary and secondary
995 screening methods to identify *CSA* genes. In the primary screen, CIN frequency at the BFP/GFP
996 locus in the individual 1067 overexpression strains was determined using flow cytometry.
997 Overexpression strains exhibiting increased CIN (23 out of 1067) were taken forward for
998 secondary screening. The secondary screen involved revalidation of the primary hits for increased
999 CIN at the BFP/GFP locus by flow cytometry. Strains which reproduced the increased CIN
1000 phenotype were further examined for yeast to filamentous transition by microscopy. **(D)** A brief
1001 overview of the *CSA* genes identified from the overexpression screen (6 out of 1067). Functional
1002 annotation of genes is based on the information available either in *Candida Genome Database*
1003 (www.candidagenome.org) or in *Saccharomyces Genome Database* (www.yeastgenome.org) on
1004 August 1, 2021.

1005
1006
1007
1008
1009
1010
1011
1012
1013
1014
1015
1016
1017
1018
1019
1020
1021
1022

1023
1024

Figure 2



1025
1026

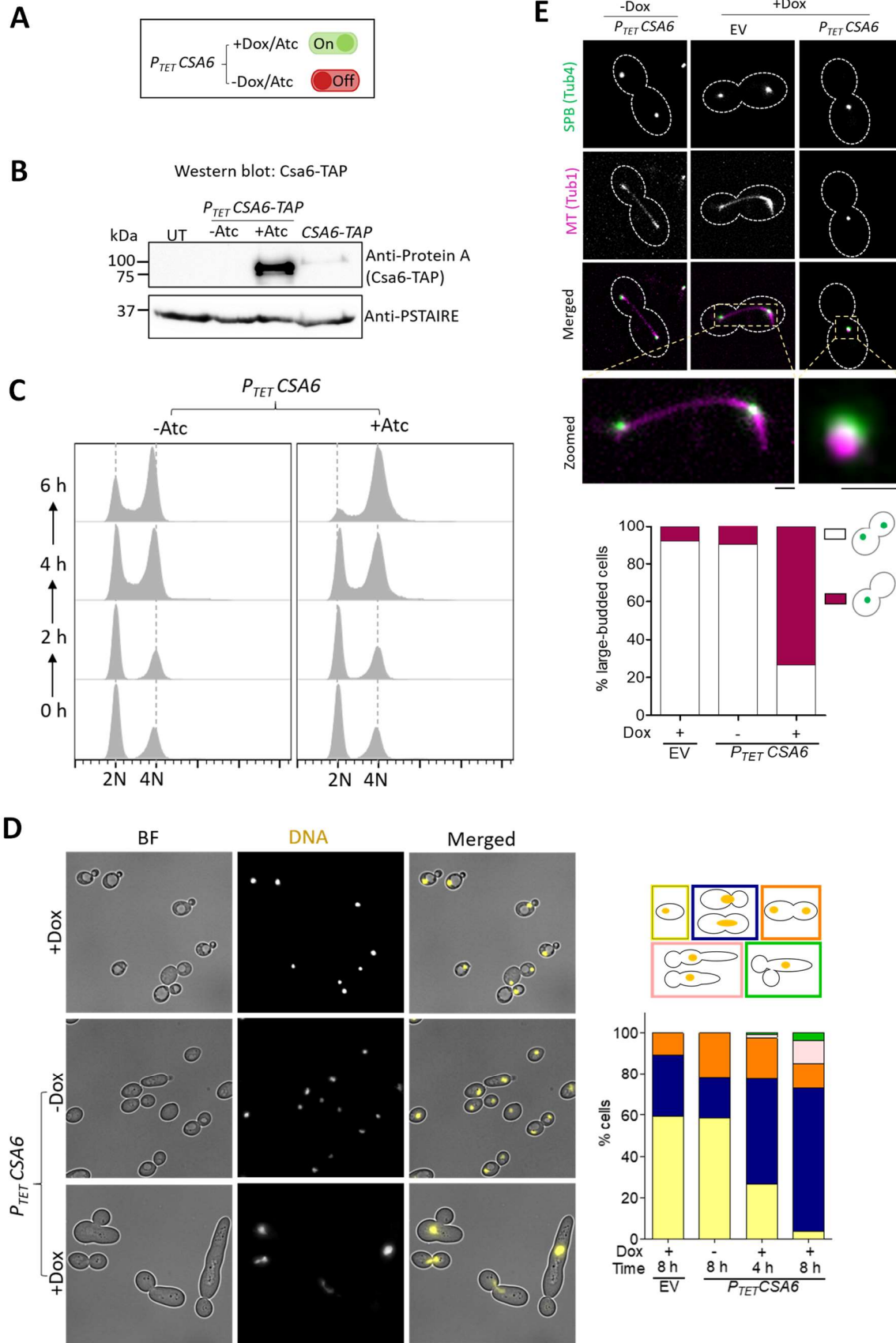
Fig. 2. Csa6 has a selective existence across fungal phylogeny and is constitutively localized

to the SPBs in *C. albicans*. (A) Phylogenetic tree showing the conservation of Csa6 across the mentioned species. The presence (filled circles) or absence (empty circles) of Csa6 in every species is marked. Each taxonomic rank is color-coded. The species mentioned under the family Debaryomycetaceae belong to the CUG-Ser clade in which the CUG codon is often translated as serine instead of leucine. The red arrow points to the CUG-Ser clade lineage that acquired Csa6. Searches for Csa6 homologs (E value $\leq 10^{-2}$) were carried out either in the *Candida Genome Database* (www.candidagenome.org) or NCBI nonredundant protein database. (B) Schematic illustrating the protein domain architecture alignment of Csa6 in the indicated fungal species.

1036 Length of the protein is mentioned as amino acids (aa). Approximate positions of the predicted
1037 coiled-coil domain, identified using HMMER (97) phmmer searches, is shown. **(C-E)** *Left*,
1038 micrographs comparing the sub-cellular localization of Csa6 with KT (Cse4) and SPB (Tub4 and
1039 Spc110) at various cell cycle stages. *Top*, Csa6-mCherry and Cse4-GFP (CaPJ119); *middle*, Csa6-
1040 mCherry and Tub4-GFP (CaPJ120), and *bottom*, Csa6m-Cherry and Spc110-GFP (CaPJ121).
1041 Scale bar, 1 μ m. *Right*, histogram plots showing the fluorescence intensity profile of Csa6-
1042 mCherry with Cse4-GFP (*top*), Tub4-GFP (*middle*) and Spc110-GFP (*bottom*) across the
1043 indicated lines.

1044
1045
1046
1047
1048
1049
1050
1051
1052
1053
1054
1055
1056
1057
1058
1059
1060
1061
1062
1063
1064
1065

1066 **Figure 3**



1067

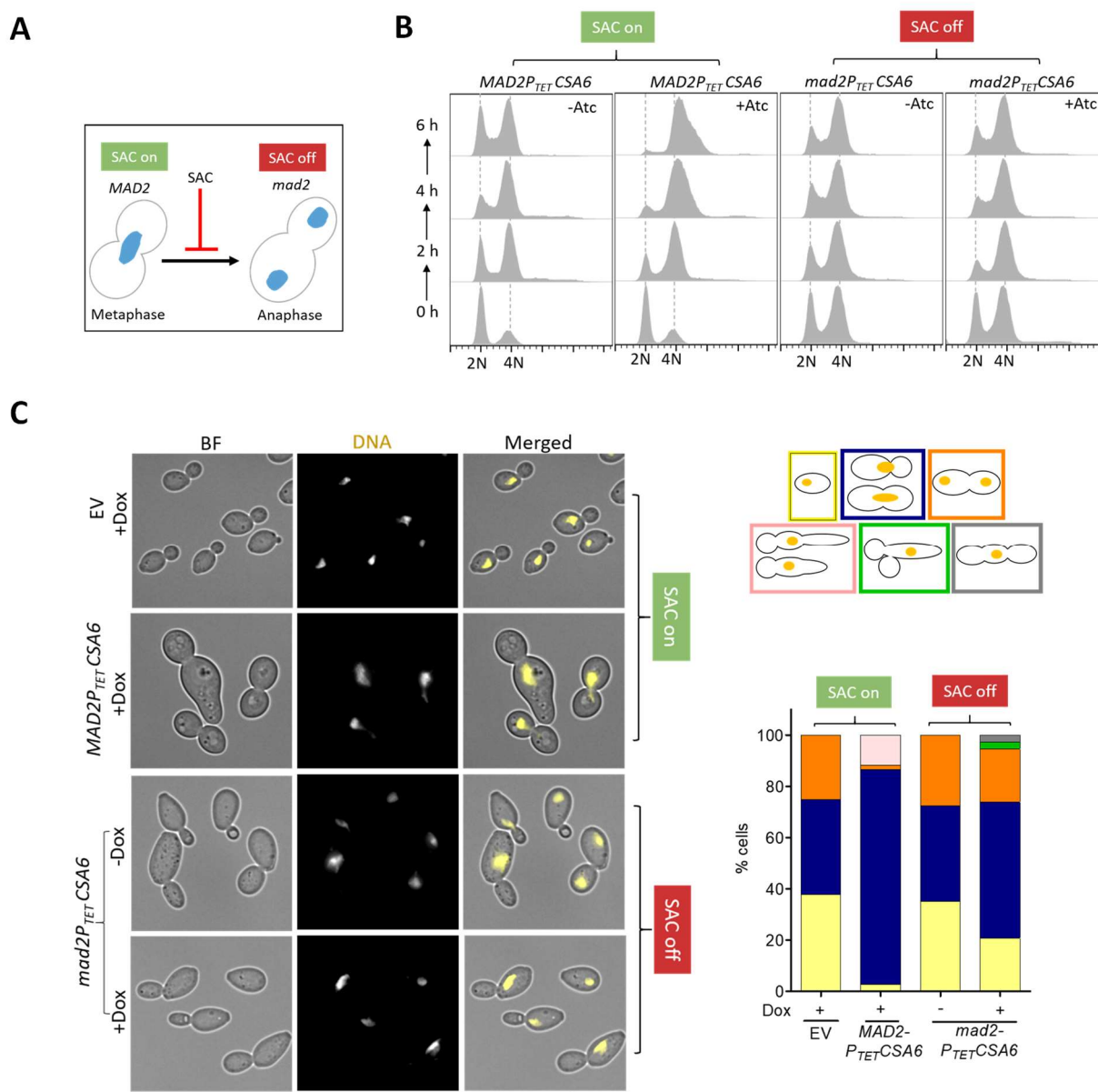
1068

1069 **Fig. 3. Overexpression of Csa6 alters the morphology of the mitotic spindle and leads to**
1070 **G2/M arrest in *C. albicans*.** (A) Atc/Dox-dependent functioning of the P_{TET} promoter system for
1071 conditional overexpression of *CSA6*. (B) Western blot analysis using anti-Protein A antibodies
1072 confirmed overexpression of *CSA6-TAP* from the P_{TET} promoter (CaPJ181), after 8 h induction in
1073 presence of Atc (3 $\mu\text{g/ml}$), in comparison to the uninduced culture (-Atc) or *CSA6-TAP*
1074 expression from its native promoter (CaPJ180); $N=2$. PSTAIRE was used as a loading control.
1075 UT, untagged control (SN148). (C) Flow cytometric analysis of cell cycle displaying the cellular
1076 DNA content of *CSA6^{OE}* strain (CaPJ176) in presence or absence of Atc (3 $\mu\text{g/ml}$) at the
1077 indicated time intervals; $N=3$. (D) *Left*, microscopic images of Hoechst-stained EV (CaPJ170)
1078 and *CSA6^{OE}* strain (CaPJ176) after 8 h of growth under indicated conditions of Dox (50 $\mu\text{g/ml}$).
1079 BF, bright-field. Scale bar, 10 μm . *Right*, quantitation of different cell types at the indicated time-
1080 points; $n \geq 100$ cells. (E) *Top*, representative micrographs of spindle morphology in the large-
1081 budded cells of EV (CaPJ172) and *CSA6^{OE}* strain (CaPJ178) after 8 h of growth under indicated
1082 conditions of Dox (50 $\mu\text{g/ml}$). SPBs and MTs are marked by Tub4-GFP and Tub1-mCherry,
1083 respectively. Scale bar, 1 μm . *Bottom*, the proportion of the large-budded cells with indicated SPB
1084 phenotypes; $n \geq 100$ cells.

1085
1086
1087
1088
1089
1090
1091
1092
1093
1094
1095
1096
1097
1098
1099
1100
1101
1102

1103 **Figure 4**

1104



1105

1106

1107 **Fig. 4. The G2/M cell cycle arrest in the *CSA6*^{OE} mutant is mediated by Mad2. (A)** The

1108 G2/M arrest posed by SAC in response to an improper chromosome-spindle attachment is

1109 relieved in the absence of Mad2, allowing cells to transit from metaphase to anaphase. (B)

1110 flow cytometric DNA content analysis in CaPJ176 (*MAD2CSA6*^{OE}) and CaPJ197 (*mad2CSA6*^{OE}) at

1111 the indicated times, in presence or absence of Atc (3 µg/ml); *N*=3. (C) *Left*, microscopic images

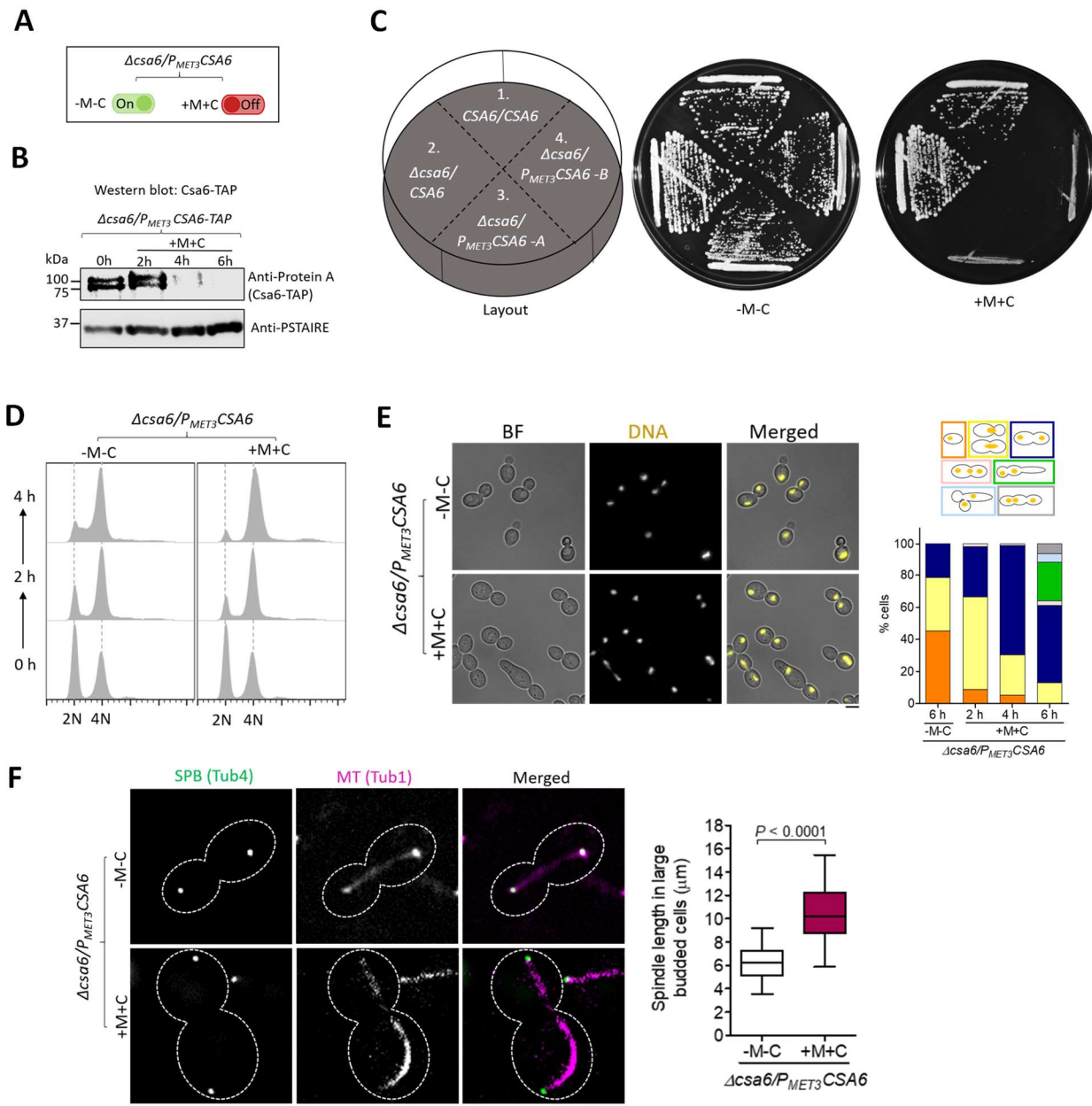
1112 of CaPJ170 (EV), CaPJ176 (*MAD2CSA6*^{OE}) and CaPJ197 (*mad2CSA6*^{OE}) following Hoechst

1113 staining, after 8 h of growth under indicated conditions of Dox (50 µg/ml). Scale bar, 10 µm.

1114 *Right*, quantitation of the indicated cell types; *n* ≥ 100 cells.

1115 **Figure 5**

1116



1117

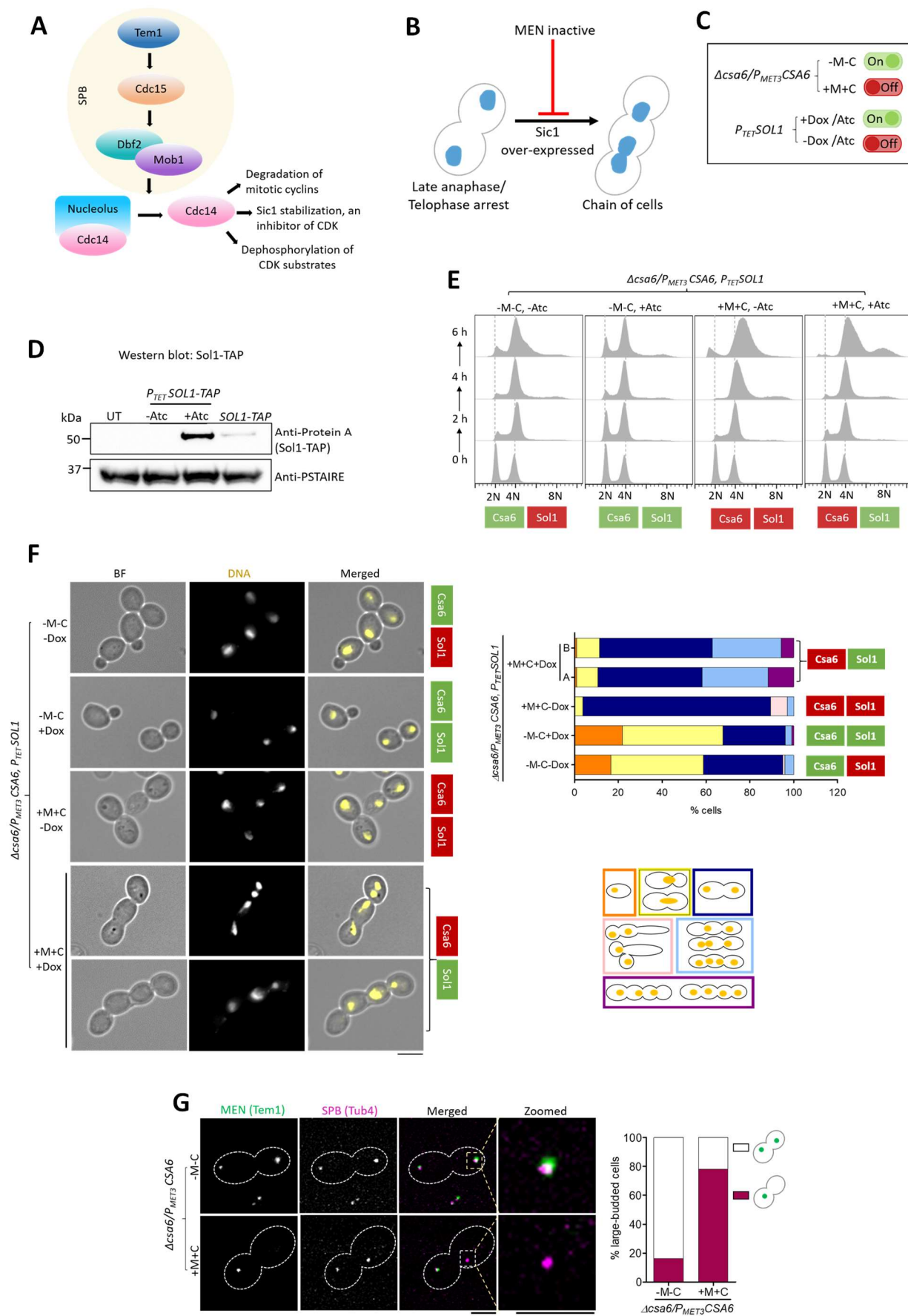
1118

1119 **Fig. 5. Csa6 depletion causes late anaphase/telophase arrest with a hyper-extended mitotic**
 1120 **spindle in *C. albicans*.** (A) The *MET3* promoter system for depleting cellular levels of Csa6. The
 1121 *MET3* promoter can be conditionally repressed in presence of methionine (Met/M) and cysteine
 1122 (Cys/C). (B) Western blot analysis using anti-Protein A antibodies revealed time dependent
 1123 depletion of Csa6-TAP in *CSA6^{PSD}* strain (CaPJ212), grown under repressive conditions (YPDU
 1124 + 5 mM Met and 5 mM Cys) for indicated time interval; *N*=2. (C) Csa6 is essential for viability in
 1125 *C. albicans*. Strains with indicated genotypes, (1) SN148, (2) CaPJ209, (3 and 4) CaPJ210 (two

1126 transformants) were streaked on agar plates with permissive (YPDU-Met-Cys) or repressive
1127 (YPDU + 5 mM Met and 5 mM Cys) media and incubated at 30°C for two days. **(D)** Cell cycle
1128 analysis of CaPJ210 (*CSA6^{PSD}*) by flow cytometry under permissive (YPDU-Met-Cys) and
1129 repressive conditions (YPDU + 5 mM Met and 5 mM Cys) at the indicated time intervals; $N=3$.
1130 **(E)** *Left*, microscopic images of Hoechst stained CaPJ210 (*CSA6^{PSD}*) cells grown under
1131 permissive (YPDU-Met-Cys) or repressive (YPDU + 5 mM Met and 5 mM Cys) conditions for 6
1132 h. BF bright-field. Scale bar, 5 μm . *Right*, quantitation of different cell types at the indicated time-
1133 points; $n \geq 100$ cells. **(F)** *Left*, micrograph showing Tub4-GFP and Tub1-mCherry (representing
1134 mitotic spindle) in the large-budded cells of CaPJ211 (*CSA6^{PSD}*) after 6 h of growth under
1135 permissive (YPDU-Met-Cys) or repressive (YPDU + 5 mM Met and 5 mM Cys) conditions.
1136 Scale bar, 3 μm . *Right*, quantitation of the distance between the two SPBs, along the length of the
1137 MT (representing spindle length), in large-budded cells of CaPJ211 (*CSA6^{PSD}*) under permissive
1138 ($n=32$) or repressive ($n=52$) conditions. Paired *t*-test, one-tailed, *P*-value shows a significant
1139 difference.

1140
1141
1142
1143
1144
1145
1146
1147
1148
1149
1150
1151
1152
1153
1154
1155
1156
1157
1158
1159

1160 **Figure 6**

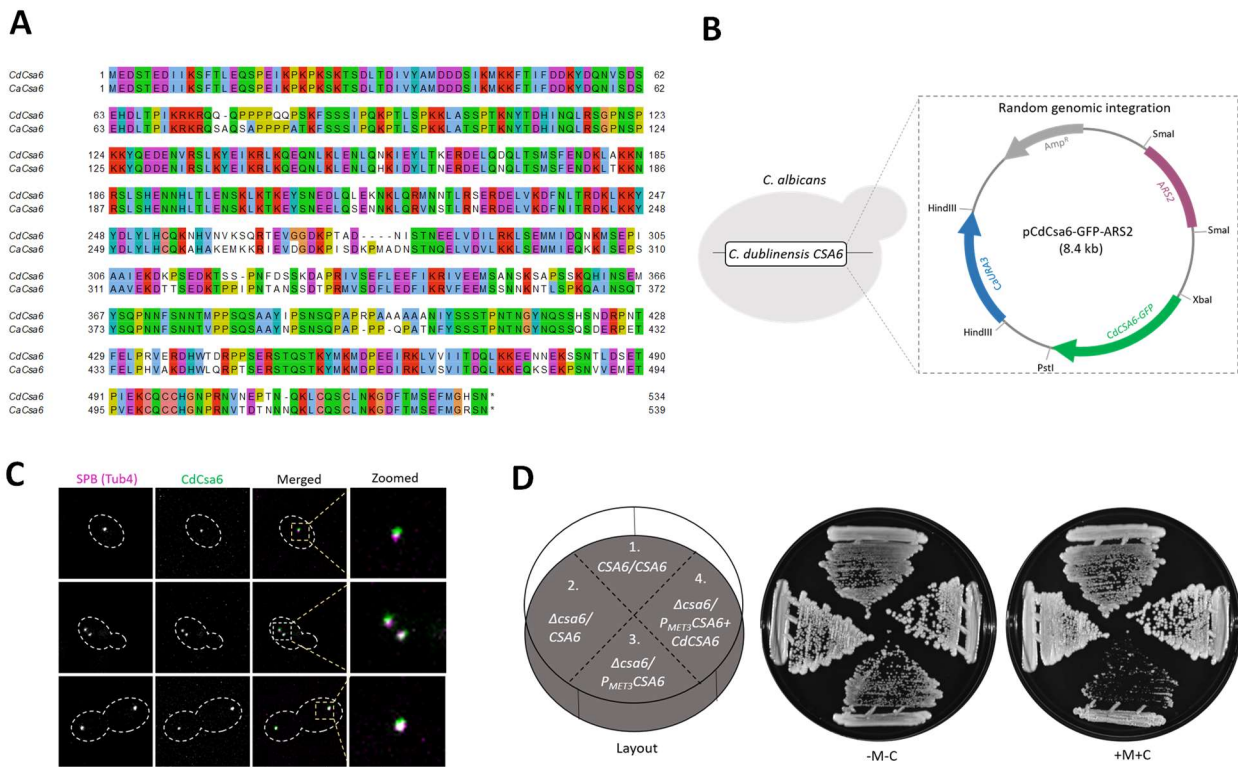


1162 **Fig. 6. Csa6 is required for mitotic exit in *C. albicans*.** (A) The MEN components in *S.*
1163 *cerevisiae*. At SPB, Nud1 acts as a scaffold. The ultimate target of the MEN is to activate Cdc14
1164 phosphatase, which remains entrapped in the nucleolus in an inactive state until anaphase. Cdc14
1165 release brings about mitotic exit and cytokinesis by promoting degradation of mitotic cyclins,
1166 inactivation of mitotic CDKs through Sic1 accumulation and dephosphorylation of the CDK
1167 substrates (64). (B) Inhibition of the MEN signaling prevents cells from exiting mitosis and
1168 arrests them at late anaphase/telophase. Bypass of cell cycle arrest due to the inactive MEN, viz.
1169 by overexpression of Sic1-a CDK inhibitor, results in the chain of cells with multiple nuclei (98,
1170 99). (C) A combination of two regulatable promoters, P_{TET} and P_{MET3} , was used to overexpress *C.*
1171 *albicans* homolog of Sic1, called *SOLI* (Sic one-like), in *Csa6*-depleted cells. The resulting strain,
1172 CaPJ215, can be conditionally induced for both *SOLI* overexpression upon Atc/Dox addition and
1173 *Csa6* depletion upon Met (M)/Cys (C) addition. (D) Protein A western blot analysis showed
1174 increased levels of Sol1 (TAP-tagged) in the *SOLI*^{OE} mutant (CaP217, $P_{TET}SOLI-TAP$) after 6 h
1175 induction in presence of Atc (3 μ g/ml) in comparison to the uninduced culture (-Atc) or *SOLI*
1176 expression from its native promoter (CaPJ216, *SOLI-TAP*); $N=2$. PSTAIRE was used as a
1177 loading control. UT, untagged control (SN148). (E) Flow cytometric analysis of cell cycle
1178 progression in CaPJ215 at indicated time intervals under various growth conditions, as indicated;
1179 $N=3$. Dox: 50 μ g/ml, Met: 5 mM, Cys: 5 mM. (F) *Left*, Hoechst staining of CaPJ215 after 6 h of
1180 growth under indicated conditions of Dox (50 μ g/ml), Met (5 mM) and Cys (5 mM); $n \geq 100$ cells.
1181 BF bright-field. Scale bar, 5 μ m. *Right*, percent distribution of the indicated cell phenotypes; n
1182 ≥ 100 cells. (G) *Left*, co-localization analysis of Tem1-GFP and Tub4-mCherry in large-budded
1183 cells of CaPJ218 (*CSA6*^{PSD}) under permissive (YPDU-Met-Cys) or repressive conditions (YPDU
1184 + 5 mM Met and 5 mM Cys). Scale bar, 3 μ m. *Right*, the proportion of the large-budded cells
1185 with indicated Tem1 phenotypes; $n \geq 100$ cells.

1186
1187
1188
1189
1190
1191
1192
1193
1194
1195

1196 **Figure 7**

1197



1198

1199

1200

1201

1202

1203

1204

1205

1206

1207

1208

1209

1210

1211

1212

1213

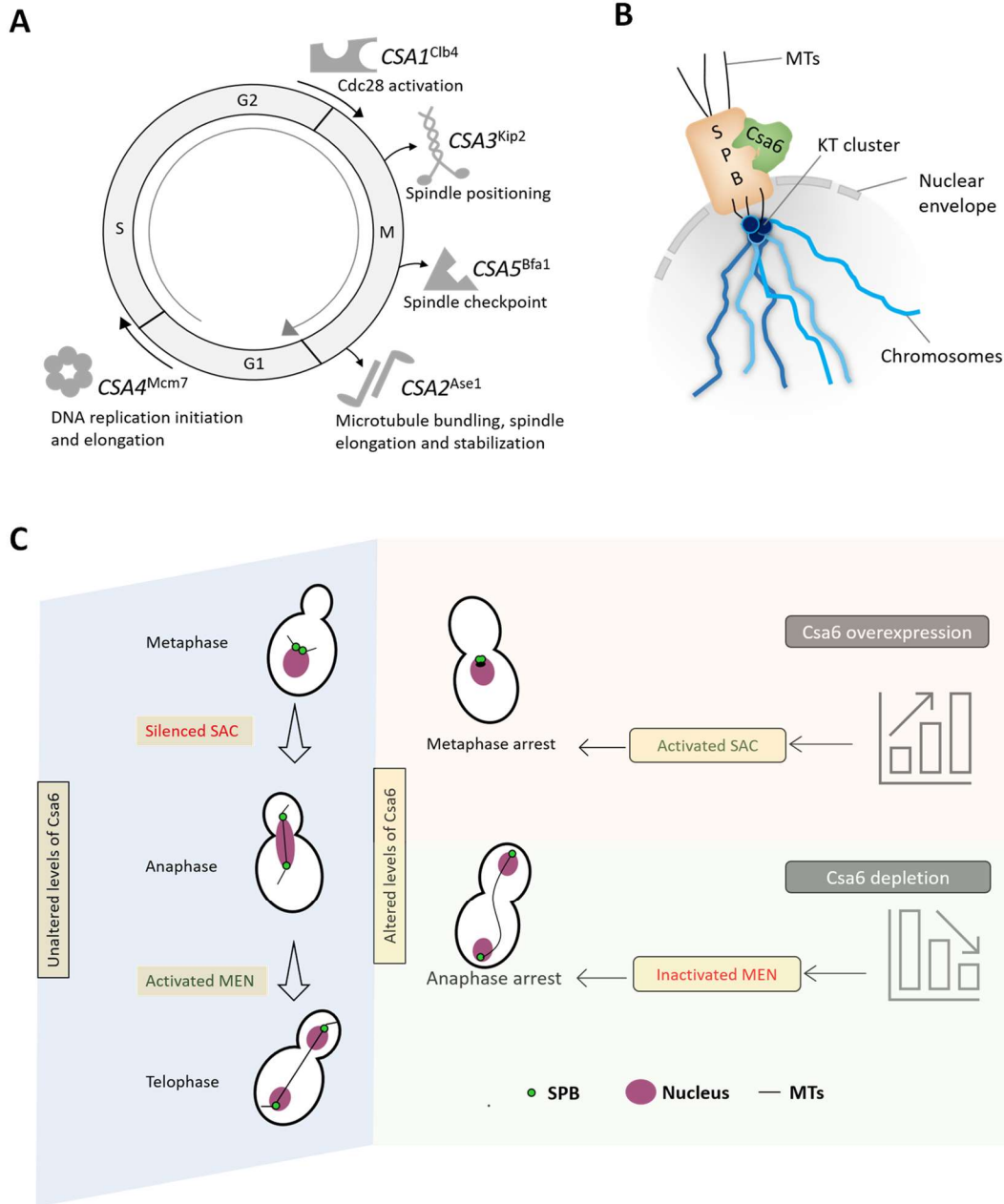
1214

1215

Fig. 7. Ectopic expression and functional conservation of CdCsa6 in *C. albicans*. (A) Pairwise alignment of amino acid sequences of Csa6 proteins in *C. albicans* (CaCsa6) and *C. dubliniensis* (CdCsa6) by Clustal Omega, visualized using Jalview. (B) Ectopic expression of CdCsa6 in *C. albicans* by random genomic integration of the ARS-containing plasmid. Vector map of pCdCsa6-GFP-ARS2 depicts the cloned sites of CaURA3, CaARS2 and CdCSA6-GFP. The CdCSA6-GFP fragment contains the GFP tag, CdCSA6 (ORF Cd36_16290) without the stop codon and the promoter region of CdCSA6. (C) CdCsa6 localizes to the SPB. Representative micrographs showing CdCsa6GFP localization at different cell cycle stages in CaPJ300. Tub4mCherry was used as an SPB marker. Scale bar, 3 μm. (D) CdCsa6 functionally complements CaCsa6. Strains with indicated genotypes, (1) SN148, (2) CaPJ300, (3) CaPJ301 and (4) CaPJ302, were streaked on agar plates with permissive (YPDU-Met-Cys) or repressive (YPDU + 5 mM Met and 5 mM Cys) media and incubated at 30°C for two days.

1216 **Figure 8**

1217



1218

1219

1220 **Fig. 8. *Csa6* levels are fine-tuned at various stages of the cell cycle to ensure both mitotic**

1221 **progression and mitotic exit in *C. albicans*. (A)** A diagram illustrating the functions of the

1222 identified *CSA* genes except *CSA6* in various phases and phase transitions of the cell cycle. **(B)**

1223 Schematic depicting the approximate position of *Csa6* with respect to SPB and KT. In *C.*

1224 *albicans*, SPBs and clustered KTs remain in close proximity throughout the cell cycle, while *Csa6*

1225 remains constitutively localized to the SPBs. **(C)** A model summarizing the effects of

1226 overexpression or depletion of *Csa6* in *C. albicans*. A wild-type cell with unperturbed *Csa6* levels

1227 progresses through the mitotic cell cycle. Overexpression of *CSA6* alters the mitotic spindle
1228 dynamics which might lead to improper KT-MT attachments, prompting SAC activation and
1229 G2/M arrest. In contrast, decreased levels of Csa6 inhibit the MEN signaling pathway, probably
1230 by affecting Tem1 recruitment to the SPBs, resulting in cell cycle arrest at the anaphase stage.

1231

1232

1233

1234

1235

1236

1237

1238

1239

1240

1241

1242

1243

1244

1245

1246

1247

1248

1249

1250

1251

1252

1253

1254 **Table 1. Overexpression phenotypes of CSA genes in *C. albicans* and *S. cerevisiae***

1255

CSA gene	<i>C. albicans</i> ORF no.	<i>S. cerevisiae</i> homolog	Overexpression phenotype (<i>C. albicans</i>)	Overexpression phenotype (<i>S. cerevisiae</i>)	Reference
<i>CSA1</i>	19.7186	<i>CLB4</i>	Increased CIN involving non-CL events	Shift towards 2N (diploid) DNA content	(100)
<i>CSA2</i>	19.7377	<i>ASE1</i>	Increased CIN involving non-CL events	i) CIN involving loss of an artificial chromosome fragment or rearrangements/ gene conversion events. ii) Spindle checkpoint dependent delay in entering anaphase upon HU treatment	(14, 75)
<i>CSA3</i>	19.1747	<i>KIP2</i>	Increased CIN involving non-CL events	Shift towards 2N (diploid) DNA content	(81, 100)
<i>CSA4</i>	19.202	<i>MCM7</i>	Shift towards 4N (diploid) DNA content, G2/M arrest	NA	NA
<i>CSA5</i>	19.608	<i>BFA1</i>	Shift towards 4N (diploid) DNA content, anaphase arrest	Shift towards 2N (diploid) DNA content, Anaphase arrest	(101)
<i>CSA6</i>	19.1447	NA	Shift towards 4N (diploid) DNA content, G2/M arrest	NA	NA

1256 NA, not available

1257

1258

1259

1260

1261

1262

1263

1264

1265